Seismic Vulnerability of Timber Bridges and Timber Substructures
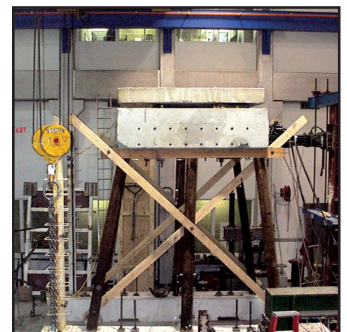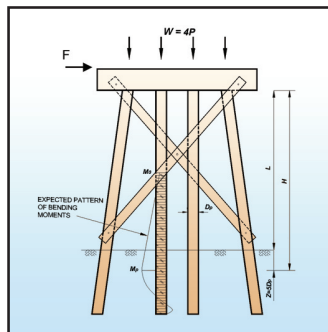
by

Ayman A. Shama, John B. Mander, Ian M. Friedland and Dion R. Allicock

NOTICE

Seismic Vulnerability of Timber Bridges
and Timber Substructures

by

Ayman A. Shama,[1] John B. Mander,[2] Ian M. Friedland[3] and Dion R. Allicock[4]

1   Structural Engineer, Parsons Transportation Group, Inc., 110 William Street, New York, NY; former Ph.D. Research Assistant, Department of Civil, Structural and Environmental Engineering, University at Buffalo, State University of New York
2   Professor of Structural Engineering, University of Canterbury, New Zealand; former Associate Professor, Department of Civil, Structural and Environmental Engineering, University at Buffalo, State University of New York
3   Bridge Technology Engineer, Federal Highway Administration; former Assistant Director for Transportation Research, Highways and Bridges, Multidisciplinary Center for Earthquake Engineering Research, University at Buffalo, State University of New York
4   Engineering Specialist III, Bridge Design Section, Dallas District, Texas Department of Transportation; former Graduate Student, Department of Civil, Structural and Environmental Engineering, University at Buffalo, State University of New York

Preface

The Multidisciplinary Center for Earthquake Engineering Research (MCEER) is a national center of excellence in advanced technology applications that is dedicated to the reduction of earthquake losses nationwide. Headquartered at the University at Buffalo, State University of New York, the Center was originally established by the National Science Foundation in 1986, as the National Center for Earthquake Engineering Research (NCEER).

Comprising a consortium of researchers from numerous disciplines and institutions throughout the United States, the Center's mission is to reduce earthquake losses through research and the application of advanced technologies that improve engineering, pre-earthquake planning and post-earthquake recovery strategies. Toward this end, the Center coordinates a nationwide program of multidisciplinary team research, education and outreach activities.

MCEER's research is conducted under the sponsorship of two major federal agencies, the National Science Foundation (NSF) and the Federal Highway Administration (FHWA), and the State of New York. Significant support is also derived from the Federal Emergency Management Agency (FEMA), other state governments, academic institutions, foreign governments and private industry.

The supporting research for this report was performed under FHWA contract number DTFH61-97-C-00029 "Effect of Seismic Loads on Timber Bridges." It was carried out at University at Buffalo under Principal Investigators John Mander and Ian Friedland. This summary report was produced under FHWA contract number DTFH61-03-P-00464 "Effect of Seismic Loads on Timber Bridges". It summarizes the research and incorporates technical comments from FHWA and external reviewers. The Principal Investigator was Jerome O'Connor and the lead author was Ayman Shama.

The seismic behavior of timber bridges is not well understood. Historically, little effort has been spent on documenting the seismic performance of these bridge types in past earthquakes or conducting research to develop an improved understanding of the seismic and/or retrofit requirements for them. This research is devoted towards: (a) documenting the seismic performance of timber bridges in past earthquakes; (b) assessing, from both theoretical as well as experimental perspectives, the strength and ductility capability of timber piled bridges in both the braced in-plane (transverse to the bridge axis) and out-of-plane (longitudinal) directions; and (c) conducting a seismic vulnerability analysis of timber bridges to assess the expected mode of failure.

In pursuit of these objectives, theories are developed to predict the performance of timber piles under lateral loading. Theoretical predictions were verified by experimental studies on full-scale timber specimens, and timber pile-to-concrete cap connections. For braced timber pile bents, a prototype timber bridge was used to develop a near-full size

physical model that was subjected to shaking table experiments and quasi-static re-versed cyclic loading tests on the laboratory strong-floor. A nonlinear force-displace-ment computational modeling study was also conducted as a companion effort to the experimental investigation. Based on the experimental and theoretical research, the seismic vulnerability study of timber bridges led to the development of fragility curves.

It is concluded that timber bridges are inherently robust and have the ability to withstand major earthquakes with minor to no damage. The main issue is in the provision of adequate deck seating on timber caps.

ABSTRACT

There is little understanding of the seismic behavior of timber bridges, as historically, little effort has been spent on documenting their performance in past earthquakes or conducting research to develop seismic and/or retrofit requirements for them. This research is devoted towards: (a) documenting the seismic performance of timber bridges in past earthquakes; (b) assessing, from both theoretical as well as experimental perspectives, the strength and ductility capability of timber piled bridges in both the braced in-plane (transverse to the bridge axis) and out-of-plane (longitudinal) directions; and (c) conducting a seismic vulnerability analysis of timber bridges to assess the expected mode of failure.

In pursuit of these objectives, theories are developed to predict the performance of timber piles under lateral loading. Theoretical predictions were verified by experimental studies on full-scale timber specimens, and timber pile-to-concrete cap connections. For braced timber pile bents, a prototype timber bridge was used to develop a near-full size physical model that was subjected to shaking table experiments and quasi-static reversed cyclic loading tests on the laboratory strong-floor. A nonlinear force-displacement computational modeling study was also conducted as a companion effort to the experimental investigation. Based on the experimental and theoretical research, the seismic vulnerability study of timber bridges led to the development of fragility curves.

It is concluded that timber bridges are inherently robust and have the ability to withstand major earthquakes with minor to no damage. The main issue is in the provision of adequate deck seating on timber caps.

ACKNOWLEDGEMENTS

TABLE OF CONTENTS

TABLE OF CONTENTS (Continued)

TABLE OF CONTENTS (Continued)

LIST OF FIGURES

LIST OF FIGURES (Continued)

LIST OF FIGURES (Continued)

LIST OF FIGURES (Continued)

LIST OF TABLES

SECTION 1
INTRODUCTION

1.1 BACKGROUND

Wood has a high strength to weight ratio and energy-absorbing properties that are desirable in bridge construction. It is also capable of supporting short-term overloads without adverse effects.   Large wooden members provide good fire-resistant qualities that meet or exceed those of other materials in severe fire exposures. Economically, wood is competitive with other materials on a first-cost basis and shows advantages when life cycle costs are compared (FPL/FHWA 2001). Timber bridges can be constructed in virtually any weather conditions, without detriment to the material. Wood is not damaged by continuous freezing and thawing and resists the harmful effects of de-icing agents, which cause deterioration in other bridge materials. Timber bridges do not require special equipment for installation and can normally be constructed without highly skilled labor. They also present a natural and aesthetically pleasing appearance, particularly in natural/rural surroundings.

In the past several years, there have been several major earthquakes in the United States and elsewhere, where numerous bridges have experienced significant damage. The performance of steel and concrete highway bridges during these earthquakes has been well documented, and significant research has gone into developing details, which can improve the performance of these structures in future earthquakes. However, little if any effort has been spent on documenting the performance of timber bridges or conducting research to develop an improved understanding of the performance and behavior of these structures during earthquakes. In addition, little guidance is provided in seismic design codes specific to timber structures, and no guidance is readily available for retrofitting seismically deficient timber bridges.

The pile bent, such as the one shown in figure 1-1, is a common form of construction for highway and railway bridges in certain parts of the United States. In this form of construction, a timber (or reinforced concrete) cap beam is attached directly to the driven timber piles. Generally, piles extending more than 2-m above the ground have their bents laterally braced as

shown in figure 1-1. Primarily designed for vertical loading, these structures may be susceptible to damage from cyclic lateral loading arising from earthquakes. Non-seismic lateral loads such as centrifugal force, stream flow and wind are designed to be resisted by battered piles and bracings.
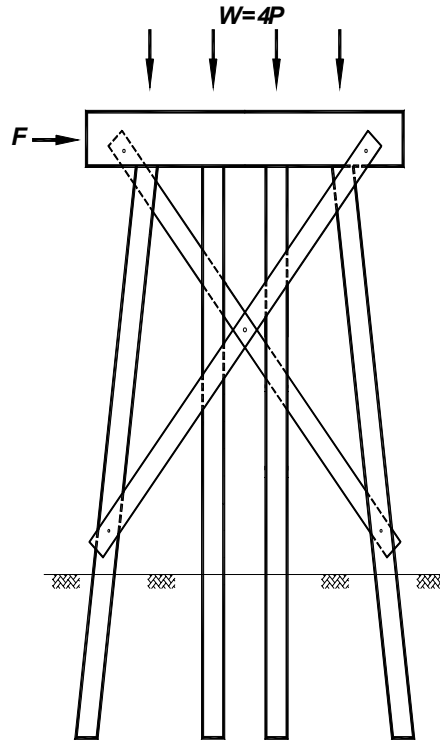
Figure 1-1. Typical timber pile supported bent.

Two typical failure modes are anticipated for these structures under earthquake loading: out-of-plane and in-plane. The out-of-plane (see figure 1-2) behavior of timber pile bents under earthquake ground motions (principally with shaking in the longitudinal direction) is characterized by formation of a plastic collapse mechanism with plastic hinging in the piles at some embedment within the soil and some opposing moment at the pile to pile cap interface. Figure 1-3 illustrates the critical connections that are vulnerable to damage from ground motions with shaking in the in-plane (braced) direction. In both situations, the local performance of the connection has a substantial effect on the overall behavior of the bridge. Therefore, it was deemed essential to evaluate the performance of these connections under cyclic loading through an extensive experimental program. The work presented in this study is an effort to contribute towards this goal.

**Figure 1-2. Timber pile bent that experienced damage in an
out-of-plane failure mode.**

CONNECTIONS
VULNERABLE TO
DAMAGE
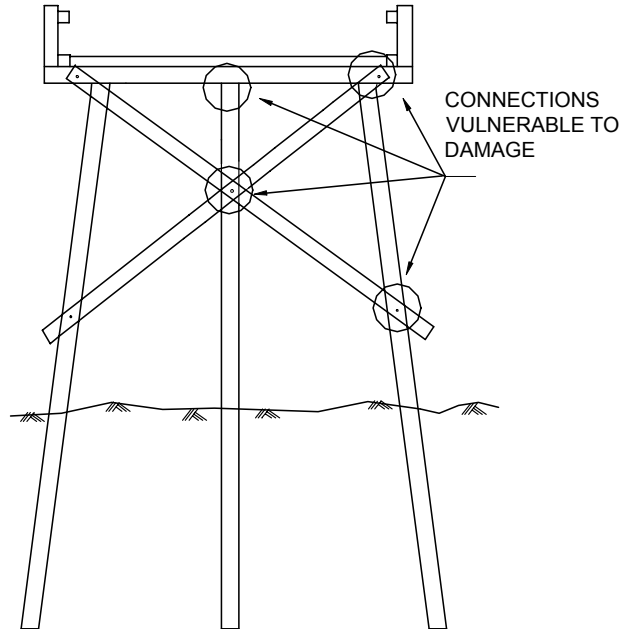
**Figure 1-3. Critical connections under earthquake loading in
braced timber pile bents (shaking in-plane direction).**

1.2 SCOPE OF RESEARCH

This research effort consists of four distinct phases:

- Documenting the performance of timber bridges in past earthquakes.

- Reviewing current timber bridge seismic design and evaluation criteria and philosophies.

- Assessing, from both a theoretical and experimental point of view, the strength and ductility capability and hence, the seismic vulnerability of timber highway bridges and timber pile-to-concrete cap connections.

- Recommending design guidelines for new construction and retrofit of existing timber highway bridges.

To achieve these objectives, theories are developed to predict the performance of timber piles under lateral loading. Theoretical predictions were validated by experiments conducted on full-scale timber specimens, and timber pile-to-concrete cap connections. Pile specimens were tested to failure using quasi-static reversed cyclic loading to assess the effect of axial load-moment interaction on both interior (vertical) and exterior (battered) piles. For braced timber pile bents, a prototype timber bridge was used to develop a near-full size physical model that was used for shaking table experiments and quasi-static reversed cyclic loading tests on the laboratory strong-floor. A nonlinear force-displacement computational modeling study was also undertaken as a companion effort to the experimental investigation. On the basis of the experimental study, a seismic damage assessment criterion is developed for bridge structures supported by pile bents

1.3 ORGANIZATION

Chapter 2 of the report covers aspects of seismic design requirements of timber bridges, and provides an overview of the performance of timber bridges during the 1964 Alaska and 1989 Loma Prieta earthquakes. Chapter 3 covers the theoretical as well as experimental study performed on timber pile bents to identify their seismic performance in both out-of-plane and in-plane directions. Chapter 4 presents the theoretical and experimental investigations conducted to evaluate the performance of timber pile-to-cap connections. Chapter 5 presents the seismic

vulnerability study of bridges supported by piled substructures. A fragility curve theory is developed based on the experimental results obtained earlier in this study. Fragility curves were developed for several case studies to demonstrate the validity of the fragility analysis. Chapter 6 draws conclusions in light of the present study and outlines recommendations for future research.

SECTION 2
SEISMIC DESIGN, EVALUATION AND PERFORMANCE OF TIMBER BRIDGES

2.1 SEISMIC DESIGN CRITERIA FOR TIMBER HIGHWAY BRIDGES

The American Association of State Highway and Transportation Officials (AASHTO) currently maintains two specifications for the design of highway bridges, the *Standard Specifications for Highway Bridges* (currently in its 17th Edition) and the *LRFD Bridge Design Specifications* (currently in its 2nd Edition, 1998, with Interim provisions through 1999). Seismic provisions in the *Standard Specifications* are contained within Division I-A, Seismic Design, while similar provisions in the *LRFD Specifications* are distributed throughout the specification and integrated into load and material resistance sections as appropriate. A number of timber bridge provisions contained in the *LRFD Specifications* are currently being updated via a joint USDA Forest Products Laboratory/FHWA project, which is conducting a specification calibration to produce improved base material resistance factors.

The stated purpose for Division I-A of the *Standard Specifications* is to establish design and construction provisions for bridges to minimize their susceptibility to damage from earthquakes. Specifically, the criteria address the applicability of the standards and lead the designer through the preliminary and final design process. The process is initiated with an inventory of seismic and soil data (the Acceleration Coefficient and Soil Site Coefficient for the area where the bridge is located) and the selection of an importance classification. On the basis of this information, the Seismic Performance Category (SPC, defined as categories A through D) of the bridge is determined.

For single-span bridges, a rigorous seismic analysis is not required; rather, design forces and displacements are calculated and checked against the capacity of the structure to accommodate these forces and displacements. For displacements, the key criteria is minimum seat width (also called the support length) at the abutment; for forces, the standards require the

calculation of a required horizontal force at the abutment, based on the tributary weight of the structure at the abutment, multiplied by the Acceleration Coefficient and the Site Coefficient.

For multiple-span bridges, the SPC determines the level of seismic analysis required for design. SPC A bridges (the lowest seismic hazard category) do not require rigorous seismic analysis, but again must be checked for seat widths (at abutments, piers, and in-span hinges) and for fixed-bearing forces equal to 0.2 times the tributary weight of the structure in each restrained direction (similar to single-span bridges). Bridges classified as SPC B, C, or D must be analyzed in a more rigorous manner, and special provisions exist in each category for structural steel and concrete (reinforced or prestressed) super- and substructures, and foundations. *There are no provisions specific to timber bridge components in these standards*.

Therefore, based on this criterion, and the knowledge that many U.S. timber highway bridges are relatively short, single-span or multiple simple-span structures, the expected minimum design and evaluation requirements were limited to connection force and displacement checks. However, because timber bridges often consist of light superstructures, the expected tributary dead weight is likely to be relatively small. Therefore, the minimum amount of connectivity provided by drift bolts and boat spikes typically found in timber bridge construction in regions of low seismicity should suffice to carry required forces. This, however, would have to be examined in more detail for timber bridges with heavier superstructures, e.g., those with concrete decks on timber pile bents.

The *LRFD Specifications* contain similar provisions. In this specification, the identification of the SPC (called Seismic Performance Zone, SPZ, with values of 1 through 4, rather than A through D) is determined in the loads section (Section 3) and material-specific resistance provisions are contained in the steel and concrete sections of the specification. Similar to the *Standard Specifications*, however, no provisions specific to timber seismic performance or resistance requirements are contained in the timber section (Section 8).

As in the *Standard Specifications*, single-span bridges designed in accordance with the *LRFD Specifications* are exempt from a formal seismic analysis and must be checked primarily for minimum connection forces in the restrained direction between the super- and substructure. The use of longitudinal restrainers is allowed on multiple-span bridges in lieu of satisfying the minimum seat width requirements for all SPZs.

The simplified design process in both specifications continues with the determination of an elastic seismic response coefficient and a response modification factor (R-factor). If an elastic analysis is conducted, the force effects resulting from the elastic analysis are divided by the specified R-factors. This is done to avoid the overconservatism inherent in a purely elastic design, when it is known that structures deform inelastically during seismic events. The elastic design displacements, however, are not reduced by these R-factors. R-factors have been defined for reinforced concrete and steel or composite pile bents, and generic R-factors are specified for single-column and multiple-column bents. *However, it is not known if these R-factors are appropriate for timber substructure elements*. Similarly, R-factors are specified for connection details, such as the connection of a superstructure to an abutment, or a column, pier, or pile bent to a cap beam or superstructure. *Again, it is not known if these R-factors are appropriate or have been validated for timber super-/substructure connections*.

It is important to note that the *LRFD Specifications* provide a significant departure from earlier codes, as structures designed in accordance with this specification are now designed for the ultimate strength limit state, and are intended to have a uniform level of safety. Design working loads are factored up by the use of partial safety factors. Dependable ultimate strength resistance is determined by assuming that ultimate concrete strains (0.003) exceed the crushing strength strain (at 0.002), and steel strains exceed the yield strain by a significant amount. This ultimate strength theory implies ductile behavior for both reinforced concrete and structural steel members. This approach is particularly meaningful for seismic resistant design where elastic design loads may (intentionally) exceed the provided strength by a wide margin on the order of three to five times. Resistance of these large seismically-generated inertia loads is via ductile action with considerable hysteretic energy dissipation.

2.2 SEISMIC DESIGN OF TIMBER RAILROAD BRIDGES

Seismic design provisions for railroad bridges are published and maintained by the American Railway Engineering and Maintenance-of-Way Association (AREMA, formerly the American Railway Engineering Association, AREA) in its *Manual for Railway Engineering*.

In general, timber bridges are considered in Chapter 9 of the AREMA manual as being the least vulnerable to seismic effects (Article 1.4.2). According to Article 1.5.7.2 of Section

1.5, *Existing Structures*, timber trestles may be screened and eliminated from further seismic evaluation if they are free of conditions that would require attention in the near future, in order to permit continuation of normal railroad traffic. For timber trestles not eliminated by screening, seismic evaluation is to be focused on the potential effect of an earthquake on deficient conditions or details.

Previous editions of the AREA manual (i.e., prior to 1996) outlined the seismic criteria for existing timber trestles per the following:

Timber trestles supporting track, which meet the following criteria, need not be analyzed for resistance to seismic loads:

Bents:

- Driven piles or framed posts of not more than three stories.

- Steel connector with a diameter of 19-mm or more at each cap-to-pile joint.

- Fully connected cross bracing providing a maximum unbraced pile or post height of 3.1-m.

- Alternate panel tower bracing for bents of more than 12.2-m from base of rail to natural ground level.

Open deck spans:

- Not fewer than two stringers per track rail.

- Stringer lapping and chord bolting at all intermediate bents.

- Full stringer-to-cap bearing at end bents.

- Full connection of stringer to cap joints by a steel connector not less than 19-mm in diameter.

Ballasted deck spans:

- Not fewer than eight stringers per panel.

- Not more than two stringers butt-jointed on any intermediate bent.

- Full stringer-to-cap bearing at end bents.

- Full connection of stringer to cap joints by a steel connector not less than 19-mm in diameter.

- Not less than 50 percent of deck board/top of stringer joints connected by appropriate steel spikes.

It appears that the vast majority of existing timber trestle railroad bridge standards comply with this criteria.

2.3 TIMBER BRIDGE MANUAL

The most comprehensive source of general information for the design, inspection, and maintenance of timber bridges can be found in the U.S. Department of Agriculture manual *Timber Bridges: Design, Construction, Inspection, and Maintenance* (Ritter, 1990). When issued, this manual provided state-of-the-art information and guidance on all aspects of timber bridge construction. Seismic considerations in the timber bridge manual refer back to the AASHTO *Standard Specifications* and the AASHTO *Guide Specifications for Seismic Design of Highway Bridges*. Because of the date of issue, the manual is no longer up-to-date in this area, as the *Guide Specifications* were incorporated into the *Standard Specifications* in 1991. This manual, therefore, does not provide any additional information or guidance for the seismic design or evaluation of timber bridges.

2.4 SEISMIC EVALUATION OF EXISTING TIMBER BRIDGES

Currently, there are no formal national specifications for the seismic evaluation of existing timber highway or railroad bridges. The most up-to-date information for all materials except wood is contained in the FHWA *Seismic Retrofitting Manual for Highway Bridges*, originally published in 1983 and more recently updated and reissued by the FHWA as a product of the FHWA/MCEER Highway Project in 1995. This bridge retrofitting manual provides guidance on the seismic hazard screening, evaluation, and retrofitting of highway bridges across the U.S. Similar to the AASHTO design specifications, this manual contains provisions specific to steel and concrete super- and substructures, but no provisions specific to timber bridges are provided.

The seismic evaluation procedures contained in the FHWA retrofitting manual are currently being extended and refined for concrete and steel bridges as part of the FHWA/MCEER Highway Project. Similar evaluation procedures can not be developed for timber bridges, at this time, since the strength and deformation capability of each member and systems comprised of these members are not readily available. It is intended that this study will partially remedy this situation through a limited testing program on timber bridge pile bents, and by ascertaining their deformation (ductility) capacity under lateral loading.

It is well known that timber is a robust material capable of resisting large dynamic impact forces. For example, traffic-induced impact loads on timber bridges need not be considered explicitly during design. There is an implicit belief that these impact forces can easily be absorbed by the visco-elastic damping inherent in wood. Additionally, timber exhibits increased strength for short duration loads. However, the extent to which large seismic overloads can be sustained is unknown. This stems from the fact that timber design is primarily based on an allowable stress philosophy. What this suggests, then, is that the deformation capability of timber bridge components, stressed well into the inelastic range, is not well understood.

2.5 PERFORMANCE OF TIMBER BRIDGES IN PAST EARTHQUAKES

2.5.1 Highway Bridges

There are a number of reports and references concerning the performance of timber buildings during earthquakes (see Foliente, 1997, for example). However, based on a review of published literature, only a limited number of reports documenting timber highway bridge damage in the U.S. and worldwide were identified. A search of MCEER Quakeline's database, which contains listings for more than 30,000 journal and conference proceeding articles, did not identify any specific reports of earthquake damage to timber highway bridges. Other online searches also identified only a few articles or reports of interest, with the exception of an analytical study discussed below. The only significant report of interest was one from the U.S. Geological Survey which documented bridge damage resulting from the 1964 Alaska earthquake (Kachadoorian, 1968).

A telephone survey was conducted of several State bridge engineers (New York, Pennsylvania, Virginia, California, Oregon, and Washington) in order to determine if there were any damage reports for timber bridges not readily available in the published literature. The only reported timber highway bridge damage occurred in Oregon in 1993, when strong ground shaking caused a timber superstructure to become unseated from its bearings. The superstructure came off its support (bearing) but did not drop from the abutment; this resulted in an approximately 76-mm bump at the end of the bridge. The Oregon State DOT considered this damage minor and easily repairable.

Although not a real case study of timber bridge performance during an earthquake, an analytical study was conducted to determine the expected performance of a historic timber covered bridge in West Virginia (Spyrakos: 1994, 1999). This analytical study modeled the structure using a finite element code, and then subjected the model to a multimode spectral analysis based on then-current AASHTO criteria. Three other spectra were also applied using increased accelerations corresponding to different earthquakes and different regions of the eastern U.S. The analysis revealed that the bridge would suffer no damage based on the AASHTO earthquake, and limited damage for even higher-magnitude events, but no collapse. However, for the worst case considered, with an acceleration coefficient of 0.35-g, the bridge would experience severe damage.

1964 Alaska Earthquake

The March 27, 1964, Alaska earthquake was the largest magnitude earthquake to affect the U.S. in recent history and possibly the most damaging overall. It had a magnitude of 8.4 and strong ground shaking lasted for between four and five minutes (the 1811 and 1812 New Madrid earthquakes, by comparison, were on the order of magnitude 8.1 with a duration of strong shaking estimated at less than one minute). The earthquake resulted in widespread damage to the infrastructure in the south-central part of Alaska.

Especially hard hit was the highway system in this part of Alaska. Of the 204 highway bridges in the region, 141 were damaged; of these, 92 were severely damaged or destroyed (Kachadoorian, 1968). Thirteen of these 141 damaged bridges were destroyed by a tsunami and nine more had to be replaced because subsidence caused them to be under water during high

tides. Therefore, 119 bridges (58.3 percent of the total bridge inventory in the area) were damaged or destroyed by ground shaking.

According to Kachadoorian:

"The intensity of damage was controlled primarily by the geologic environment (including depth of the water table) upon which the highway structures rested, and secondarily by the engineering characteristics of the structures. Structures on bedrock were only slightly damaged if at all, whereas those on unconsolidated sediments were slightly to severely damaged, or were completely destroyed by seismic shaking....

The chief engineering characteristics responsible for the type and intensity of damage include (1) thickness of roadway fills, (2) type of pile bents and masonry piers, (3) the weight ratio between the substructure and superstructure, and (4) the tie between the substructure and superstructure.

The thicker the roadway fills, the more severe the damage. Wooden piles did not break as extensively as piles constructed of three railroad rails welded together. Bridges that had relatively heavy superstructures, for example those with concrete decks on wooden piles, were more severely damaged than those with all-wood or concrete decks on concrete piers. Failure first occurred at the tie between the superstructure and substructure; the poorer this tie, the sooner the failure."

Table 2-1 summarizes the type and extent of damage for bridges with timber substructures which were in the region of damage from the earthquake. As can be seen, only 20 percent (four of 20) of bridges with timber superstructures were severely damaged or destroyed, whereas 81 percent (22 of 27) of bridges with concrete decks were damaged or destroyed. As examination of the data provided in the report also shows that in virtually every case where there was severe damage or collapse, a significant amount of ground deformation at the abutments and/or under the piers also occurred.

There are several important issues that should be noted as a result of Kachadoorian's report, including the following:

- The majority of damage was a result of soil amplification effects of the ground motion for structures founded in soft soils. Bridges founded on bedrock were only minimally damaged, if at all.

- Most bridge damage resulted from soil liquefaction and lateral spreading. Liquefaction can cause a loss of vertical support or lateral stability, while lateral spreading causes large pressures and displacements on foundations and substructures.

- In general, bridges with timber substructures performed better than those with welded steel rail substructures.

- Bridges with heavier concrete decks and timber substructures performed much worse than similar bridges with timber decking and timber substructures.

- The most susceptible structural detail appears to be the connection between the superstructure and substructure, especially between the pier cap and piles.

Unfortunately, available reports documenting bridge damage from the 1964 Alaska earthquake do not provide sufficient structural detail on the damaged bridges or failed components. Reports refer to light or small connections between the superstructure and substructure, or between the pier caps and timber piles. Based on typical timber bridge construction employed at the time, it is therefore assumed that these connections were primarily 12-mm or 19-mm diameter drift or anchor bolts.

Table 2-1. Timber highway bridge damage during the 1964 Alaska earthquake.

Superstructure	Substructure	Foundation	Extent of Damage (no. of bridges)			
			None	Slight	Moderate	Severe or Destroyed
Timber	Timber	Bedrock	-	1	-	-
Timber	Timber	Sediment	1	13	2	4
Concrete	Timber	Sediment	3	2	-	22
Steel	Timber	Bedrock	1	-	-	-
Steel	Timber	Sediment	1	-	1	7

Kachadoorian (1968)

2.5.2 Railroad Bridges

1964 Alaska Earthquake

The 1964 Alaskan earthquake resulted in widespread damage to both highway and railroad bridges, including many timber trestle structures (McCulloch and Bonilla, 1970). Similar to the earlier discussion on highway bridges, it appears that much of the timber railroad bridge damage that occurred during this event was due to ground liquefaction and lateral spreading, where the lateral ground spreading caused large horizontal displacements and failures in the railroad bridge foundations (McCulloch and Bonilla, 1970, Byers, 1996 and Pauschke, 1990). According to McCulloch and Bonilla:

> *"Bridge superstructures were compressed and failed by lateral buckling, or more commonly were driven into, through, or over bulkheads. Piles and piers were torn free of super-structures by moving sediments, crowded toward stream channels, and lifted in the center. The lifted piles arched the superstructures. Vertical pile displacement was independent of the depth of the pile penetration in the sediment and thus was due to vertical movement of the sediments, rather than to differential compaction. The fact that bridge piles were carried laterally without notable tilting suggests that mobilization exceeded pile depths, which averaged about 6.1 m."*

There were two primary modes of superstructure to substructure connectivity failures noted in this earthquake. The first was where the bolts securing the stringers to the pile caps pulled free or fractured, while the pile caps remained attached to the piles. The second mode was where the drift bolts securing the pile cap to the pile failed, but the cap remained attached or partially attached to the stringers.

In all, 125 Alaska railroad bridges were damaged or destroyed during the earthquake; in nearly every documented case, pile bents were shifted both horizontally and vertically as a result of liquefaction and lateral spreading at stream crossings. It is important to recognize that these types of ground failures are likely to result in similar failure modes regardless of whether the substructure and foundation are constructed of steel, concrete, or timber piling.

1989 Loma Prieta Earthquake

During the October 17, 1989, Loma Prieta earthquake near San Francisco, California, a large number of highway bridges (none of which were timber) sustained damage of varying degrees, including several structures, which fully collapsed. In addition, several Southern Pacific

Railroad bridges sustained minor damage, as described below. Following the earthquake, the firm of Modjeski and Masters, Inc. was employed to assist in on-site inspections and evaluations of these damaged structures.

The inspection reports noted that the epicenter of the earthquake was in close proximity to a large number of railroad bridges on main lines and branch lines. In spite of this and the magnitude of the earthquake, there was virtually no significant damage to most railroad structures. In fact, the main line reportedly did not sustain any structural damage during the earthquake.

Overall, four Southern Pacific structures were damaged during the earthquake, one of which had minor superstructure damage while the other three sustained substructure damage. Although there was some movement between the girders and the top of the pier caps, the bearings were of sufficient size and the available seat widths on top of the pier caps were large enough that the movement did not cause any spans to drop.

One of the damaged Southern Pacific structures was an open deck timber trestle at Watsonville, California, located about 19.3-km south east of the epicenter on a branch line. The soil at the bridge site is very soft clay. The damage to this bridge was relatively minor and repairable, and it was attributed to both ground deformations and ground shaking. Gaps in the soil along the bridge and transverse to the tracks were noted. In addition, fissures were seen in an adjacent farm field with mud expelled from the cracks. An area near the timber trestle approach subsided causing the track and deck to drop between 102-mm and 152-mm. Some of the damage can be attributed to ground lateral spreading toward the channel crossing. There were also gaps in the soil next to the piles which were most likely caused by ground shaking.

The most notable damage was the tipped pile cap and the cracked brace connecting the cap and the piles. The bent has five piles and the cap is connected to each pile through a vertical 22-mm by 559-mm drift bolt at the center of the pile. This type of connection offers very little resistance to rotation of the cap although it is quite common in timber bridge construction (for both highway and railroad bridges). Some timber trestle standards call for 63-mm by 10-mm metal straps with thru-bolts connecting the cap to each pile. Such straps may have prevented the twisting of the cap in this case.

It should be noted that the occurrence of seismic damage to buildings in the past has been linked to soft soil conditions. According to a number of surveys and reports (for example see Anderson, 1952), for areas of strong earthquake motions, the observed damage rate for wooden structures decreases quickly when the structure has been built on intermediate soils. On hard soils, the observed damage rate for wooden buildings is usually very small and minor in nature.

Another section of the previously mentioned bridge includes five 18.3-m long through-plate girder spans over the Pajaro River. Each pier consists of a pair of wrought iron cylinder casings filled with concrete, constructed on top of timber piling. Bracing between cylinders consists of angle cross-frames (X-bracing) with the end piers having a concrete beam to support the approach timber stringers.

The cylinder piers were all in good condition, except pier 1, where the concrete beam between cylinders was twisted, tilted and pulled up from the top of one cylinder. Most of the cylinders exhibited movement, as noted by soil heave adjacent to the cylinders. Piers 3 and 4 remained stationary.

The five girder spans were in end contact with each other but had no structural damage. Other than repairs to pier 1, only several bolster shoes required repositioning in order to reset the girder stiffeners over the bearings. To expedite opening the bridge to traffic, a pile bent was driven on both sides of pier 1 to support the girder span and approach timber span.

There are a number of reports documenting the performance of timber railroad bridges during earthquakes around the world. In general, these structures performed quite well. However, there are several major differences between timber railroad bridges and timber highway bridges, which must be recognized. To begin with, the design live load on railroad bridges is much greater than the corresponding design live load on highway bridges (Cooper E80 railroad engine and uniform trailing loads versus H15, HL93, HS20 or, more recently, HS25 highway design truck loads). Railroad bridges also have the advantage of the continuous steel rails, which provide longitudinal continuity and resistance. In addition, non-seismic horizontal design loads for railroad bridges are much larger than those corresponding to highway bridges, since railroad bridges are designed for longitudinal traction and breaking forces, and transverse nosing forces. Another consideration is that most timber railroad trestle structures are well braced, both longitudinally and transversely, while timber pile bents for highway bridges may

have only minimal transverse bracing between piles and, in many cases, no longitudinal bracing. Also, many timber railroad bridge pile-to-cap connections include thru-bolted steel straps while older timber highway bridges do not. It should be noted, though, that timber railroad bridges are designed to resist vertical and horizontal loads in a purely elastic manner.

As a result, railroad bridges that are not seismically designed may have better performance under small-to-moderate earthquakes than similar non-seismically designed highway bridges. It is for this reason that lessons learned from railroad bridge performance during earthquakes can lead to parallels for highway bridge performance, but not necessarily directly applicable conclusions.

2.6 SUMMARY OF TIMBER RESEARCH BY BC HYDRO

In a report published by British Columbia Hydro (BC Hydro, 1992), Borg Madsen from the University of British Columbia (UBC) presents a significant amount of information on the performance of timber piles that is germane to this project (volume 2, appendix A). The UBC tests were conducted in conjunction with BC Hydro to investigate the seismic resistance of timber pile foundations used to support heavy-duty electrical transformers. The piles evaluated in the UBC experimental study are essentially the same as those used in timber bridge construction throughout North America, i.e., Douglas Fir.

As a result of seismic activity, these piles may be susceptible to displacements in the order of 1-m. Current methods of analysis predict that timber pile foundations would fail under such displacement magnitudes. However, this is not in consonance with the performance of transformer towers in past earthquakes. The UBC program sought to determine whether or not these structures could accommodate large horizontal displacements resulting from earthquake activity and still maintain their design vertical load.

2.6.1 UBC Laboratory Testing of Timber Piles

There are three key items directly affecting the ability of timber pile foundations to carry vertical loads while undergoing large lateral displacements that may result from earthquakes:

- Magnitude of the lateral displacement.

- Moment-curvature or bending response of timber piles and their ability to sustain axial load after "failing in bending.

- Fixity provided both by the soil and the concrete pile caps.

An obvious laboratory simulation of the field loading conditions, as shown in figure 2-1, would be to construct a loading arrangement as shown in figure 2-2(a). In this setup, a timber pile could be supported at the bottom to simulate the pile segment embedded in the non-liquefied soil, with a free "cantilevered" portion at the top simulating the segment within the liquefied soil. Horizontal displacement and the design vertical load could be facilitated by using two independent hydraulic pistons. This method was not selected due to the large travel requirement (1-m) in the piston controlling the horizontal displacement and the difficulty in maintaining a constant vertical load during horizontal translation of the pile top.
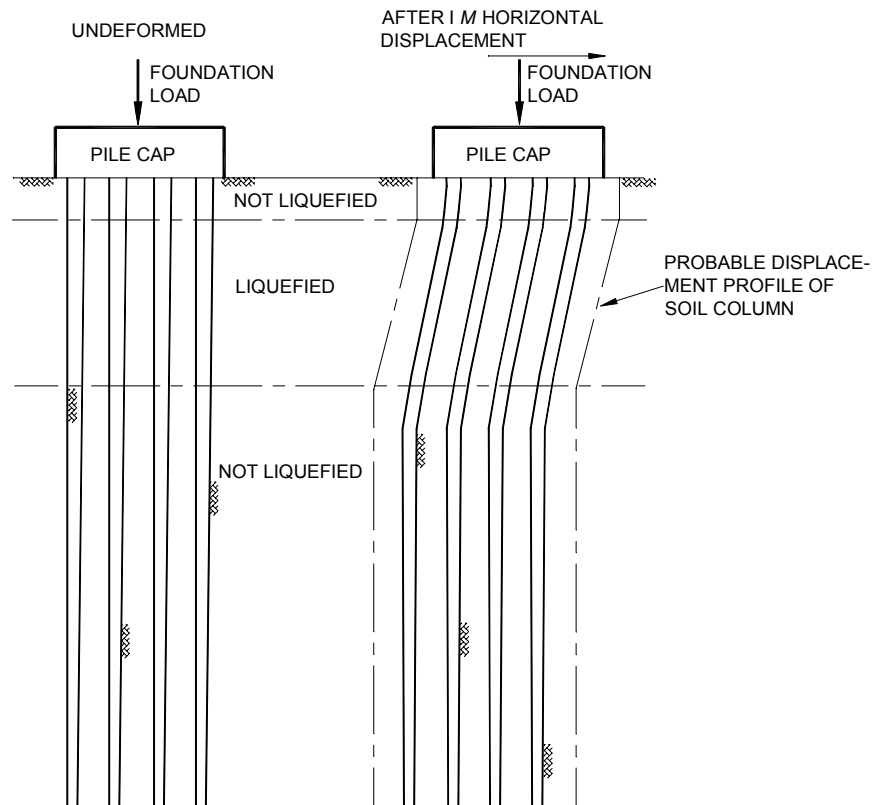
Figure 2-1. Pile displacement due to ground motion.

Figure 2-2(b) shows the actual laboratory test setup (turned 90°). This is, in fact, a simple beam bending setup with an added feature of applying a constant axial load. The location of the transverse load application point was selected so that the required equivalent maximum displacement of 1-m at the pile cap can be achieved by a much smaller displacement at the load point, about 0.38-m. In this case, the location of the hydraulic piston for the axial load can be fixed relative to the axis of the undeformed pile.
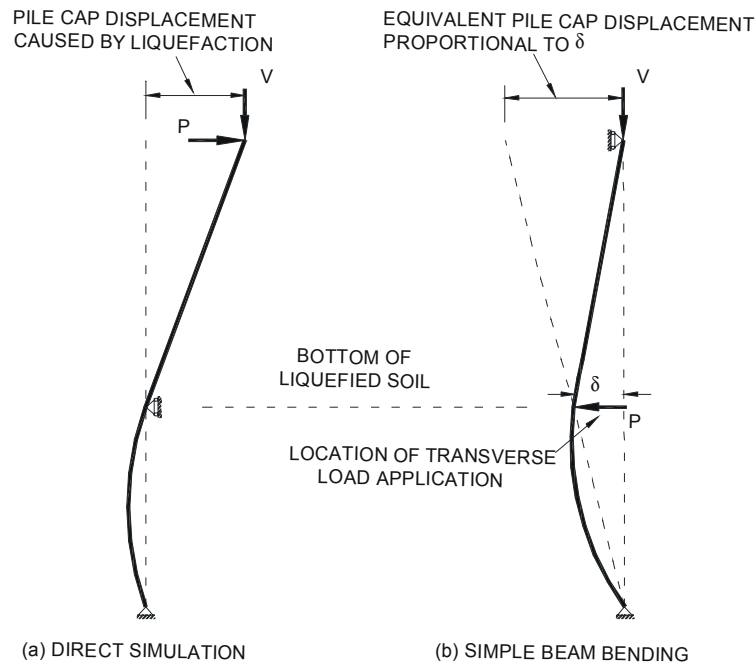
BC Hydro 1992

**Figure 2-2. Laboratory test methods to approximate field
loading conditions.**

2.6.2 Results of UBC Tests

The UBC research program clearly demonstrated the capability of timber piles to withstand large horizontal displacements. Specific conclusions from this laboratory testing of 27- to 300-mm diameter piles, all cut to 8-m lengths, were as follows:

1. The strength and stiffness values of all piles tested were not noticeably affected by having their moisture content varied from 22 to 44 percent. This is consistent with

the concept that the strength properties of wood products are unaffected by moisture content changes above the fiber saturation point.

2. The median modulus of rupture of the Douglas Fir piles tested was 39-MPa, which is about twice the bending strength recommended by the Canadian Standards Association.

3. Moment-curvature data obtained for all piles tested showed a very large scatter, which is typical of timber products.

4. The deflections at final failure were about 30 percent greater than at maximum transverse load and about 100 percent larger than at the linear elastic limit. It is reasonable to include plastic deformation (past yield) in the ultimate design of timber piles to resist lateral loading.

5. Four of the piles tested had an inclinometer casing epoxied in a formed groove. Four of the piles had been treated with creosote and had been in service for roughly three to four years. The results from the bending tests indicated no statistically significant differences. Creosote does not affect the material properties of wood.

6. The results from a single timber crushing test indicate that with increasing lateral displacements applied to the pile cap, a plastic hinge would occur in the pile at or immediately below the concrete cap. These hinges would most likely limit the shear and moment capacity within the pile.

7. It was estimated that Douglas Fir timber piles subjected to field loading may survive up to 1-m horizontal displacement.

The following conclusions were inferred from the field testing of 3- to 350-mm diameter piles about 10-m long:

1. All three tests attained a maximum displacement of 1-m, the limit of the horizontal travel of the load frame. No definitive final failure point was identified in these tests, as the pile was able to support the weight of the pile cap of 89-kN to its maximum displacement. Although the moment-curvature relationship indicated that the pile had already crushed in bending at this point, the residual structural capacity of the pile was able to support axial loads in excess of 89-kN.

2. There were two locations with relatively large curvature values for each laterally loaded test pile. These locations, one close to the bottom of the pile cap and the other at a depth of 0.2- to 0.6-m below the bottom of the slurry pit, were approximately the same for all three tests.

3. The moments developed in the field test piles were 10 to 20 percent larger than, but within the scatter, of the laboratory test results. At failure, the former piles were able to sustain curvatures three to four times larger than those that were laboratory tested.

4. The large settlement of the pile caps (about 100-mm) measured during the tests most likely resulted from the kinematics of the 'rigid body' rotation, rather than those caused by pile yielding, punching and/or uplift.

5. The probability of timber piles surviving large horizontal displacements is very high, but the integrity of the pile foundation depends on the actual magnitude of the displacements.

SECTION 3
SEISMIC PERFORMANCE OF TIMBER SUBSTRUCTURES

The seismic performance of timber substructures is not well established in comparison to other substructure types. Accordingly, an extensive investigation of its behavior under cyclic loading is necessary.

This section presents the experimental study conducted to evaluate the seismic performance of timber pile bents with shaking in the longitudinal (out-of-plane) direction followed by a theoretical model for predicting the force-deformation behavior. The results from this model are compared to the experimental results. Finally, a dual experimental-computational modeling program is presented that investigates the seismic resistance of typical braced timber bridge pile bents (in-plane direction).

3.1 STRENGTH AND DUCTILITY CAPABILITY OF TIMBER PILES

The main objective of this section is to assess the flexural strength and ductility capability of timber piles and pile bents with shaking in either the longitudinal (out-of-plane) or transverse (in-plane) direction. In pursuit of this objective, four timber round Douglas Fir timber pile specimens with a nominal diameter of 250-mm were tested to failure using quasi-static reversed cyclic loading to assess the effective axial load-moment interaction on both interior (vertical) and exterior (battered) piles. All poles were obtained from Bell Atlantic and were all chemically treated with creosote preservative. Since they were all used as telephone poles and were not actual piles, they possessed no residual stresses due to driving

Figure 3-1 shows a timber pile bent, laterally braced, and the rationale used to determine the configuration of the experimental substructure. The expected boundary conditions, i.e., the points of zero and flexural moments, M_o and M_p, respectively, are shown for the shaded region. The pile is imbedded in low strength concrete poured into a central cavity of the beam,

which is anchored to the laboratory strong floor. Axial load is applied directly via a lever-beam system, while lateral load is applied at the theoretical point of zero moment, M_o.
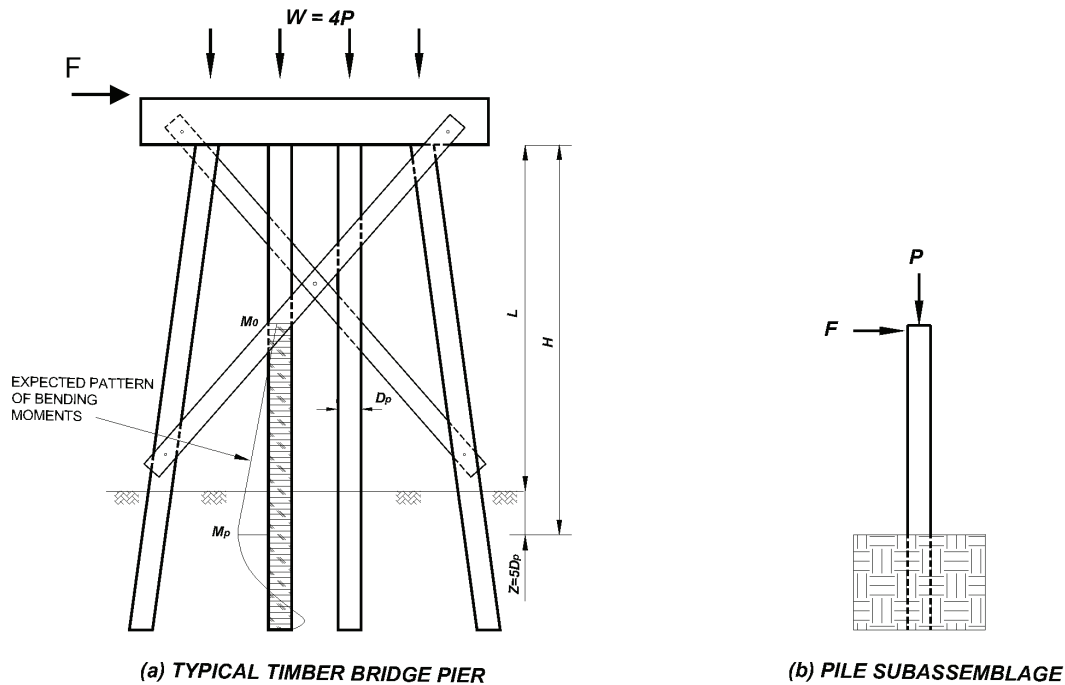
Figure 3-1. Physical modeling rationale for timber pile bents (in-plane behavior).

The testing program was divided into three stages with the following configuration and loads: (1) interior pile with no axial load; (2) interior pile with a constant axial load; and (3) exterior pile with a varying axial load. The first two tests were designed to act as controls in assessing the axial load-moment interaction of an interior pile. The objective for the last two experiments was to investigate a battered exterior pile and its variable axial-lateral load relationship. Most exterior piles are battered, i.e., inclined, to increase the lateral stability of the pile bent. This geometry introduces a varying axial load in the pile, which is dependent on the lateral load. The last two experiments investigate the effect of this varying axial load on the strength and ductility of the pile.

The test specimens utilized in this program were all of different diameters and fell into two categories with regard to their physical condition; the heights, except for the first test, were

all the same (see table 3-1). Specimens S1 and S2 were highly weathered and aged in comparison to S3 and S4. It should be noted that the values listed are the effective diameters, where the splitting of the specimens are taken into account.

Table 3-1. Characteristics of the different pile specimens.

Specimen No.	Height (mm)	Bottom Diameter (mm)	Top Diameter (mm)
S1	2438	244	223
S2	2000	217	208
S3	2000	257	239
S4	2000	277	262

3.1.1 Design and Construction of Reinforced Concrete Beam

As previously mentioned, four pile specimens were tested in this study. However, instead of constructing four separate models, one reinforced concrete test beam with dimensions of 3,658-mm by 914-mm by 762-mm, was designed with a central diametral cavity of 457-mm. The pile was placed into it and low-strength concrete grout was poured. This grout was designed to have a target strength of 14-MPa at 28 days to facilitate some bending and deformation below the top of the grout pocket in order to avoid a sharp region of fixity (and an infinite shear stress) at the top of the grout. This cavity was created by using a steel drum, which facilitated both the placement and removal of the pile and the grout.

The confining beam was designed to resist the plastic moment developed in the hinge zone during testing. For this design, an upper bound plastic overstrength moment was defined as

$$M_p^o = 1.18\lambda f_b S_x \tag{1}$$

where the overstrength factor, λ is 1.4, the resistance in flexure, f_b is 50-MPa, and the diameter, d is 406-mm. This concrete beam was constructed with ready-mix concrete having a specified strength of 31-MPa and a slump of 51-mm. Grade 60 (415-MPa) deformed steel reinforcement was used. The adequacy of the section was checked to ensure it exceeded the capacity of a 400-mm diameter pile in bending. During construction, a framework to maintain proper vertical alignment supported these piles.

Figure 3-2 illustrates the reinforcement used. Longitudinally, the beam was reinforced with four 25-mm (#8) rebars top and bottom. For transverse reinforcement, 12 10-mm (#3) rebars spaced at 300-mm centers were used. A drum of 457-mm diameter formed the central cavity. Further, after the beam was cured, it was prestressed using four 31-mm (#10) high alloy prestressing thread bars, resulting in a total force of 894-MN being applied to the block for a stress of 1.3-MPa.

(a) PLAN

(b) SIDE ELEVATION   *(c) FRONT ELEVATION*
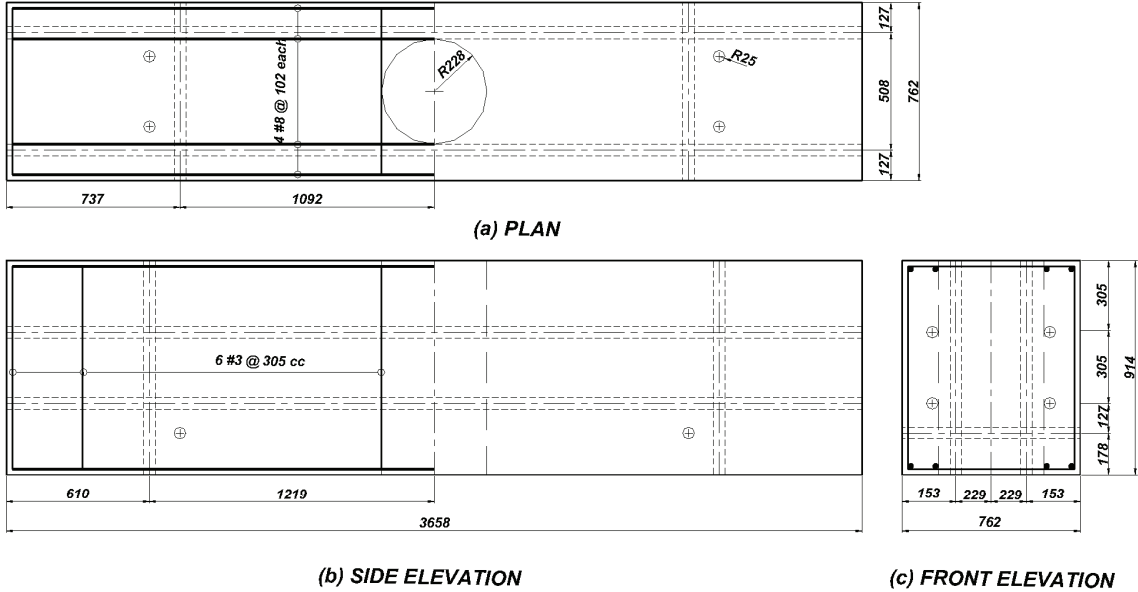
Note:

1) Cover to all rebars is 25 mm
2) All ducts are 51 mm φ

Figure 3-2. Test beam for out-of-plane experimental program showing details of reinforcement.

3.1.2 Experimental Setup

The test rigs utilized for testing the different specimens are shown in figure 3-3. To provide restraint against both translation and uplift during testing, four 25-mm (#8) threadbars (DYWIDAG) inserted through the anchoring ducts of the beam were stressed to provided a total vertical force of 218-MN.

Lateral load was provided by a 250-kN capacity MTS servo-hydraulic actuator with a stroke of ± 305-mm operated in displacement control. This actuator was attached to the pile

through a pin connection, which allowed rotation only about one axis, as shown in figure 3-3(b). The other end of the actuator was bolted to a rigid reaction frame through a swivel-base connection. This connection allowed out-of-plane motion in order to provide a method of aligning the actuator and test specimen. The test rig did not employ any bracing to actively prevent out-of-plane motion of the pile. However, the pin connection at the pile provided adequate passive restraint against these undesirable displacements. Slight out-of-plane motion could be tolerated by the system and was expected in the unstable (lateral buckling) push direction.
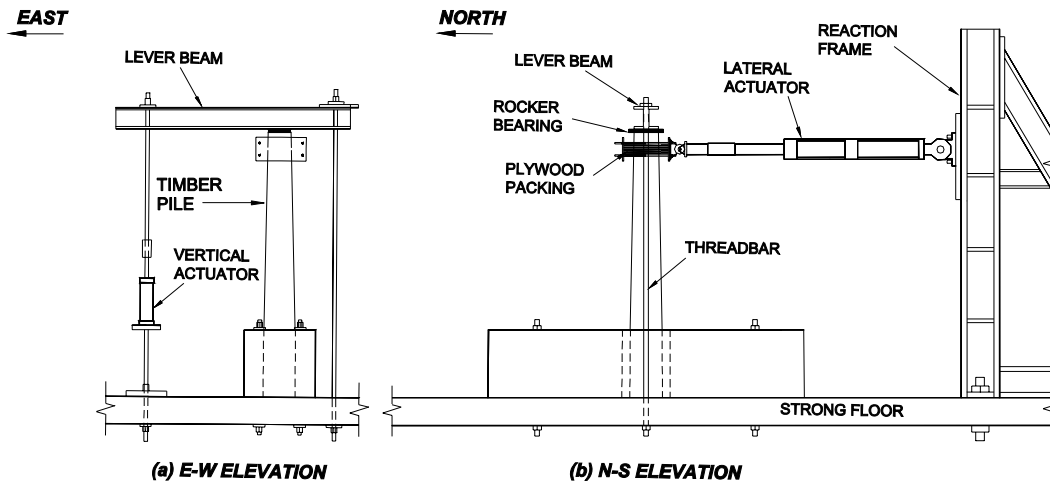
Figure 3-3. Typical experimental setup for various loading regimes (out-of-plane experiments).

Axial load was provided by a 311-kN capacity, ± 102-mm stroke Parker servo-hydraulic actuator operated in load control. The actuator load was applied to the pile through a W10 x 77 lever beam seated on a rocker bearing at the top of the pile in a direction transverse to the axis of the lateral load, as shown in figure 3-3(a). This bearing allowed the lever beam to rotate relative to the pile while transmitting the necessary load. Rotation was only allowed in the plane of the east-west axis of the pile. This rotation was necessary since the vertical actuator operated in load control; the actuator piston was free to move during the test in order to achieve the required load. The pile, located at the fulcrum, was at a distance of 1,676-mm from the actuator. This geometry resulted in an amplified axial load of 16/5 P_{va} at the pile, where P_{va} equals the vertical actuator

force. The reaction at the opposite end of the 3,048-mm lever beam was provided by a 32-mm diameter DYWIDAG bar. Both this bar and the actuator were anchored to the strong floor with rocker bearings that allowed the lever beam to move with the pile during the course of the tests. The testing procedure employed a quasi-static, cyclic lateral load, which followed a sinusoidal wave form. A MTS 436 control panel was used for the hydraulic supply to provide the frequency control for the test. MTS 406 servo-controllers provided program input to the actuators.

In order to prevent slipping at the lateral actuator-pile interface, two 450-mm by 305-mm by 25-mm mild steel plates confined six 450 by 305 by 19-mm pieces of ply (see figure 3-4). These ply each had a central, circular hole, marginally smaller than the pile diameter at the related location, and were cut at an offset of 25-mm from their centerline to facilitate placement and clamping. This arrangement was clamped to the pile by four 25-mm threaded bars, which were subsequently stressed to prevent any slippage.
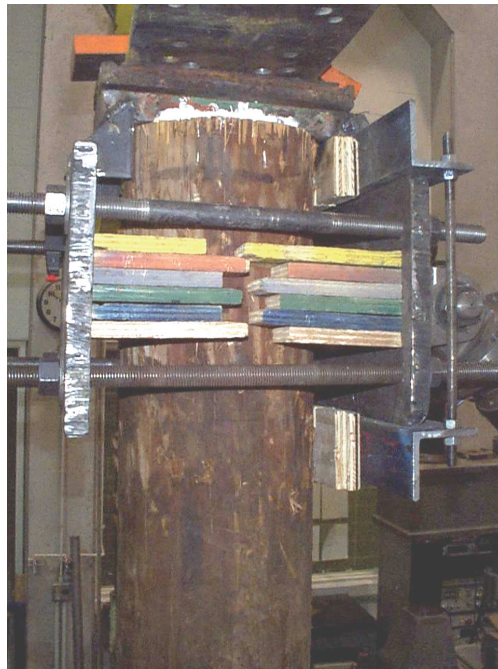
Figure 3-4.   Clamping and load transfer arrangement.

For the case where the actuator was inclined, additional reinforcement in the form of two 89-mm by 76-mm by 6-mm angles connected by two 12-mm threaded rods were used. The

purpose of these rods was to adjust the opening between the angles so as to snugly accommodate the plate. The top angle was welded to the rocker on the southern end, while the 25-mm plate was welded to the rocker on the northern end. Figure 3-5 illustrates the details of the attachment. In the push direction, the lateral load was directly transferred to the pile through the above-mentioned adapter plate; in the pull direction, four 25-mm threaded rods, which were connected and fastened to the two steel plates, transferred this load.
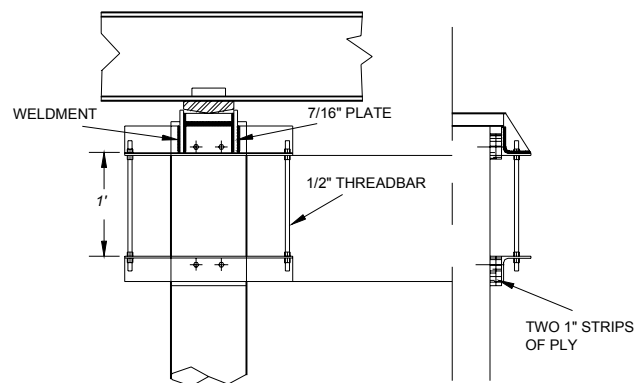
Figure 3-5. Details of attachment for inclined loading.

3.1.3 Instrumentation and Data Acquisition

Three different types of measurements were recorded during each test utilizing three types of instrumentation: sonic transducers, linear resistance potentiometers and load cells.

Seven sonic transducers, mounted on a reference frame to the north of the pile in the configuration (shown in figure 3-6), were used to measure transverse pile displacements. These displacements were monitored relative to the fixed base at several points along the pile (T1 through T7). Of these seven sonic transducers, six were attached to the bottom of the specimen at varying heights, while one was attached at the centerline of the point of lateral load application to provide the input signal for the lateral actuator. The transducers were all MTS transducers with variable strokes. Load cells attached in series to their respective actuators measured lateral

31

and vertical forces. These load cells were 250-kN and 311-kN devices supplied with the MTS and Parker actuators, respectively.
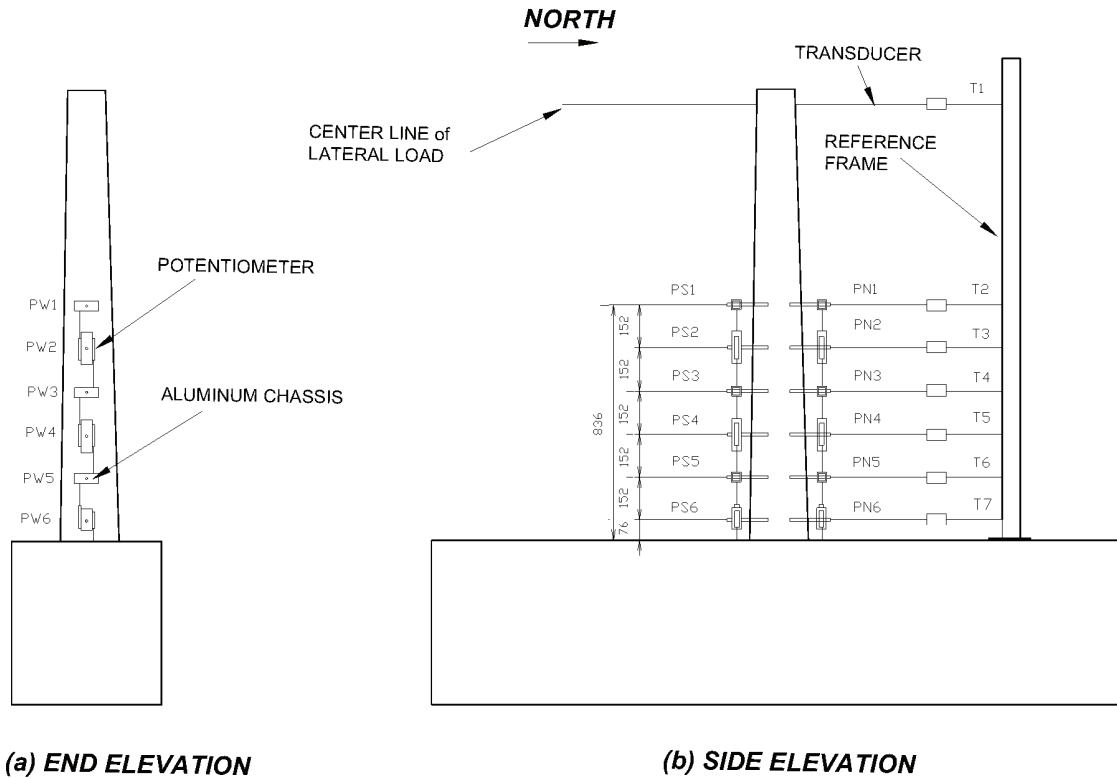
Figure 3-6. Configuration of instrumentation (out-of-plane experiments).

The arrangement of linear resistance potentiometers utilized to measure rotations/curvatures over sequential gauge lengths of the pile is shown in figure 3-6. The gauge length was shortened at the joint region in order to provide higher resolution in the hinge zone, where larger rotations were expected. Twelve potentiometers were utilized to measure column curvatures in pairs. Two were each mounted on an aluminum chassis fabricated from a rectangular tube, one covering the upper gauge length, the other covering the adjacent lower one. Each chassis was bolted to a 9-mm diameter threaded rod that was screwed into the pile. Aluminum tubes serving as contact surfaces for the brass rods coupled to the potentiometers were also similarly attached at alternate gauge lengths. The potentiometers used had strokes ± 6 - mm, ± 13 -mm, and ± 25 -mm. For each specimen except S2, the bottom pair of potentiometers had a stroke of ± 6 -mm, while the remaining ones had a stroke of ± 25 -mm. Due to the

malfunctioning of a few ± 25-mm stroke potentiometers, a couple of ± 13-mm stroke potentiometers were used during the testing of S2 at station number three.

During testing, an Optim Megadac 5533A data acquisition system was used to collect and store the data in an ASCII format at a sampling rate of 3 Hz. Supplies that allowed for separate zero adjustment of each instrument operated transducers and potentiometers. Prior to each test, the potentiometers and transducers were manually checked to ascertain their functionality and all the instruments were zeroed-out, i.e., set at their balance point. The output voltages of all the instruments were recorded during testing. While testing, the force of the lateral actuator along with the displacement of the top-most transducer were plotted on a Hewlett-Packard 7090A measurement plotting system. In addition to being a backup recorder, this system provided immediate insight into the behavior of the pile.

Of the transducers, the top provided the input signal for the lateral actuator, which operated in displacement control. Drift levels indicated in this report are equal to the displacement at this transducer divided by the height from the top of the beam to this same transducer, or

$$\theta = \frac{\Delta_p}{L} \tag{2}$$

where θ is the drift angle; Δ_p is the deflection of the pile tip; and L is the height of the cantilevered pile measured from the top of the beam to the centerline of the lateral actuator.

Located at identical positions as the lower temposonics were pairs of potentiometers used to measure the rotations/curvatures of the specimen. Rotations over the i-th gauge length are defined by the formula

$$\alpha_i = \frac{\Delta_{pi}}{L_{pi}} \tag{3}$$

Correspondingly, curvatures at this point are defined as

$$\phi_i = \frac{\alpha_i}{L_{gi}} = \frac{\Delta_{pi}}{L_{pi} \, L_{gi}} \tag{4}$$

where i is the level of the gauge length; Δ_{pi} is the algebraic difference of recordings from the potentiometers; L_{pi} is the center-center distance between the potentiometers; and L_{gi} is the gauge length.

3.1.4 Experimental Program and Results

Testing of the pile specimens was conducted under displacement control where a command signal was provided by an analog function generator in the form of a positive sine wave. The specimen was therefore first pushed then pulled. Each of the four specimens were tested for a minimum of two reversed cycles at specified drift levels of ± 1, ± 2, ± 3, ± 4, ± 5 and 6 percent, respectively. Specimens S1, S2 and S4 were also subjected to drifts of ± 7 percent; in the case of S1, this was done for two distinct time periods that closely followed one another, the first being for a single cycle. Additionally, S4 was subjected to drift amplitude of ± 8 percent. In each case, the displacement function had a period of one cycle per minute. Table 3-2. summarizes the characteristic data of the test specimens for this study.

Table 3-2. Characteristic data of test specimens (out-of-plane experiments).

Test Spec.	Total Axial Load (kN)	Max. Shear Force (kN)	Yield Drift (percent)	Drift at Failure (percent)	Length of Pile (mm)	Displacement (mm)
S1	0	24.6	3.6	5	2438	125
S2	50	23.3	2.8	6	2000	80
S3	5+ 0.2F	42	2.7	5	2000	100
S4	31 + 0.64F	49.2	3.6	2	2000	160

F is horizontal applied force

The experimental results of this study are summarized as follows.

Specimen S1

This specimen was tested with two complete reversed cycles of loading at ±1, ±2, ±3, ±4, ±5, and ±6 percent, respectively; additionally, eleven complete reversed cycles of loading was

done at ± 7 percent. No vertical (axial) load was applied. The loading was applied through the 250-kN MTS actuator, which was mounted horizontally and operated in displacement control at a height of 2,438-mm above the base of the pile (height/diameter aspect ratio of 10).

The force-drift behavior of this specimen is illustrated in figure 3-7. For this specimen, failure occurred at 22.5-kN and 24.6-kN in the push and pull directions, respectively, each within the ±5 percent drift subtest; the theoretical yield force of 27-kN was not attained. Upon failing in the pull direction, there was an 8-kN drop in strength resulting from the tensile fracture of the outermost fibers. Previous to this, within the same cycle, the load peaked at 22.5-kN in the push direction, then experienced a drop in strength of 12-kN, resulting from the partial snapping of fibers on the prevailing tensile surface. Although the pile failed at the ±5 percent drift angle, it was able to sustain loads equivalent to at least 50 percent of its original strength to a drift angle of ±7 percent. Ten additional cycles of lateral loading was applied at the ±7 percent drift amplitude, whereupon the behavior was observed to be stable with little loss of strength.
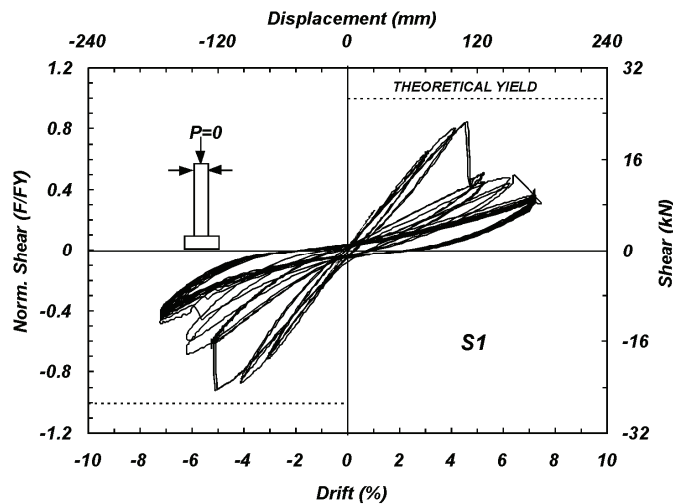
Figure 3-7. Force-drift behavior of specimen S1.

Specimen S2

In addition to two complete reversed cycles of loading up to ±7 percent provided by the horizontal actuator, this specimen was also subjected to a constant compressive axial load of 14-kN held by the 311-kN MTS vertical actuator for the duration of the test. This resulted in an amplified axial load equivalent to 45-kN being transferred to the pile. This load is considered to

be representative of the typical dead load a timber highway bridge transfers to a timber pile within a bent. The lateral loading was applied at a height of 2,000-mm above the base of the pile, giving an aspect ratio of 9.2.

This specimen exhibited three failure modes, as shown in figure 3-8, each occurring at succeeding drift amplitudes following initial failure. The loss in capacity at initial failure was only three percent. This phenomenon resulted directly from the applied axial load, causing less stretching of the tension surface of the specimen. After the force peaks at its limit load of 23.3-kN in the push direction within the ±4 percent drift subtest, there is evidence of fibers snapping, resulting in a drop in strength 0.6-kN; it then rises within the same cycle to roughly its peak value. For the next drift level, the peak force is above the previous fall-off value; however, strength degradation continues and the tensile splitting of fibers is more noticeable. For the succeeding drift of ±6 percent, the peak force attained is 20-kN. This is followed by the tensile fracture of additional fibers, leading to a loss in strength of 7.5-kN in the push direction. The maximum strength of this specimen, i.e., 23.3-kN, is marginally less than that for S1. This lesser strength reflects both the fact that the diameter of S2 was less than S1 and the inherent inhomogeneous nature of timber. Further, the species may not have been identical: upon examination, this pole was actually found to be less dense than the one previously tested.
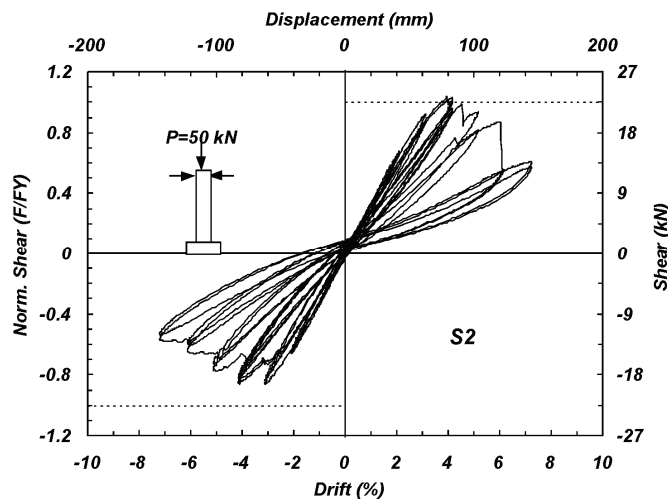
Figure 3-8. Force-drift behavior of specimen S2.

Specimen S3

Coupled with two complete reversed cycles of loading up to ±6 percent, this specimen was also subjected to a varying axial load to investigate the effects on an exterior/battered pile in a group. The loading regime consisted of an actuator inclined at 40° to the horizontal pushing upwards, together with a vertical actuator pulling downwards. For this specimen, a gravity load of P_g = 10-kN was applied. The objective of this low level of axial load was to investigate the effect of the pile response in tension (when the actuator acted in the push direction), as well as compression. The lateral actuator was coupled to the pile at a height of 2,000-mm above the base, for an aspect ratio of 7.8.

The performance of S3 is shown in figure 3-9. The loads at failure here are 42-kN and 36.3-kN in the push and pull directions, respectively. This specimen was able to surpass its theoretical yield strength in the push direction. After peaking at its maximum strength of 42-kN within the ±5 percent drift subtest, there is roughly a four percent loss in strength of 1.5-kN. This behavior is primarily indicative of the superior physical state of the specimen. For the succeeding drift level, the attained strength of 40.7-kN is just greater than that recorded at the fall-off point for the previous drift amplitude.
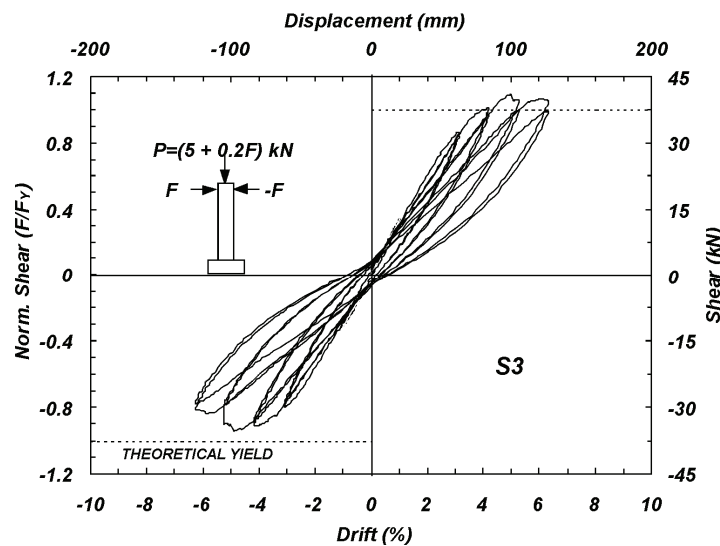
Figure 3-9. Force-drift behavior of specimen S3.

Specimen S4

This test was performed to accurately emulate the variable axial load conditions on an exterior pile in a bent. As such, the entire configuration was similar to S3, but the axial load was increased to P_g is 39-kN. Once again, the lateral actuator was coupled to the pile at a height of 2,000-mm above the base for an aspect ratio of 7.2, and provided two complete reversed cycles of loading up to ±8 percent.

The behavior of S4 is illustrated in figure 3-10, where the maximum loads attained were 43.7-kN and 49.2-kN in the push and pull directions, respectively. It is easily discerned that this specimen achieved its theoretical yield strength in the pull direction. This specimen was unable to achieve its ultimate load due to the limitations of the test rig, i.e., it did not fail. Although in this case, the peak shear force attained, i.e., 49.2-kN, is greater than that for S3, there is absolutely no evidence of failure.
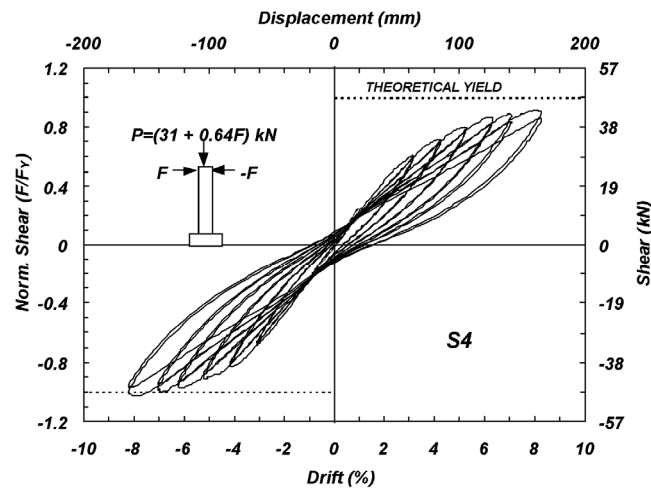
Figure 3.10. Force-Drift Behavior of Specimen S4.

Figure 3-10. Force-drift behavior of specimen S4.

This specimen was tested under combined axial load and bending and achieved 49-kN maximum load at eight percent drift amplitude.

Some basic observations can be inferred from this experimental program: (i) timber piles are capable of sustaining drift angles in excess of seven percent; (ii) the strength capacity up to a three percent drift angle can be maintained; and (iii) for drifts greater than three percent, the

strength is dependent on the physical condition of the wood. If the wood is in good condition, a capacity of not less than the yield strength can be maintained.

3.2 THEORETICAL MODELING OF LATERAL BEHAVIOR OF TIMBER PILE BENTS

3.2.1 Theoretical Stress-Strain Relationship of Timber

The theoretical stress-strain relation proposed in this study is based on the well-known Mander model for concrete (Mander et al., 1988) that uses the Popovics (1973) stress-strain relationship:

$$\sigma = \frac{\varepsilon\, E_o}{1 + (\lambda - 1)\left(\dfrac{\varepsilon}{\varepsilon_o}\right)^r} \tag{5}$$

In which σ is the timber stress for a given strain ε; E_o is Young's modulus of elasticity; ε_o is the strain at peak stress; and the other parameters (λ, r) are defined as follows:

$$\lambda = \left|\frac{\varepsilon_o\, E_o}{f_{max}}\right| \tag{6}$$

where f_{max} is the maximum timber stress in either tension or compression and

$$r = \frac{\lambda}{\lambda - 1} \tag{7}$$

Comparisons of the theoretical relationship to results of different coupon tests under compression and tension are shown in figure 3-11. The coupon specimens and testing procedures conform to ASTM D 143-94. It is clearly seen that the theoretical curve models the experimental result very well.
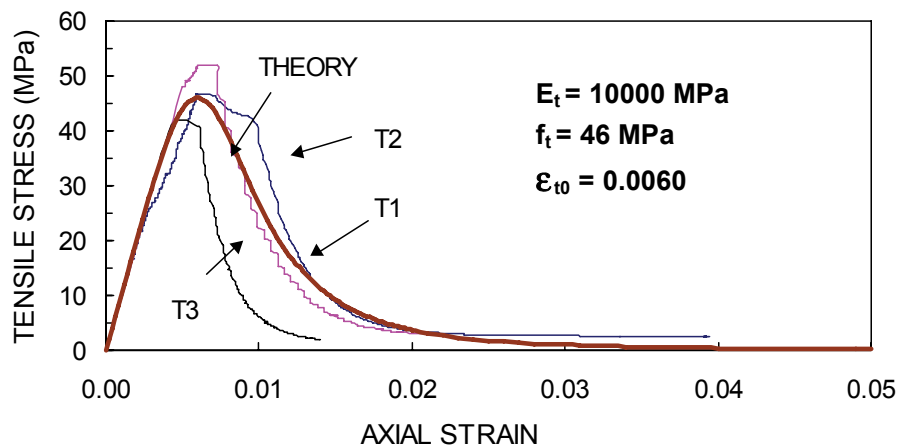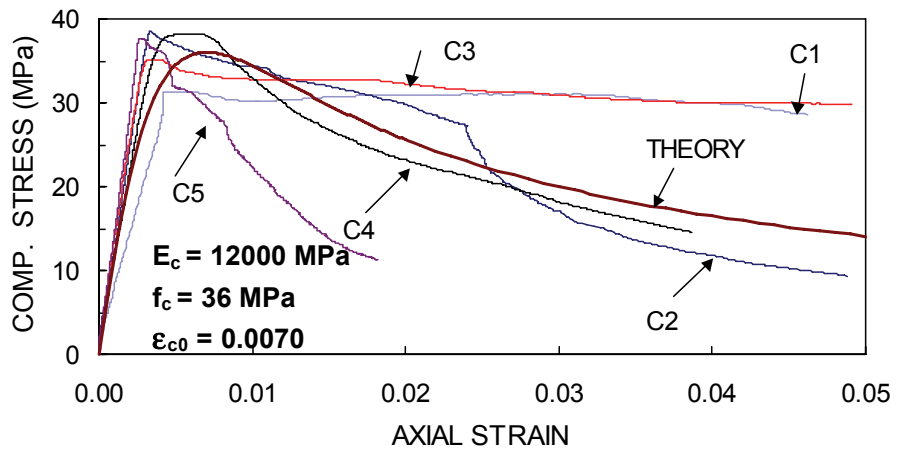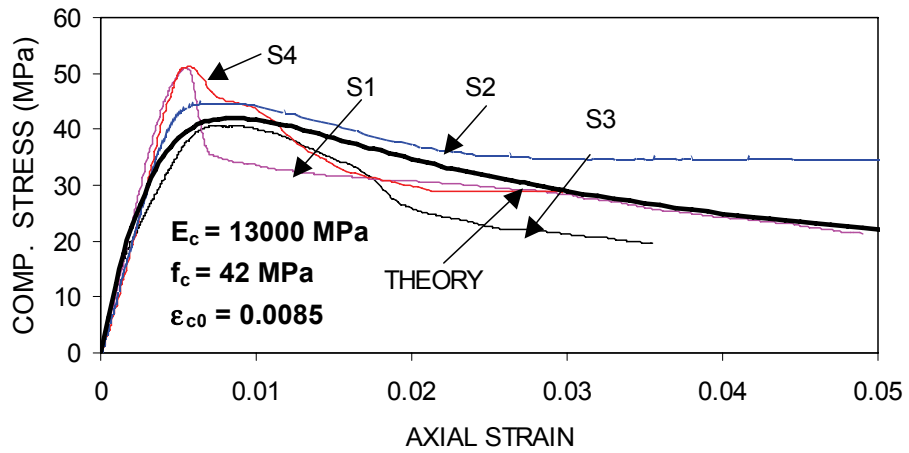
Figure 3-11. Comparison of the theoretical relationship to experimental results: (a),(b) coupon tests under compression and (c) coupon tests under tension.

It should be noted that values for the material parameters in the absence of specific tests could be taken from the AASHTO *LRFD Design Code*. However, AASHTO does not provide sufficient information for the strains at the peak compression and tension stress (ε_{co} and ε_{to}). Therefore, in the absence of this information, it is suggested that these strains be inferred by adopting λ equal to 2.5 and 1.3 for compression and tension, respectively. These values are based on calibrating the constitutive model to the experimental results.

Figure 3-12 shows a typical stress-strain relationship for the timber piles that were tested. The curve labeled "Experiment" is the theoretical curve modeled on Popovics' equation using values derived from the coupon tests. A comparison of the two theoretical stress-strain curves shows that they are indeed similar. They differ principally in the values of f_c and f_t, the experimentally obtained values being roughly double the value of those found in the AASHTO *LRFD Design Code*.
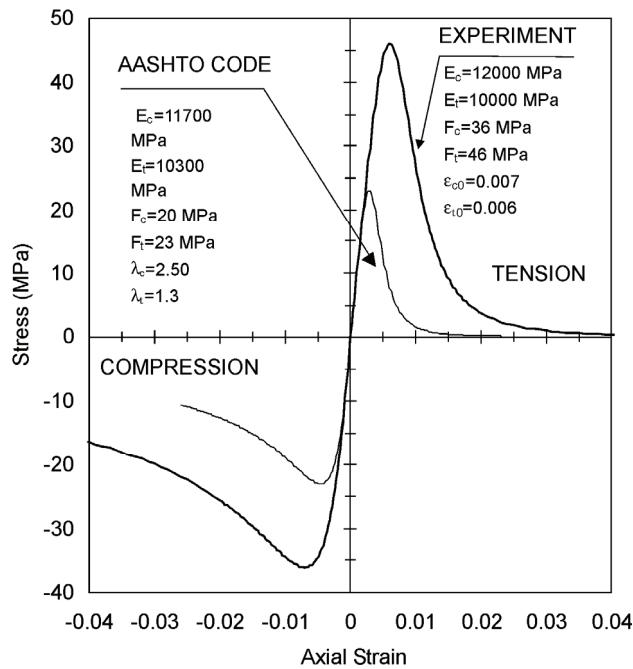
Figure 3-12. Stress-strain relationship for Douglas Fir timber used in the pile specimen.

3.2.2 Moment-Curvature Analysis for Uni-axial Bending

When conducting a moment-curvature analysis, it will be implicitly assumed that shear stresses do not have a significant effect on the stress-strain relationships. Therefore, uni-axial

stress-strain relations are assumed over the entire section. This assumption holds true providing the member has an appropriately slender aspect ratio i.e., $M/(VD)$ is greater than two, where M is the moment, V is the shear force and D is the diameter of the cross section, respectively. It is also assumed that Bernoulli's hypothesis holds true, i.e., plane sections remain plane before and after bending. Thus, the strain at any fiber across the timber section is given by the following linear relationship:

$$\varepsilon = \varepsilon_{oo} + \varphi\, y \tag{8}$$

where ε_{oo} is the strain at the centroid of the section; y is the ordinate from the axial and ϕ is the curvature on the section.

Figure 3-13 shows a timber pile cross-section, with the assumed strain profile based on the above equation, and the resulting stresses that exist across the section. Integration of these stresses provides the resulting axial force and moment actions applied to the pile. These can be calculated from the following:
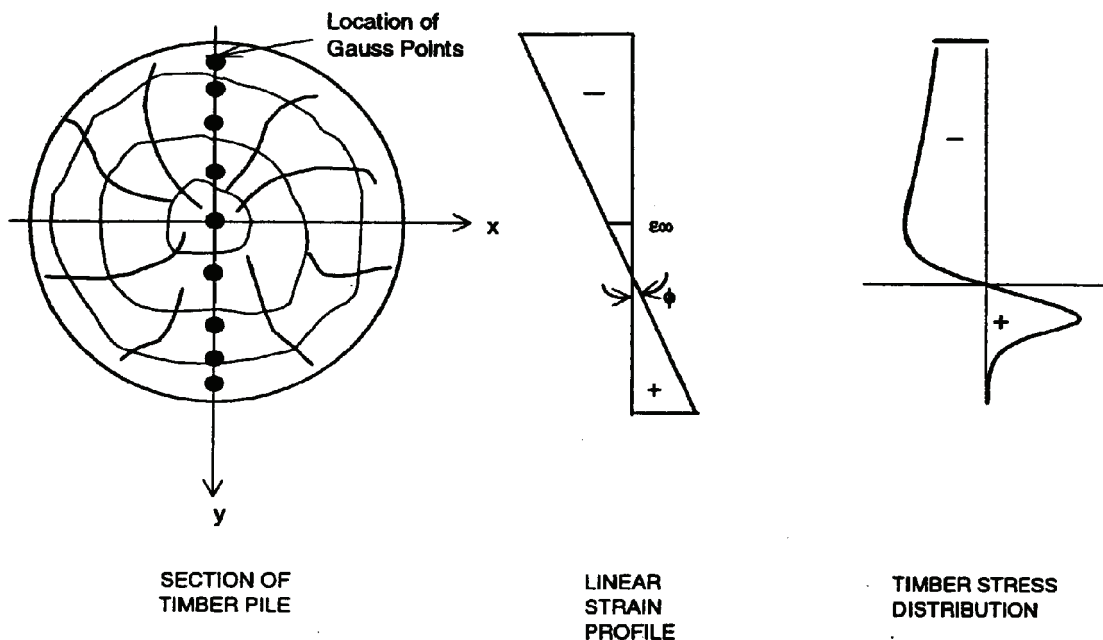
Figure 3-13. Basis of the moment curvature analysis.

$$P = \int \sigma\, b(y)\, dy = \frac{1}{2} D \sum w_i\, \sigma_i\, b_i \tag{9}$$

$$M = \int \sigma\, y\, b(y)\, dy = \frac{1}{4} D^2 \sum w_i\, \xi_i\, \sigma_i\, b_i \tag{10}$$

where b is the width of the section, which may be a variable. In the above equations, the right hand side gives a Gaussian quadrature numerical integration solution where, for i Gauss points, w_i and ξ_i are the weighting and position factors, respectively.

Therefore, if the centroidal strain ε_{oo} and the curvature ϕ are provided, the stress throughout the section is defined via the constitutive relationships in Eq. (5), and the axial force P and the moment M can be directly calculated by using Eqs. (9) and (10), respectively.

However, if the stress-strain relationships are highly nonlinear, it is conceivable that, for a given strain profile, the required axial force on the section does not correspond to the target value. Therefore, a correction may need to be applied (ΔP_i), which can be found by solving the following matrix equation:

$$\begin{Bmatrix} \Delta P \\ \Delta M \end{Bmatrix}_i = \begin{bmatrix} \dfrac{\partial P}{\partial \varepsilon_{oo}} & \dfrac{\partial P}{\partial \phi} \\[2ex] \dfrac{\partial M}{\partial \varepsilon_{oo}} & \dfrac{\partial M}{\partial \phi} \end{bmatrix}_i \begin{Bmatrix} \Delta \varepsilon_{oo} \\ \Delta \phi \end{Bmatrix}_i \tag{11}$$

where ΔP_i and ΔM_i are the incremental forces needed to reach the specified forces, P and/or M, from the state of stresses across the section for the i-th solution. By using a numerical differentiation strategy as described in the following, one can derive the elements in the matrix.

To define $\dfrac{\partial P}{\partial \phi}$, hold ε_{oo} constant and determine:

$$\frac{\partial P}{\partial \phi} \cong \left(\frac{\Delta P}{\Delta \phi} \right)_i = \frac{P_{i+1} - P_i}{\Phi_{i+1} - \Phi_i} \tag{12}$$

Similarly, to define $\dfrac{\partial P}{\partial \varepsilon_{oo}}$, hold ϕ_i constant and determine:

$$\frac{\partial P}{\partial \varepsilon_{oo}} \cong \left(\frac{\Delta P}{\Delta \varepsilon_{oo}}\right)_i = \frac{P_{i+1} - P_i}{(\varepsilon_{oo})_{i+1} - (\varepsilon_{oo})_i} \qquad (13)$$

3.2.3 Force Deformation Analysis

Upon integrating the curvature in a timber member, it is possible to obtain the flexural deformation as follows:

$$\Delta_F = \int_0^L \phi(l)\,dl \qquad (14)$$

where l is the length of pile measured from an inflection point; $\phi(l)$ is the flexural curvature as a function of position (along the length) and; L is the overall length of a cantilever column (pile) from the point of application of load to the point of fixity as shown in figure 3-14.
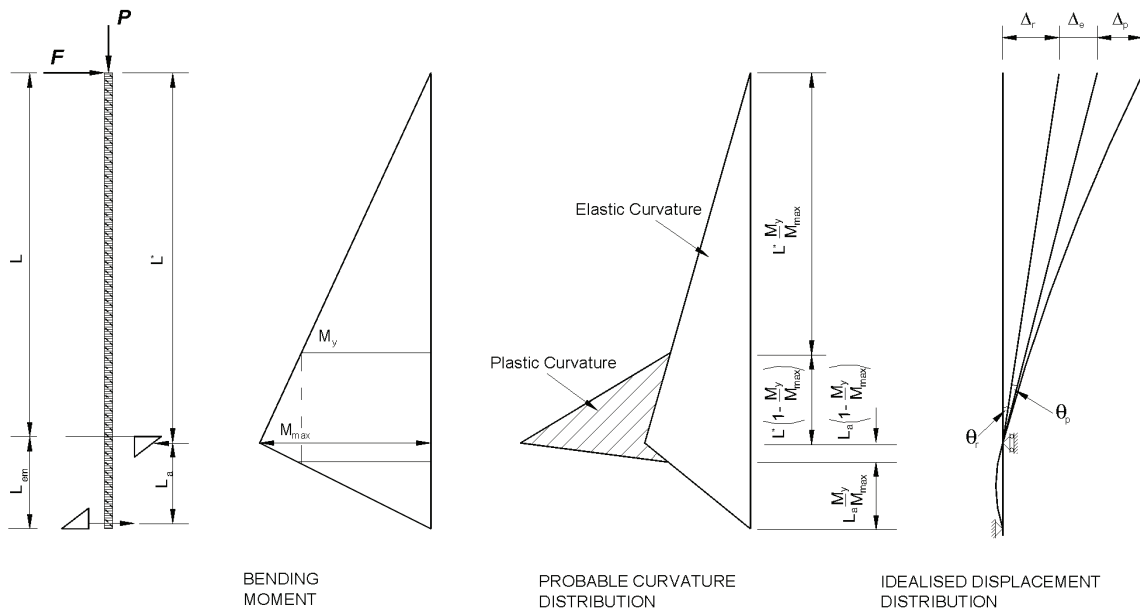
Figure 3-14. Assumed distribution of moments and curvatures for timber piles.

In order to quantify the total flexural displacement of a timber pile, one may proceed by determining its different components with reference to figure 3-14. Hence, the displacement due to deformation within the anchor zone is quantified as:

$$\Delta_r = \theta_r L* \tag{15}$$

where θ_r equals rotation obtained in the anchorage and L* equals the actual lever arm of the pile. θ_r can be found from the area of the curvature diagram within that zone as :

$$\theta_r = \frac{1}{2}\frac{M_{max}L_a}{EI} \tag{16}$$

where L_a is the distance between points of reactions of the linear stress blocks within the embedded zone. The deflection component, as a result of anchorage flexibility, is:

$$\Delta_r = \frac{1}{2}\frac{M_{max}L_a L*}{EI} \tag{17}$$

The elastic displacement of the pile is determined as:

$$\Delta_e = \frac{FL*^3}{3EI} = \frac{M_{max}L*^2}{3EI} \tag{18}$$

The total elastic displacement is found by combining Eqs. (17) and (18), giving

$$\Delta_r + \Delta_e = \frac{M_{max}L*^2}{3EI} + \frac{M_{max}L_a L*}{2EI} \tag{19}$$

The plastic displacement is given by

$$\Delta_p = \theta_p L \tag{20}$$

where θ_p is the plastic rotation given by

$$\theta_p = \frac{1}{2}\phi_p\left[(L*+L_a)\left(1-\frac{M_y}{M_{max}}\right)\right] \tag{21}$$

In the above equation, M_y is the elastic yield moment; $L*+L_a \approx L+L_{em}$; and M_{max} is the maximum applied moment at critical section. Therefore, the plastic deformation can be obtained as:

$$\Delta_p = \frac{1}{2}\phi_p L(L+L_{em})\left(1-\frac{M_y}{M_{max}}\right) \tag{22}$$

However, plastic curvature can be expressed in terms of the current ultimate curvature (ϕ_u) as follows:

$$\phi_p = \phi_u - \frac{M_{max}}{EI} \tag{23}$$

Where upon substituting the total plastic curvature

$$\Delta_p = \frac{L^2}{2}\left(\phi_u - \frac{M_{max}}{EI}\right)\left(1 + \frac{L_{em}}{L}\right)\left(1 - \frac{M_y}{M_{max}}\right) \tag{24}$$

The theory presented in this section was implemented in a Fortran code. The value in developing that code is that it will enable future extensions to accommodate cyclic loading effects in the analysis. The P-Δ effects as modeled by the experimental setup (figure 3-15) were implemented in the code as follows.
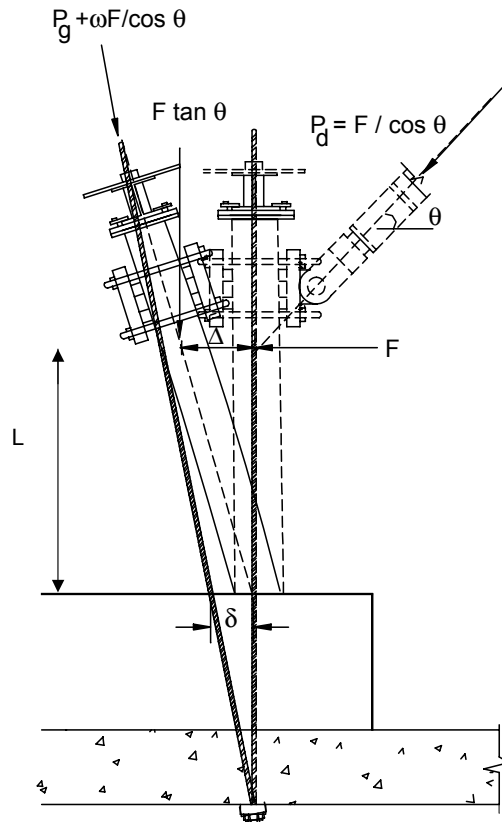
Figure 3-15. Accommodation of the effects of P-Δ in the experimental setup in the Fortran code.

The horizontal applied force F to the specimen is quantified as:

$$F = \frac{M - P_g \delta}{\alpha} \tag{25}$$

where M is the total moment applied at the connection (determined from moment-curvature analysis); P_g is the gravity load as applied in the experiment; δ is the effective displacement at the concrete base; and α is the coefficient to account for the effect of axial load on the test specimen defined as:

$$\alpha = L + \frac{\omega}{\cos \theta} \delta + \Delta \tan \theta \tag{26}$$

where L is the cantilever length of the pile; ω is the factor that adjusts the fraction of load transferred from the lateral actuator to the vertical actuator; Δ is the displacement at the point of load application; and θ is the angle of inclination of the lateral actuator to the horizontal.

3.2.4 Verification of the Lateral Force-Deformation Theory

The best way of ascertaining the validity of the foregoing theory is to apply it to the available experiment results. The specimens tested in this experimental program were embedded to 900-mm length into the concrete base. The effect of variation of embedment depth of the pile into the concrete base is implemented in the theory in the next section. Material properties of the specimens are shown in table 3-3.

Figures 3-16 and 3-17 display the cyclic horizontal-force displacement relationships for the four specimens tested in the experimental program described above. The theoretical monotonic pushover curves are also plotted in the same figures with the experimental results. It can be observed that the monotonic pushover curves satisfactorily converged to the cyclic experimental results. Hence, the constitutive model proposed in this study, as well as the theoretical pushover modeling, is considered to be validated.
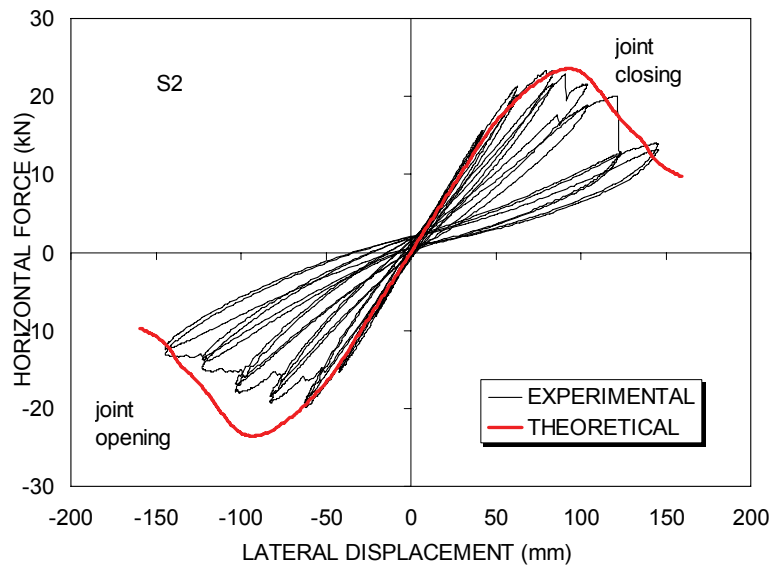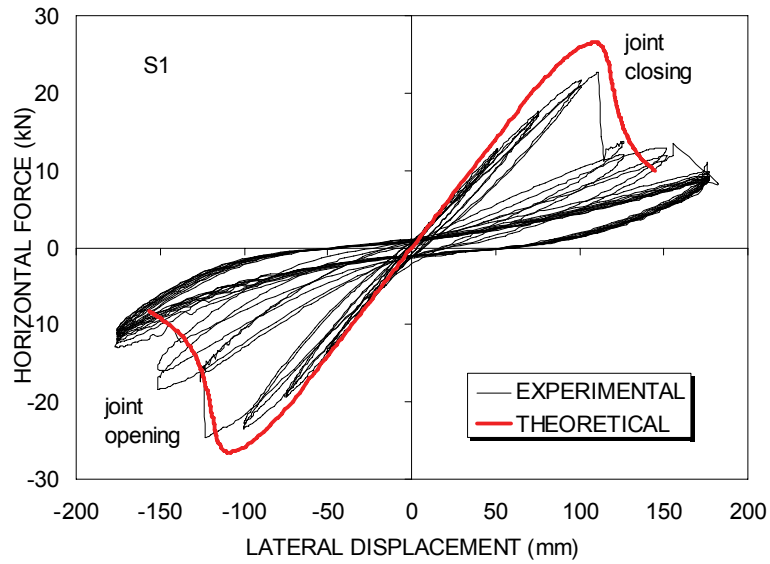
Figure 3-16. Comparison of the theoretical model for timber behavior with experimental results. Upper shows comparison with specimen S1. Lower shows comparison with specimen S2.
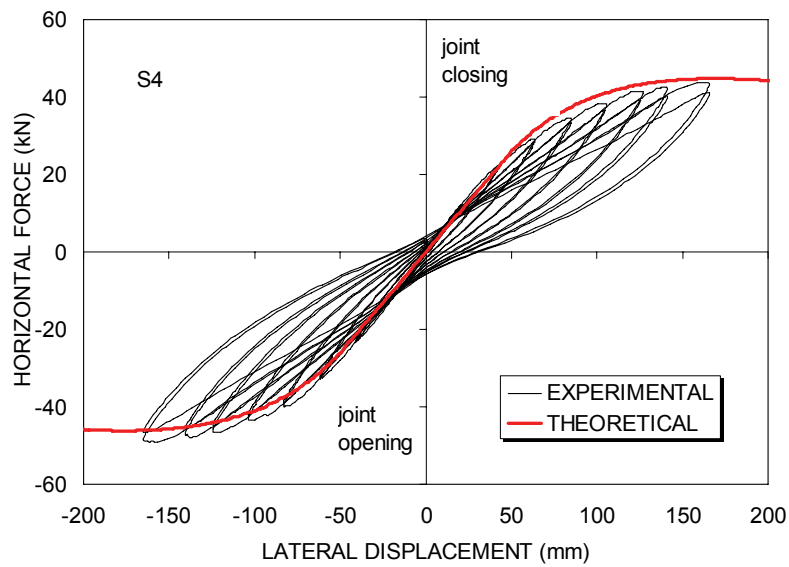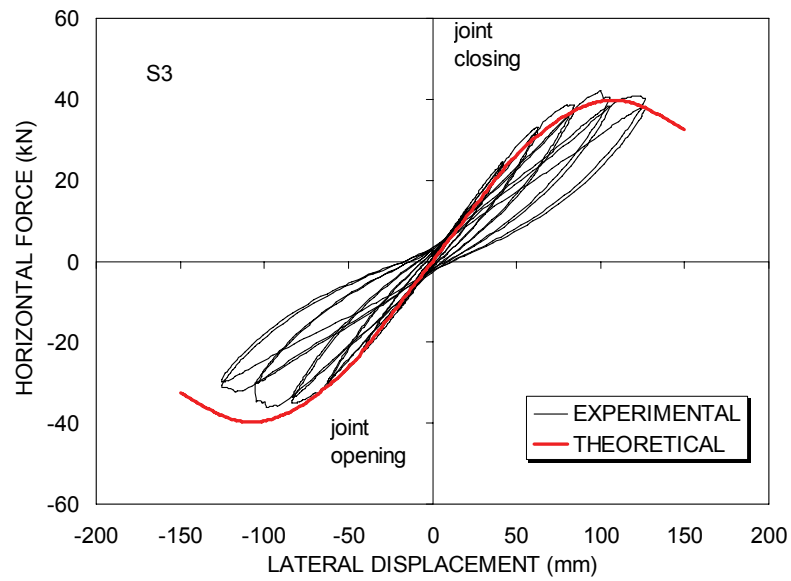
Figure 3-17. Comparision of the theoretical model for timber behavior with experimental results. Upper shows comparison with specimen S3. Lower shows comparison with specimen S4.

Table 3-3. Material properties for test specimens.

Spec.	f_{c0} (MPa)	f_{t0} (MPa)	E_{c0} (MPa)	E_{t0} (MPa)	ε_{c0}	ε_{t0}
S1	31	40	10000	9000	0.0040	0.0050
S2	31	40	11000	9000	0.0045	0.0050
S3	31	40	11000	9000	0.0050	0.0055
S4	30	32	10000	8000	0.0085	0.0080

f_{c0}, f_{t0} = maximum compression and tension stress
E_{c0}, E_{t0} = Young's modulus for compression and tension
$\varepsilon_{c0}, \varepsilon_{t0}$ = strain at peak stress for compression and tension, respectively

3.3 SEISMIC PERFORMANCE OF BRACED TIMBER PILE BENTS

Experimental and theoretical studies on steel pile bents (Shama et al., 2001b) indicated that the overall behavior of the unbraced bents is dominated by the bending strength of individual piles. This criterion is also applicable to unbraced timber pile bents. Therefore, one can conclude from the experimental study that unbraced timber pile bents have a very ductile performance, as the individual piles are capable of sustaining drift angles up to seven percent. They also can maintain their elastic performance up to a three percent drift angle. The study also showed that the strength of such structures is relatively low and depend on the maximum bending stress of the individual piles and the number of piles in a bent.

Compared to unbraced timber pile bents, the behavior of braced bents under lateral loads is usually governed by the stiffness of the bracing rather than the strength of the piles. This comparison is illustrated in figure 3-18. One can also expect that the connection between the bracing and the piles may play an important role in the overall behavior of braced timber pile bents.
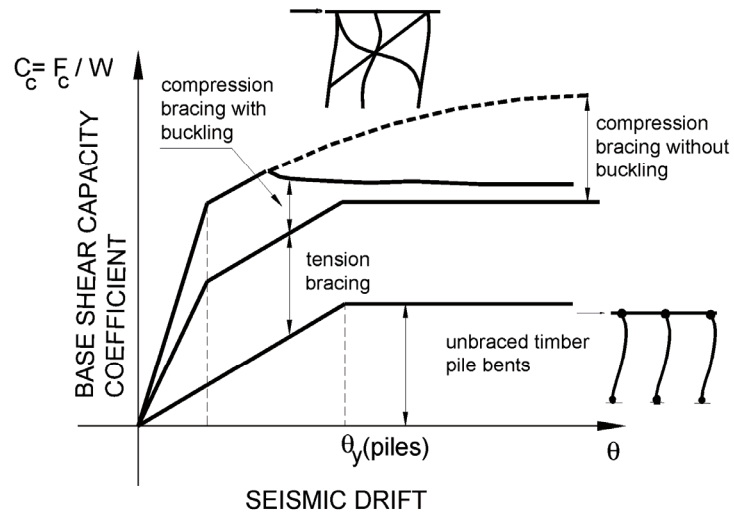
Figure 3-18. Expected seismic performance of braced and unbraced timber pile bents.

3.4 COMPUTATIONAL MODELING OF BRACED TIMBER PILE BENTS

As a means to identify and quantify the earthquake-induced damage to braced timber bridge pile bents, a computational modeling study has been undertaken. The DRAIN-2DX computer code (Prakash et al., 1992) was used for this purpose.

The basic geometric dimensions of one bent were established by placing joints (nodes) on the structure. The structure geometry was completed by connecting the predefined joints with nonlinear elements. The timber cap-beam and the piles were modeled using beam elements with same section and material properties of the experimental model. Connection elements (type 04) were used to model the rotational flexibility at the cap beam-pile head joints. An elastic bilinear force displacement relationship was assigned for this element. This relationship is shown in figure 3-19(a). Two nodes were assigned at each beam-to-pile connection with identical coordinates. The X and Y displacements of each pair of nodes were slaved to be equal, so that the connection became rigid translationally. The nodes were connected rotationally by inelastic connection elements. The connections were assumed initially to be very stiff. Therefore, 1×10^{-5} radian was assigned for the yielding rotation, and the yielding moment was determined according to the following equation:

(

51

$$M_y = 0.4Pd_p \qquad\qquad (27)$$

where M_y is the yielding moment of the cap beam-pile connection; P is the concentrated gravity vertical load at each pile; and d_p is the pile diameter at the connection. A post yield stiffness ratio of 0.003 was used. A detailed derivation of equation (27) is found in section 4.2.3.
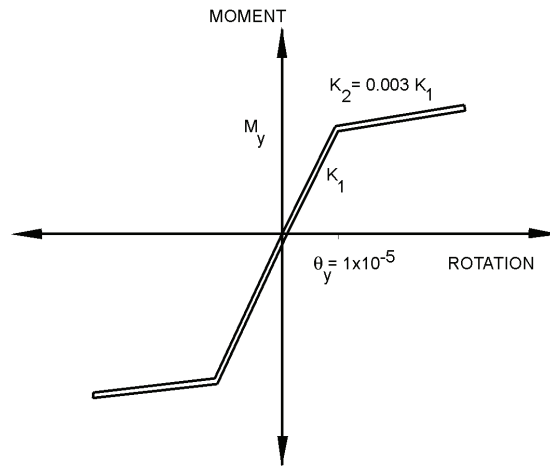
(a) CONNECTION ELEMENT WITH ELASTIC
UNLOADING PROPERTY AT THE HEAD
OF THE PILE INTO THE PILE CAP
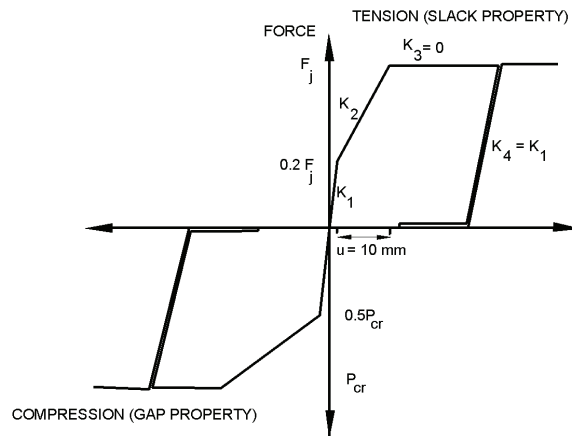
(b) LINK ELEMENTS FOR BRACING
SYSTEM

Figure 3-19. Computational modeling for force-deformation relationships.

One of the most important points in the development of this structural model was to assign the geometrical as well as the material properties that may capture the physical performance of the braces. It is expected that the overall behavior of the structure under cyclic loading will be governed by two basic behaviors: (i) the performance of the braces, which will be affected by its material and section properties; and (ii) the behavior of the connection between the brace and the pile, which will be affected by the type and properties of the connection. Therefore, in order to capture the appropriate cyclic performance of the structure, link elements (Type 09) were utilized to model the bracing/connection behavior. Link elements in DRAIN-2DX are uniaxial with finite length and arbitrary orientation. An element can be specified to act in tension or compression. Two link elements acting in parallel were assigned for each bracing member, one with gap property and another with slack property. The ultimate force of a brace in tension is governed by the bearing resistance of its connection with the pile. Hence, this force was determined as:

$$F_j = d_b t f_c \qquad (28)$$

where F_j is the bearing resistance of the connection; d_b is the diameter of the lag screw used at the brace-pile connection; t is the thickness of the timber brace; and f_c is the compressive strength of the timber brace.

On the other hand, the behavior of the brace in compression is governed by the lesser of the bearing resistance of the connection; the in plane Euler buckling load of the brace; or the out of plane Euler buckling load of the brace defined in this study as:

$$P_{cr} = \pi^2 \frac{E_c bt}{12} \left(\frac{t}{L} \right)^2 \qquad (29)$$

where P_{cr} is the Euler buckling load of the timber brace; E_c is the modulus of elasticity of the timber brace in compression; b is the width of the timber brace; t is the thickness or height of the brace; and $L = L$ is the buckling length of the brace taken as half the full length of the member because the connection at the intermediate pile provided restraint against translation. It was assumed that the bearing between the lag screw and the timber brace will govern its initial stiffness. Therefore, the initial stiffness was determined according to the following equation:

$$K_1 = \frac{E_c t d_p}{L} \quad (30)$$

Yielding was assumed to occur at one fifth of the bearing resistance of the connection in tension and at half the Euler buckling load in compression and continues over a slotting displacement ± 10-mm. These values were verified using the experimental results. Once the hole slotting exceeded this value, the structure acted in an elasto-perfectly plastic fashion i.e., K_3 equals zero, and K_2 was quantified in tension as:

$$K_2 = \frac{0.8F_j}{u} \quad (31)$$

and in compression as:

$$K_2 = \frac{0.5P_{cr}}{u} \quad (32)$$

where u equals ± 10-mm hole slotting at the connection. The unloading stiffness K_4 was taken as the same as the initial stiffness K_1. Figure 3-19b shows the force displacement relationship used for both tension and compression to model the bracing system.

3.5 PHYSICAL MODELING OF BRACED TIMBER PILE BENTS

Based on an examination of the FHWA *Standard Plans* (see "Standard Plans," 1979), it has been established that the seismic performance of braced timber pile bents is potentially critical, but the extent of this remains unknown. Therefore, a prototype timber bridge was used to develop a near-full size physical model that was used for shaking table experiments and quasi-static reversed cyclic loading tests on the laboratory strong-floor. Most timber highway bridges do not appear to deviate markedly from the FHWA *Standard* for the construction of timber bridges. Accordingly, the experimental model consisted of two identical pile bents. Each was three-quarter scale of a prototype timber bridge pile bent designed in accordance with FHWA *Standard Plans*. The assumed prototype timber bridge structure had five 300-mm diameter piles per bent with a span length of 8-m and deck width of 6.5-m. Based on an analysis of typical all-timber bridge decks, a distributed dead load of 4-kPa was assumed to represent the deck.

Accordingly, each pile in the prototype was supposed to carry 41.5-kN concentrated vertical force.

Three 225-mm diameter piles were used in the experimental model. Typical lag screws of 16-mm diameter were used at the brace-pile and cap beam-pile connections. Timber braces (pine) were 40-mm by 190-mm and cap beam was 200-mm by 200-mm. The model structure was also tested under quasi-static cyclic loading with 100-mm by 150-mm Hemlock braces. The prototype bridge was not assumed to be located in any particular seismic zone, rather the intent of this research was to investigate the level of seismic drift that would induce various states of damage in a prototypical timber bridge. Details of the physical model topology are shown in figure 3-20.

3.6 SHAKING TABLE EXPERIMENTS

Shaking table experiments are useful in identifying the dynamic characteristics of the structure at different stages of performance. The shaking table used for the experiments in this study is 3.66-m by 3.66-m. It has five controlled degrees of freedom (excluding the transverse translational movement), a payload of 500-kN and a useful frequency range of 0- to 50-Hz. The table is furnished with a reinforced concrete testing platform of 6.1-m by 3.66-m plan dimensions. The longitudinal (horizontal), vertical and roll degrees of freedom are programmable with feedback control to simultaneously control displacement, velocity, and acceleration. The performance envelope of the table is ± 150-mm displacement, 762.0-mm/sec velocity and 1.15-g acceleration at a payload of 195.0-kN in the horizontal direction, and ± 750-mm displacement, 508.0-mm/sec velocity and 2.30-g acceleration in the vertical direction. A photograph of the model structure on the shaking table is shown in figure 3-21.

SIDE ELEVATION

END ELEVATION
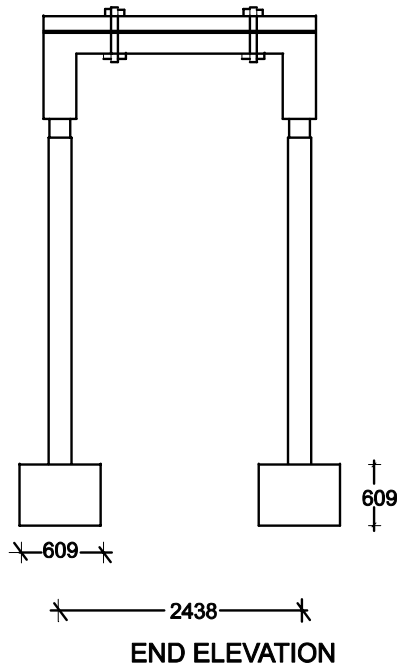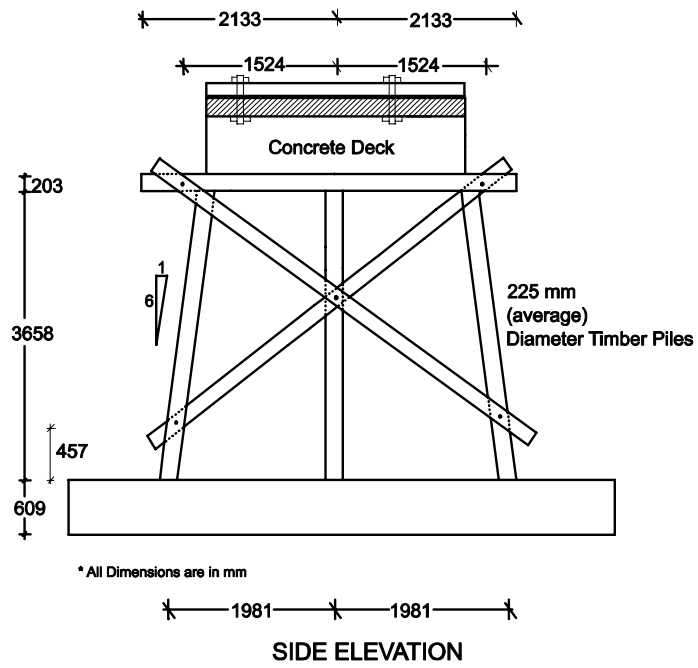
Figure 3-20. Timber bridge three-quarter scale model structure.
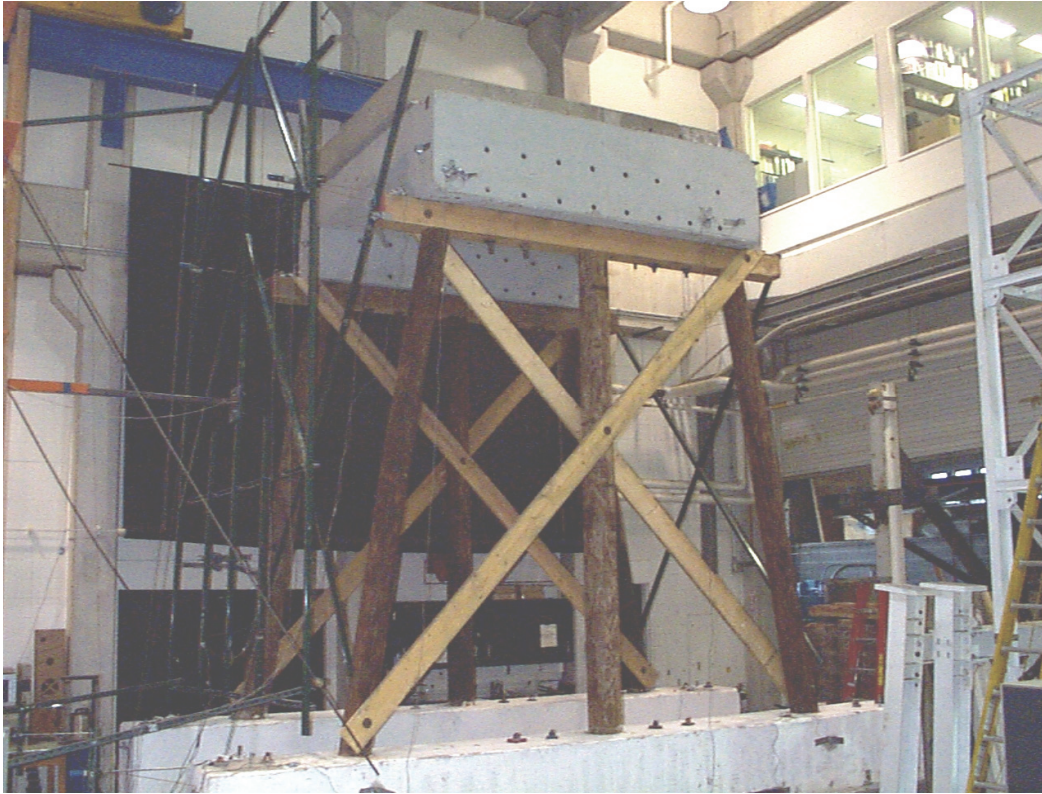
Figure 3-21. Braced timber pile bent bridge on the shaking table.

3.6.1 Similitude Requirements

Basic similitude requirements of the model must be satisfied for proper modeling of its dynamic behavior. Table 3-4 shows the scale factors for various parameters used to model the structure. As shown in table 3-4, the constant acceleration scaling was used in this study, and the same material properties were considered in the model design. This consideration required additional mass that translates into an additional weight of 70-kN per bent with three piles. Therefore, with the same material being used, the same stresses and strains in the prototype and model structure were attained for a geometry scale factor of three-quarters.

3.6.2 Instrumentation and Data Acquisition

A total of 24 data channels, including displacement transducers and accelerometers, were used to monitor the response of the model structure at the foundation, cap beam and deck

(concrete weight) level. The displacement transducers had global displacement ranges of ± 150-mm, ± 200-m and ± 250-m. The transducers were conditioned by a generic power supply and manufacturer amplifier-decoders; they were calibrated for the respective full scale displacement per 10 volts. Resistive accelerometers were used to measure the absolute accelerations at the cap beam and deck level. The accelerometers were conditioned with 2310 Vishay Signal Conditioning Amplifiers, which filtered frequencies above 25-Hz., calibrated for an acceleration range of ± 2-g per 10 volts The analog output readings from instrumentation were recorded digitally using an Optim Megadac 5533 Data Acquisition System. The output recordings were stored on a local personal computer at a frequency of 100-Hz seconds.

3.6.3 Selection of the Ground (Shaking Table) Excitation

Earthquake ground motions may vary widely in magnitude, peak ground acceleration, duration, and frequency content. Peak ground accelerations primarily influence the vibration amplitudes. Duration of ground motion has a pronounced effect on the severity of shaking and the evolution of damage. Frequency content relates to the periods of vibration of a structure. Since the prototype bridge was not assumed to be located in any particular seismic zone, an earthquake should therefore be chosen such that large magnitudes of base motion occur over a wide range of frequencies.

Therefore, two historically significant ground motions were chosen, Taft 1952 N21E and El Centro 1940 NS, for the shaking table motion to excite the model structure. The original Taft accelerogram, shown in figure 3-22(a), has a total ground excitation time history of 54.4 seconds with a peak ground acceleration (PGA) of 0.156-g at 9.1 seconds. The unscaled El Centro original accelerogram, shown in figure 3-23(a), has a total ground excitation time history of 53.8 seconds with a peak ground acceleration (PGA) of 0.348-g at 2.12 seconds. To satisfy time similitude requirements of the actual earthquake for the three-quarter scale model (see table 3-4), a scale factor of $\sqrt{0.75}$ is used to compress the time history of the accelerogram. The scaled ground motions for the signals are shown in figures 3-22(b) and 3-23(b).
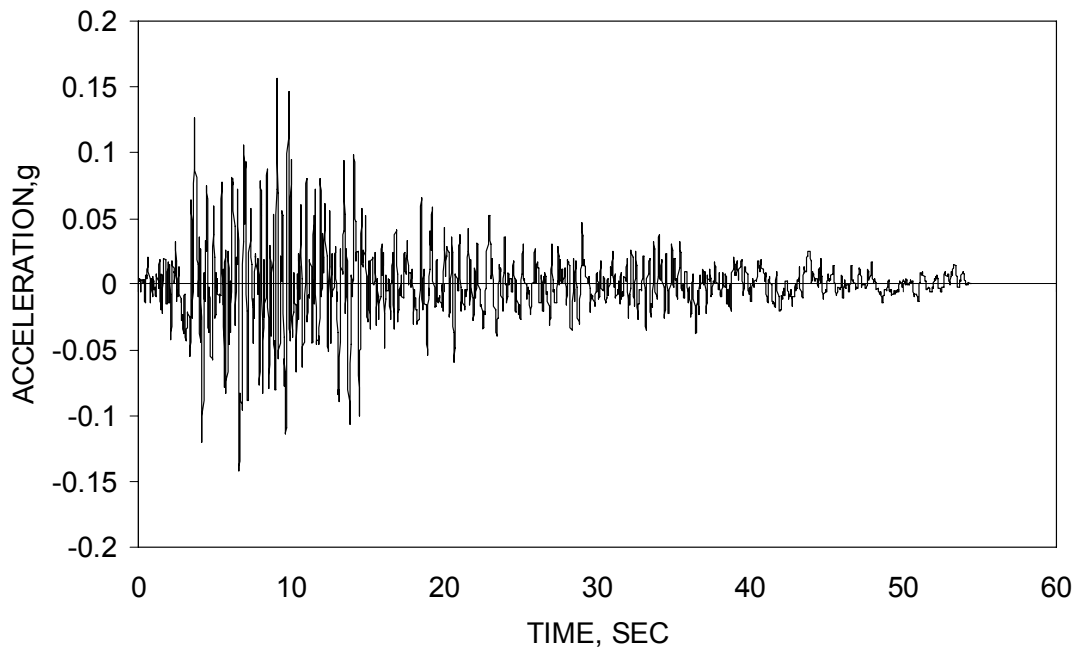
(a) Full Scale Taft NS1e
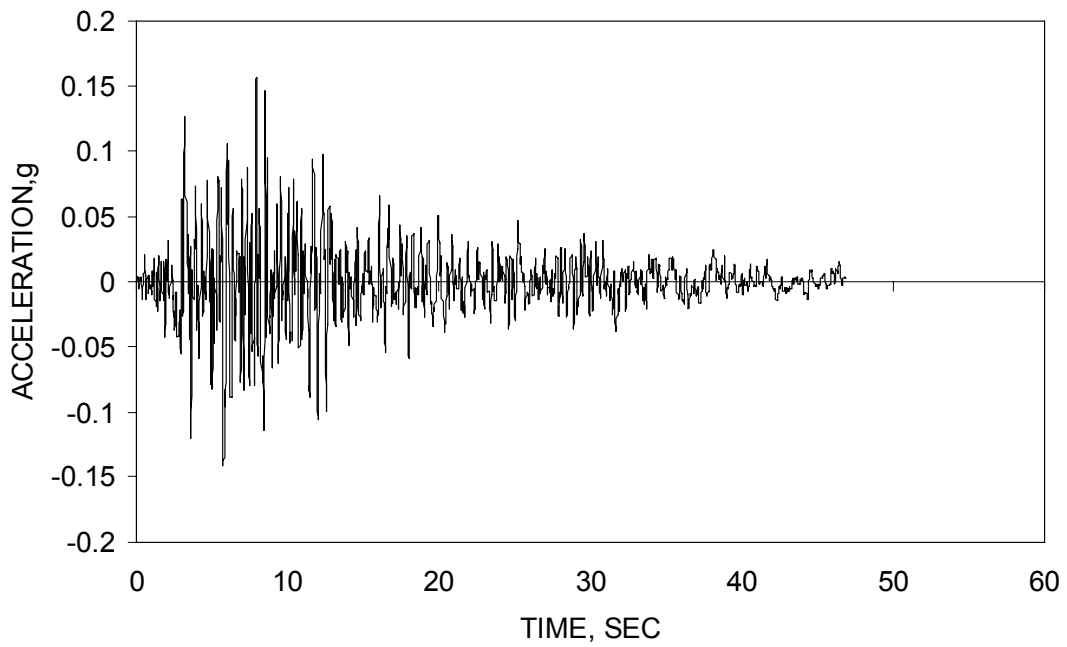
(b) Time Scaled Taft NS1e

Figure 3-22. Ground motions for the Taft N21E accelerogram component.
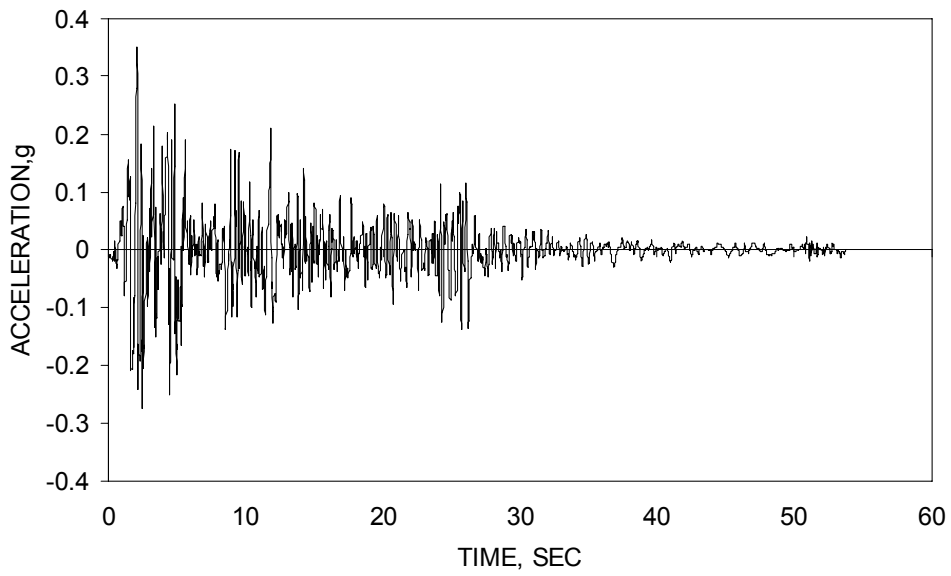
(a) Full Scale El CentroNS
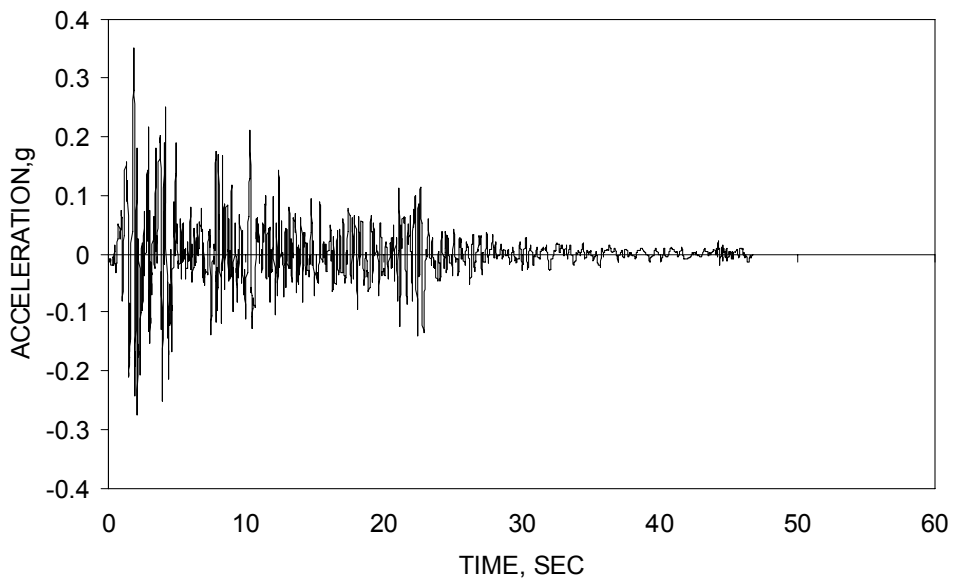
(b) Time Scaled El CentroNS

Figure 3-23. Ground motions for the El Centro 1940NS accelerogram component.

Table 3-4. Similitude requirements for the three-quarter scale timber bridge pier bent.

Quantity	Symbol	Dimension	Scale Factor	Scale Factor Used
Acceleration	a	LT^{-1}	1	1
Elastic Modulus	E	FL^{-2}	1	1
Linear Dimension	L	L	S_L	1.33
Displacement	Δ	L	S_L	1.33
Drift	θ	—	S_θ	1
Time	T	T	$\sqrt{S_L / S_a}$	1.15
Stress	f_0	FL^{-2}	S_E	1
Concentrated Load	P	F	$S_E \cdot S_L^2$	1.7689
Frequency	f	T^{-1}	$1 / S_T$	0.87
Velocity	V	LT^{-1}	S_L / S_T	1.15

3.6.4 System Identification

White-noise experiments were conducted before and after each simulated ground motion experiment in order to identify the structural dynamics characteristics of the model structure. White-noise excitations were banded 0-50 Hz with a peak table acceleration of 0.05-g. Dynamic properties of the test structure were then determined from the transfer functions (TF). The Hanning windowing technique was employed with a 50 percent overlap (total of seven averages over 4,096 data points) along the time axis of the acceleration time histories.

Identified natural periods of vibration and equivalent viscous damping ratios showed a distinct dependence on the amplitude of the response. This was expected as the model structure responded at higher amplitudes, the out-of-plane buckling of the braces introduced further flexibility and friction induced at the connections resulted in higher damping ratios. Hence, identified natural periods of vibration ranged between 0.23 sec for low-amplitude white-noise and 0.51 sec for high-amplitude El Centro (250 percent) excitations as shown in figure 3-24.
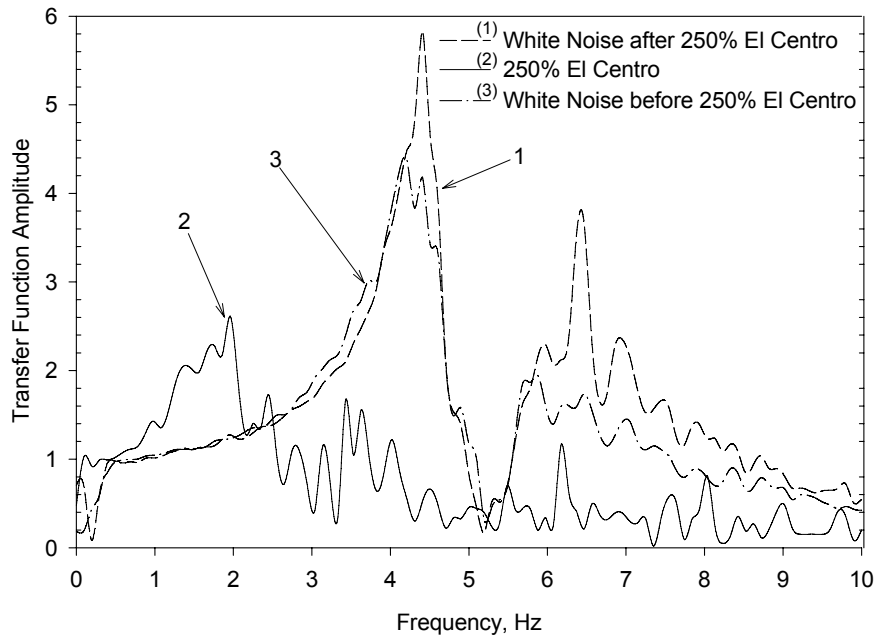
**Figure 3-24. Transfer function comparison before and after the
250 percent El Centro experiment.**

Corresponding calculated equivalent viscous damping ratios were 10 and 20 percent, respectively.

3.6.5 Experimental Results

The model structure was subjected to the two simulated ground motions at various peak ground acceleration (PGA) levels. The PGA values varied from 0.15-g to 0.85-g, representing minor to major ground shaking. A complete list of the ground motion experiments is given in table 3-5. Also listed in the table are the recorded maximum accelerations at the deck level as well as the maximum deck displacements. Experimental base shear coefficient versus deck displacement hysteresis are shown in figure 3-25. The corresponding deck displacement time histories are plotted in figures 3-26 and 3-27.
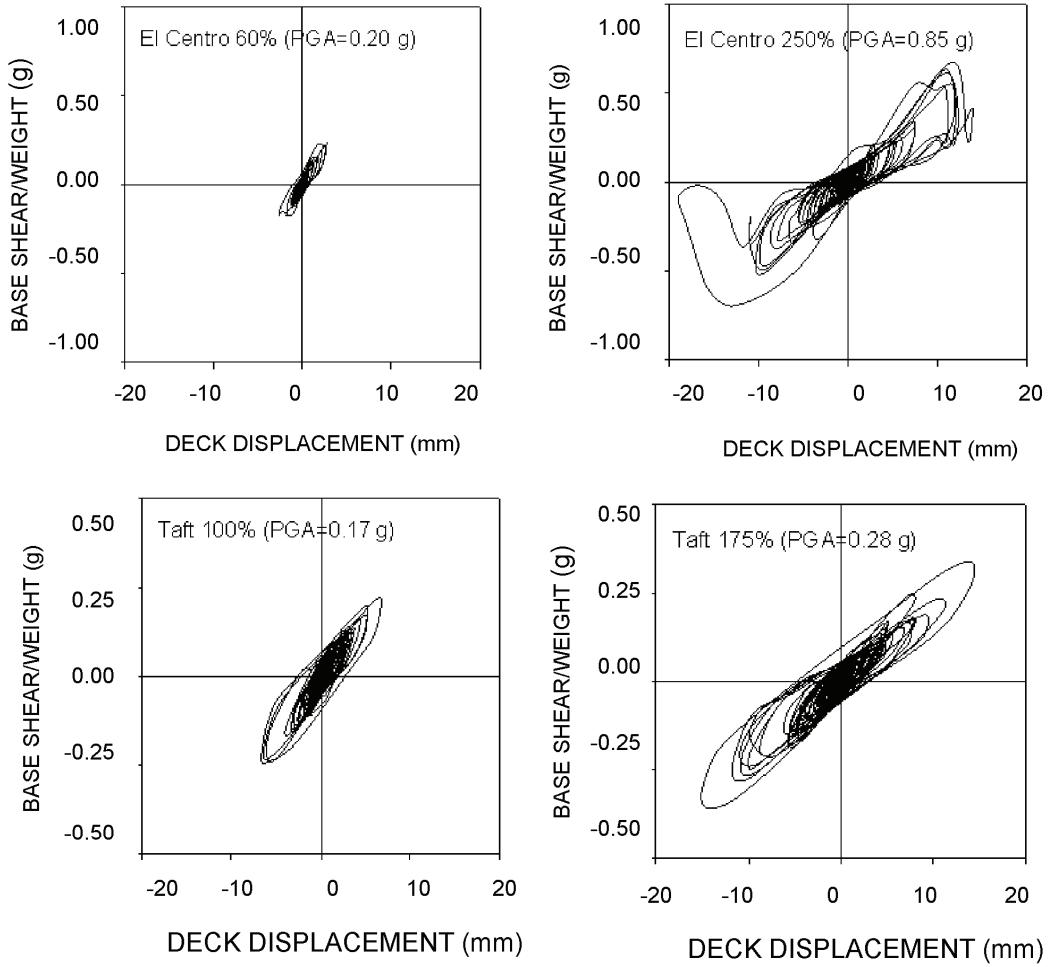
Figure 3-25. Base shear coefficient versus deck displacement hysteresis for different ground motions.
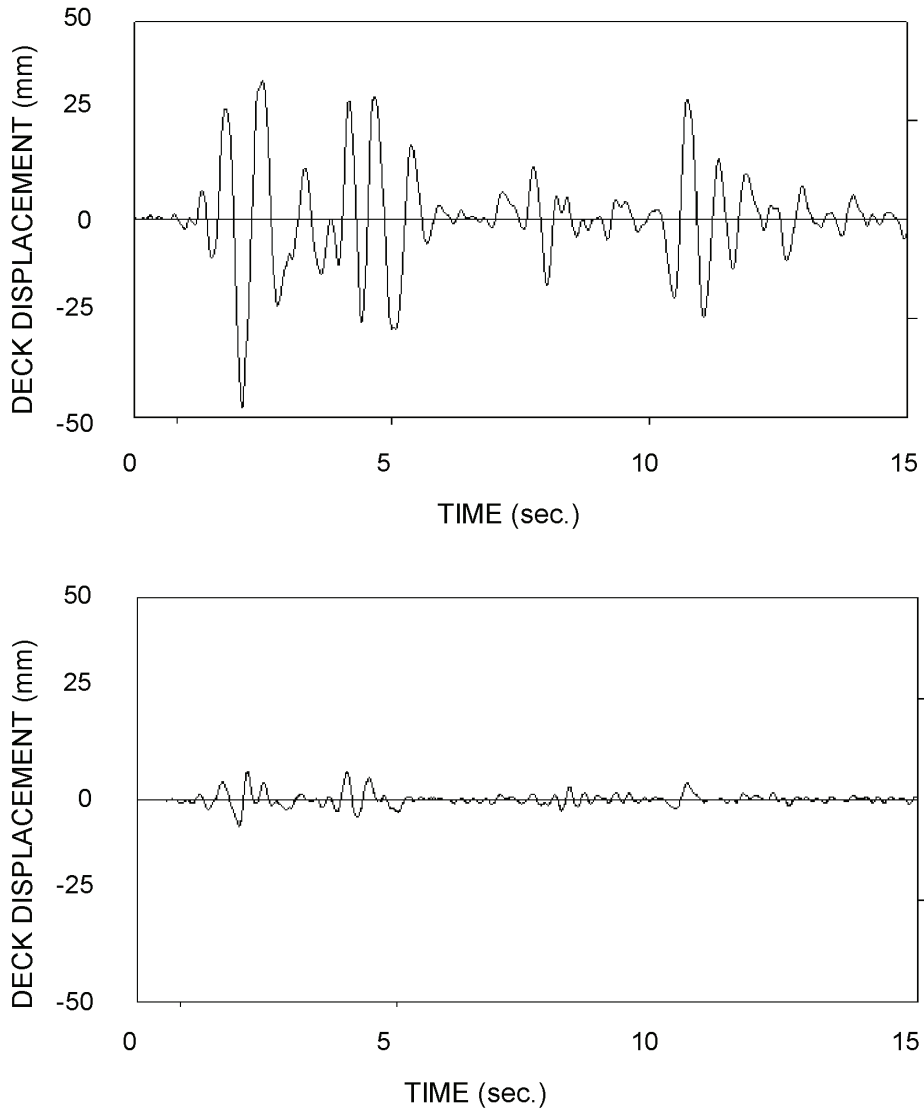
**Figure 3-26. Shaking table experiment results for El Centro 1940 N-S (a) 250 percent
(PGA = 0.85-g) and (b) 60 percent (PGA=0.20-g).**
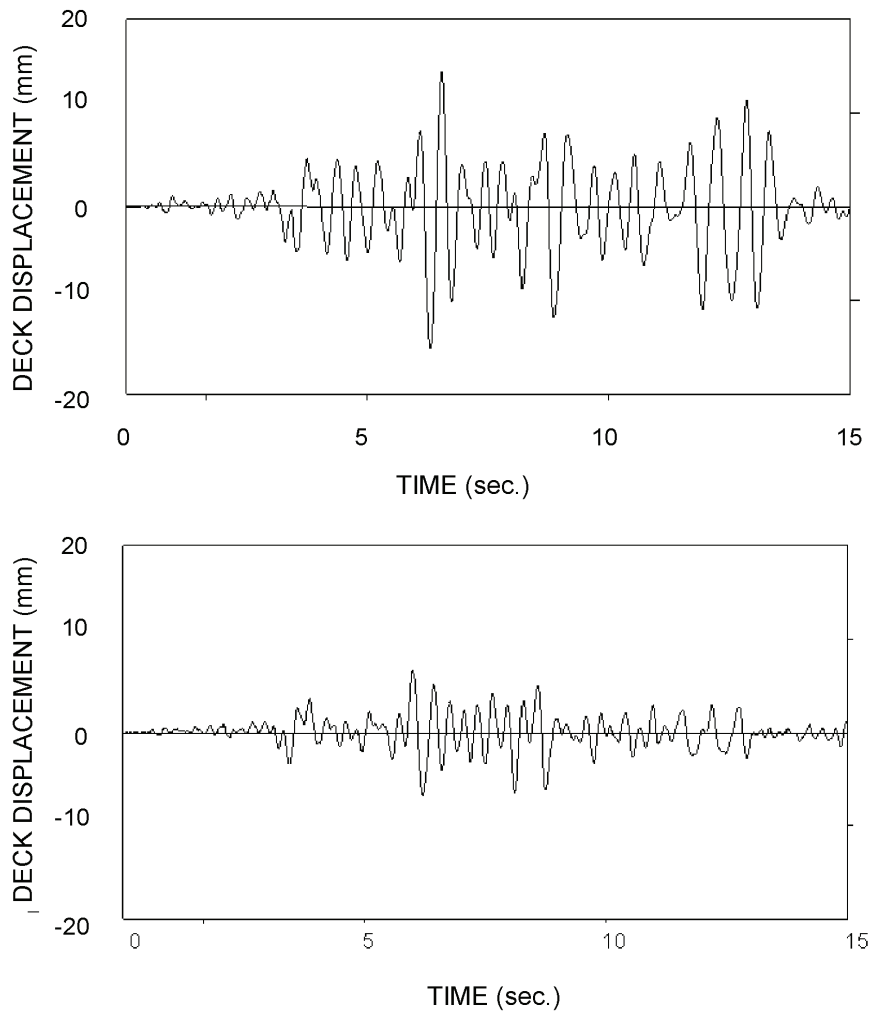
Figure 3-27. Shaking table experiment results for Taft N21E (a) 175 percent (PGA = 0.28-g) and (b) 100 percent (PGA = 0.17-g).

Table 3-5. Summary of shaking table experiments.

	Taft N21E (PGA = 0.16 g)		El Centro NS (PGA = 0.35 g)		
	100 percent	175 percent	40 percent	60 percent	250 percent
Peak Ground Acceleration (PGA)	0.17	0.28	0.14	0.20	0.85
Deck Acceleration (g)	0.25	0.36	0.15	0.24	0.70
Deck Displacement (mm)	7	15	4	7	47

The model structure responded elastically when subjected to minor and moderate ground motions with PGAs up to 0.28-g. During the Taft 175 percent experiment, which had a PGA of 0.28-g, distress in the brace elements and its connections was observed as the maximum deck displacements reached up to 15-mm (0.4 percent drift). An inspection of the model structure following this experiment revealed several minor splits in the cap beam and brace elements. No visible damage was observed at the bolted connections.

The model structure was then subjected to El Centro ground motion at a PGA of 0.85-g that represented a typical major earthquake. Recorded maximum deck drift was 47-mm (1.3 percent drift) and significant damage due to crushing of the wood around the bolts was observed. However, this damage did not affect structural stability. Transfer function comparison of figure 3-24 also indicates that the model structure, although damaged, had comparable overall capacity to withstand minor to moderate ground excitations before and after this experiment.

Finally, it must be noted that the recorded hysteresis (base shear vs. deck drift) shown in figure 3-25 represent energy dissipation (hence damping) due to both friction at the connections and inelastic response of the braces.

3.6.6 Verification of Computational Model with Shaking Table Experiments

The computational model was used to predict the shaking table experiments response behavior. For this purpose, first, a modal analysis was performed on the structure using its

linear-elastic properties. The corresponding natural period of vibration was found to be 0.21 sec, which is in good agreement with the experimental value obtained from the low-amplitude white-noise experiments. Next, the structure was subjected to a lateral drift of 0.4 percent (15-mm deck displacement) using a nonlinear static pushover analysis. This drift value corresponded to the incipient out-of-plane buckling of the braces. Following the pushover analysis, another modal analysis was performed and the natural period of vibration corresponding to the final state of the model was found to be 0.54 sec, which is also in good agreement with the value obtained from the high-amplitude El Centro experiment. Experimental base shear coefficient versus deck displacement hysteresis and corresponding deck displacement time histories are compared and plotted in figures 3-28 and 3-29. It can be observed that a good agreement between the experimentally recorded and analytically predicted response is evident. However, due to the obvious complexities involved in the modeling of the out-of-plane response (in a 2D model) of the braces and the modeling of the friction induced at the connections, the computational model cannot capture the entire response history, especially for high-amplitude excitations.

3.7 QUASI-STATIC REVERSED CYCLIC LOADING EXPERIMENTS

Although the shaking table experimentation was successfully completed, the near full-sized timber bridge model still had considerable remaining life. In order to understand the actual failure mechanisms under cyclic loading, it was considered necessary to test the model to destruction on the laboratory strong floor under quasi-static reversed cyclic loading. Hence, the principal objective of the quasi-static reversed cyclic loading experiments was to capture any potential failure modes that were not attained when the structure was tested on the shaking table, due to the limitation of the imposed earthquake-induced displacements.

Two different bracing systems were investigated in this study. Parameters like section properties, type of wood, seasoning, and moisture content were also included in this investigation. In the first quasi-static reversed cyclic loading experiment, the structure was configured in the same manner as before but with new diagonal bracing members designed to resist buckling. The 100-mm x 150-mm Hemlock timber braces that were used had a measured compressive strength of f_c equals 20-MPa. Table 3-6 summarizes the different properties of the two bracing systems employed in this experimental study.
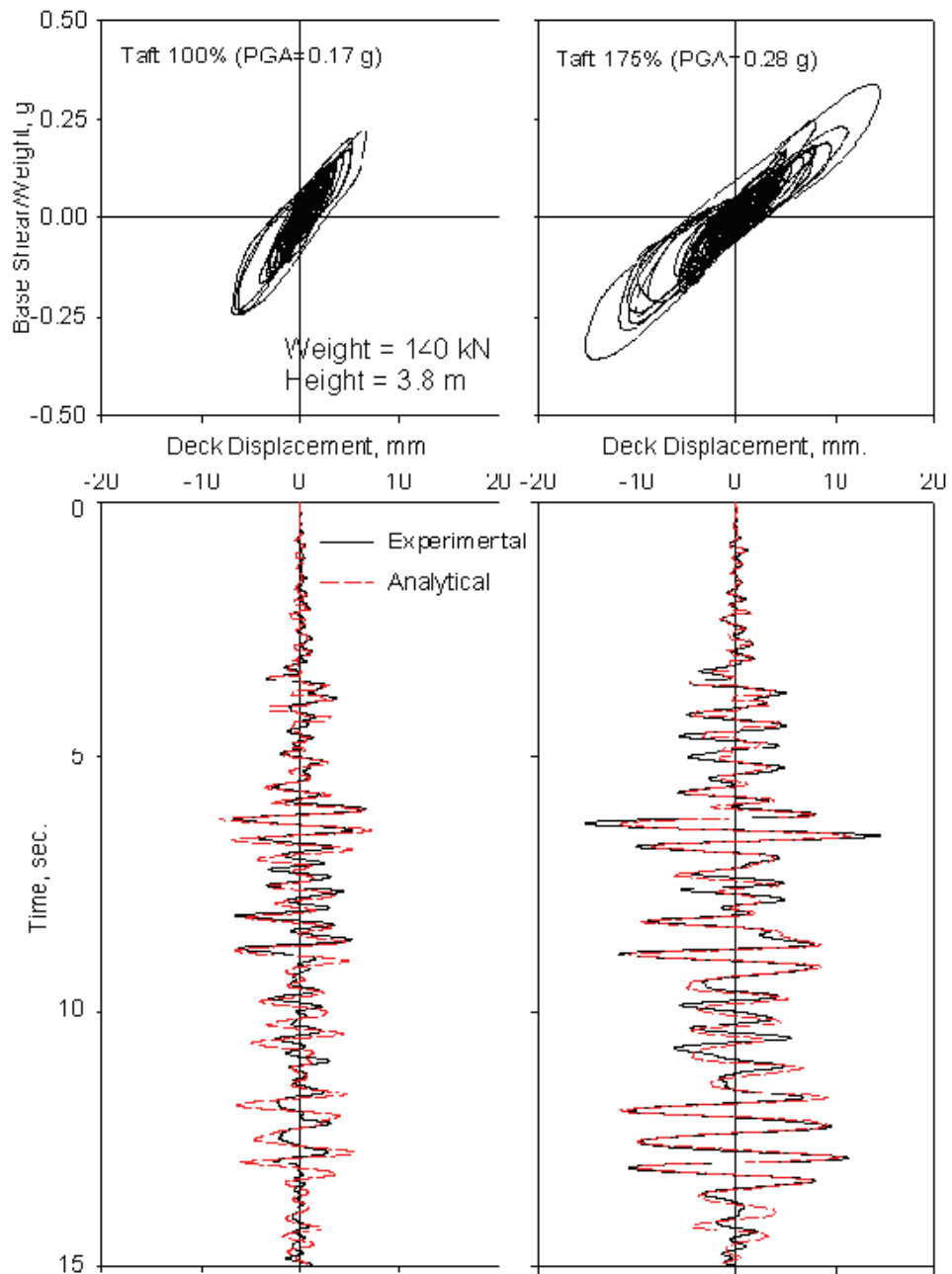
Figure 3-28. Shaking table experiment results in comparison with computational model: Taft N21E.
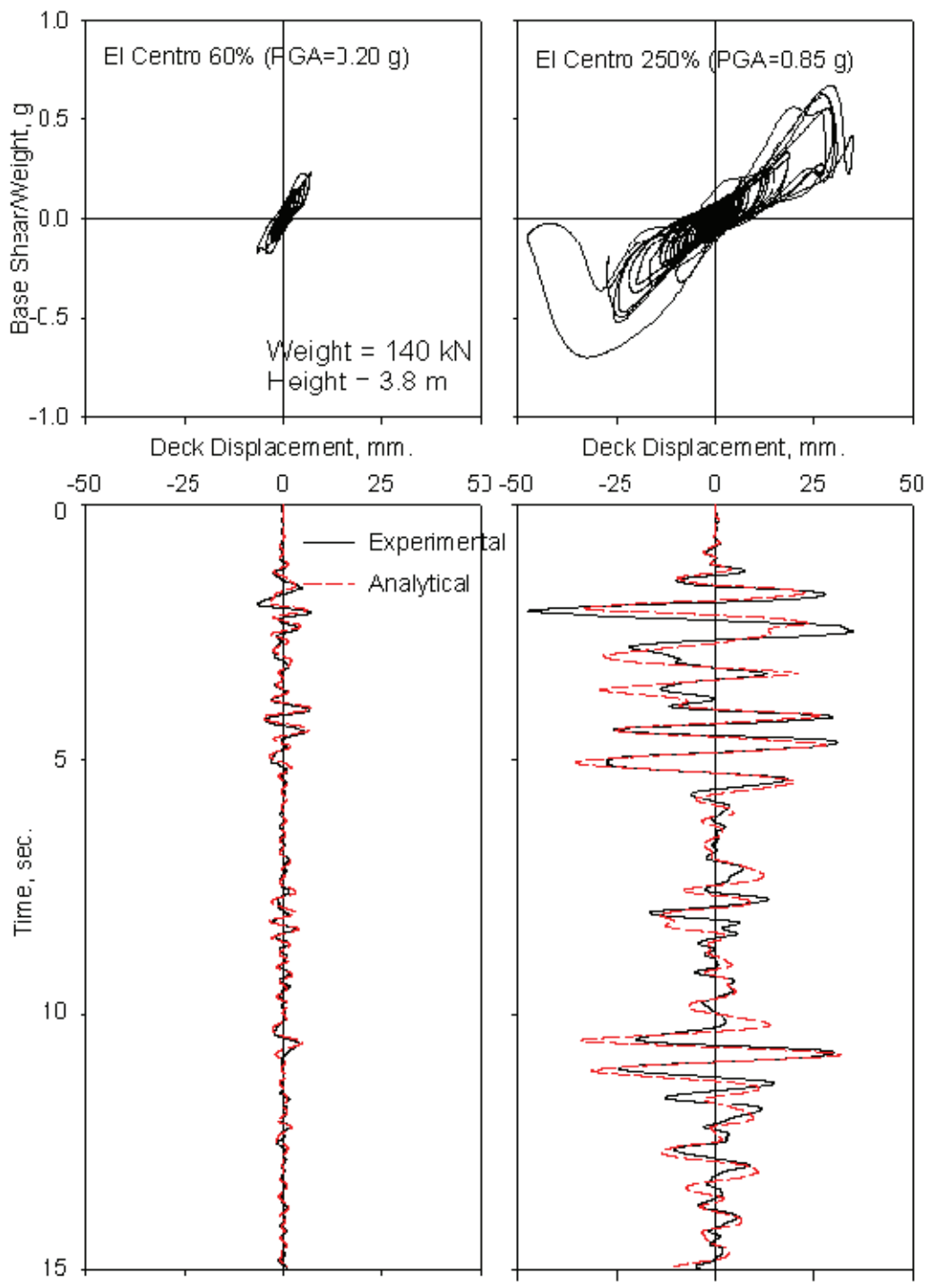
Figure 3-29. Shaking table experiment results in comparison with computational model: El Centro 1940 N-S.

Table 3-6. Properties of the braces employed in the quasi-static reversed cyclic loading test.

Test #	Bracing Dimension (mm)	Wood Species	Moisture Content (percent)	Compressive Stress (MPa)[1]	Theoretical Connection Capacity[2] (kN)	Theoretical Buckling Capacity[3] (kN)
1	40 x 190	Southern Pine	8 (Dry)	38	24	15[4]
2	100 x 150	Hemlock	54 (Green)	20	32 [4,5]	190

1. The compressive stresses are based on coupon tests.
2. Connection capacity was determined according to equation (28)
3. Theoretical buckling capacity was determined according to equation (29)
4. is the governing case for compression
5. is the governing case for tension

3.7.1 Experimental Setup and Instrumentation

The test rig employed for these experiments is shown in figure 3-30. The specimens were anchored to the strong floor to provide restraint against both horizontal translation and uplift during testing. Anchoring was provided using 32-mm diameter high alloy prestressing threadbars that were used to post-tension the concrete anchor beams to the laboratory strong floor.

Lateral load was provided by a 500-kN servo-controlled hydraulic actuator that had an available stroke of ± 127-mm. Concrete weights, 140-kN in total, were placed on top of the timber cap beams of the braced timber pile bents to represent the weight of two spans in a timber bridge. The MTS servo-controlled hydraulic actuator was attached to the lower of these concrete weights and horizontal lateral load was applied from a reaction frame through the center of mass, thus representing seismic inertia loads.

The instrumentation used for the experiment consisted of sonic displacement transducers, linear resistance potentiometers, and load cells. Two ± 150-mm sonic displacement transducers were used to measure the lateral displacements at the top of the timber cap beams of each pier bent. These instruments were mounted on an independent reference frame which was anchored to the laboratory strong floor. Another two sonic transducers were included as a precautionary device to measure translation of the anchor beams of each bent relative to the strong floor. Due to the high level of prestress applied to hold down the anchor beam, no relative movement with the strong floor was detected.
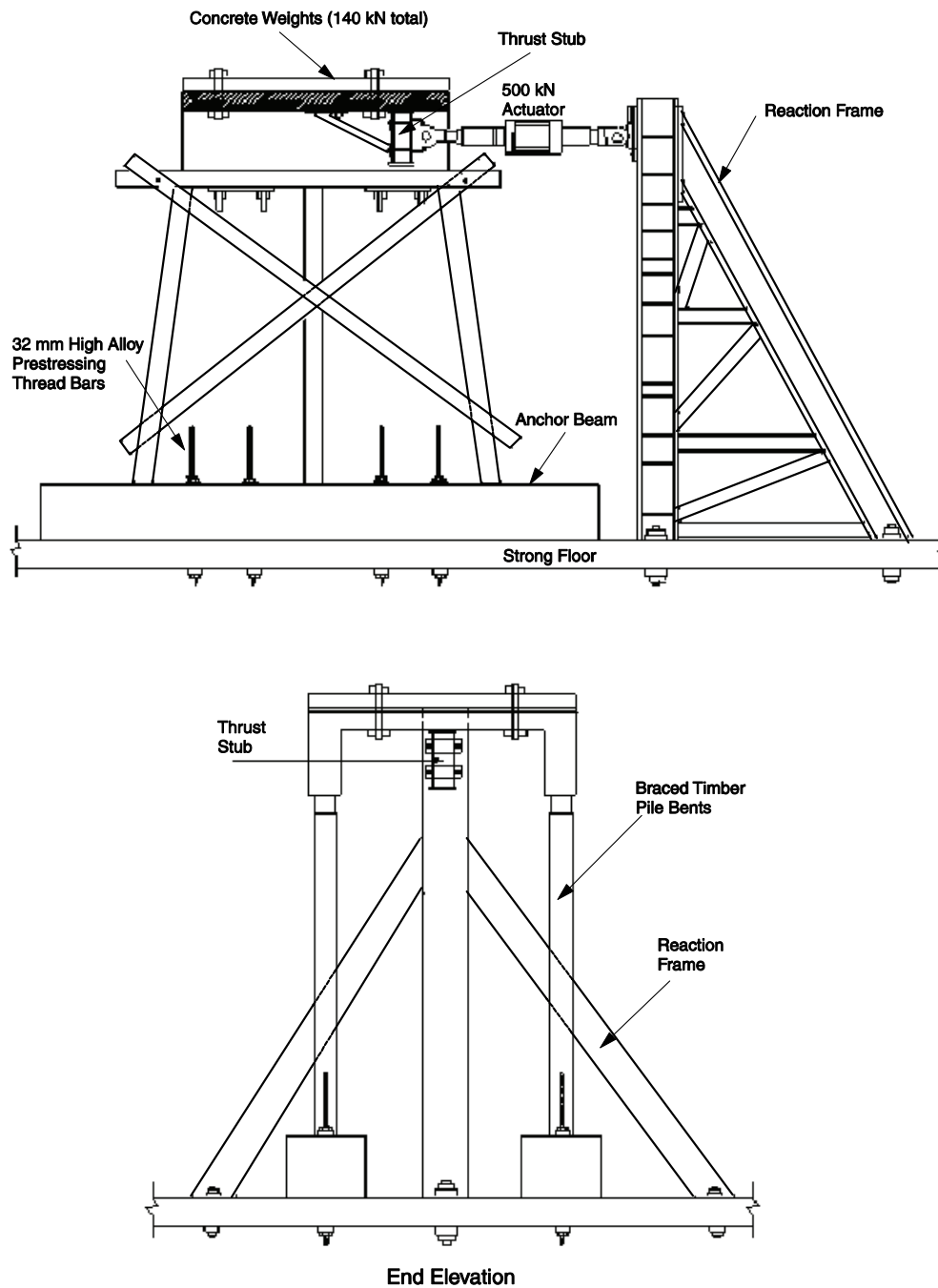
Figure 3-30. Quasi-static cyclic loading experimental setup.

Figure 3-31. Locations of potentiometers to measure the relative displacement: between bracing and cap beam (left); and between bracing and piles (right).

Linear resistance potentiometers were utilized to measure rotations (and hence infer curvatures) over sequential gauge lengths of the interior pile. They were also used to measure the relative displacement of both the timber cap beam and the bracing system with respect to the piles. Photographs displaying the locations of these potentiometers are shown in figure 3-31.

3.7.2 Experimental Results

Quasi-Static Test 1: Pier Bent with 40-mm x 190-mm Dry Pine Timber Bracing
The pier bent was tested in this experiment, with 40-mm by 190-mm dry pine timber bracing, under two reversed cycles at nominal drift amplitudes in the range of ±0.5 percent and ±2 percent. The end distance between the center of the bolt and the end of the X-bracing member was 180-mm in accordance with standard detailing practice. However, 300-mm was used in one connection, to investigate the effect of changing this distance on the bearing resistance of the connection under cyclic loading. Failure occurred at about 100-kN lateral applied load in the X-

bracing due to the accumulation of the crushing of the wood surrounding the bolts that connected the bracing to the timber piles and caps. The testing was terminated due to longitudinal splitting that developed in the diagonal X-bracing - much of the splitting was caused as a result of the out-of-plane buckling.

The experimental results indicated that the overall structural behavior of the braced timber pile bent was governed by the inelastic (post yield) performance of the bracing system as well as the connection between the bracing and the piles. The force-displacement behavior for this experiment is shown in figure 3-32 (top). The observed pinching in the loops resulted from a combination of the out-of-plane buckling of the braces in compression and the slip-lock behavior of braces in tension. The experiment indicated that 180-mm distance between the center of the bolt and the end of the X-bracing member is not suitable for seismic considerations, for the section considered in this test. This distance should ideally be increased to at least 300-mm in order to avoid undesirable splitting in the connection region during large seismic drifts. Braces with 180-mm distance to edge experienced dramatic splitting in the connection at ±1 percent drift amplitude. These connections were damaged by the end of the test at the ±2 percent drift amplitude. Damage was concentrated in the timber brace in the form of longitudinal splits forming in the wood (see photographs in figure 3-33). The lag screws, however, did not exhibit any damage. The connection with 300-mm edge distances were not damaged during the test. They, however, experienced ± 10-mm splitting in the timber bracing. This splitting was traced using the potentiometers installed for that purpose and was observed after the test during replacement of these bracing. Figure 3-34 presents the variation of the hole splitting created with time during the test and a photograph showing this splitting.

Quasi-Static Test 2: Pier Bent with 100-mm x 150-mm Green Hemlock Timber Bracing

A second strong-floor experiment was performed in order to investigate improvements to be made in the diagonal bracing. Accordingly, the 100-mm x 150-mm green Hemlock timber bracing sections were used during that test. Nominal drift angles of ± 0.5, ±1 and ± 2 percent, respectively, were first applied as in the previous test. A modest improvement in the performance of the structure was observed. No buckling was encountered in the bracing as in the case of the first test. Moreover, at the completion of the ±2 percent drift amplitude, it was considered that the overall structure, including the bridge piles with the bracing, was still in reasonably good
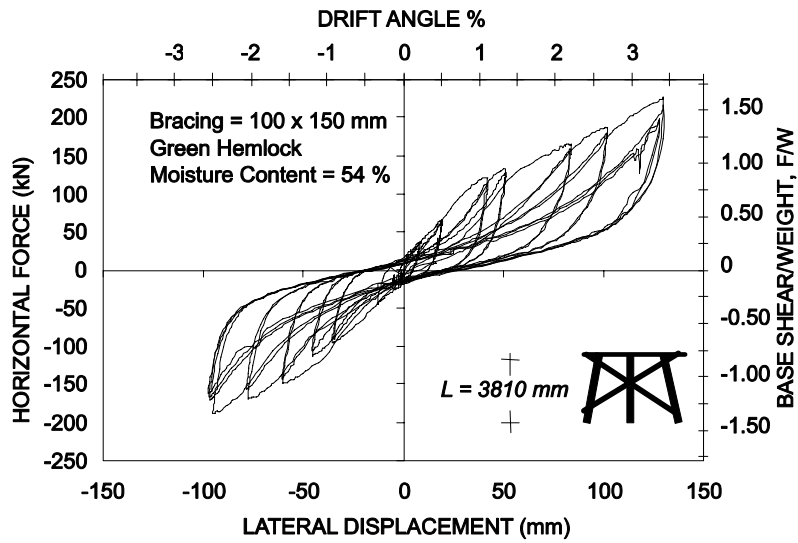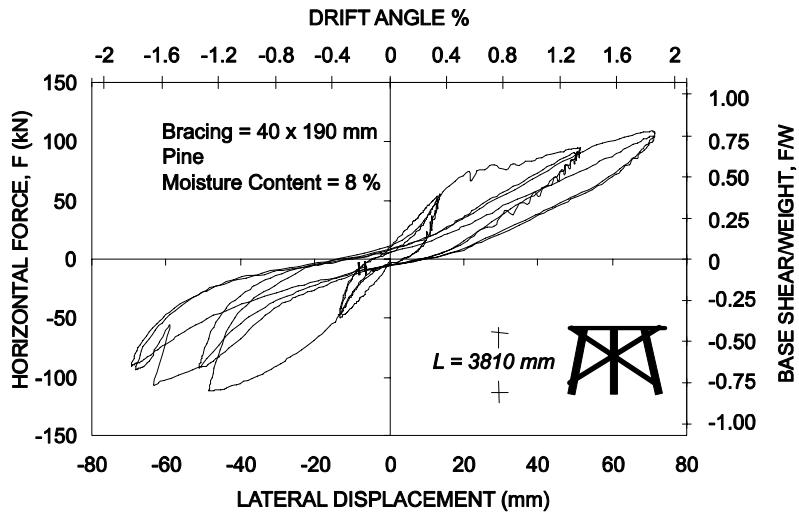
Figure 3-32. Quasi-static reversed cyclic load test results: test # 1, standard bracing (top); and test # 2, buckling resistant bracing (bottom).
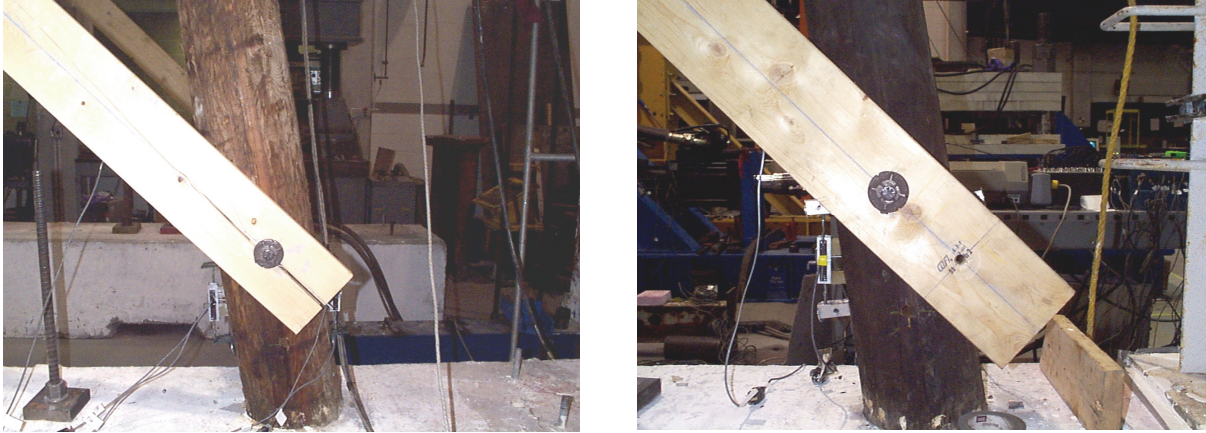
Figure 3-33. Effect of changing the end distance between the center of the bolt and the end of the southern pine X-bracing member. Photo on the left shows splitting damage of connection with insufficient length; photo on the right shows undamaged connection with sufficient length.
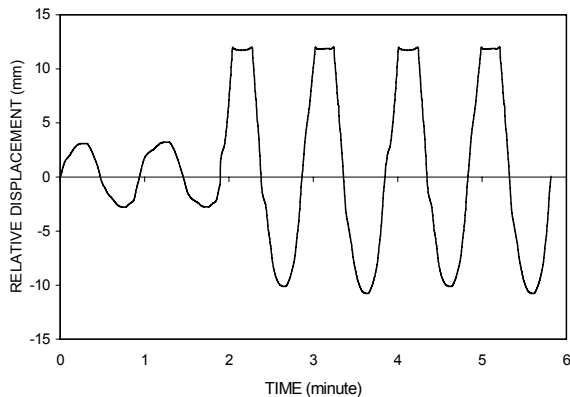
Figure 3-34. Hole slotting that occurred to the bracing at the connection (300-mm edge distance). The graph shows the variation of the splitting with time; and the photo shows such splitting after test.

condition. Therefore, the test was concluded with four cycles at nominal drift amplitude of ±3 percent. This was over a displacement range of +130-mm and -100-mm; the maximum that could be delivered by the actuator applying the lateral load. A photograph of the structure under testing is shown in figure 3-35. Although this test was considered to be very successful, some

minor longitudinal splintering in the timber bracing was observed (figure 3-36 left). This was attributed to the high moisture content of the Hemlock wood used in this test, which affected its compressive and bending strength. The connections also exhibited splitting in the Hemlock braces as shown in figure 3-36 (right). The pinching in the force-displacement loops (figure 3-37 bottom) was indicative of such splitting. It is worth noting that in all of the above testing, no observable damage was noticed in the timber pile. This is because the theoretical "yield" drift that would lead to the onset of some splitting damage in the piles is at ±3 percent. Moreover, based on earlier tests that had been done on piles alone (when tested in a free cantilever condition under cyclic loading), it was observed that damage commenced at ±4 percent drift. For this reason, the damage to the braced timber pier bent was restricted to the bracing itself, and some limited local splitting around the bracing that passed through both the bracing and the cap beams.
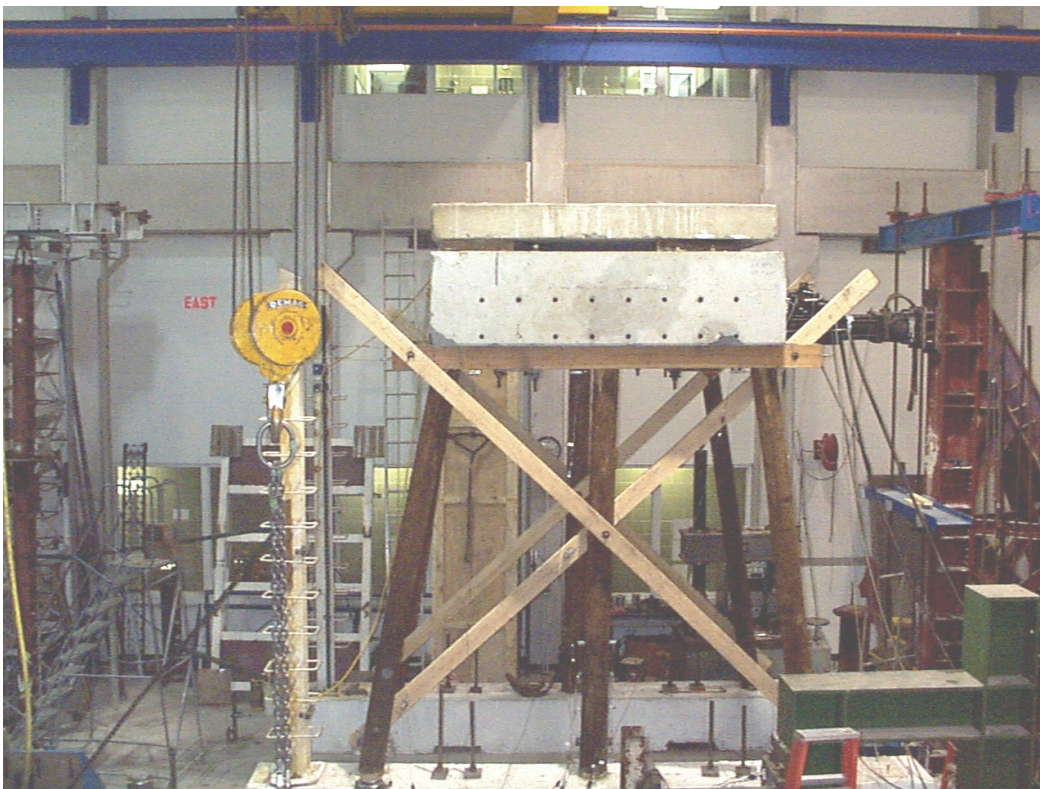
Figure 3-35. Braced timber pile bent bridge under quasi-static experiment with green hemlock bracing.

Figure 3-36. Hemlock bracing after test. Photo on left shows minor splintering; photo on right shows splitting in the connection.

By the end of the second experiment, it was noted that the transverse timber cap beam exhibited some damage in the form of longitudinal splintering and splitting at the rigid connection between the beam and the piles. Photographs of such damage are shown in figure 3-37. This damage was almost cumulative as a result of loading the structure in different experiments.
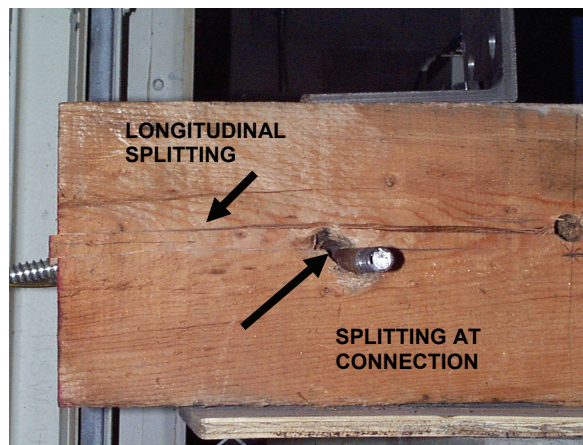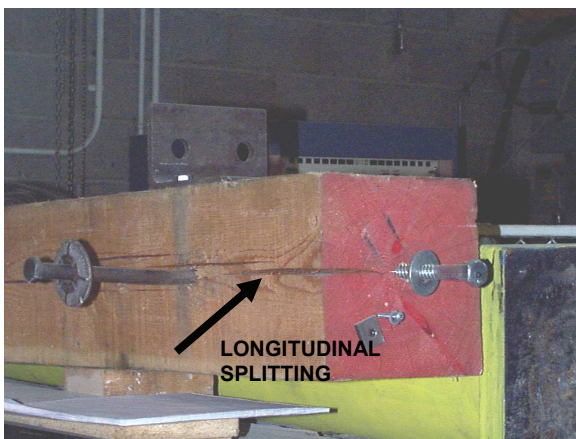
Figure 3-37. Damage occurred to the transverse cap beam by the end of experiments. Photo on the left shows longitudinal splintering; and the photo on the right shows splitting at the connection due to horizontal shear.

3.7.3 Verification of the Computational Model with Strong Floor Experiments

Quasi-Static Test 1:

The computational model was cycled in displacement control with the force computed at each event change (timber crushing, brace buckling, etc.). The same cyclic displacement history as used in the first experiment was implemented in this computational analysis. Results of the computer simulation are shown in figure 3-38 (top). The experimental results are also displayed in the figure (bottom) for comparison. From these results, it is evident that the computational modeling strategy effectively captures the general behavior (particularly the strength and unloading stiffness characteristics) of the braced timber pier bent when under cyclic loading with significant inelastic response. Some differences, however, should be noted. In particular is the reloading stiffness (and hence force) during each reloading cycle, when the load amplitudes are small. Evidently, the computational model does not reflect the friction inherent in the structural system. Also, the slight degradation of strength that occurred during load cycling was not captured.

Quasi-Static Test 2

Results of the computer simulation for this experiment are shown in figure 3-39 (top). Reasonable agreement between the experimental and the computational models is evident, particularly the envelope of the force response. Nevertheless, differences between the observed experimental results and the computational simulation do exist. As before, these are most noticeable under loading reversals when the load levels and/or displacements are small. Here, much of the resistance is provided by friction in the connections. Such behavior was not modeled computationally. Including frictional effects in the connections remains the subject of future theoretical research.
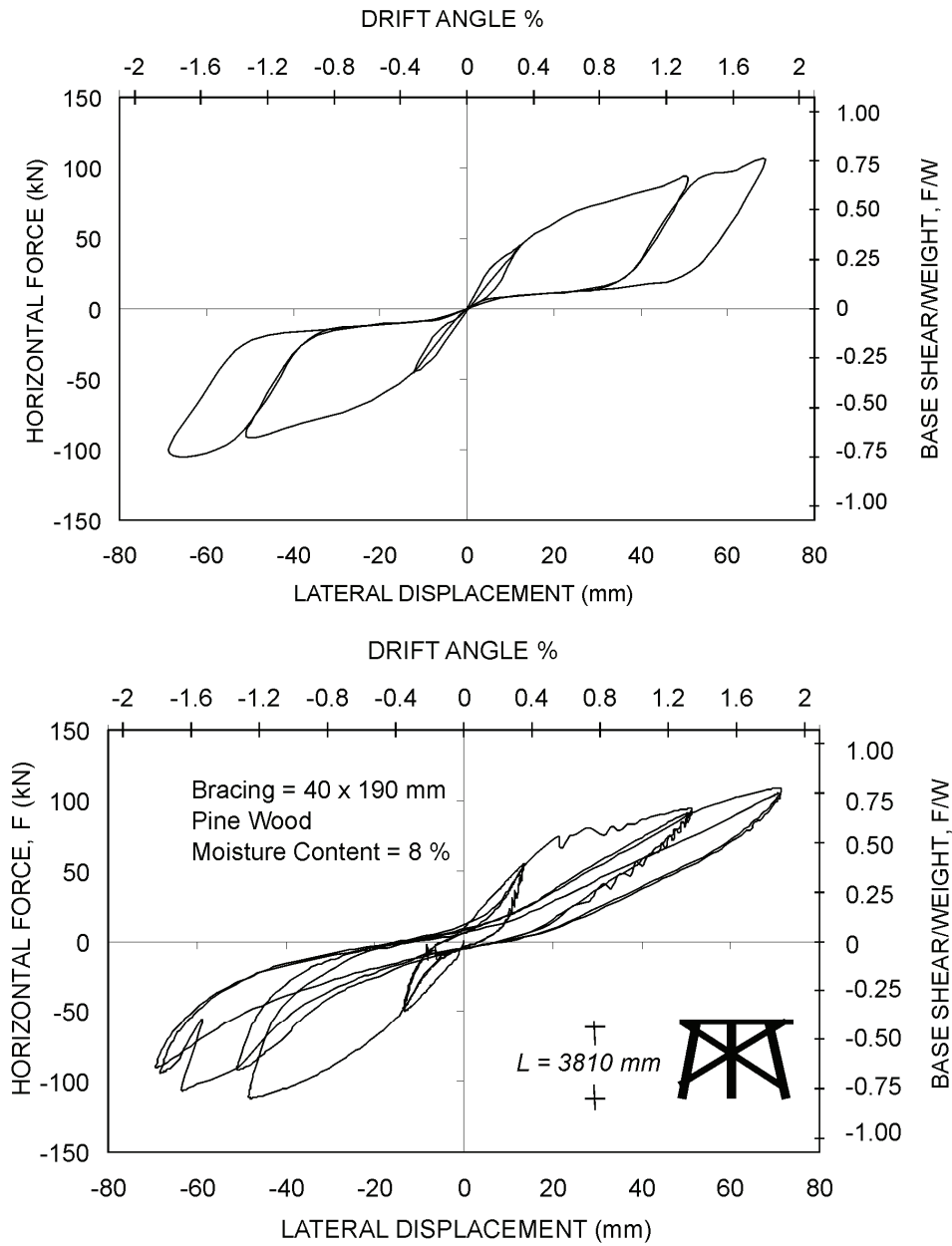
Figure 3-38. Computational-experimental comparison results for quasi-static reversed cyclic load test # 1: top shows computational results; bottom shows experimental results.
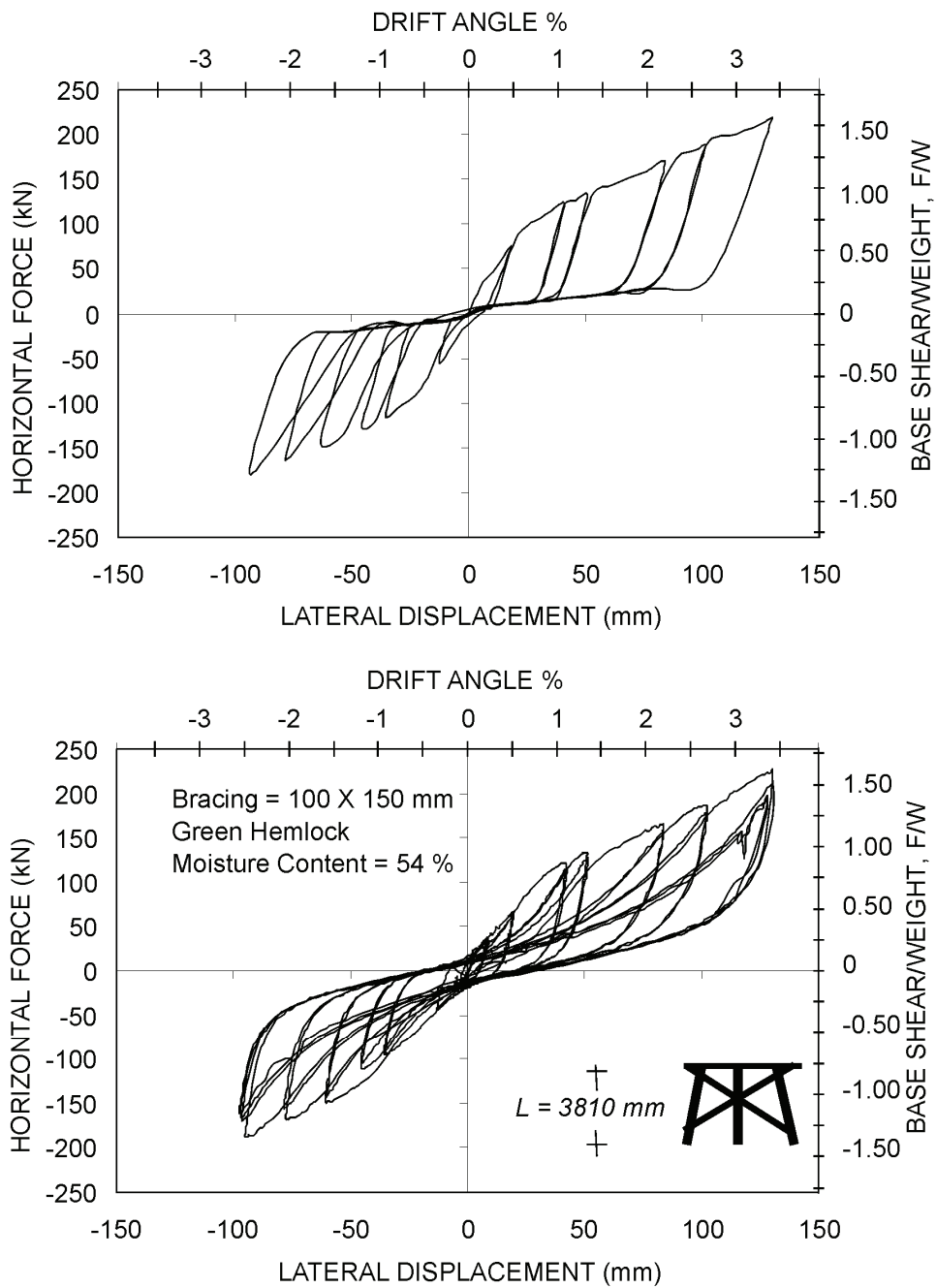
Figure 3-39. Computational-experimental comparison results for quasi-static reversed cyclic load test # 2: top shows computational results; bottom shows experimental results.

3.8 SUMMARY AND CONCLUSIONS

The performance of a bridge on timber pile bents was investigated in this section. An experimental study was presented to elaborate the behavior of timber pile bents with shaking in the out-of-plane direction. A constitutive material model was proposed for timber. This model was employed in a theoretical pushover modeling of unbraced timber piles. The model results were compared favorably to the observed experimental results. Finally, a dual experimental-computational research approach was adopted for braced timber pile bents. A prototype bridge was used to develop a near-full size physical model that was used for shaking table experiments and quasi-static reversed cyclic loading tests on the laboratory strong-floor. A nonlinear force-displacement computational modeling study was also undertaken as a companion effort to the experimental investigation. Based on the results, the following conclusions are drawn:

- The constitutive model proposed in this study and implemented in the theoretical pushover modeling of unbraced timber pile bents effectively modeled their experimental behavior. This constitutive model can be further extended in the future to incorporate the cyclic behavior of such structures.

- The experimental program overviewed in this study for unbraced timber pile bents showed that these structures have a very ductile performance under cyclic lateral loading and their strength is governed by the maximum bending stress of the individual piles and the physical condition of the wood. These experiments have demonstrated that braced timber piles bents have considerable strength and deformability capability.

- Although timber bridges have considerable robustness, they are not immune from earthquake damage. If ground shaking is strong, particularly in the long period range (this can be exacerbated by soft-soil effects), damage can be expected.

- Damage to braced timber pier bents resulting from strong ground motions transverse to the axis of the bridge deck will be mostly restricted to the timber X-bracing in the vicinity of the bolted connections. Such damage is not really serious as the bracing can easily be removed (while the bridge remains in service, but under speed restriction) and replaced.

- By installing X-braces that will resist out-of-plane buckling, a modest improvement in the seismic performance (due to improved hysteretic energy dissipation characteristics) can be expected. This means using, for example, 140-mm by 190-mm members, instead of the usual 75-mm by 200-mm members as recommended in the *Standard Plans* (1979).

- The computational model developed in the present study for the performance of braced timber pile bents under cyclic lateral loading successfully captured the shaking table response as well as behavior in the strong floor experiments. Hence, it can be used for future investigations for such structures after adding the frictional effects in the connections.

- Quasi-static reversed cyclic loading experiments were more efficient than shaking table experiments in capturing the potential failure modes of the structure. They can be used with an appropriate computational model as an alternative to shaking table experiments for further investigations of braced timber pile bents.

SECTION 4
EXPERIMENTAL INVESTIGATION OF TIMBER PILE-TO-FOUNDATION CONNECTIONS UNDER CYCLIC LATERAL LOADING

In this chapter, a theory is developed to predict the capacity of timber pile-to-foundation connections. This is followed by development of the experimental procedures and setup necessary to conduct the tests on full-scale timber specimens. Finally, results of the experimental program are outlined and comparisons with the theoretical predictions are established.

4.1 THEORETICAL MODELING OF TIMBER PILE-TO-FOUNDATION CONNECTIONS

Wood is an anisotropic material and a certain degree of familiarity with its nature is necessary to understand the factors that affect the strength properties and behavior of the material. Herein, a theory is developed that accounts for the anisotropy of wood to predict the behavior of timber pile-to-cap connections. The theory is described in the following paragraphs.

The behavior of timber pile-to-cap connections under lateral loading is mainly governed by two different mechanisms (figure 4-1):

- Flexural strength of the pile.
- Crushing of the wood perpendicular to the grain within the embedment depth.

The overall connection capacity is usually dominated by the lesser of the two mechanisms. The residual rocking capacity of the connection is associated with these mechanisms and becomes very effective under high cyclic drifts when the bond between the wood and concrete breaks down. The basic mechanisms are explained below.
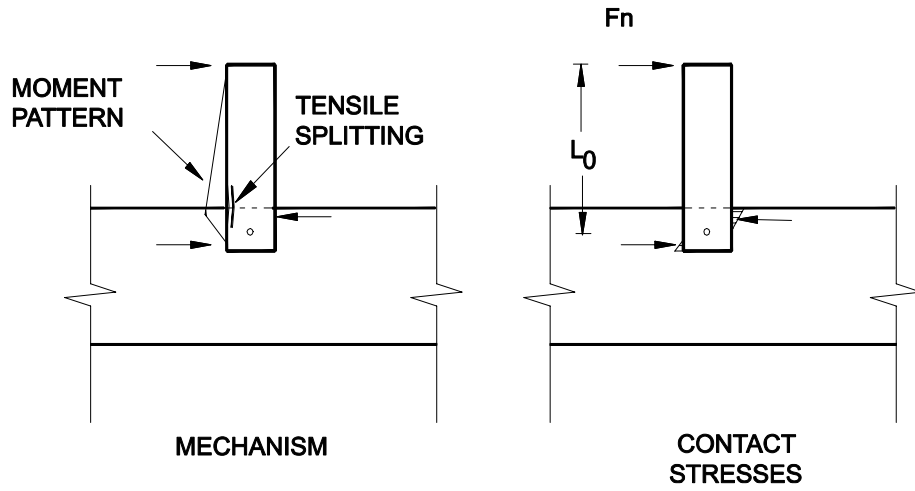
a) Mechanism 1: Tensile Flexural Splitting of Wood
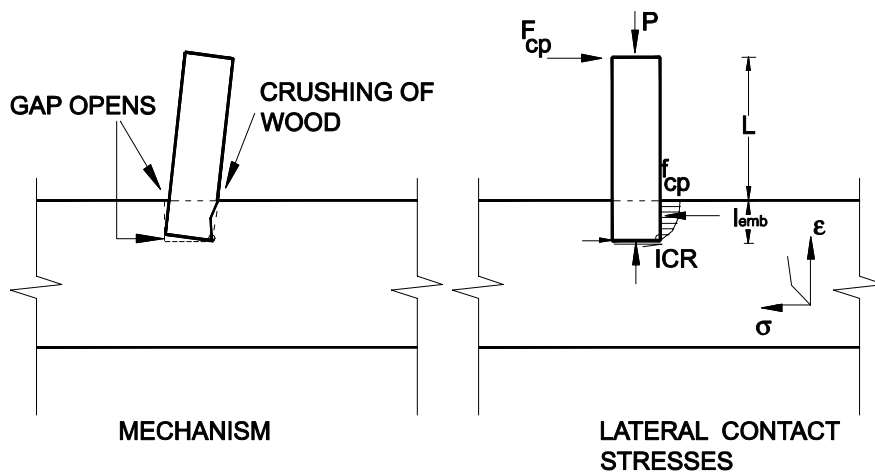
b) Mechanism 2: Crushing of Wood Perpendicular to the Grain

Figure 4-1. Potential failure mechanism for timber pile-to-concrete cap connections.

4.1.1 Failure Mechanism 1: Flexural Strength of Wood pile

Based on the AASHTO LRFD code (AASHTO LRFD, 1994) the nominal flexural strength of a timber pile is based on an amplified moment capacity at first yield, thus

$$M_n = 1.18 M_y \tag{33}$$

where M_y is the yield moment given by:

$$M_y = f_b S_x \tag{34}$$

in which f_b is the flexural bending stress of wood; and S_x is the elastic section modulus. For a circular section this is

$$S_x = \frac{\pi d_p^3}{32} \tag{35}$$

where d_p is the diameter of the timber pile.

Note that the nominal moment capacity of the pile will be attained only if a sufficient embedment depth of the pile in the concrete cap is provided.

4.1.2 Failure Mechanism 2: Wood-crushing Perpendicular to the Grain

The compressive strength perpendicular to the grain for wood is very low when compared to the compressive strength of concrete. This criterion is the basis of *Mechanism 2* explained herein.

Based on the experimental stress-strain relationship for wood perpendicular to the grain (figure 4-2a), its compressive stress can be expressed in a polynomial form as:

$$f_{cp} = f_{cp0} \left(\frac{\varepsilon_{cp}}{\varepsilon_{cp0}} \right)^{\frac{1}{n}} \tag{36}$$

where f_{cp} is the compressive stress of wood perpendicular to the grain; f_{cp0} is the nominal compressive strength of wood perpendicular to the grain; ε_{cp} is the strain corresponding to the stress f_{cp}; ε_{cp0} is the strain corresponding to the nominal compressive strength perpendicular to the grain; and n is the polynomial order.

$$f_{cp} = f_{cp0} \left(\frac{\varepsilon_{cp}}{\varepsilon_{cp0}} \right)^{1/n}$$
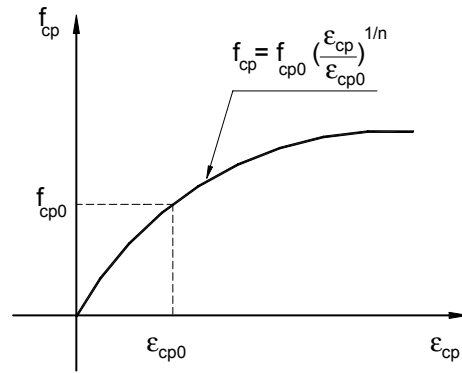
a) Proposed Stress-Strain Relationship for
Compression Perpendicular to the Grain
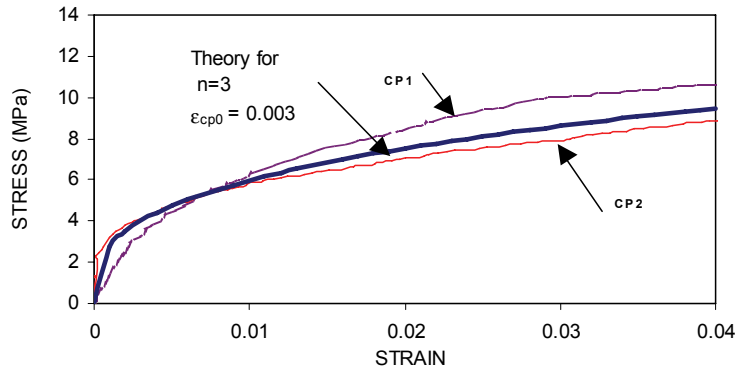
b) Experimental Stress-Strain Relationship

For Compression Perpendicular to Grain
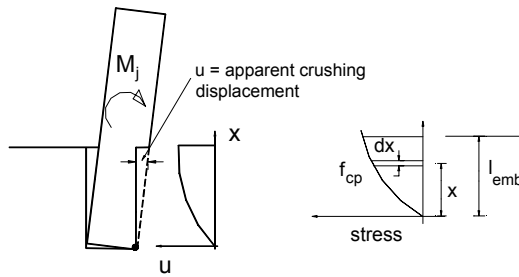
c) Distribution of Forces along the
Embedment Depth

**Figure 4-2. Criterion proposed for determining joint moment due to crushing
perpendicular to grain.**

With reference to figure (4-2c), the moment exerted by this mechanism can be obtained as:

$$M_j = \int_0^{l_{emb}} x f_{cp} d_p dx \qquad (37)$$

where M_j is the moment due to crushing in joint perpendicular to the grain; d_p is the diameter of the pile cross section; and l_{emb} is the embedment of the pile inside the concrete beam. Substitute equation (36) into (37), so that:

$$M_j = \int_0^{l_{emb}} x f_{cp0} d_p \left(\frac{\varepsilon_{cp}}{\varepsilon_{cp0}} \right)^{\frac{1}{n}} dx \qquad (38)$$

The strain ε_{cp} can be expressed in terms of joint rotation θ as:

$$\varepsilon_{cp} = \frac{\theta x}{d_p} \qquad (39)$$

By substituting equation (37) into (36) and integrating, the joint moment M_j can be evaluated as:

$$M_j = f_{cp0} d_p \left(\frac{\theta}{d_p \varepsilon_{cp0}} \right)^{\frac{1}{n}} \left(\frac{n}{2n+1} \right)^{2+\frac{1}{n}} l_{emb}^{2+\frac{1}{n}} \qquad (40)$$

Further simplification of equation (39) gives:

$$M_j = \frac{f_{cp0}}{\varepsilon_{cp0}^{1/n}} \left(\frac{n}{2n+1} \right) \left(\frac{l_{emb}}{d_p} \right)^{2+1/n} d_p^3 \theta^{1/n} \qquad (41)$$

By adopting a value of n equals 3, equation (38) can be further simplified:

$$M_j = \frac{3}{7} \frac{f_{cp0}}{\varepsilon_{cp0}^{0.333}} \left(\frac{l_{emb}}{d_p} \right)^{2.33} d_p^3 \theta_j^{0.333} \qquad (42)$$

4.1.3 Residual Moment Capacity of Connection

Consider the compressive zone in figure 4-3. The ratio of the area in compression, A_c, to the total area of the timber circular cross section, A_g, can be evaluated as (Dutta and Mander 1998):
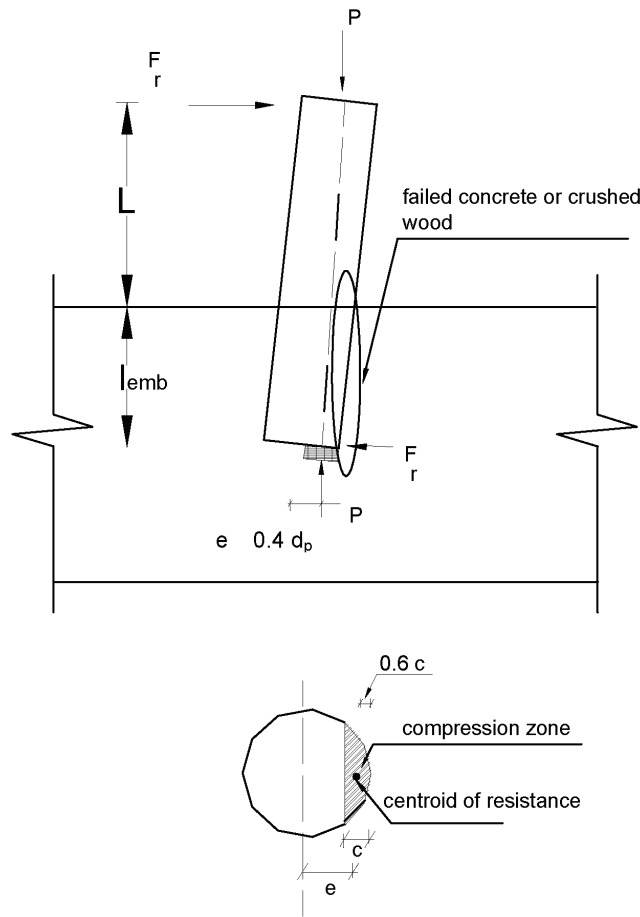
Figure 4-3. Residual moment capacity of connection.

$$\frac{A_c}{A_g} = \frac{1}{2\psi}(\psi - \sin \psi)$$
(43)

where ψ is the angle subtended at the center by the chord; c is the depth of the circular stress block; and d_p is the diameter of the pile. Equation (43) can be further simplified as:

$$\frac{A_C}{A_g} = 1.32\left(\frac{c}{d_p}\right)^{1.36} \tag{44}$$

Hence:

$$\frac{c}{d_p} = 0.757\left(\frac{A_c}{A_g}\right)^{0.725} \tag{45}$$

The moment exerted by the axial load is

$$M_r = Pe = f_c A_c \left(0.5d_p - 0.6c\right) \tag{46}$$

Further simplification of equation (46) leads to the following relationship:

$$\frac{M_r}{f_c A_g d_p} = 0.5\frac{A_c}{A_g}\left(1 - 0.9\left(\frac{A_c}{A_g}\right)^{0.725}\right) = \frac{\psi}{2}\left(1 - 0.9\psi^{0.725}\right) \tag{47}$$

where

$$\frac{A_c}{A_g} = \frac{A_c f_c}{A_g f_c} = \frac{P}{P_y} = \psi \tag{48}$$

Substituting equation (48) into (47) and simplifying gives:

$$M_r = \frac{Pd_p}{2}\left(1 - 0.9\psi^{0.725}\right) \tag{49}$$

Suppose a typical value of ψ is 0.1 is assumed, then equation (49) can be further simplified to give:

$$M_r = 0.415Pd_p \tag{50}$$

Hence, the residual rocking capacity F_r can be approximated as:

$$F_r = \frac{0.4Pd_p}{L} \tag{51}$$

The residual rocking behavior can occur following the occurrence of any of the three critical mechanisms.

4.2 IMPLEMENTATION OF MECHANISM 2 IN THE THEORETICAL PUSHOVER MODELING

The computational force-displacement method previously explained in chapter 3 is summarized in the following after adding mechanism 2 to it.

1. Determine a curvature ϕ_i.

2. Perform moment-curvature analysis and determine the connection moment M_i.

3. Calculate elastic displacement Δ_e using equation (18):

$$\Delta_e = \frac{M_i L *^2}{3EI} + \frac{M_i L_a L *}{2EI} \tag{52}$$

in which $L*$ is the actual lever arm of the pile; L_a is the distance between points of reactions of the linear stress blocks within the embedded zone; E is young's modulus of elasticity; and I is the moment of inertia of the pile cross section.

4. Calculate the flexural plastic deflection using equation (24):

$$\Delta_p = \frac{L^2}{2}\left(\phi_i - \frac{M_i}{EI}\right)\left(1 + \frac{L_{em}}{L}\right)\left(1 - \frac{M_y}{M_i}\right) \tag{53}$$

5. Calculate joint rotation due to crushing of wood perpendicular to grain from equation (42):

$$\theta_j = \frac{\varepsilon_{cp0}}{d_p^{3n}}\left(\frac{M_i}{f_{cp0}}\right)^n\left(\frac{2n+1}{n}\right)^n\left(\frac{d_p}{l_{emb}}\right)^{2n+1} \tag{54}$$

6. Calculate the joint deflection due to crushing of wood perpendicular to grain:

$$\Delta_j = (L + l_{emb})\theta_j \tag{55}$$

7. Obtain overall deflection Δ_T:

$$\Delta_T = \Delta_e + \Delta_p + \Delta_j \tag{56}$$

8. Calculate the P-Δ moment due to axial forces.

9. Determine the lateral force F as:

$$F = \frac{M_i - P\Delta}{L} \qquad (57)$$

10. Add an incremental curvature to the current curvature ϕ_I and resume steps 2 to 9.

In order to illustrate the significance of joint rotation due to crushing of wood perpendicular to grain, the method presented above was employed and force deformation relationships were established for three different cases. The following parameters were used in the analysis: d_p is 300-mm, L is 1800-mm, and f_{c0} is 32-MPa.

The influence of embedment length was investigated, and the results are shown in figure 4-4a. It is observed that the crushing of wood perpendicular to grain has a dramatic effect on the lateral resistance of the connection. As the embedment length increases, the connection lateral resistance increases. On the other hand, adjusting the embedment length will render a more ductile connection.

Results of varying the axial load and its effect on the connection performance are shown in figure 4-4b for two different cases, the fixed case (i.e $l_{emb}/d_p \geq 3$), and the case of l_{emb}/d_p is 0.8. It is shown that increasing the axial load lowers the lateral resistance of the connection, which is attributed to the P-Δ effects.

The influence of wood hardness as indicated by the relative strength ratio f_{cp0}/f_{c0} is shown in figure 4-4c. As expected, the ultimate lateral resistance is more for hardwood than for softwood.
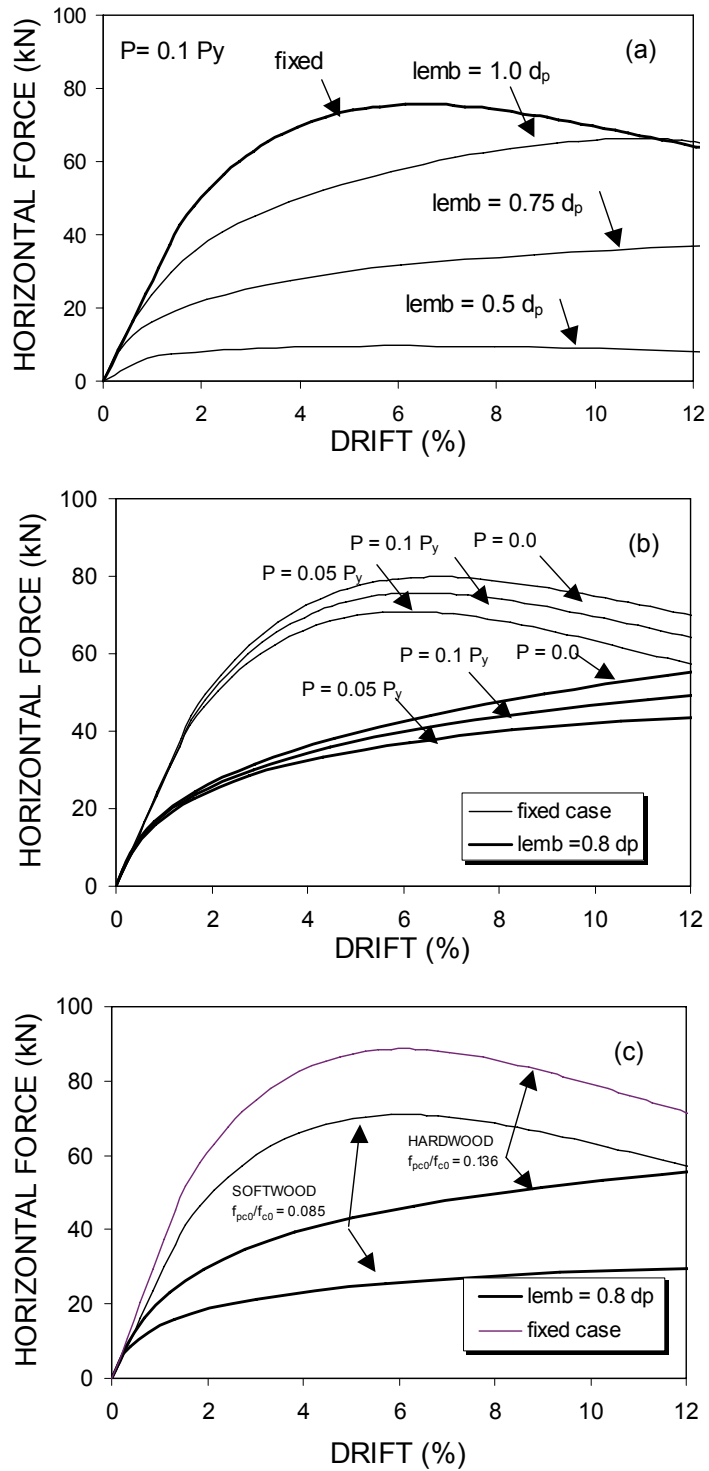
Figure 4-4. Effect of joint rotation due to crushing perpendicular to the grain on its lateral resistance.

4.3 SOIL-STRUCTURE INTERACTION REPRESENTATION
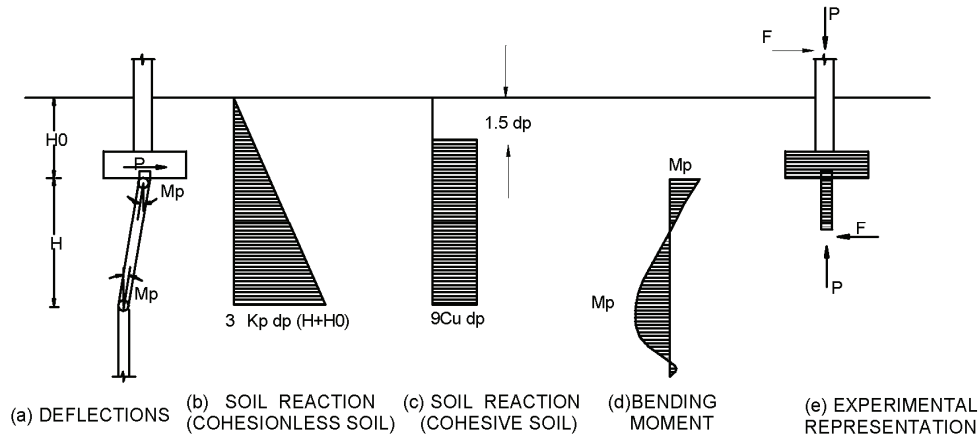
Figure 4-5. Soil-structure interatction representation in plastic mechanism of timber pile foundations.

Applying the theory of virtual work for the mechanism shown in figure 4-5, the following equations relating the normalized effective length of timber pile specimens to the soil properties can be obtained. Refer to Shama (2000) for a detailed derivation. Therefore, for cohesive soil:

$$\frac{L}{d_p} = \frac{1}{6}\left(\frac{M_p}{C_U d_p^3}\right)^{\frac{1}{2}} \tag{58}$$

and for cohesionless soil:

$$\frac{L}{d_p} = \frac{K_{buried}}{3}\left(\frac{2M_p}{\gamma K_p d_p^4}\right)^{\frac{1}{3}} \tag{59}$$

where for non-buried foundations $K_{buried} = 1$ and for buried foundations

$$K_{buried} = \frac{\left(1 + 0.12\,{}^{H_0}\!/\!{}_{d_p}\right)^{\frac{2}{3}}}{\left(1 + 0.08\,{}^{H_0}\!/\!{}_{d_p}\right)\left(1 + 3\frac{H_0}{d_p}\left(\frac{1 + 0.12\,{}^{H_0}\!/\!{}_{d_p}}{\frac{2M_p}{\gamma K_p d_p^4}}\right)^{\frac{1}{3}}\right)} \tag{60}$$

93

in which L is the effective length of pile defined as the distance from the inflection point to the plastic hinge at the connection with the pile cap; C_u is the cohesion of soil determined from undrained triaxial, direct shear or vane tests; d_p is the diameter of the timber pile; H_0 is the buried depth of the cap beam; γ is the unit weight of the soil considered ; K_p is the Rankine coefficient of passive earth pressure; and M_p is the flexural moment of the timber pile evaluated as:

$$M_p = 1.18M_y = \frac{1.18\pi f_b d_p^3}{32} \tag{61}$$

Equations (58) and (59) are employed to provide relationships between the normalized effective length of the pile (L/d_p is M/Vd_p) and parameters for cohesionless and cohesive soils, respectively. These relationships are shown graphically in figure 4-6.

Based on these relationships, an effective length L/d_p is 6 was chosen for specimens in the present study. Consequently, the cantilever length of the timber pile foundation experiments was taken as 1.42-m. Extracting the shaded portion in figure 4-5e and inverting it, a test specimen is formed when anchored to the laboratory strong floor. Axial loads were applied to the specimens by a vertical actuator acting via a lever beam system. Lateral loads were applied so that it acted at the theoretical inflection point of the pile.

4.4 MATERIAL TESTS

Visual inspection of piles used in this testing program indicated the species was Douglas Fir. The mechanical properties of the timber were characterized by performing a series of bending, axial compression parallel to the grain, and axial compression perpendicular to the grain tests. The coupon tests were performed on samples prepared in accordance with ASTM D 143-94. The tests were conducted using a TINIUS OLSEN Universal test machine.
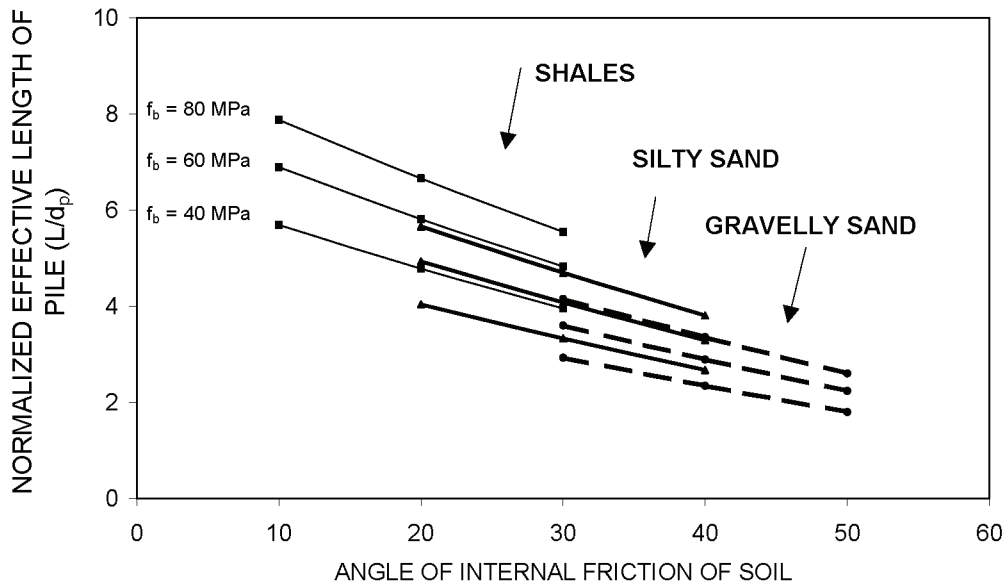
(a) Cohesionless Soil
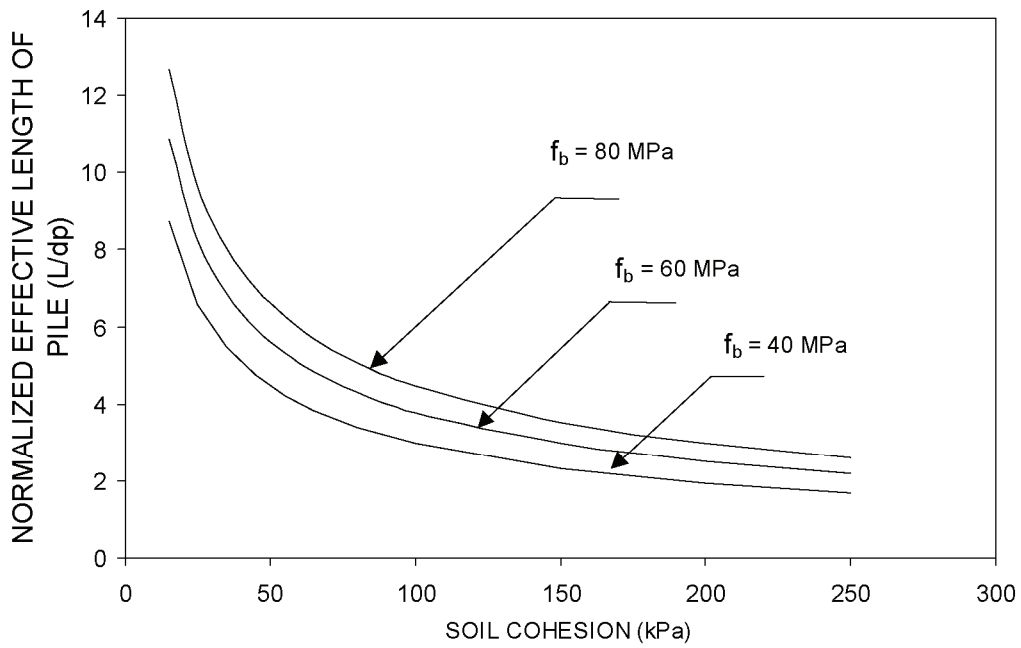
(b) Cohesive soils

Figure 4-6. Effect of soil parameters on the effective length of timber pile specimens.

4.4.1 Static Bending Test

Four 50-mm by 50-mm by 760-mm coupons were used for the static bending test. These coupons were cut from the two pile specimens employed for the lateral cyclic loading experiments. Two of these coupons conformed in dimensions with the ASTM standards i.e., 50-mm by 50-mm by 760-mm. The other two were 38-mm by 38-mm by 760-mm. A photograph of the specimens is shown in figure 4-7. Displacements were measured by a pair of $\pm$ 25-mm stroke potentiometers affixed to an aluminum frame, which was attached to the coupons at their center; a $\pm$ 50-mm transducer was also attached to the movable crosshead of the machine to provide comparative data. The load was applied continuously throughout tests at a rate of motion of the movable crosshead of 2.5-mm/min. A photograph of a coupon under bending test is shown in figure 4-8. The apparent modulus of elasticity in bending was determined as:

$$E = \frac{PL^3}{48\Delta I} \tag{62}$$

where Δ is the deflection at the center; I is the moment of inertia; L is the span length; and P is the applied load. Table 4-1 outlines the resulting data for Young's modulus (E), bending strength (f_b). The dominant failure mode of the first three coupons was simple tension. The fourth coupon, however, failed in a cross-grained tension mode showing inferior resistance with respect to the other coupons. This may be attributed to the presence of knots in the test coupon.

The bending stress-strain relationships for these tests are shown in figure 4-10(b).

Figure 4-7. Tangential surfaces of bending specimens.
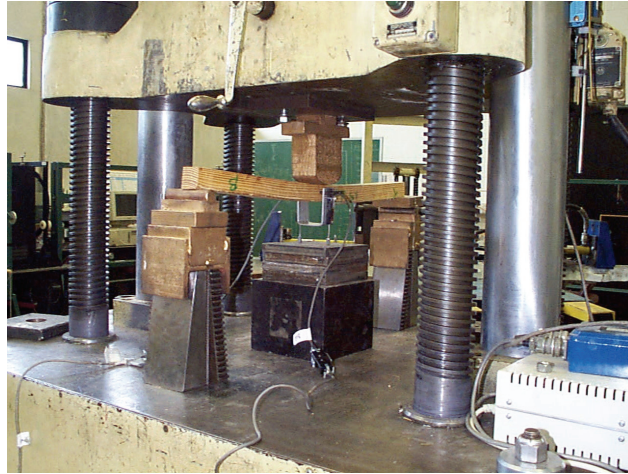
Figure 4-8. Static bending test.

Table 4-1. Results of bending tests.

Test No.	Specimen No.	Coupon Cross-section Area (mm^2)	Young's Modulus E_b (MPa)	Bending Resistance f_b (MPa)
1	B1	2500	11850	67
2	B2	1444	12450	70
3	B3	2500	13500	82
4	B4	1444	5000	48

4.4.2 Compression Parallel to Grain Test

Four 50-mm by 50-mm by 200-mm coupons were used for the compression parallel to grain test. Special care was taken to ensure that the end grain surfaces of each coupon were parallel and at right angle to the longitudinal axis. A ± 25-mm stroke linear resistance potentiometer attached to an aluminum-measuring device measured axial displacements (see a photograph of the test in figure 4-9). Table 4-2 presents the resulting data for these tests. The stress-strain relationships are illustrated in figure 4-10a.

Table 4-2. Results of compression parallel to the grain tests.

Test No.	Specimen No.	Young's Modulus E (MPa)	Compresion Resistance f_c (MPa)	Strain at Peak Stress ε_0
1	C1	10700	51	0.005
2	C2	9600	45	0.006
3	C3	9700	50	0.005
4	C4	10200	40	0.008
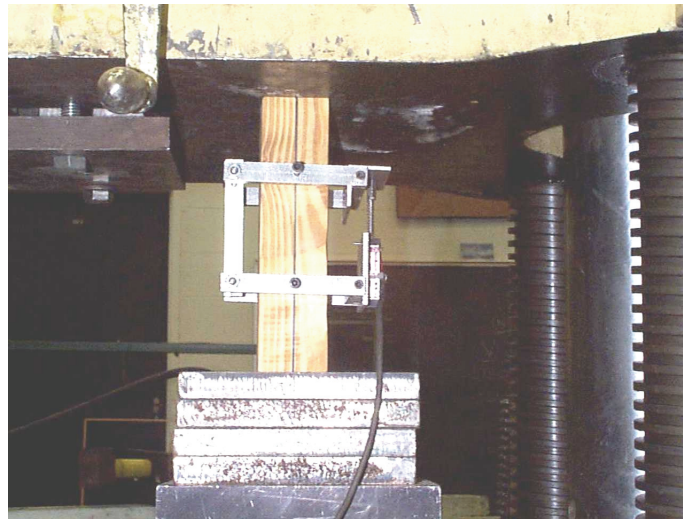
Figure 4-9. Compression parallel to grain test.

4.4.3 Compression Perpendicular to Grain Test

The compression perpendicular to the grain tests were made on two 38-mm by 38-mm by 150-mm specimens. The load was applied through a metal bearing plate 50-mm in width, placed across the upper surface of the specimen at equal distances from the ends and at right angle to the length. The load was applied continuously throughout the test at a rate of motion of the movable crosshead of 0.3-mm. The compression strength was determined at a compression strain of 0.003. Results of these coupon tests are shown in figure 4-10c.
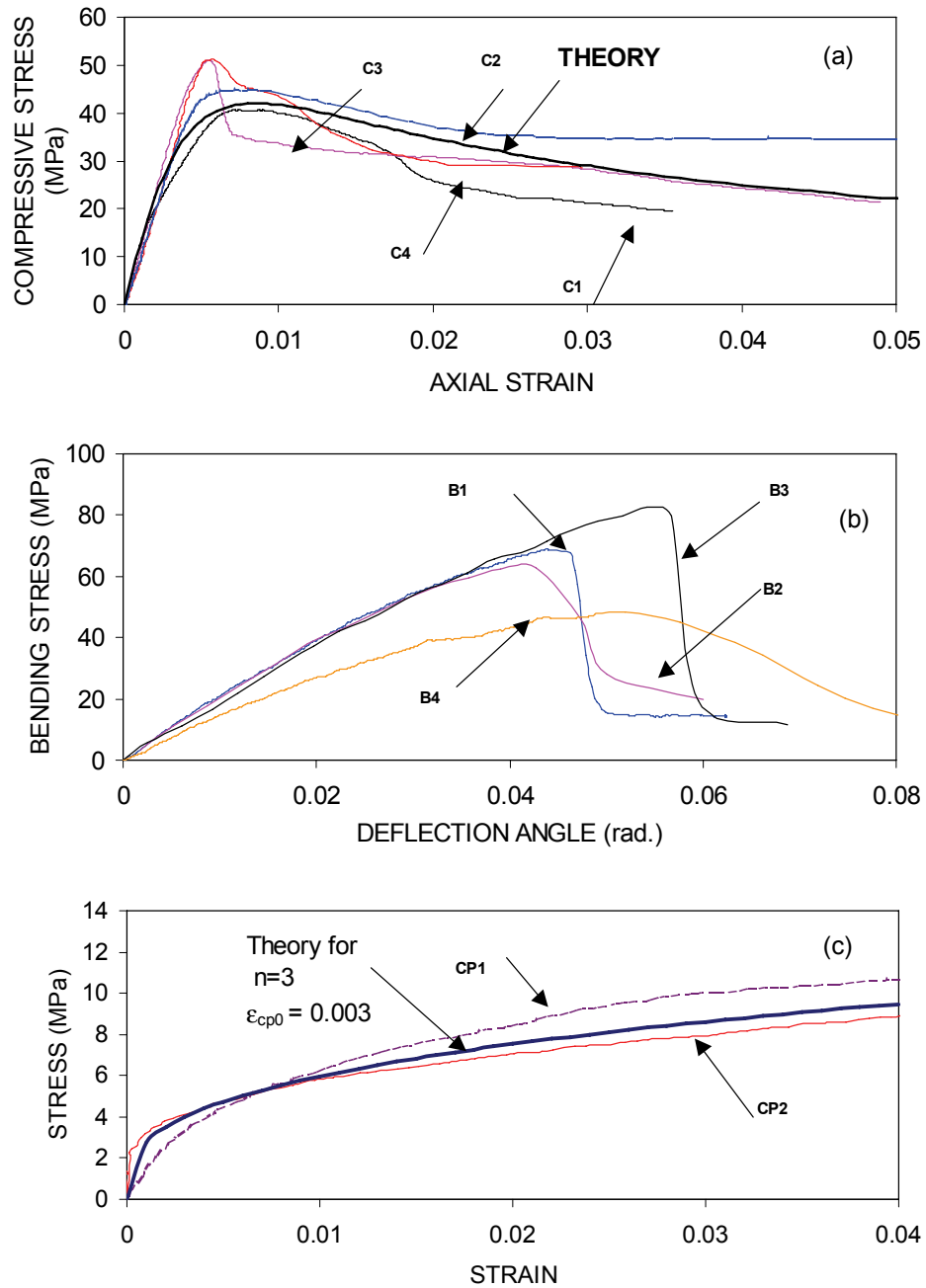
Figure 4-10. Constitutive relationships for timber as determined from experiments: (a) compression parallel to grain (b) bending, and (c) compression perpendicular to grain.

4.4.4 Moisture Content of the Timber

The moisture content of the specimens was determined according to the following relationship:

$$M = \frac{W_W}{W_S} \tag{63}$$

in which W_W is the weight of water in the specimen; and W_S is the weight of solid wood in the specimen. The weight of the specimens was determined before and after being placed in an oven at 100 Celsius for 24 hours. The moisture content was obtained as:

$$M = \frac{W_b - W_a}{W_a} \tag{64}$$

where W_b is the weight of the specimen before drying out; and W_a is the weight of the specimen after drying out. Several specimens were obtained from each pile and the moisture content was determined for each specimen. An average moisture content value of 10 percent was obtained.

4.4.5 Concrete Strength

The concrete used for the cap beam was an early strength ready-mix. Its ultimate compressive strength was determined from the results of three 150-mm by 300-mm cylinder tests at 7, 21, and 28 days. Results are shown in table 4-3.

4.5 DESIGN AND CONSTRUCTION OF THE SPECIMEN

The experimental program involved in this investigation consisted of two timber specimens with a different embedment depth of the pile into the concrete cap beam. Specimen T1 represents an exterior pile with l_{emb} is d_p consistent with present "as-built" practice.

Table 4-3. Results of 150-mm by 300-mm concrete cylinder tests.

Spec. #	Compressive Strength (MPa)		
	7 Days	21 Days	28 Days
1	19	25	34
2	23	28	28
3	24	30	30
f'_c	22	28	31

Specimen T2 represents an exterior pile with l_{emb} is $1.5d_p$ consistent with design recommendations for new timber pile foundations as proposed herein. Another reason for embedding the pile this distance was to determine whether or not retrofitting of existing bridge foundations is an economical and/or worthwhile process. Instead of constructing two separate foundations, the two pile specimens were installed into one reinforced concrete foundation cap beam with dimensions of 2,724-mm by 914-mm by 914-mm. The cap beam was reinforced with two layers of Grade 60 (414-MPa) 25-mm diameter deformed bars (# 8) at 300-mm centers as shown in figure 4-11. This reinforcement is consistent with what is customarily used in practice. An additional U Shape 28-mm diameter deformed bar (# 9 rebar) was added for specimen T2 to counteract forces that may cause spalling of the concrete in the end region of the cap. The two pile specimens utilized in this program were of different diameters.

Specimen diameters just above connections were 228-mm and 238-mm for specimen T1 and T2, respectively. The respective embedment lengths for specimens T1 and T2 were 228-mm (l_{emb} is $1d_p$) and 357-mm (l_{emb} is $1.5 d_p$). Each specimen was chemically treated with creosote.

During construction, a wooden framework to maintain proper vertical alignment was constructed to support these piles (see construction photographs, figure 4-12). The specimen was designed so that it could be clamped to the laboratory strong floor to resist horizontal sliding while lateral load testing was conducted. The clamping force was provided by an anchoring beam that was post-tensioned with a high strength threadbars system to the strong floor.

#8 @ 300

#9 U-bar

914

457 — 1828 — 457

PLAN

SPECIMEN T2
dp = 238 mm

SPECIMEN T1
dp = 229 mm

#8 @ 300

357

229

embedment
= 1.5 dp

embedment
= 1dp

SIDE ELEVATION

DIMENSIONS
IN mm

1828

1/1.5 dp

914

END ELEVATION
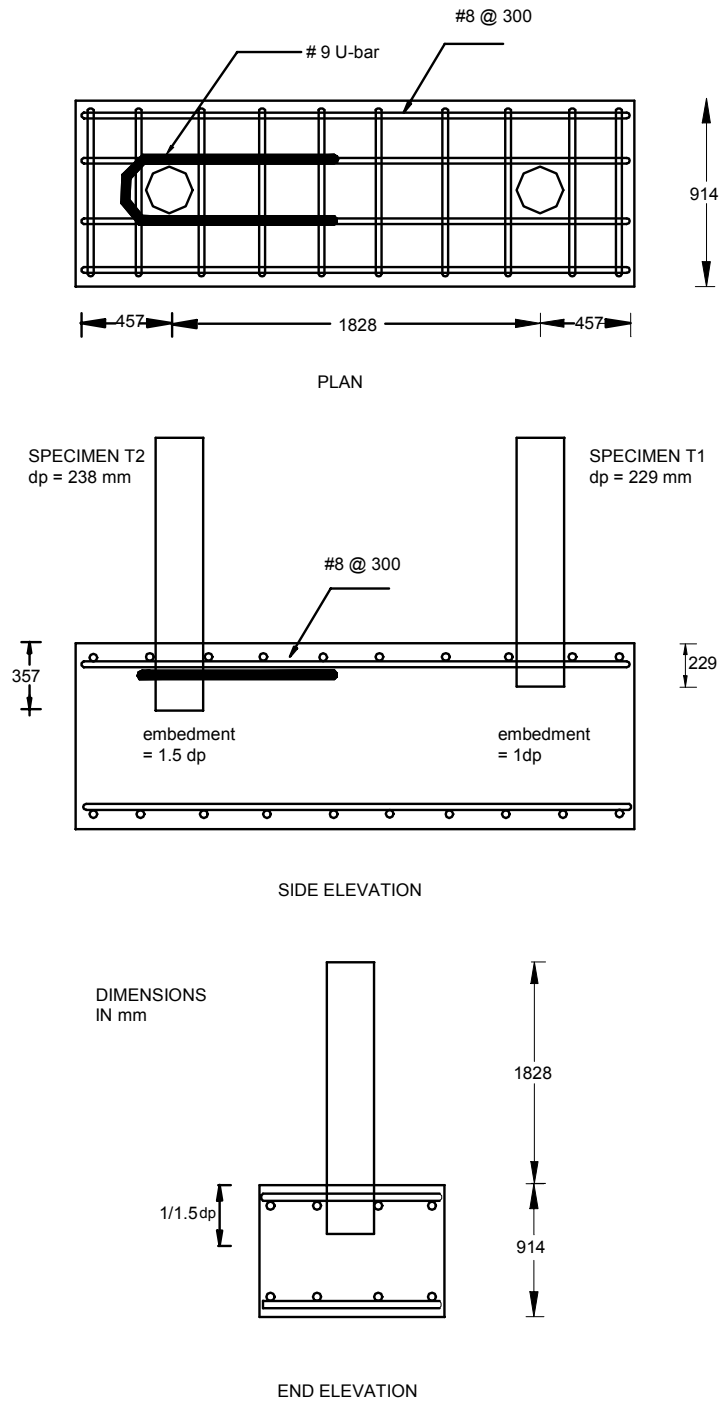
Figure 4-11. Geometry and reinforcement of timber pile foundation specimens.
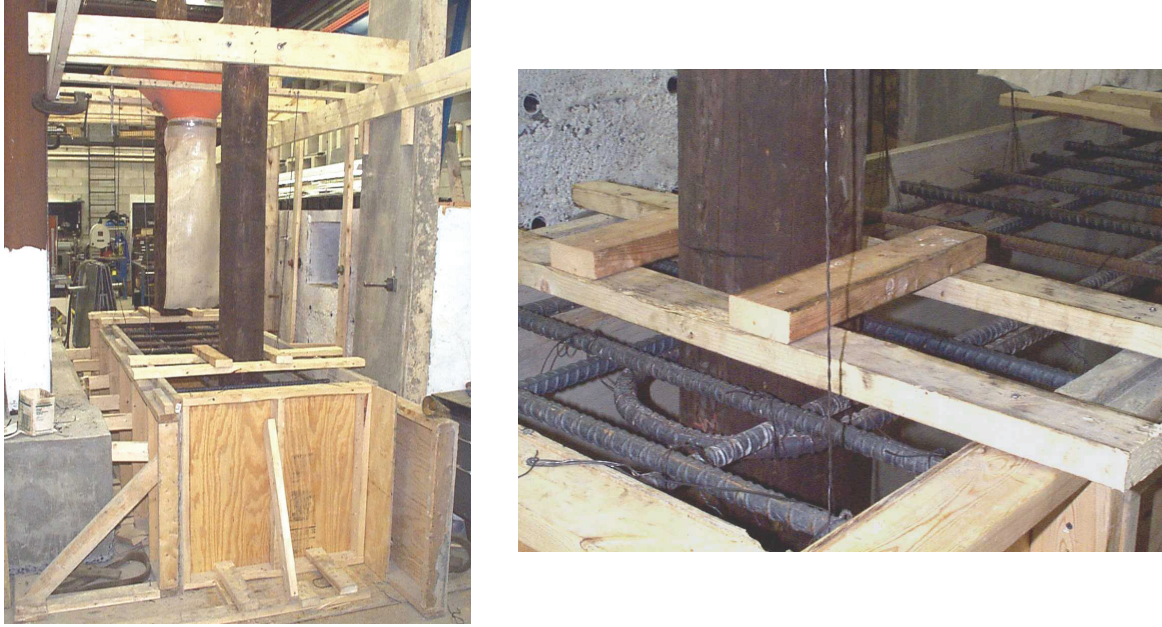
Figure 4-12. Construction of the timber pile foundation. Photo on the left shows the formwork with the timber pile specimens; photo on the right shows a close up view of specimen T2.

4.6 EXPERIMENTAL SETUP

The test rig employed for the testing of these specimens was similar to that used for the steel pile foundation specimens (Shama et al., 2002). Lateral load was supplied by a 500-kN MTS hydraulic actuator anchored to the reaction frame at an angle of 56° to the horizontal and connected to the specimen. To prevent slipping at the lateral actuator-pile interface, two 450-mm by 305-mm by 25-mm mild steel plates confined six 450 by 305 by 19-mm pieces of plywood. The plywood each had a central, circular hole, marginally smaller than the pile diameter at the related location, and were cut at an offset of 25-mm from their centerline to facilitate placement and clamping. This arrangement was clamped to the pile by four 25-mm threadbars, which were subsequently stressed to prevent any slippage (see photographs, figure 4-13).

The vertical load due to gravity was provided by a 350-kN capacity ± 50-mm stroke Parker servo-controlled hydraulic actuator. This actuator was operated in load control and connected to the W10 by 77 lever beam. This beam was anchored to the strong floor at one end using a pair of 32-mm diameter high-strength prestressing threadbars. The force in the MTS lateral actuator actively controlled the vertical actuator.

Figure 4-13. Test rig of the timber pile foundation specimens showing: (left) connection between actuator and specimen, and (right) anchor beam.

The W10 by 88 steel beam was employed to anchor the specimen to the strong floor to provide sufficient restraint against translation and uplift during the tests. The beam was set on a rocker bearing, which transmitted the anchoring load to the concrete cap specimen. The steel beam was anchored to the laboratory strong floor at one end using a pair of 32-mm high alloy prestressing threadbars and was anchored from the other side using three thread rebars. The two 32-mm bars were prestressed to a force of 310-kN each. The resulting force clamping the specimen to the strong floor via the beam was 1860-kN.

4.7 INSTRUMENTATION AND DATA ACQUISITION

The instrumentation used for this experiment consisted of sonic transducers, linear resistance potentiometers, and load cells. The load cells were 500-kN and 650-kN devices supplied with the MTS and Parker actuators, respectively. Two sonic transducers (S-T) [MTS Temposonics] model number DCTM-4002-1 with stroke length of $\pm$ 150-mm was used for the measurement of lateral displacement. The upper one (as shown in figure 4-14) was at the same height as the centerline of the inclined actuator. The second transducer was mounted at the same

CENTER LINE of
LATERAL LOAD

56^0

REFERENCE
FRAME

POTENTIOMETERS
FOR MEASURING
CURVATURES

S-T FOR LOAD CONTROL
ANCHOR BEAM

L2

L1
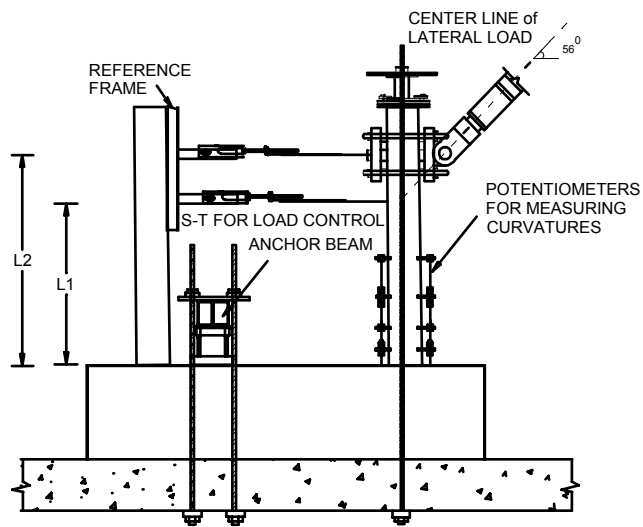
(a) SIDE ELEVATION

	PHASE1	PHASE2
L1	1400	800
L2	1980	1380

|← 1372 →|← 1067 →|

LEVER ARM

VERTICAL
ACTUATOR

DIMENSIONS
IN mm
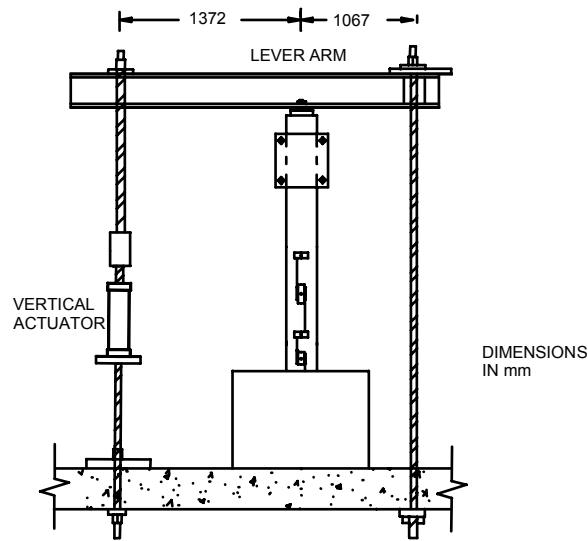
(b) END ELEVATION

**Figure 4-14. Instrumentation configuration for timber pile
experiments.**

height of the point of action of the actuator that is at the lateral loading inflection point and was used to provide the input signal for the inclined actuator, which operated in displacement control.

Eight linear resistance potentiometers were utilized to measure pile rotations/curvatures in pairs. Two were each mounted on an aluminum chassis fabricated from a rectangular tube, one covering the upper gauge length, the other covering the adjacent lower one. The stroke for these linear potentiometers was $\pm$ 13-mm. Each chassis was bolted to a 75-mm threaded rod that was screwed into the pile. Aluminum tubes serving as contact surfaces for the brass rods coupled to the potentiometers were also similarly attached at alternate gauge lengths. Prior to each test, the potentiometers and transducers were manually checked to ascertain their functionality and all the instruments were set at their balance point.

Curvature and rotations (ϕ_i, α_i) over the I-th gauge length were calculated from:

$$\phi_i = \frac{\Delta_{pi}}{L_{pi}L_{gi}} \tag{65}$$

and

$$\alpha_i = \frac{\Delta_{pi}}{L_{gi}} \tag{66}$$

in which Δ_{pi} is the algebraic difference of readings from potentiometer pairs, L_{pi} is the center-to-center distance between the potentiometer pairs and L_{gi} is the gage length.

4.8 EXPERIMENTAL PROGRAM AND RESULTS

The experimental program consisted of testing both specimens in two phases. The specimens in phase one were tested at cyclic drift amplitudes that ranged from $\pm$ 1 to $\pm$ 6 percent with an average M / Vd_p ratio of six. This value is representative of a class of friction piles embedded in soils characterized by high shear strength (see figure 4-6). In the second phase, however, the length of the same specimens were reduced so that an average M / Vd_p ratio of 3.5 was obtained. This value is representative of a broad range of cohesionless and cohesive soils. As a result of reducing the effective length of the specimens, greater drift angles could be

106

obtained. This enabled the performance of the connection to be examined under drifts that may not be attained because of the actuator stroke limitations in the first phase. Therefore, the specimens in phase two were tested at cyclic drift amplitudes that ranged from ± 3 to ± 12 percent. Another reason for conducting the second phase of testing for each specimen was to examine the theoretical results obtained. One important result is the independence of the connection resistance with respect to the effective length of the pile.

Each of the specimens was tested for a minimum of two cycles per drift amplitude. Testing was conducted under displacement control where the specimens were first pushed then pulled. The command signal was provided by an analog function generator in the form of a sine wave with a one-minute cycle period. A constant gravity load was taken as 133-kN for specimen T1 in the first phase and the following relationship was used to relate the lateral actuator force to that of the vertical actuator:

$$P_{va} = \frac{7}{16}\left(133 + 0.325P_{da}\right) \tag{67}$$

It was observed, however, that no tension uplift was attained using this relationship because of the high value chosen for the constant gravity load. One of the main goals of this experimental study is to investigate the performance of the connection under variable tension and compression uplift. Consequently, the following relationship was utilized in the other three experiments:

$$P_{va} = \frac{7}{16}\left(100 + 0.88P_{da}\right) \tag{68}$$

The vertical actuator increased the axial force in the pile when the lateral actuator was pushing and decreased it during pulling.

4.8.1 Specimen T1

Specimen T1 represents an exterior timber pile foundation with a typical "as-built" pile-cap connection. The specimen was tested with a variable axial load considered to be representative for this class of pile.

Phase (1)

The 500-kN MTS servo-hydraulic actuator operated in displacement control was used to induce the lateral load. The actuator was mounted at an angle of $56°$ along with the axial actuator to simulate the uplift that may be exerted in a physical scenario. The 350-kN Parker servo-hydraulic vertical actuator induced the variable axial load. Both actuator outputs are related to induce a total axial load governed by equation (68). The specimen had a clear height of 1,400-mm $\left(M/Vd_p = 6.2\right)$ above the concrete base surface.

In this experimental phase, the specimen was tested with two reversed cycles at drift amplitudes of ± 1, ± 2, ± 3, ± 4, ± 5, and ± 6 percent, respectively. The specimen behavior conformed well to the theoretical model proposed in this study. According to the theoretical model, it was expected that the failure of the specimen would not occur, as the crushing perpendicular to the grain governs the specimen strength. Such wood crushing occurred during the course of the test. The marked pinching of the force displacement plot (figure 4-15) is indicative of such crushing perpendicular to the grain within the embedment. A gap between the timber pile and the concrete appeared on the pull side of the four percent drift. This gap opened and closed during the course of testing at the five percent and six percent cycles (see photographs of the opening and closing of the gap in figure 4-17). Apart from some minor cracks at the cap beam surface, no pronounced damage was observed in both the timber pile at the hinge zone or on the cap beam.

Figure 4-16 plots the theoretical and experimental moment-axial load interaction diagram for specimen T1. The maximum lateral force achieved during that test was 65-kN. The vertical component of this force was not enough to induce tension uplift during the pulling of the specimen. The maximum horizontal force achieved was 36-kN, which is well below the yielding strength of the specimen. This observation assesses the theoretical model. According to equation (40), the wood crushing resistance is 38-kN, which is well below the flexural strength of the pile (61-kN).
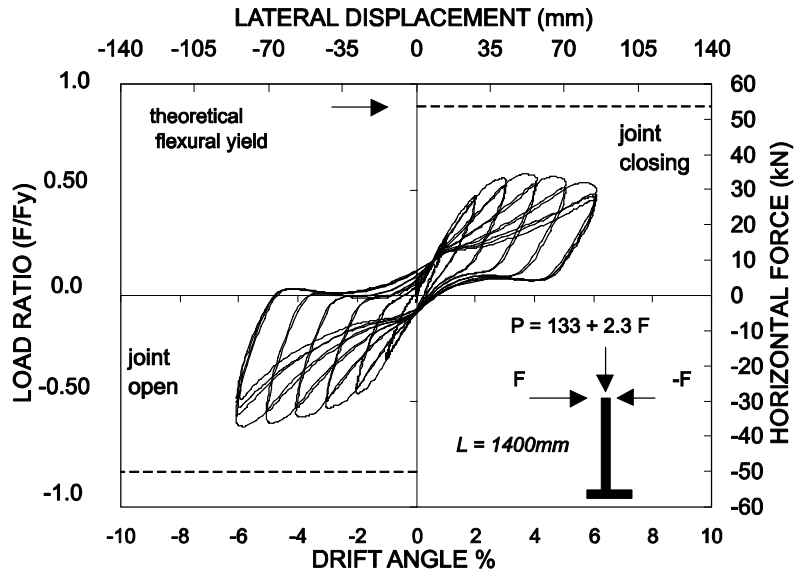
Figure 4-15. Timber pile specimen T1 (phase 1); lateral load-displacement relationship.
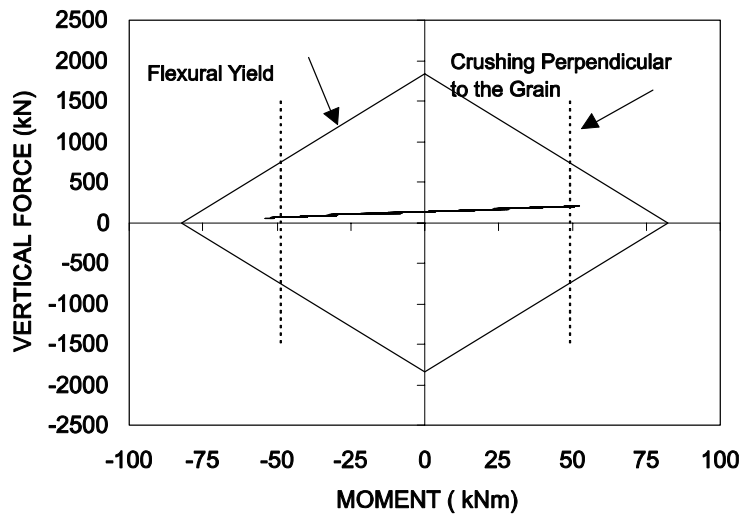
Figure 4-16. Experimental and theoretical lateral load-axial load interaction diagram for specimen T1 (phase 1).
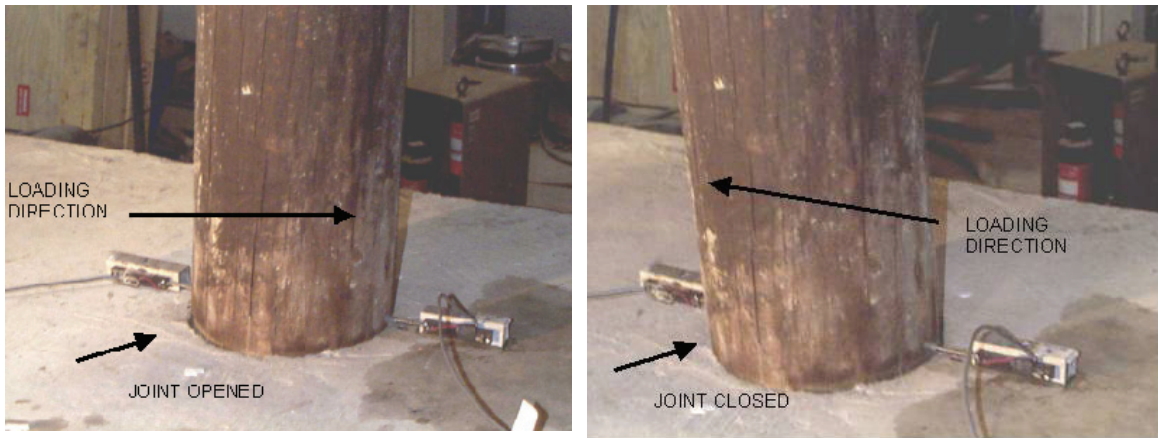
Figure 4-17. Gap that occurred between the pile and the concrete cap. The top photograph shows the joint opening, while the lower photograph shows the joint closing.

Phase (2)

The specimen clear height was reduced to 800-mm $\left(M/Vd_p = 3.55\right)$ in this experimental phase. The specimen was then tested with two reversed cycles at drift amplitudes of ± 3, ± 6, ± 8, ± 10, and ± 12 percent drift, respectively. Figure 4-18 presents the horizontal force displacement relationship. The pile behaved in a similar manner to previous phase one tests during the course of the ± 3 and ± 6 percent drifts. The width of the gap between the pile and concrete increased, and was very pronounced at the eight percent drift as a result of crushing of the wood within the embedment zone. The specimen exhibited tension uplift during this experimental phase (see figure 4-19). The tension uplift helped in slipping of the pile within the embedment zone as the pile walked out of the socket during the 10 and 12 percent drifts (see photographs of the connection under 12 percent drift in figure 4-20). It was obvious at the conclusion of testing (at the end of the second cycle at 12 percent drift), that no noticeable damage was observed in either the timber pile at the hinge zone or on the cap beam. The maximum horizontal force achieved was 68-kN. Figure 4-21 displays the performance of specimen T1 with the two phases of loading shown in terms of drift-moment relationship.
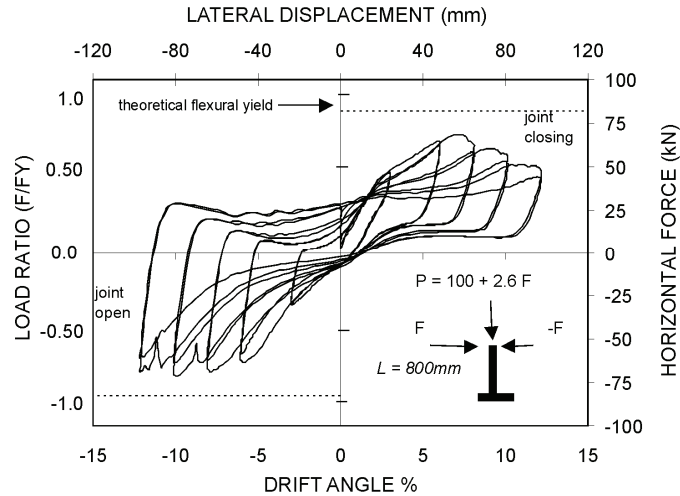
Figure 4-18. Timber pile specimen T1 (phase 2): lateral load-displacement relationship

4.8.2 Specimen T2

Specimen T2 represents a conservative design for an exterior pile to cap connection. According to this design, the pile was embedded to a distance of 1.5 d_p in the concrete foundation base. An additional U shape # 9 rebar was added to the original reinforcement to counteract forces that may cause spalling of the concrete in the end region of the cap. The objective of the experiment is to determine whether or not this design will improve the seismic performance of the connection.

Phase (1)

The lateral load was exerted by the 500-kN MTS servo-hydraulic actuator operated in displacement control and mounted at an angle of $56°$. The 350-kN Parker servo-hydraulic vertical actuator induced the variable axial load. Both actuator outputs are related to induce a total axial load governed by the equation (68). The specimen had a clear height of 1,400-mm $(M/Vd_p = 6.2)$ above the concrete base surface.

111
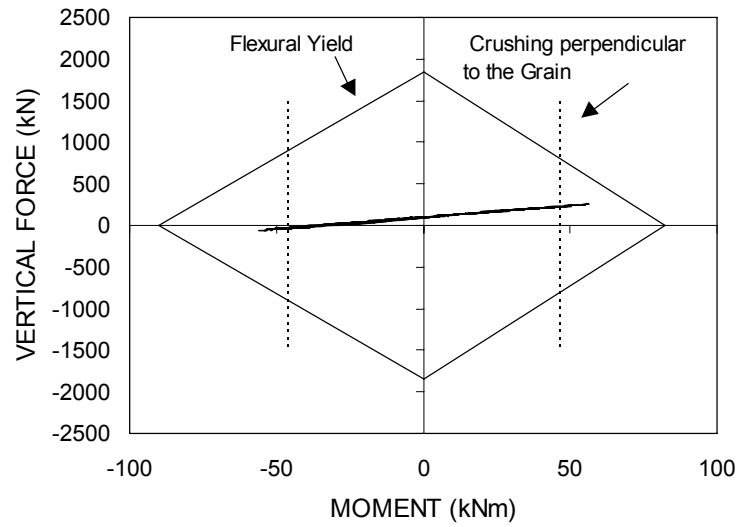
Figure 4-19. Experimental and theoretical lateral load-axial load interaction diagram for specimen T1 (phase 2).
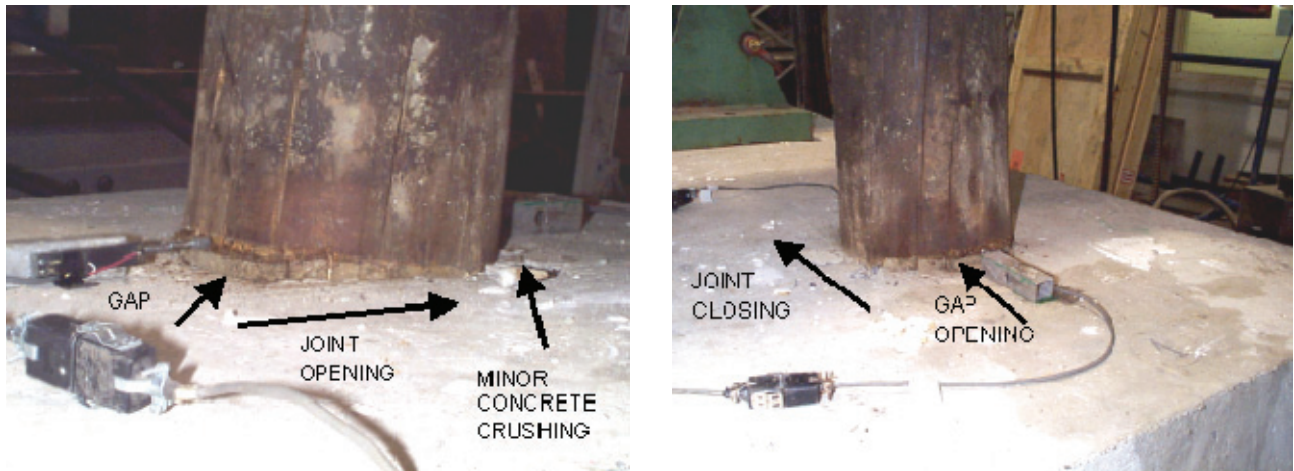
Figure 4-20. Specimen T1 connection under high drifts (phase 2). Joint opening shown on left; joint closing shown on right.
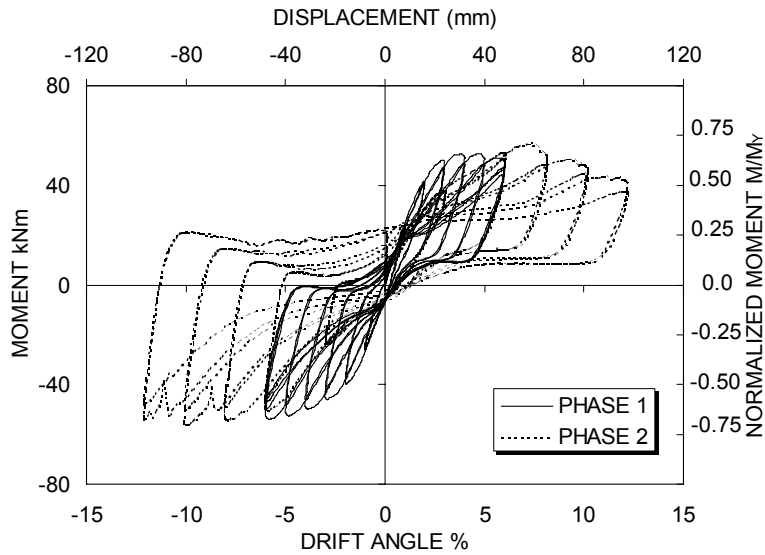
Figure 4-21. Moment rotation relationship of specimen T1.

In this experimental phase, the specimen was tested with two reversed cycles at drift amplitudes ± 1, ± 2, ± 3, ± 4, ± 5 and ± 6 percent, respectively. The force-drift behavior of the specimen during this experimental phase is illustrated in figure 4-22. The specimen did not attain the theoretical flexural yield up to the end of the ± 3 percent drift. A gap was observed between the timber pile and the adjacent concrete during the first cycle at the ± 4 percent drift.
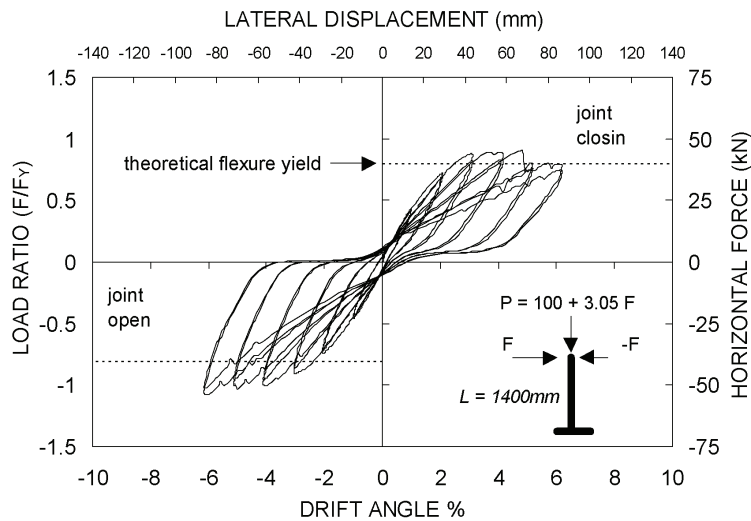
Figure 4-22. Timber pile specimen T2 (phase 1): lateral load-displacement relationship.

113

This gap continued to increase in width by alternately opening and closing during the course of cyclic testing. In fact, this behavior agrees with the assumption made for determining the theoretical nominal flexural capacity of the pile. During the $\pm$ 5 percent drift, there was evidence of tension fibers fracturing, resulting in a drop in strength of 8-kN. Strength degradation continued during the $\pm$ 6 percent drift, and tensile splitting of fibers was more pronounced.

Figure 4-23 plots the theoretical and experimental moment-axial load interaction diagram for the first experimental phase of specimen T2. The maximum horizontal force achieved during that test was 45-kN and 54-kN in push and pull, respectively. The theoretical yield force was attained. However, the nominal flexural capacity of the pile was not achieved.
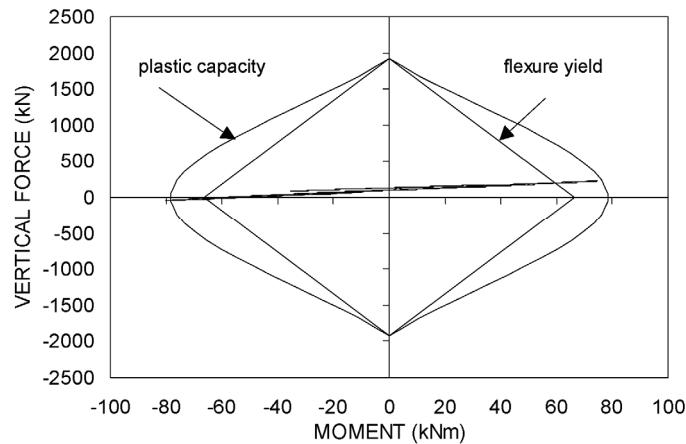
**Figure 4-23. Experimental and theoretical moment-axial load
interaction diagram for specimen T2 (phase 1).**

Phase (2)

In the second experimental phase, the specimen clear height was reduced to 800-mm $(M/Vd_p = 3.50)$ and then tested with two reversed cycles at drift amplitudes $\pm$ 3, $\pm$ 6, $\pm$ 8 and $\pm$ 10 percent, respectively. The force-drift behavior of the specimen during this experimental phase is illustrated in figure 4-24. Fiber fracturing was very pronounced during the second cycle at $\pm$ 6 percent drift. Accordingly, strength degradation was very noticeable at the $\pm$ 8 percent drift and tensile splitting of fibers was obvious. Two more cycles at $\pm$ 10 percent evidenced that the connection failed in flexural bending mode. The concrete base did not experience any major damage, except for some surface cracks within the cover zone. Photographs of the connection after failure are shown in figure 4-26.

Figure 4-25 plots the theoretical and experimental moment-axial load interaction diagram for the second experimental phase of specimen T2. The maximum horizontal forces attained during that test were 62-kN and 78-kN in push and pull, successively. The specimen exhibited an over-strength value of 1.1. Figure 4-27 displays the performance of specimen T2 under these two experimental phases.
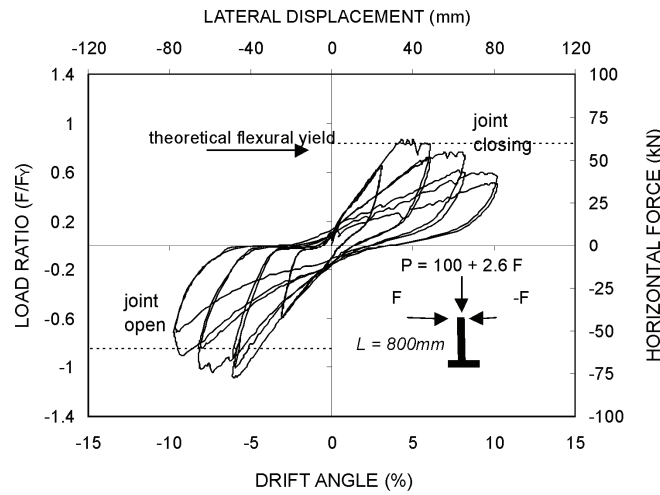
Figure 4-24. Timber pile specimen T2 (phase 2): lateral load-displacement relationship.
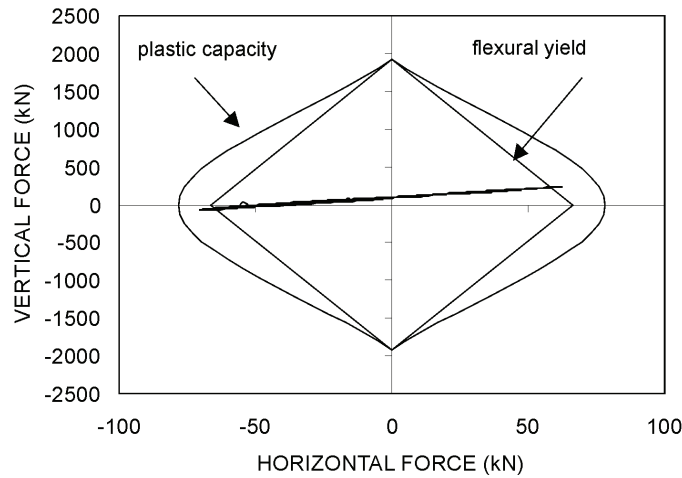
Figure 4-25. Experimental and theoretical lateral load-axial load interaction diagram for specimen T2 (phase 2).

Figure 4-26. Specimen T2 connection after failing in flexural bending mode. Photo on left shows the front view; photo on right shows the rear view.
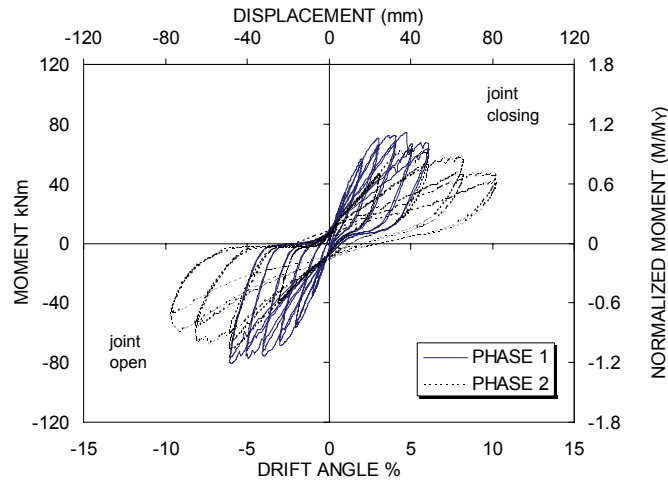
Figure 4-27. Moment rotation relationship of specimen T2.

4.9 PUSHOVER THEORY VERIFICATION USING EXPERIMENTAL RESULTS

The force displacement algorithm presented in this section, incorporating the effect of joint rotation due to crushing perpendicular to the grain, is validated by comparing its results to those from the experimental program.

Figures 4-28 and 4-29 display the cyclic horizontal-force displacement relationships for the two specimens tested in the experimental program described above. The computational

monotonic pushover curves are displayed in the same figures. It can be observed that the monotonic curves effectively captured the cyclic experimental behavior for the two experiments.

It should be noted that the effect of joint rotation due to crushing perpendicular to the grain was not pronounced for specimen T2 experiments, as flexural bending failure dominated the connection behavior. Expectedly, the computational model converged well to the experiment in its two phases, as this is the same case that was examined in the previous section. Specimen T1, which exhibited crushing perpendicular to the grain, also converged satisfactorily to the theoretical model. Hence, the theoretical model for such connections is validated.

4.10 DESIGN REQUIREMENTS FOR TIMBER PILE-TO-CAP CONNECTIONS

Theory and experiments have shown that pile-to-cap connections constructed with an embedment depth equal to one pile diameter had very ductile performance under cyclic lateral loading. On the other hand, increasing the embedment of these connections to 1.5 d_p resulted in a stronger but slightly less ductile connection. For design purposes, both behaviors are preferred to occur simultaneously. Therefore, the following condition should be satisfied for design objectives:

$$\lambda M_y = M_j(\theta) \tag{69}$$

in which λ is an over-strength factor. By substituting equations 34 and 42 into 69 and simplifying, an expression for the normalized embedment depth for such specimens can be obtained as:

$$\left(\frac{l_{emb}}{d_p}\right) = 0.5\left(\frac{f_{b0}}{f_{pc0}}\right)^{\frac{3}{7}}\left(\frac{\varepsilon_{cp0}}{\theta_j}\right)^{\frac{1}{7}} \tag{70}$$

where ε_{cp0} equals 0.003 and θ_j is the design connection rotation arising from crushing perpendicular to the grain. It is suggested that θ_j is 0.03 rad.
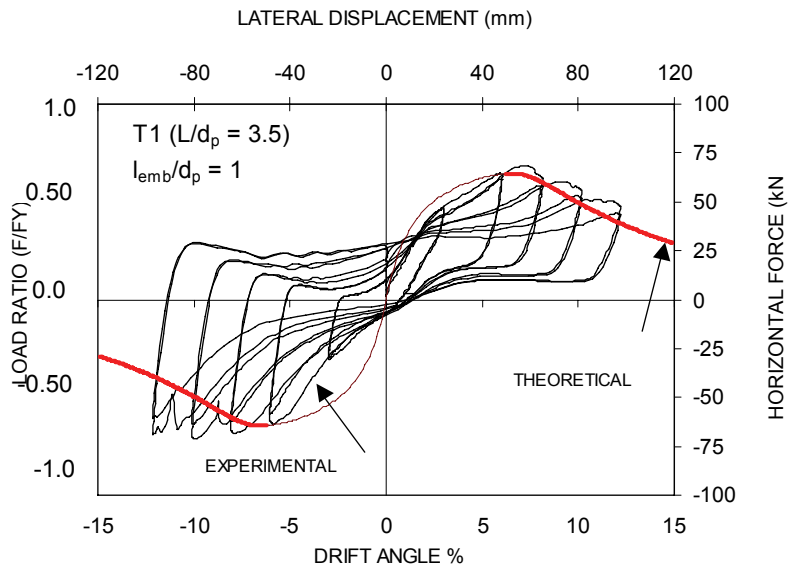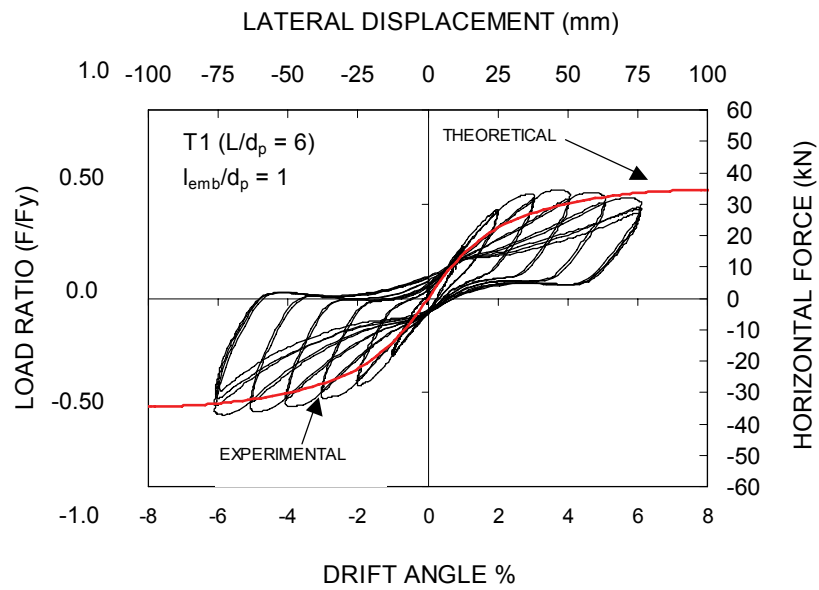
Figure 4-28. Comparison of the theoretical model for timber behavior with Specimen T1.
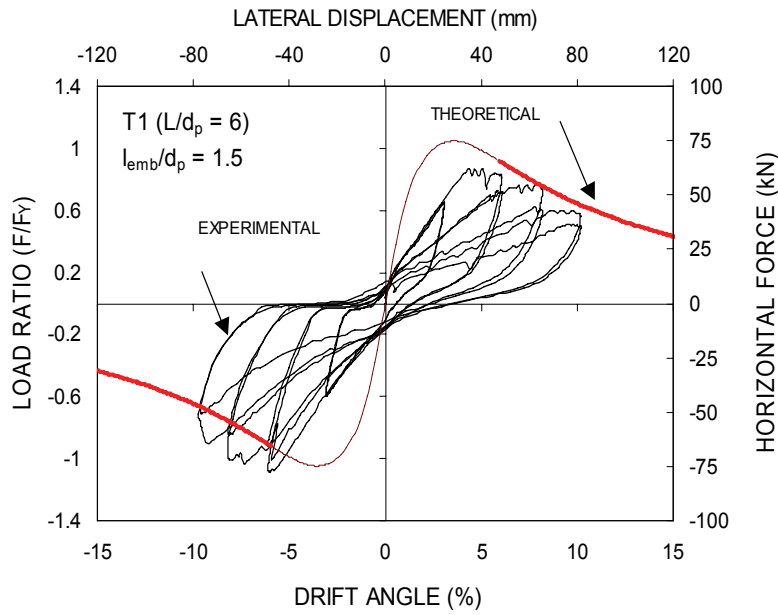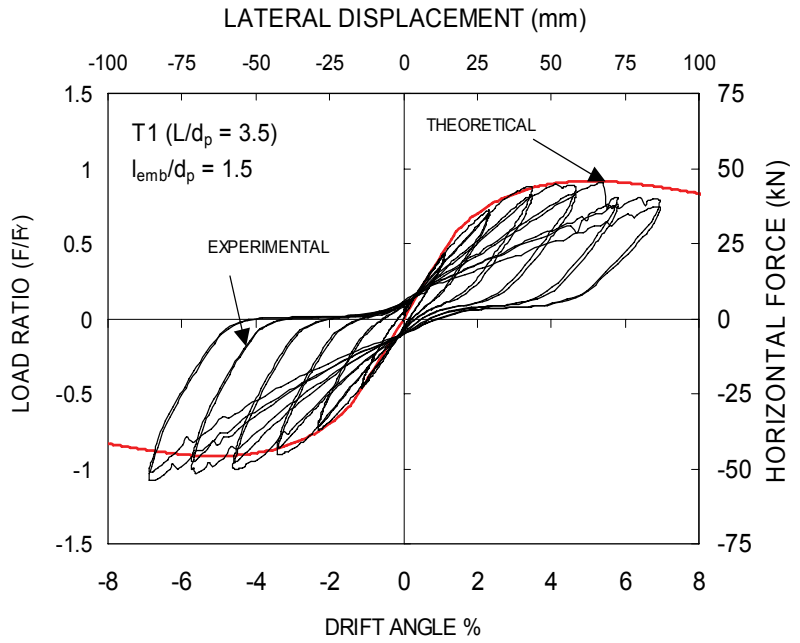
Figure 4-29. Comparison of the theoretical model for timber behavior with specimen T2.

4.11 SUMMARY AND CONCLUSIONS

In this section, comprehensive theoretical and experimental studies were performed on timber pile foundations to evaluate the seismic performance of the pile-to-concrete cap connection. A theory was developed to determine the performance of such a connection under lateral loads. The theory was implemented in a comprehensive computational pushover algorithm. A series of experiments were conducted to validate the theory. The following conclusions can be drawn from this study:

1. The extensive study performed showed the significance of the compression perpendicular to the grain in evaluating the performance of timber pile-to-concrete cap connections under lateral loads.

2. The study showed that as the embedment length increases, the connection lateral resistance increases. On the other hand, adjusting the embedment length will render a more ductile connection.

3. The influence of wood hardness is very important in determining the ultimate lateral resistance of timber pile-to-concrete cap connections. As the ratio f_{cp0}/f_{c0} (which is an indication of wood hardness) increases, its ultimate lateral resistance capability improves.

4. The embedment depth of the timber pile inside the concrete pile cap foundation is governed by bending as well as compression perpendicular to the grain stresses of the timber pile.

5. The expected maximum seismic drift and base shear capacity coefficient are two important parameters in determining and optimizing the required embedment depth of the timber pile into the concrete cap beam.

6. The study showed that pile-to-cap connections constructed with an embedment depth equal to one pile diameter performed very satisfactorily and does not require any retrofit. On the contrary, increasing the embedment depth of such connections without looking into the material properties may result in a stronger, but slightly less ductile connection.

7. The theoretical model developed in the present study for determining the lateral force-deformation resistance of timber pile-to-cap connections compared favorably to the experimental results.

SECTION 5
SEISMIC VULNERABILITY ANALYSIS OF TIMBER BRIDGES

Damage to transportation systems can lead to traffic flow disturbance, as has been well documented in past earthquakes. Bridges, key elements of a transportation system, need to be functional after an earthquake to prevent essential services in the traffic network from being interrupted. Consequently, it is necessary to assess how vulnerable these structures are to earthquakes of varying intensities.

The likelihood of structural damage caused by various levels of ground motion is usually expressed by a damage probability matrix or with fragility curves. The damage probability matrix provides probabilities of various anticipated damage states to a structure at a particular ground motion level. A fragility curve, however, describes the probability of a specific type of damage to the structure at different levels of ground motion. Fragility curves are developed in the present study to evaluate the seismic vulnerability of bridges under consideration.

5.1 REVIEW OF PREVIOUS WORK

Historically, fragility curves have been based on empirical field observations following damaging earthquakes (Basoz and Kiremidjian, 1997). More recently, Dutta and Mander have developed a fundamental mechanics-based approach from which fragility curves could be derived from first principles (Dutta and Mander, 1998). They validated this approach against experimental data. Detailed and simplified analytical models can be used when earthquake or test data do not provide sufficient information. The steps involved in these detailed analyses are summarized as follows:

- A structure is represented by an appropriate model, which includes inelastic behavior of all structural components.

- Artificial earthquake acceleration time histories corresponding to various seismological parameters (e.g., local soil conditions; epicentral distances; and magnitudes) are generated.

- Uncertainties in both the ground motion and structural component behavior are quantified to establish a set of earthquake-structure samples.

- A nonlinear time history analysis is performed for each sample and damage to structural components is assessed according to predefined damage criteria. These damage criteria are usually established from the available experimental results.

- From the severity of damage to various structural elements, an overall damage state is assigned to the entire structure.

- Fragility curves, which display the relationship of damage states and ground shaking parameters (e.g., peak ground acceleration), are then established.

One can realize that the analytical approaches followed thus far by various researchers (Hwang and Jaw, 1989; Hwang and Huo, 1994; Mullen and Cakmak, 1997) require high computational costs and substantial time and effort to perform, particularly when the structural model is more sophisticated.

An increasingly popular way of characterizing the seismic performance of structures is through the use of the capacity spectrum method (Shama et al., 2001a). In this method, the pushover capacity of the structure is converted to the acceleration-displacement response spectrum format and displayed in the same graph with the demand spectrum. In a deterministic analysis, the intersection of the two curves gives the expected level of performance. However, there are uncertainties associated with both structural capacity and variability of seismic demand. Based on these uncertainties, it is evident that there is a wide range of possible performance states, and the problem needs to be treated non-deterministically through the use of fragility curves.

The approach presented in this study to develop fragility curves stems from the capacity spectrum method, and takes the randomness associated with the structural capacity as well as the seismic demand into account. This method utilizes some experimental data from the present study in the formulation of the fragility curves.

5.2 FRAGILITY CURVE THEORY

5.2.1 Expected Seismic Resistance

The seismic demand of a structure can be represented in terms of a design code-like response spectrum. Based on the AASHTO guide specification for isolation, which adopts a linearized spectrum approach, the seismic demand is given by the lesser of

$$C_d = \frac{2.5A}{B_S} \tag{71}$$

and

$$C_d = \frac{SA}{T_{eff} B_L} \tag{72}$$

where C_d is the base shear demand; A is the peak ground acceleration at the site; S is the soil type factor; T_{eff} is the effective period of vibration and B_L, B_S are spectral reduction factors used to modify the elastic response spectrum for high damping; i.e., when the structure responds in the inelastic range to account for hysteretic damping resulting from nonlinear effects.

It is assumed here (in the same way as in the capacity spectrum method) that the peak response of the nonlinear structure is equal to the displacement of a substitute SDOF system with an effective period (T_{eff}) given by:

$$T_{eff} = 2\pi\sqrt{\frac{M}{K}} = 2\pi\sqrt{\frac{W/g}{F_y/\Delta}} = 2\pi\sqrt{\frac{\Delta}{C_c g}} \tag{73}$$

where Δ is the maximum displacement response; $C_c = F_y/W$ is the base shear capacity, in which F_y equals yield force of the pile bent; and W is the tributary weight.

The capacity spectrum method requires the intersection of the capacity and appropriately damped demand curve at a point that represents the inelastic displacement of the structure. By adopting this criterion and replacing the base shear demand in equations (71) and (72) with the

structural base shear capacity and rearranging, the peak ground acceleration can be determined by taking the <u>greater</u> of:

$$A = 0.4\,C_c\,B_s \qquad (74)$$

or

$$A = \frac{2\pi}{S}\sqrt{\frac{C_C\Delta}{g}}\,B_L \qquad (75)$$

For the present study, is assumed that the pile bent supporting the deck will govern the damage state of the entire bridge. Therefore, C_c in the above two equations denotes the base shear capacity coefficient of the bridge. Note that for bridge structures supported by flexible steel

5.2.2 Accounting for Uncertainty and Randomness in Fragility Curves

The nonlinear static capacity spectrum approach has gained wide acceptance among the earthquake engineering community during the last few years. This method does not account for any associated uncertainty with both the capacity and demand curves. Figure 5-1 shows a capacity spectrum graph, where the acceleration-displacement response spectrum for the ground motion is plotted with the pushover capacity of a bridge. Both the capacity and demand will have some probabilistic variation as shown in the figure. Therefore, there is a wide range of possible performance outcomes. The uncertainty associated with the final outcome results from the uncertainty in both the demand and capacity.

The uncertainty in the demand arises from the fact that the code-specified spectrum was established as a result of a statistical analysis, that was performed for a broad range of response spectra from actual earthquakes which occurred at different sites with common local soil conditions. At the location of the bridge considered, one can expect a series of seismic events with associated response spectra that may follow, or not, the ensemble used to establish the general code-specified spectrum at a particular site.

The uncertainty in the capacity can be due to different sources such as (i) the variability of structural material properties associated with strength, (ii) inelastic energy absorption and damping and (iii) dispersion in calculating the response due to approximations in modeling.
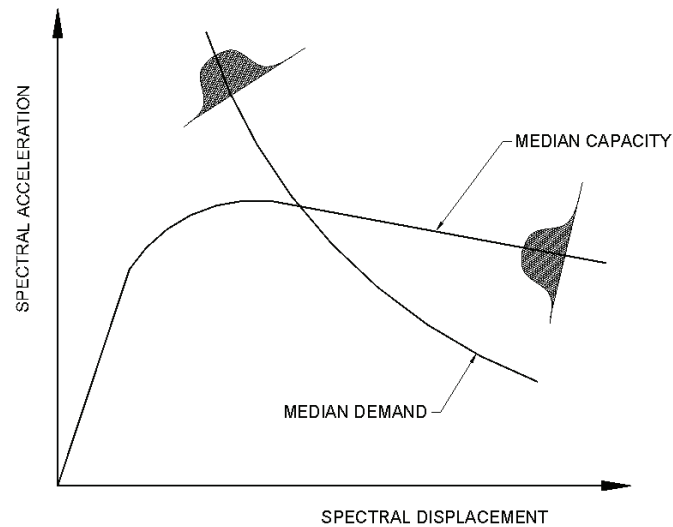
Figure 5-1. Capacity-demand acceleration-displacement spectra showing randomness in structural behavior and ground motion response.

The following assumptions are drawn in the present study following Kennedy et al., 1980:

The entire fragility curve and the uncertainty in that curve can be expressed in terms of the median ground acceleration, A, for a given drift limit to be attained times the product of two random variables. Thus, the ground acceleration $\breve{A}$ corresponding to a particular damage state is given by:

$$\breve{A} = A\varepsilon_c\varepsilon_d \tag{76}$$

where ε_c is the random variable with a median of unity that represents the uncertainty associated with capacity and ε_d is the random variable with a median of unity that represents the uncertainty associated with demand.

- Both ε_c and ε_d are log-normally distributed with logarithmic standard deviation of β_c and β_d, respectively.

- Both ε_c and ε_d are an accumulation of many small additive random variables. The distributions of these additive random variables are not necessary, since the central

125

limit theory can be applied. This theory states that, under very general conditions, as the number of variables in the sum becomes large, the distribution of the sum of random variables will approach the log-normal distribution irrespective of the distributions of the individual variables.

- Since both ε_c and ε_d are log-normally distributed, they can be represented by a composite log-normal random variable ε with a median of unity and logarithmic standard deviation β given by:

$$\beta = \sqrt{\beta_c^2 + \beta_d^2} \tag{77}$$

Hence, equation (76) can be rewritten as:

$$\breve{A} = A\varepsilon \tag{78}$$

The main advantage of this formulation is that the entire fragility curve and its uncertainty can be expressed by only two parameters, a median expected value (the 50th percentile) and a normalized logarithmic standard deviation.

Characteristics of the lognormal distribution which are useful to keep in mind when generating estimates of $\breve{A}$ and β are summarized in the following paragraphs (Benjamin and Cornell, 1970; Ang and Tang, 1975).

A random variable Y is said to be log-normally distributed if its natural logarithm X given by

$$X = \ln Y \tag{79}$$

where X is normally distributed with a mean value m_X equals $\ln \Theta$, in which Θ is the median of Y, and with the standard deviation of X equal to β, which will be called the logarithmic standard deviation of Y. Then, the coefficient of variation (COV) of Y is given by the relationship:

$$COV = \sqrt{(\exp \beta^2) - 1} \tag{80}$$

for β values less than about 0.5, this equation becomes approximately

$$COV \approx \beta \tag{81}$$

For a log-normal distribution, the median value Θ is used as the characteristic parameter of central tendency, and the logarithmic standard deviation β or the coefficient of variation are used as a measure of the dispersion of the distribution. The corresponding cumulative probability distribution function is given by:

$$F_Y(y) = \Phi\left[\frac{1}{\beta}\ln\left(\frac{y}{\Theta}\right)\right]$$
(82)

where Φ = standard Gaussian cumulative distribution function. Equation (82) can now be used to express uncertainty in terms of cumulative probability for a given ground acceleration. With perfect knowledge (i.e., only accounting for the random variability β), the cumulative probability $F(S_a)$, for a given spectral acceleration level, S_a can be obtained as:

$$F(S_a) = \Phi\left[\frac{\ln(S_a/A)}{\beta}\right]$$
(83)

where Φ (.) is the standard normal cumulative distribution function; S_a is the spectral acceleration amplitude for a period of $T = 1$ sec; A is the the median (expected value) peak ground acceleration for the given drift limit to be attained, as deterministically assessed by equation (75); and β is the normalized composite log-normal standard deviation, which combines aspects of uncertainty and randomness for both capacity and demand, determined according to equation (77). Based on the study by Peckan (1998) on the uncertainties arising from seismic ground motion, and Dutta and Mander (1998) on the randomness associated with different parameters affecting the structural capacity (e.g., material properties, model simplification, etc.), it is recommended that $\beta = 0.6$. This value was validated by Basoz and Mander (1999) against experiential fragility curves obtained from data gathered from the 1994 Northridge and 1989 Loma Prieta earthquakes.

5.2.3 Defining Bridge Capacity

Timber piles

If the principal of virtual work is adopted, one can obtain an expression for the base shear capacity of timber piles as:

$$C_c = \frac{(1+\rho)}{8\psi} \frac{f_{b0}}{f_{c0}} \frac{D}{H} \tag{84}$$

where D is the diameter of the timber pile; f_{b0} is the bending strength of the timber pile; f_{c0} is the compressive strength of the timber pile; and ψ is defined for this case as:

$$\psi = \frac{P}{P_y} = \frac{4wBL}{\pi n f_{c0} D^2} \tag{85}$$

The fixity efficiency of the plastic hinge given by $\rho = M_j/M_y$ participating in resistance and expressed in terms of the pile-to-cap connection efficiency is:

$$\rho = \frac{M_j}{M_y} = 3.7 \left(\frac{f_{pc0}}{f_{b0}} \right) \left(\frac{l_{emb}}{d_p} \right)^{2.33} \left(\frac{\theta_i}{\varepsilon_{cp0}} \right)^{0.33} \tag{86}$$

By substituting equation (84) into (75), one can obtain an expression for the expected peak ground acceleration for timber pile-to-cap connections:

$$A = \frac{2\pi}{S} \sqrt{(1+\rho)\frac{f_{b0}}{f_{c0}} \frac{D}{8\psi g} \theta_i} \ B_L \tag{87}$$

Braced Timber Pile Bents

Consider the braced timber pile bent shown in figure 5-2a, subjected to a lateral force C_{cb} W, where C_{cb} is the base shear capacity of the braced bent and W is the tributary weight from the deck. Applying the principle of virtual work for the potential mechanism shown in figure 5-2b yields:

$$EWD = IWD \tag{88}$$

$$C_{cb}W\Delta = \delta(T + C) \tag{89}$$

where Δ is the maximum displacement response of the bent; δ is the axial deformation of the braces; and T,C is the maximum tension and compression forces in the braces.

If the braces are rigid and no buckling will occur, the ultimate force of a brace in tension and compression is governed by the bearing resistance of its connection with the pile, hence:

$$T = C = f_c d_b t \tag{90}$$

in which d_b is the diameter of the lag screw used at the brace-pile connection; t is the thickness of the brace; and f_c is the compressive strength of the timber bracing.

Substituting equation (90) into (89) and rearranging, therefore, the base shear capacity of the braced timber bent can be expressed as:

$$C_{cb} = \frac{2f_c d_b t}{W} \cos\alpha = \frac{2f_c d_b t \cos\alpha}{n\psi \frac{\pi}{4} D^2 f_c} = \frac{8}{\pi} \frac{d_b}{D} \frac{t}{D} \frac{\cos\alpha}{n\psi} \tag{91}$$

in which α is the inclination angle of the bracing to the horizontal.

Substituting equation (91) into (75), and rearranging gives:

$$A = \frac{2\pi}{S} \sqrt{C_c \frac{\Delta}{g}} B_L = \frac{2\pi}{S} \sqrt{\frac{8}{\pi} \frac{d_b}{D} \frac{t}{D} \frac{\cos\alpha}{n\psi} h\theta_i} \ \ B_L \tag{92}$$

This equation defines the theoretical capacity of a braced timber pile bent in the transverse direction, where θ is the column/pile drift for the ith damage state.

5.2.4 Defining Displacement /Damage States

In Basoz and Mander (1999), five damage states are defined for highway system components. These are (1) none, (2) slight/minor, (3) moderate, (4) extensive and (5) complete. These damage states are adopted in the present study for bridges supported by steel and timber substructures. Table 5-1 lists these damage states for timber pile substructures and the corresponding failure mechanisms in developing analytical fragility curves adopted herein.

$F_b = C_{cb}W$

T

C

α

Δ

$F_b = T \cos \alpha + C \cos \alpha$

$C_{cb} = \dfrac{F_b}{W} = \dfrac{T+C}{W} \cos \alpha$
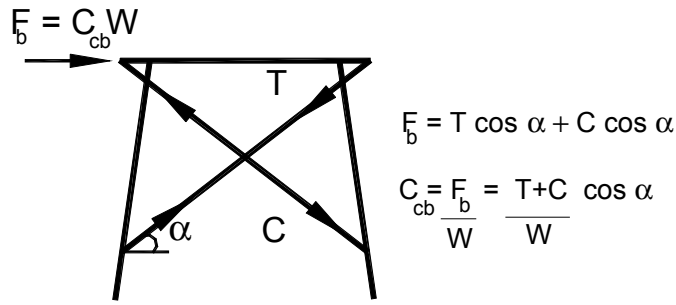
(a) Typical Geometry of Braced Timber
Pile Bent

Δ

δ

δ

δ
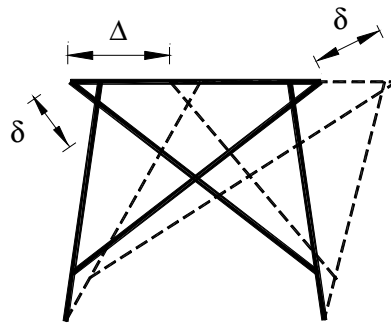
(b) Plastic Mechanism

Figure 5-2. Analysis of braced timber pile bents capacity.

5.2.5 Evaluation of Structural Damping

The spectral reduction factors can be obtained according to the equations given by Cheng and Mander (1997). These equations are based on regression analysis on the values given by Newmark and Hall (1982), and derived from an equivalent damping formulation as:

$$B_S = \left(\frac{\xi_{eff}}{0.05}\right)^{0.5} \tag{93a}$$

and

$$B_L = \left(\frac{\xi_{eff}}{0.05}\right)^{0.3} \tag{93b}$$

where ξ_{eff} is the effective viscous damping.

One way to evaluate energy absorption capability is to translate the hysteretic energy dissipation into equivalent viscous damping factors. The equivalent viscous damping ratio is defined as:

$$\xi_{eq} = \frac{1}{2\pi} \frac{E_{cycle}}{F_{max} \Delta_{max}}$$

(94)

in which E_{cycle} is the area enclosed within one cycle of loading; F_{max} is the average maximum strength observed in the push and pull directions during one cycle of loading; and Δ_{max} is the average maximum displacements in the push and pull directions of loading. The theoretical effective damping can be expressed in terms of drift amplitude as:

$$\xi_{eff} = \xi_o + \frac{2}{\pi}\eta\left(1 - \frac{1}{\mu}\right) = \xi_o + \frac{2}{\pi}\eta\left(1 - \frac{\theta_y}{\theta_i}\right)$$

(95)

in which ξ_o is the base damping ratio that is representative of the visco-elastic effects inherent in the structure; θ_y is yield drift amplitude; θ_i is the ith drift damage state; η is the energy absorption efficiency with respect to pure elasto-plastic behavior ($\eta = E_{cycle} / E_{EPP}$, where E_{EPP} equals the energy absorption capacity of one fully-reversed elastoplastic cycle).

Figure 5-3 presents experimental results for the piles with shaking in the longitudinal direction, where the effective damping is plotted against the ductility amplitude. The analytical curves associated with these experimental results are plotted in the same figure.

Based on the experimental results, the following values for efficiency and base damping ratio are suggested: $\xi_o = 0.03$, and $\eta = 0.15$ for wood that is in good condition. If the wood is weathered and prone to splitting, the above values should be reduced to two-thirds of the above—that is, $\xi_o = 0.02$ and $\eta = 0.10$.

Braced Pile Bents

The energy absorption characteristics of the braced timber pile bent subassembly tested during the course of this study are displayed in figure 5-4. The structure exhibited early inelastic behavior represented by the frictional effects in the connections. This led to high damping at low amplitude levels. Based on these plots, a value of 0.08 is suggested for the base damping ratio.

Table 5-1. Damage states for bridges supported by timber pile substructures.

Substructure Type	Damage State	Drift Limit (%)	Description of Damage
Unbraced Timber Pile Bents	Pre-Yield (DS=1)	2	No damage
	Onset of Damage (DS = 2)	3	Beginning of tensile splitting of fibers
	Moderate Damage (DS =3)	4	Noticeable splitting of fibers
	Extensive Damage (DS =4)	5	Noticeable fiber fracturing accompanied with loss of strength
	Complete Damage (DS =5)	7	Complete failure of pile and collapse of span
Braced Pile Bents	Pre-Yield (DS =1)	1	No damage
	Slight Damage (DS =2)	2	Minor longitudinal splintering in the timber bracing
	Moderate Damage (DS =3)	3	Local splitting around lag screws passing through the bracing and cap beam
	Extensive Damage (DS =4)	4	Extensive splitting in the bracing
	Complete Damage (DS =5)	5	Failure of bracing due to splitting and out-of-plane buckling
Timber Pile Foundation	Pre-Yield (DS =1)	2	No Damage
	Slight Damage (DS =2)	4	Beginning of crushing of wood perpendicular to the grain within the embedment length of the pile into the cap
	Moderate Damage (DS =3)	8	Gap occurs between the pile and concrete cap beam and crushing of wood perpendicular to grain increases
	Extensive Damage (DS =2)	10	The pile tends to walk-out from its socket and minor cracks in the concrete cap beam
	Complete Damage (DS =2)	15	Failure of foundation due to local failure in connection

Pile-to-Concrete Cap Foundations

The energy absorption characteristics of specimen T1 ($l_{emb}/d_p = 1$) in its two experimental phases are plotted in figure 5-5a, in terms of the drift angle-damping ratio relationship. The experimental results converged satisfactorily with the theoretical curve. On the basis of this graph, the following values are suggested for such a specimen: ordinary structural damping $\xi_o = 0.07$; and cyclic energy absorption efficiency $\eta = 0.20$.

Figure 5-5b presents experimental results as well as the theoretical relationship for specimen T2 ($l_{emb}/d_p = 1.5$) in its two experimental phases. The following values for efficiency and base damping ratio are suggested for such a specimen: ordinary structural damping $\xi_o = 0.06$; and cyclic energy absorption efficiency $\eta = 0.15$.

5.3 APPLICATION TO TIMBER PILE BENTS

The expected peak ground motion for unbraced timber pile bents can be expressed according to equation (87):

$$A = \frac{2\pi}{S}\sqrt{(1+\rho)\frac{f_{b0}}{f_{c0}}\frac{D}{8\psi g}\theta_i}\ \ B_L \tag{96}$$

and for braced timber pile bents as:

$$A = \frac{2\pi}{S}\sqrt{\frac{C_c\Delta}{g}}B_L = \frac{10}{S}\sqrt{\frac{d_b\, t\,\theta_i\, h}{n\psi D^2 g}}\cos\alpha\ \ B_L \tag{97}$$

The following assumptions have been made in the analysis:

- Timber can be represented by a median bending and compressive strengths of 40-MPa and 35-MPa, respectively.

- The number of piles in a bent or a pile cap is taken as $n = 5$ and the diameter of timber piles is assumed to be $D = 300$-mm.

- Dry pine is used for the bracing with dimensions 75-mm by 250-mm.

- The deck width is taken as for a two-lane roadway with $B = 8.5$-m.
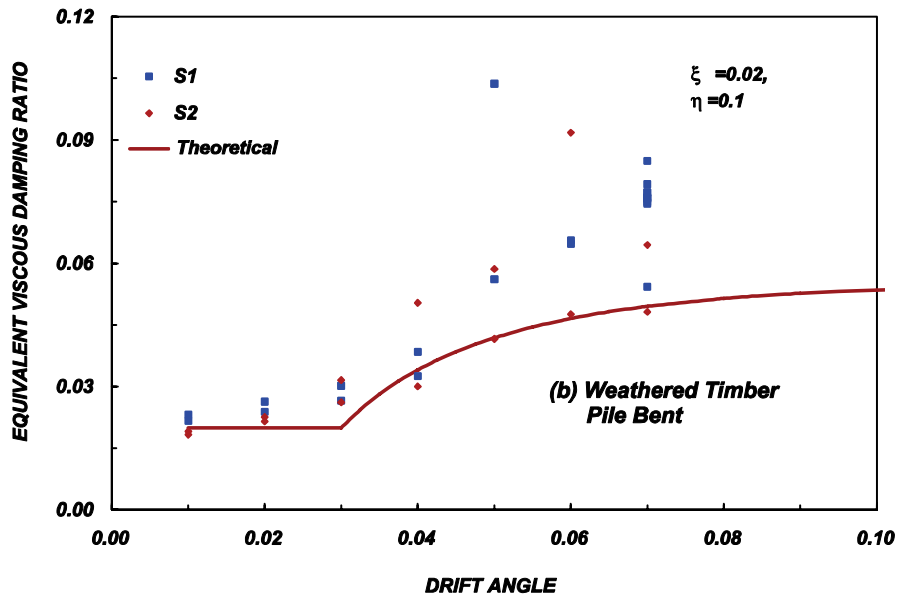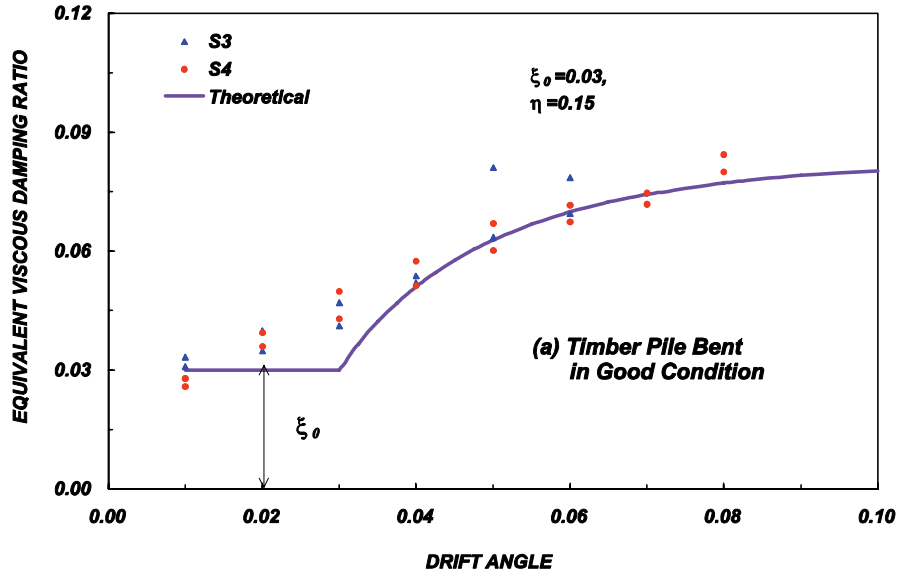
Figure 5-3. Energy absorption characteristics of unbraced timber pile bents.
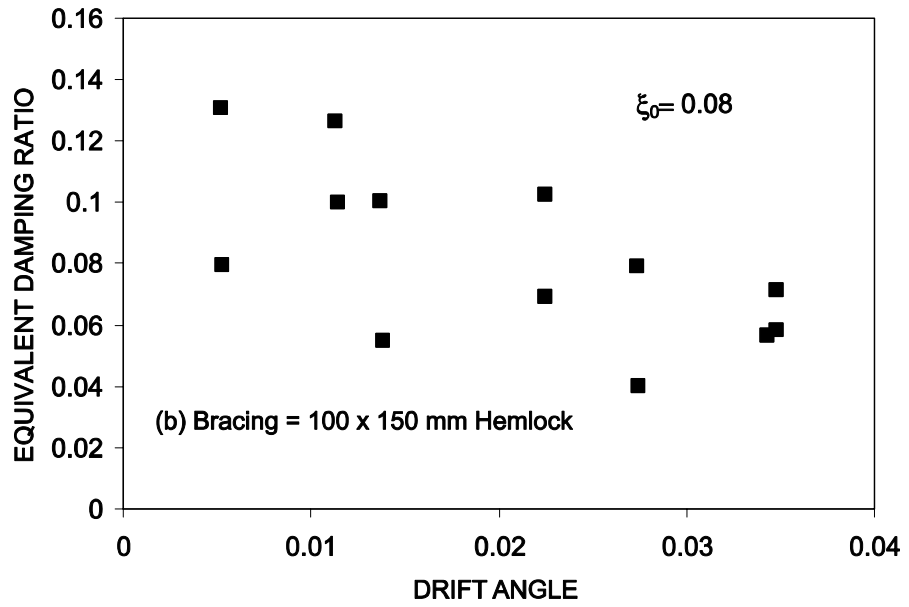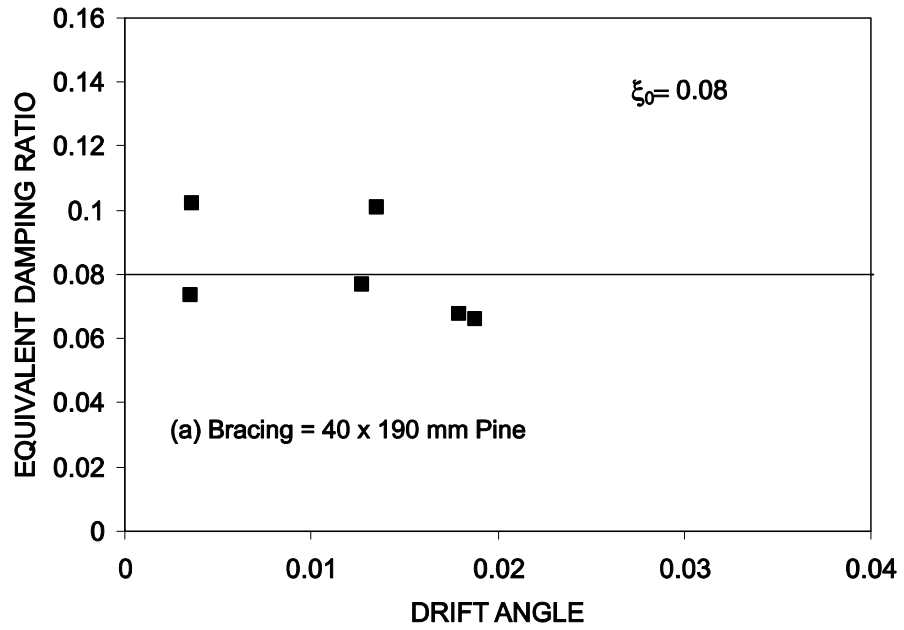
Figure 5-4. Energy absorption characteristics of braced timber pile bents.
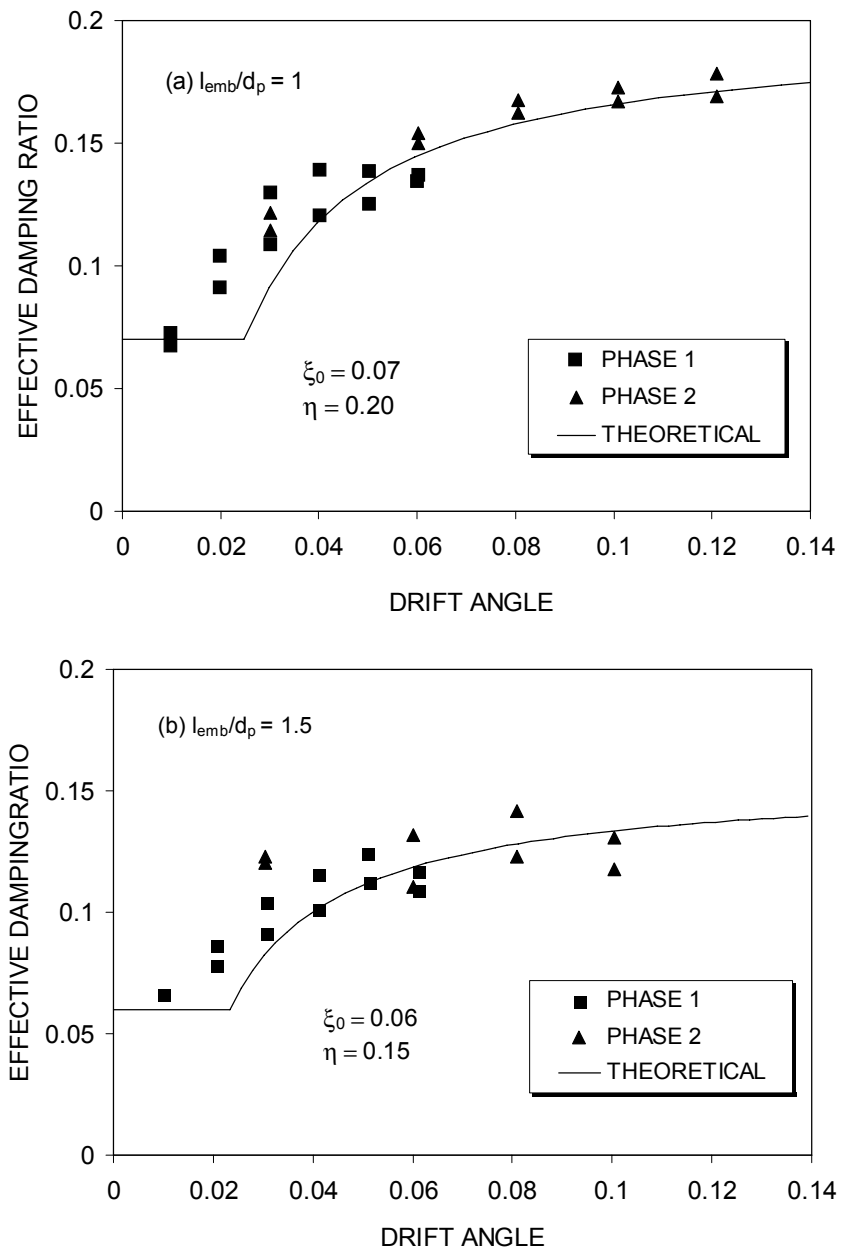
Figure 5-5. Energy absorption characteristics of timber pile-to-cap connections.

- The unit weight of all-timber and timber-concrete decks is w = 4-kPa and 7-kPa, with representative span lengths of L = 6-m and 8-m, respectively.

- Lag screws with diameter 22-mm are used for the connections between the bracing and the piles.

- The vertical distance h from the connection of the bracing to the transverse beam is 4-m. Consequently, the inclination of the bracing α can be determined as:

$$\alpha = COS^{-1} \frac{B}{\sqrt{B^2 + h^2}} = 25^0$$

Based on the above assumptions, the ratio of the axial applied load to the axial yield load ψ was determined according to equation (85) as 0.02 and 0.038 for timber and concrete decks, respectively.

Table 5-2 presents the different values for the parameters used in determining the expected peak ground acceleration of braced timber pile bents for different damage states.

Figures 5-6 and 5-7 display fragility curves for bridges supported by braced timber pile bents, with motion along the transverse and longitudinal directions for different states of damage. One can observe that concrete deck bridges are more vulnerable to damage than timber deck bridges, which corroborates the aforementioned empirical field evidence from the 1964 Alaska earthquake. For example, 43 percent of timber pile bents will experience slight damage in their bracing for spectral acceleration S_a = 0.4-g if the deck is concrete. On the other hand, only 29 percent of timber pile bents will sustain damage for the same spectral acceleration if the deck is timber. Furthermore, 32 percent of timber pile bents will sustain slight damage in the piles at S_a = 0.4-g if the deck is concrete. This value may reduce to 14 percent if the deck is timber.

Figure 5-8 presents a comparison between concrete and timber deck bridges on timber pile bents. This comparison was done in terms of slight damage for different orientations of ground motions. It can be observed that the bracing system is very vulnerable to damage. However, such damage is not serious, as the bracing can easily be replaced while bridge is in service.

Table 5-2. Expected peak ground motions for existing timber pile bents.

Damage State	Drift (percent)	B_L (spectral reduction factor)	A_i Transverse (braced) (g)		A_i Longitudinal (unbraced) g	
			Timber Deck	Concrete Deck	Timber Deck	Concrete Deck
1	0.02	1.17	0.43	0.31	0.35	0.25
2	0.03	1.26	0.53	0.38	0.46	0.33
3	0.04	1.30	0.61	0.44	0.65	0.48
4	0.05	1.33	0.68	0.49	0.79	0.58
5	0.07	1.36	0.80	0.58	1.01	0.73
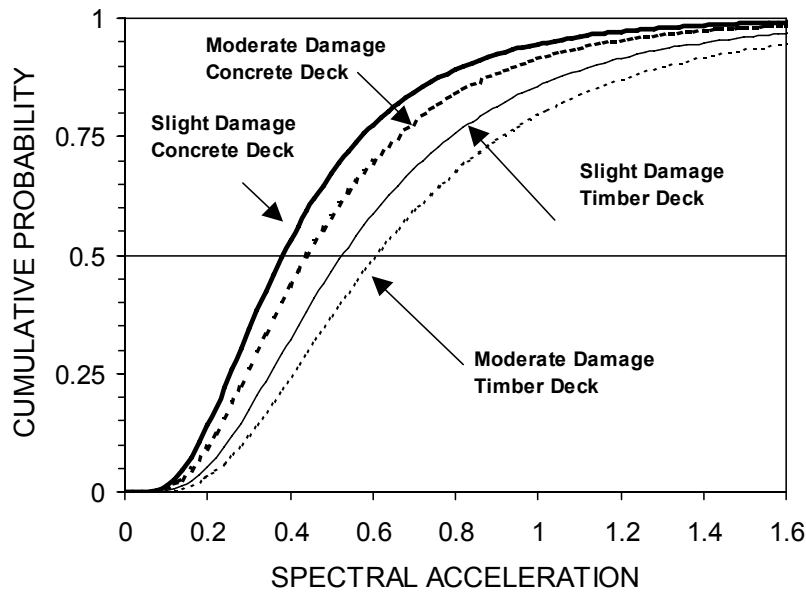
Figure 5-6. Fragility curves for bridges supported by braced timber pile bents with shaking along the transverse direction.
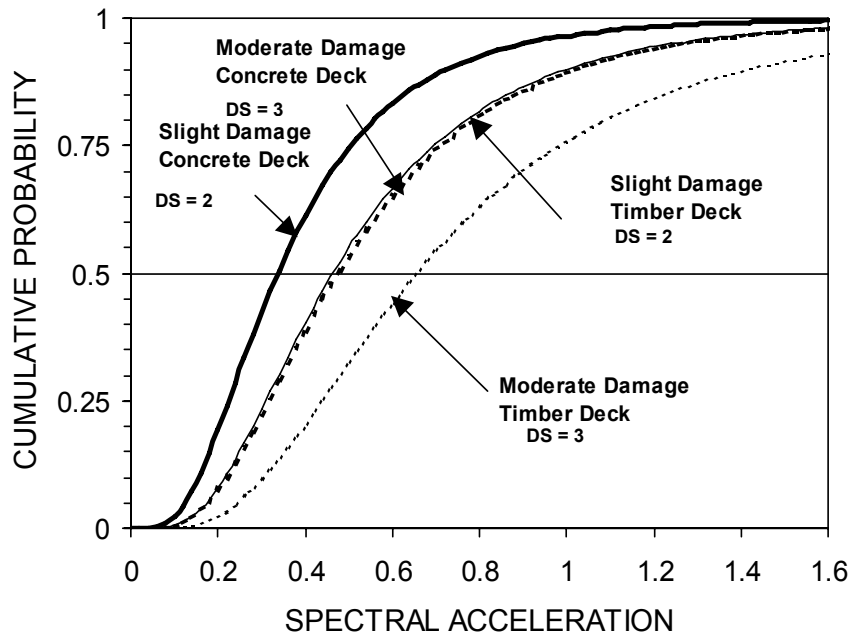
Figure 5-7. Fragility curves for bridges supported by braced timber pile bents with shaking along the longitudinal direction.
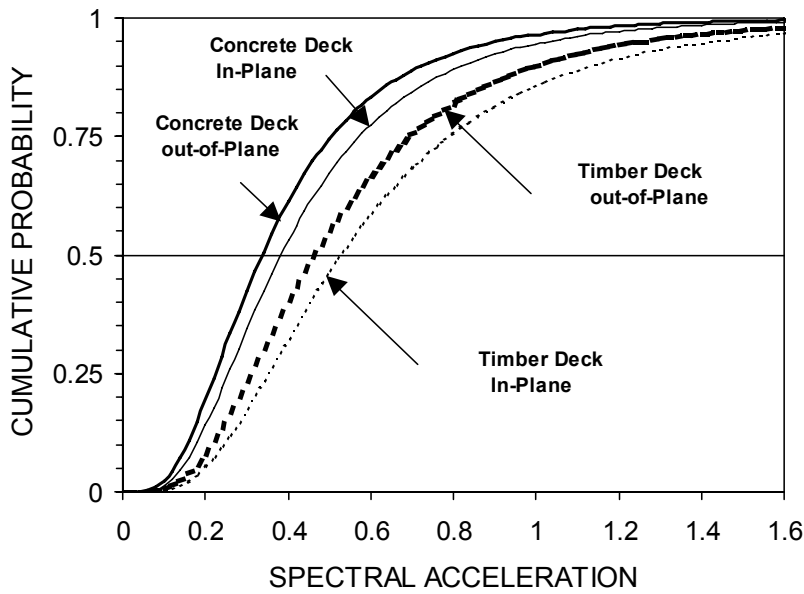
Figure 5-8. Comparisons of concrete and timber deck bridges for slight damage in terms of ground motion orientation.

5.4 APPLICATION TO STRONG PIER/WEAK PILE FOUNDATION SYSTEM

In certain situations, such as the case shown in figure 5-9, a weak piled foundation system may support a strong superstructure system. This may occur if the piles supporting the bridge pier are driven in different saturated soil layers and the first layer is prone to liquefaction during ground shaking. The strength of this layer is expected to be reduced, often drastically, to the point where it is unable to remain stable and appears to flow as fluids. In this case, plastic hinging will occur in the foundation system instead of the strong superstructure system. Consequently, the seismic performance of the entire bridge structure will be dominated by the behavior of the pile-to-concrete cap connections of the foundation system. In this subsection, comparisons are made in terms of performance between timber and steel pile-to-cap connections and fragility curves are developed for bridge structures supported by these two types of piles.

The expected peak ground motion for bridges on steel pile foundations can be expected, according to Shama (2000), as:

$$A = \frac{2\pi}{S} \sqrt{\frac{\Lambda d_p \theta_i}{2\psi g}} \; B_L \qquad B_L = \frac{2\pi}{S} \sqrt{\frac{(1+\rho)d_p \theta_i}{2\psi g}} \; B_L \qquad (98)$$

and for bridges on timber pile foundations according to equation (87), adding to it the soil reactions :

$$A = \frac{2\pi}{S} \sqrt{(1+\rho)\frac{f_{b0}}{f_{c0}} \frac{D}{8\psi g}\theta_i + \frac{2}{\pi}\frac{\gamma k_p H^3}{\psi f_{c0} g}\theta_i} \; B_L \qquad (99)$$

where the connection efficiency can be evaluated according to equation (86)

$$\rho = 3.7 \left(\frac{f_{pc0}}{f_{b0}}\right)\left(\frac{l_{emb}}{D}\right)^{2.33}\left(\frac{\theta_i}{\varepsilon_{cp0}}\right)^{0.33} \qquad (100)$$

H is the distance between the plastic hinges and can be evaluated for non-buried foundations as:

$$H = 0.6 D^{0.67}\left(\frac{f_b}{\gamma k_p}\right)^{0.333} \qquad (101)$$

140

A detailed derivation of equation (101) can be found in Shama (2000). The following assumptions are made in the analysis:

- Ground motion is effective along the strong bending axis of the steel piles. The bridge is supported on steel pile bents with section HP 10 by 42. Consequently, d_p and b_f are taken as 246-mm and 256-mm, respectively.

- The bridge deck is concrete with unit weight w = 8-kPa, and representative span length and width of L = 8-m and B = 14-m.

- The number of piles in a pile cap equal six.

- The median compressive strength of the deck concrete f'_c = 30-MPa.

- The median yield stress of the steel piles f_y = 300-MPa.

- Timber pile can be represented by a median bending, compressive, and compression perpendicular to the grain strengths of 40-MPa , 35-MPa, and 4-MPa, respectively.
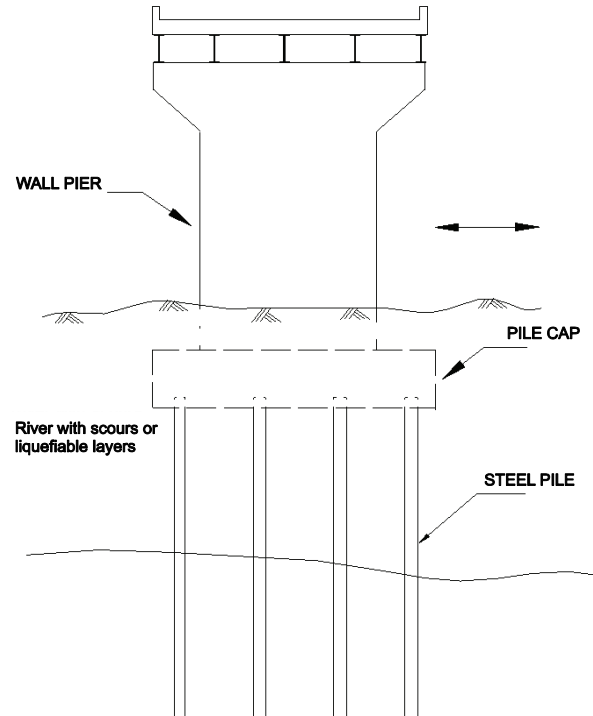
Figure 5-9. Illustration of a strong wall-weak piled foundation system.

- The diameter of timber piles is assumed to be D = 300-mm.

- The total dead load will be multiplied by a factor of 1.15 to account for the additional weight of the pier wall.

Table 5-3 presents the different values of the parameters used to evaluate the expected peak ground acceleration of such structures.

Table 5-3. Expected peak ground motions for bridges on weak pile foundations.

Bridge on Steel Pile Foundations					Bridge on Timber Pile Foundations			
DS	ρ	Drift %	B_L	A_i g	ρ	Drift %	B_L	A_i g
1	1	0.004	1	0.25	0.62	0.02	1.12	0.38
2	0.82	0.01	1.36	0.50	0.79	0.04	1.27	0.64
3	0.36	0.02	1.45	0.65	0.99	0.08	1.44	1.07
4	0.24	0.04	1.49	0.90	1.07	0.10	1.47	1.24
5	0.1	0.05	1.50	0.96	1.22	0.15	1.51	1.60

Figure 5-10 compares timber to steel piles in terms of slight and moderate damage. It can be observed that bridges on timber piles perform better than those on steel piles during seismic motions. As an example, more than 40 percent of bridges will sustain slight damage for $S_a > 0.4$-g if steel piles are used. On the contrary, less than 15 percent will sustain such damage if timber piles are used. Figure 5-11 displays the effect of liquefaction of soils on the performance of bridge structures. It is shown that bridges on liquefiable soils are more vulnerable to damage than bridges on strong soils.
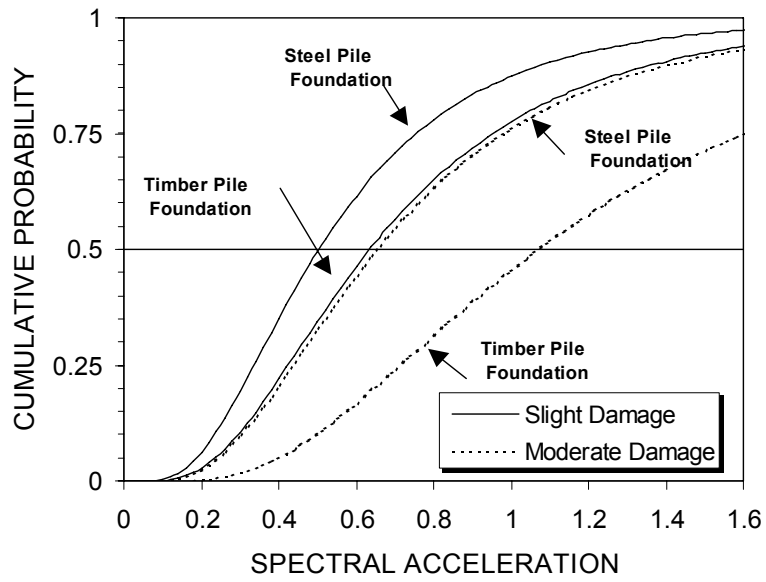
Figure 5-10. Comparison of steel to timber piles in terms of damage.
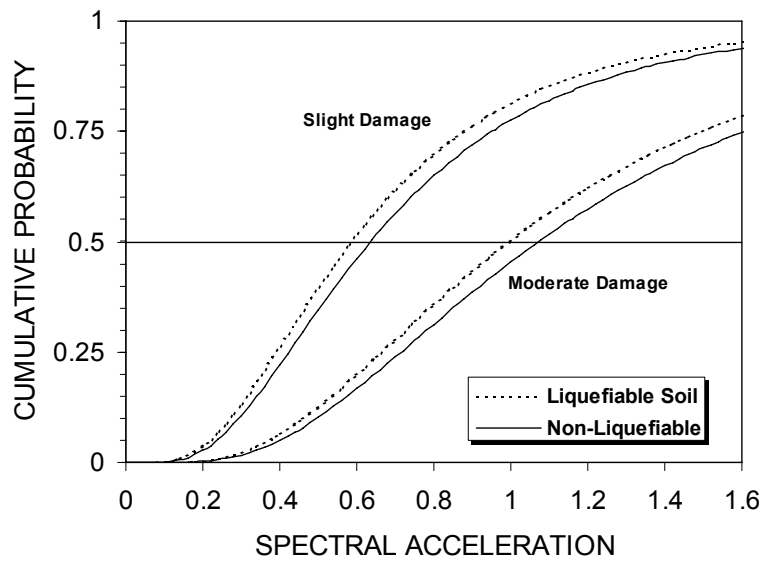
Figure 5-11. Effect of liquefaction on the performance bridge pile foundations.

5.5 SUMMARY AND CONCLUSIONS

A method to evaluate the seismic vulnerability of bridges supported by timber piled substructures was developed in the present section. Simplified equations were developed for the expected peak ground motions for each structural type investigated in this study. The method utilized fragility curves to describe the probability of a specific type of damage of the bridge at different ground shaking levels. A simplified method, which originates from the nonlinear capacity spectrum method, was adopted to develop fragility curves. The method accounted for the randomness associated with the structural capacity as well as seismic demand. The experimental results obtained were used to formulate the fragility curves.

Based on the fragility analysis in this section, the following conclusions can be drawn:

- Theoretical fragility curves are an elegant way to represent the degree of damage expected in major earthquakes. They also provide some insight into the major factors that lead to bridge damage and/or collapse.

- Timber bridges with concrete decks, being more massive than timber bridges with timber decks, are more prone to damage.

- Fragility curves presented in this section verified that timber piles are just as suitable or more suitable when compared to steel piles for use in seismic areas.

SECTION 6
CONCLUSIONS AND RECOMMENDATIONS

The present research investigated the performance of timber piled bridges and included several experimental studies. The first experimental study was performed on timber pile bents with shaking in the longitudinal direction. This study was carried out to determine the strength and ductility capability of timber substructures, without regard to the connections and bracing. In pursuit of this objective, four timber pile specimens were tested to failure using quasi-static reversed cyclic loading.

A second experimental study was performed to evaluate the behavior of timber pile bents in the transverse direction. For this study, an experimental model consisting of two identical pier bents was tested. Each of the two identical pier bents was a three-quarter scale of a prototype timber pile bent, designed in accordance with the FHWA standard plans. A series of shaking table experiments were conducted on the model structure. The structure was then tested to destruction on the laboratory strong floor under quasi-static reversed cyclic loading, as it still had considerable remaining life after the shaking table experiments. Parameters like bracing section properties, type of wood, seasoning, and moisture content were included in the strong floor experiments. Furthermore, a computational model for the model structure was also developed. The computational model efficiently simulated both the shaking table and strong floor experiments.

A third extensive experimental program was performed on timber pile-to-concrete cap foundation connections. The experimental study was undertaken on full scale prototypical specimens to validate the theory developed herein to evaluate the behavior of such connections under lateral loading. Four specimens with different M/Vd_p and different embedment depths were tested during this experimental study. A proposed uniaxial stress-strain relationship was extended and a theoretical model, based on the compression perpendicular to the grain for timber, was developed for such connections. The model was implemented in a theoretical

pushover algorithm and compared favorably to the backbone curve for experimental data of the four experiments conducted for these connections.

Finally, based on the experimental study, a method to evaluate the seismic vulnerability of timber piled bridges was developed. Simplified equations were developed for the expected peak ground motions for each structural type investigated in this study. The method utilized fragility curves to describe the probability of a specific type of damage to the bridge at different ground motion levels. A simplified method, which stems from the nonlinear capacity spectrum method, was adopted to develop fragility curves. The method accounted for the randomness associated with the structural capacity as well as seismic demand.

6.1 CONCLUSIONS

Based on this experimental and analytical investigation, the following conclusions can be drawn:

Timber Pile Bridges

1. The extent of damage depends on the deck type and condition of the timber piles. Timber bridges with concrete decks, being more massive than timber bridges with timber decks, are more prone to damage. Timber piles that have some splits, knots, etc., are less ductile than sound timber piles in good (un-split) condition.

2. Experiments have demonstrated that timber piles have considerable deformation capability. Provided that the timber is in good condition, drift limits of eight percent are possible. This is also true for weathered timber; however splitting may lead to a loss of about 50 percent of the original strength.

3. From the analysis of damping, it is evident that for large drift amplitudes (in excess of five percent), equivalent viscous damping ratios of nine percent may be assumed; however, if the wood is weathered or damaged, a value of six percent is more appropriate.

4. The computational model developed in the present study favorably captured the shaking table and strong floor experiments.

5. Quasi-static reversed cyclic loading (strong-floor) experiments were effective in inducing and observing the potential failure modes of the structure.

6. Although timber bridges have considerable strength, they are not immune from seismic damage. If ground motion is strong, particularly in the long period range (this can be exacerbated by soft-soil effects), damage can be expected.

7. Damage to braced timber pier bents resulting from strong ground motions transverse to the axis of the bridge deck will mostly be limited to the timber X-bracing in the vicinity of the bolted connections. Such damage is not considered serious, as the bracing can easily be replaced while the bridge remains in service.

8. Using X braces that will resist out-of-plane buckling instead of the usual 75-mm by 200-mm members as recommended in the *Standard Plans* can improve the seismic performance of such structures. It is thus recommended that 100-mm by 150-mm timbers be used as the diagonal bracing.

Timber pile-to-concrete cap connections

1. The present study revealed the importance of the compression perpendicular to the grain in investigating the performance of timber pile-to-concrete cap connections under lateral loads.

2. The uniaxial stress-strain relationships proposed in the study and implemented in the theoretical pushover analysis of pile-to-cap connections effectively modeled their experimental behavior.

3. The relative wood-hardness, as given by the f_{cp}/f_c stress ratio, is a significant factor in determining the ultimate lateral resistance of timber pile-to-concrete cap connections. The ultimate lateral resistance of such connections improves as the relative perpendicular to parallel compressive strength increases.

4. The study showed that pile-to-cap connections, constructed with embedment depth equal to one time the diameter of the pile, performed satisfactorily and strictly do not require retrofitting. However, for new structures, these connections should be detailed based on timber design stresses.

5. Timber piles showed high ductility when compared to other pile materials like steel and concrete. Hence, timber piles are recommended as satisfactory for high seismic zones.

6.2 RECOMMENDATIONS FOR FUTURE RESEARCH

1. The theoretical model based on the proposed stress-strain relationship for timber needs to be extended to cover the cyclic behavior of the connections.

2. Improving the connection of the braces to the piles, for timber pile bents, can improve the seismic performance of the structure. In the present study, lag screws were used for this connection. The effect of using other types of timber fasteners and their effect on the overall performance of the structure needs to be investigated. For example, shear ring connectors may well increase the strength, but damageability remains an unanswered question.

3. In order to improve the cyclic loading force-deformation predictions, especially under reloading, it will be necessary to study and include the frictional effects for the connections in the two-dimensional computational model.

4. The experimental pile-to-cap connections study needs to be extended to cover other types of piles such as pipe piles and precast-concrete piles.

5. Further research is recommended for some unusual cases of high timber bents with no longitudinal bracing, or damaged transverse bracing, where stability of the bent becomes an important issue.

SECTION 7
REFERENCES

AASHTO, LRFD, (1994), *Bridge Design Specifications*, 1st edition, American Association of State Highway and Transportation Officials, Washington, DC.

AASHTO, (1996), *Standard Specifications for Highway Bridges*, 16th edition, American Association of State Highway and Transportation Officials, Washington, DC.

Ang, A.H-S. and Tang, W.H., (1975), *Probability Concepts in Engineering Planning and Design,* John Wiley & Sons, Inc.

Anderson, A.W., (1952), "Lateral Forces of Earthquake and Wind," *Transactions ASCE*, Vol. 117, pp. 716-722.

Basöz, N. and Kiremidjian, A.S., (1997), *Evaluation of Bridge Damage Data from the Loma Prieta and Northridge, CA Earthquakes,* Technical Report No. 127, John A. Blume Earthquake Engineering Center, Civil Engineering Department, Stanford University, Stanford, California.

Basöz, N. and Mander, J.B., (1999), *Enhancement of the Highway Transportation Lifeline Module in HAZUS*, Final Pre-Publication Report prepared for the National Institute of Building Sciences.

Benjamin, J.R. and Cornell, C.A., (1970), *Probability Statistics and Decisions for Civil Engineers,* McGraw-Hill, New York.

BC Hydro, (1992), *Seismic Withstand of Timber Piles*, Hydroelectric Engineering Division, Geotechnical Department, Report No. H2607, (Vol. 1, *Evaluation of Practice Versus Theory*; Vol. 2, *Detailed Test Procedures and Test Results*).

Buckle, I.G. and Friedland, I.M., (1995), *Seismic Retrofitting Manual for Highway Bridges*, FHWA-RD-94-052, Office of Engineering and Highway Operations Research and Development, Federal Highway Administration, McLean, Virginia, 309 pages.

Byers, W.G., (1996), "Railroad Bridge Behavior During Past Earthquakes," *Proceedings of Structures Congress XIV*, Chicago, Illinois, April 15-18, 1996, American Society of Civil Engineers, New York, Vol. 1, pp. 175-182.

Cheng, C-T, and Mander, J.B., (1997), *Seismic Design of Bridge Columns Based on Control and Reparability of Damage*, Technical Report NCEER-97-0013, National Center for Earthquake Engineering Research, University at Buffalo, Buffalo, New York.

Dutta, A., and Mander, J.B., (1998), "Seismic Fragility Analysis of Highway Bridges," *INCEDE-MCEER Center-to-Center Workshop on Earthquake Engineering Frontiers in Transportation Systems.*

Foliente, G. C., (1997), *Earthquake Performance and Safety of Timber Structures*, Forest Products Society, Madison, WI, 146 pages.

Forest Products Laboratory (FPL) and Federal Highway Administration (FHWA), (2001), *Timber Bridge Economics*, Research Paper FPL-RP-593, Madison, WI, 40 p.

Hwang, H.H.M. and Huo, J-R., (1994), *Generation of Hazard-Consistent Fragility Curves for Seismic Loss Estimation Studies*, Technical Report NCEER-94-0015, National Center for Earthquake Engineering Research, University at Buffalo, Buffalo, NY.

Hwang, H.H.M. and Jaw, J-W., (1989), "Seismic Fragility Analysis of Shear Wall Structures," *Proceedings of the 5th International Conference on Structural Safety and Reliability*, San Francisco, California, pp. 399-406.

Kachadoorian, R., (1968), *Effects of The Earthquake of March 27, 1964, on The Alaska Highway System*, Geological Survey Professional Paper 545-C.

Kennedy R.P., Cornell, C.A., Campbell, R.D., Kaplan, S. and Peria, H.F., (1980), "Probabilistic Seismic Safety Study of an Existing Nuclear Power Plant," *Journal of Nuclear Engineering and Design*, Vol. 59, pp. 315-338.

Mander, J.B., Priestley, M.J., and Park, R., (1988), "Theoretical Stress-Strain Model for Confined Concrete," *Journal of Structural Engineering*, Vol. 114, No. 8, pp. 1804-1826.

McCulloch, D.S. and Bonilla, M.G. (1970), *Effects of the Earthquake of March 27, 1964, on the Alaska Railroad*, U.S. Geological Survey Paper 545-D, U.S. Government Printing Office, Washington, DC.

Mullen, C.L. and Cakmak, A.S., (1997), *Seismic Fragility of Existing Conventional Reinforced Concrete Highway Bridges*, Technical Report NCEER-97-0017, National Center for Earthquake Engineering Research, University at Buffalo, Buffalo, NY.

Newmark, N.M., and Hall, W.J., (1982), *Earthquake Spectra and Design*, Earthquake Engineering Research Institute, Oakland, California.

Pauschke, J.M., (1990), "Seismic Damage to Railroad Bridges in the United States," *Fourth U.S. National Conference on Earthquake Engineering, Proceedings*, Earthquake Engineering Research Institute, Oakland, California, Vol. 1, pp. 1017-1026.

Pekcan, G., (1998), *Design of Seismic Energy Dissipation Systems for Concrete and Steel Structures*, Ph.D. Dissertation, University at Buffalo, State University of New York, Buffalo, NY.

Popovics, S. (1973), "A Numerical Approach to the Complete Stress-Strain Curves for Concrete," *Cement and Concrete Research*, Vol. 3, No. 5, pp. 583-599.

Prakash, V., Powell, G.H., and Fillippou, F.C., (1992), *DRAIN-2DX: Base Program User Guide*, Report No. UCB/SEMM-92/29, University of California, Berkeley, California.

Ritter, M., (1990), *Timber Bridges Design, Construction, Inspection, and Maintenance*, United States Department of Agriculture.

Shama, A.A., Mander, J.B. and Aref, A.J., (2002), "Seismic Performance and Retrofit of Steel Pile to Concrete Cap Connections," *ACI Structural Journal*, Vol. 99, No. 1, pp. 51-61.

Shama, A., Mander, J.B., Chen, S. and Aref, A.J., (2001a), " Ambient Vibration and Seismic Evaluation of a Cantilever Truss Bridge," *Engineering Structures Journal*, Elsevier, Vol. 23, No. 10, pp. 1281-1292.

Shama, A.A., Mander, J.B., Blabac, B.B. and Chen, S., (2001b), *Experimental Investigation and Retrofit of Steel Pile Foundations and Pile Bents Under Cyclic Lateral Loading*, Technical Report MCEER-01-0006, Multidisciplinary Center for Earthquake Engineering Research, University at Buffalo, Buffalo, NY.

Shama, A.A., (2000), *On the Seismic Analysis and Design of Pile-to-Cap Connections*, Ph.D. Dissertation, University at Buffalo, State University of New York, Buffalo, NY.

Spyrakos, C.C., Kemp, E.L., and Venkatareddy, R., (1994), "Seismic Study of Historic Bridges in Eastern United States," *Proceedings of Structure Congress 94*, ASCE, New York, NY, pp. 380-386.

Spyrakos, C.C., Kemp, E.L., and Venkatareddy, R., (1999), "Seismic Study of An Historic Covered Bridge," *Engineering Structures*, Vol. 21, No. 9, pp. 877-882.

United States Department of Transportation (USDOT), (1979), *Standard Plans for Highway Bridges*, *Vol. III, Timber Bridges*, Washington, DC.

MCEER Technical Reports

MCEER publishes technical reports on a variety of subjects written by authors funded through MCEER. These reports are available from both MCEER Publications and the National Technical Information Service (NTIS). Requests for reports should be directed to MCEER Publications, MCEER, University at Buffalo, State University of New York, Red Jacket Quadrangle, Buffalo, New York 14261. Reports can also be requested through NTIS, 5285 Port Royal Road, Springfield, Virginia 22161. NTIS accession numbers are shown in parenthesis, if available.

NCEER-87-0001 "First-Year Program in Research, Education and Technology Transfer," 3/5/87, (PB88-134275, A04, MF-A01).

NCEER-87-0002 "Experimental Evaluation of Instantaneous Optimal Algorithms for Structural Control," by R.C. Lin, T.T. Soong and A.M. Reinhorn, 4/20/87, (PB88-134341, A04, MF-A01).

NCEER-87-0003 "Experimentation Using the Earthquake Simulation Facilities at University at Buffalo," by A.M. Reinhorn and R.L. Ketter, to be published.

NCEER-87-0004 "The System Characteristics and Performance of a Shaking Table," by J.S. Hwang, K.C. Chang and G.C. Lee, 6/1/87, (PB88-134259, A03, MF-A01). This report is available only through NTIS (see address given above).

NCEER-87-0005 "A Finite Element Formulation for Nonlinear Viscoplastic Material Using a Q Model," by O. Gyebi and G. Dasgupta, 11/2/87, (PB88-213764, A08, MF-A01).

NCEER-87-0006 "Symbolic Manipulation Program (SMP) - Algebraic Codes for Two and Three Dimensional Finite Element Formulations," by X. Lee and G. Dasgupta, 11/9/87, (PB88-218522, A05, MF-A01).

NCEER-87-0007 "Instantaneous Optimal Control Laws for Tall Buildings Under Seismic Excitations," by J.N. Yang, A. Akbarpour and P. Ghaemmaghami, 6/10/87, (PB88-134333, A06, MF-A01). This report is only available through NTIS (see address given above).

NCEER-87-0008 "IDARC: Inelastic Damage Analysis of Reinforced Concrete Frame - Shear-Wall Structures," by Y.J. Park, A.M. Reinhorn and S.K. Kunnath, 7/20/87, (PB88-134325, A09, MF-A01). This report is only available through NTIS (see address given above).

NCEER-87-0009 "Liquefaction Potential for New York State: A Preliminary Report on Sites in Manhattan and Buffalo," by M. Budhu, V. Vijayakumar, R.F. Giese and L. Baumgras, 8/31/87, (PB88-163704, A03, MF-A01). This report is available only through NTIS (see address given above).

NCEER-87-0010 "Vertical and Torsional Vibration of Foundations in Inhomogeneous Media," by A.S. Veletsos and K.W. Dotson, 6/1/87, (PB88-134291, A03, MF-A01). This report is only available through NTIS (see address given above).

NCEER-87-0011 "Seismic Probabilistic Risk Assessment and Seismic Margins Studies for Nuclear Power Plants," by Howard H.M. Hwang, 6/15/87, (PB88-134267, A03, MF-A01). This report is only available through NTIS (see address given above).

NCEER-87-0012 "Parametric Studies of Frequency Response of Secondary Systems Under Ground-Acceleration Excitations," by Y. Yong and Y.K. Lin, 6/10/87, (PB88-134309, A03, MF-A01). This report is only available through NTIS (see address given above).

NCEER-87-0013 "Frequency Response of Secondary Systems Under Seismic Excitation," by J.A. HoLung, J. Cai and Y.K. Lin, 7/31/87, (PB88-134317, A05, MF-A01). This report is only available through NTIS (see address given above).

NCEER-87-0014 "Modelling Earthquake Ground Motions in Seismically Active Regions Using Parametric Time Series Methods," by G.W. Ellis and A.S. Cakmak, 8/25/87, (PB88-134283, A08, MF-A01). This report is only available through NTIS (see address given above).

NCEER-87-0015 "Detection and Assessment of Seismic Structural Damage," by E. DiPasquale and A.S. Cakmak, 8/25/87, (PB88-163712, A05, MF-A01). This report is only available through NTIS (see address given above).

NCEER-87-0016 "Pipeline Experiment at Parkfield, California," by J. Isenberg and E. Richardson, 9/15/87, (PB88-163720, A03, MF-A01). This report is available only through NTIS (see address given above).

NCEER-87-0017 "Digital Simulation of Seismic Ground Motion," by M. Shinozuka, G. Deodatis and T. Harada, 8/31/87, (PB88-155197, A04, MF-A01). This report is available only through NTIS (see address given above).

NCEER-87-0018 "Practical Considerations for Structural Control: System Uncertainty, System Time Delay and Truncation of Small Control Forces," J.N. Yang and A. Akbarpour, 8/10/87, (PB88-163738, A08, MF-A01). This report is only available through NTIS (see address given above).

NCEER-87-0019 "Modal Analysis of Nonclassically Damped Structural Systems Using Canonical Transformation," by J.N. Yang, S. Sarkani and F.X. Long, 9/27/87, (PB88-187851, A04, MF-A01).

NCEER-87-0020 "A Nonstationary Solution in Random Vibration Theory," by J.R. Red-Horse and P.D. Spanos, 11/3/87, (PB88-163746, A03, MF-A01).

NCEER-87-0021 "Horizontal Impedances for Radially Inhomogeneous Viscoelastic Soil Layers," by A.S. Veletsos and K.W. Dotson, 10/15/87, (PB88-150859, A04, MF-A01).

NCEER-87-0022 "Seismic Damage Assessment of Reinforced Concrete Members," by Y.S. Chung, C. Meyer and M. Shinozuka, 10/9/87, (PB88-150867, A05, MF-A01). This report is available only through NTIS (see address given above).

NCEER-87-0023 "Active Structural Control in Civil Engineering," by T.T. Soong, 11/11/87, (PB88-187778, A03, MF-A01).

NCEER-87-0024 "Vertical and Torsional Impedances for Radially Inhomogeneous Viscoelastic Soil Layers," by K.W. Dotson and A.S. Veletsos, 12/87, (PB88-187786, A03, MF-A01).

NCEER-87-0025 "Proceedings from the Symposium on Seismic Hazards, Ground Motions, Soil-Liquefaction and Engineering Practice in Eastern North America," October 20-22, 1987, edited by K.H. Jacob, 12/87, (PB88-188115, A23, MF-A01). This report is available only through NTIS (see address given above).

NCEER-87-0026 "Report on the Whittier-Narrows, California, Earthquake of October 1, 1987," by J. Pantelic and A. Reinhorn, 11/87, (PB88-187752, A03, MF-A01). This report is available only through NTIS (see address given above).

NCEER-87-0027 "Design of a Modular Program for Transient Nonlinear Analysis of Large 3-D Building Structures," by S. Srivastav and J.F. Abel, 12/30/87, (PB88-187950, A05, MF-A01). This report is only available through NTIS (see address given above).

NCEER-87-0028 "Second-Year Program in Research, Education and Technology Transfer," 3/8/88, (PB88-219480, A04, MF-A01).

NCEER-88-0001 "Workshop on Seismic Computer Analysis and Design of Buildings With Interactive Graphics," by W. McGuire, J.F. Abel and C.H. Conley, 1/18/88, (PB88-187760, A03, MF-A01). This report is only available through NTIS (see address given above).

NCEER-88-0002 "Optimal Control of Nonlinear Flexible Structures," by J.N. Yang, F.X. Long and D. Wong, 1/22/88, (PB88-213772, A06, MF-A01).

NCEER-88-0003 "Substructuring Techniques in the Time Domain for Primary-Secondary Structural Systems," by G.D. Manolis and G. Juhn, 2/10/88, (PB88-213780, A04, MF-A01).

NCEER-88-0004 "Iterative Seismic Analysis of Primary-Secondary Systems," by A. Singhal, L.D. Lutes and P.D. Spanos, 2/23/88, (PB88-213798, A04, MF-A01).

NCEER-88-0005 "Stochastic Finite Element Expansion for Random Media," by P.D. Spanos and R. Ghanem, 3/14/88, (PB88-213806, A03, MF-A01).

NCEER-88-0006   "Combining Structural Optimization and Structural Control," by F.Y. Cheng and C.P. Pantelides, 1/10/88, (PB88-213814, A05, MF-A01).

NCEER-88-0007   "Seismic Performance Assessment of Code-Designed Structures," by H.H-M. Hwang, J-W. Jaw and H-J. Shau, 3/20/88, (PB88-219423, A04, MF-A01). This report is only available through NTIS (see address given above).

NCEER-88-0008   "Reliability Analysis of Code-Designed Structures Under Natural Hazards," by H.H-M. Hwang, H. Ushiba and M. Shinozuka, 2/29/88, (PB88-229471, A07, MF-A01). This report is only available through NTIS (see address given above).

NCEER-88-0009   "Seismic Fragility Analysis of Shear Wall Structures," by J-W Jaw and H.H-M. Hwang, 4/30/88, (PB89-102867, A04, MF-A01).

NCEER-88-0010   "Base Isolation of a Multi-Story Building Under a Harmonic Ground Motion - A Comparison of Performances of Various Systems," by F-G Fan, G. Ahmadi and I.G. Tadjbakhsh, 5/18/88, (PB89-122238, A06, MF-A01). This report is only available through NTIS (see address given above).

NCEER-88-0011   "Seismic Floor Response Spectra for a Combined System by Green's Functions," by F.M. Lavelle, L.A. Bergman and P.D. Spanos, 5/1/88, (PB89-102875, A03, MF-A01).

NCEER-88-0012   "A New Solution Technique for Randomly Excited Hysteretic Structures," by G.Q. Cai and Y.K. Lin, 5/16/88, (PB89-102883, A03, MF-A01).

NCEER-88-0013   "A Study of Radiation Damping and Soil-Structure Interaction Effects in the Centrifuge," by K. Weissman, supervised by J.H. Prevost, 5/24/88, (PB89-144703, A06, MF-A01).

NCEER-88-0014   "Parameter Identification and Implementation of a Kinematic Plasticity Model for Frictional Soils," by J.H. Prevost and D.V. Griffiths, to be published.

NCEER-88-0015   "Two- and Three- Dimensional Dynamic Finite Element Analyses of the Long Valley Dam," by D.V. Griffiths and J.H. Prevost, 6/17/88, (PB89-144711, A04, MF-A01).

NCEER-88-0016   "Damage Assessment of Reinforced Concrete Structures in Eastern United States," by A.M. Reinhorn, M.J. Seidel, S.K. Kunnath and Y.J. Park, 6/15/88, (PB89-122220, A04, MF-A01). This report is only available through NTIS (see address given above).

NCEER-88-0017   "Dynamic Compliance of Vertically Loaded Strip Foundations in Multilayered Viscoelastic Soils," by S. Ahmad and A.S.M. Israil, 6/17/88, (PB89-102891, A04, MF-A01).

NCEER-88-0018   "An Experimental Study of Seismic Structural Response With Added Viscoelastic Dampers," by R.C. Lin, Z. Liang, T.T. Soong and R.H. Zhang, 6/30/88, (PB89-122212, A05, MF-A01). This report is available only through NTIS (see address given above).

NCEER-88-0019   "Experimental Investigation of Primary - Secondary System Interaction," by G.D. Manolis, G. Juhn and A.M. Reinhorn, 5/27/88, (PB89-122204, A04, MF-A01).

NCEER-88-0020   "A Response Spectrum Approach For Analysis of Nonclassically Damped Structures," by J.N. Yang, S. Sarkani and F.X. Long, 4/22/88, (PB89-102909, A04, MF-A01).

NCEER-88-0021   "Seismic Interaction of Structures and Soils: Stochastic Approach," by A.S. Veletsos and A.M. Prasad, 7/21/88, (PB89-122196, A04, MF-A01). This report is only available through NTIS (see address given above).

NCEER-88-0022   "Identification of the Serviceability Limit State and Detection of Seismic Structural Damage," by E. DiPasquale and A.S. Cakmak, 6/15/88, (PB89-122188, A05, MF-A01). This report is available only through NTIS (see address given above).

NCEER-88-0023   "Multi-Hazard Risk Analysis: Case of a Simple Offshore Structure," by B.K. Bhartia and E.H. Vanmarcke, 7/21/88, (PB89-145213, A05, MF-A01).

NCEER-88-0024   "Automated Seismic Design of Reinforced Concrete Buildings," by Y.S. Chung, C. Meyer and M. Shinozuka, 7/5/88, (PB89-122170, A06, MF-A01). This report is available only through NTIS (see address given above).

NCEER-88-0025   "Experimental Study of Active Control of MDOF Structures Under Seismic Excitations," by L.L. Chung, R.C. Lin, T.T. Soong and A.M. Reinhorn, 7/10/88, (PB89-122600, A04, MF-A01).

NCEER-88-0026   "Earthquake Simulation Tests of a Low-Rise Metal Structure," by J.S. Hwang, K.C. Chang, G.C. Lee and R.L. Ketter, 8/1/88, (PB89-102917, A04, MF-A01).

NCEER-88-0027   "Systems Study of Urban Response and Reconstruction Due to Catastrophic Earthquakes," by F. Kozin and H.K. Zhou, 9/22/88, (PB90-162348, A04, MF-A01).

NCEER-88-0028   "Seismic Fragility Analysis of Plane Frame Structures," by H.H-M. Hwang and Y.K. Low, 7/31/88, (PB89-131445, A06, MF-A01).

NCEER-88-0029   "Response Analysis of Stochastic Structures," by A. Kardara, C. Bucher and M. Shinozuka, 9/22/88, (PB89-174429, A04, MF-A01).

NCEER-88-0030   "Nonnormal Accelerations Due to Yielding in a Primary Structure," by D.C.K. Chen and L.D. Lutes, 9/19/88, (PB89-131437, A04, MF-A01).

NCEER-88-0031   "Design Approaches for Soil-Structure Interaction," by A.S. Veletsos, A.M. Prasad and Y. Tang, 12/30/88, (PB89-174437, A03, MF-A01). This report is available only through NTIS (see address given above).

NCEER-88-0032   "A Re-evaluation of Design Spectra for Seismic Damage Control," by C.J. Turkstra and A.G. Tallin, 11/7/88, (PB89-145221, A05, MF-A01).

NCEER-88-0033   "The Behavior and Design of Noncontact Lap Splices Subjected to Repeated Inelastic Tensile Loading," by V.E. Sagan, P. Gergely and R.N. White, 12/8/88, (PB89-163737, A08, MF-A01).

NCEER-88-0034   "Seismic Response of Pile Foundations," by S.M. Mamoon, P.K. Banerjee and S. Ahmad, 11/1/88, (PB89-145239, A04, MF-A01).

NCEER-88-0035   "Modeling of R/C Building Structures With Flexible Floor Diaphragms (IDARC2)," by A.M. Reinhorn, S.K. Kunnath and N. Panahshahi, 9/7/88, (PB89-207153, A07, MF-A01).

NCEER-88-0036   "Solution of the Dam-Reservoir Interaction Problem Using a Combination of FEM, BEM with Particular Integrals, Modal Analysis, and Substructuring," by C-S. Tsai, G.C. Lee and R.L. Ketter, 12/31/88, (PB89-207146, A04, MF-A01).

NCEER-88-0037   "Optimal Placement of Actuators for Structural Control," by F.Y. Cheng and C.P. Pantelides, 8/15/88, (PB89-162846, A05, MF-A01).

NCEER-88-0038   "Teflon Bearings in Aseismic Base Isolation: Experimental Studies and Mathematical Modeling," by A. Mokha, M.C. Constantinou and A.M. Reinhorn, 12/5/88, (PB89-218457, A10, MF-A01). This report is available only through NTIS (see address given above).

NCEER-88-0039   "Seismic Behavior of Flat Slab High-Rise Buildings in the New York City Area," by P. Weidlinger and M. Ettouney, 10/15/88, (PB90-145681, A04, MF-A01).

NCEER-88-0040   "Evaluation of the Earthquake Resistance of Existing Buildings in New York City," by P. Weidlinger and M. Ettouney, 10/15/88, to be published.

NCEER-88-0041   "Small-Scale Modeling Techniques for Reinforced Concrete Structures Subjected to Seismic Loads," by W. Kim, A. El-Attar and R.N. White, 11/22/88, (PB89-189625, A05, MF-A01).

NCEER-88-0042   "Modeling Strong Ground Motion from Multiple Event Earthquakes," by G.W. Ellis and A.S. Cakmak, 10/15/88, (PB89-174445, A03, MF-A01).

NCEER-88-0043   "Nonstationary Models of Seismic Ground Acceleration," by M. Grigoriu, S.E. Ruiz and E. Rosenblueth, 7/15/88, (PB89-189617, A04, MF-A01).

NCEER-88-0044   "SARCF User's Guide: Seismic Analysis of Reinforced Concrete Frames," by Y.S. Chung, C. Meyer and M. Shinozuka, 11/9/88, (PB89-174452, A08, MF-A01).

NCEER-88-0045   "First Expert Panel Meeting on Disaster Research and Planning," edited by J. Pantelic and J. Stoyle, 9/15/88, (PB89-174460, A05, MF-A01).

NCEER-88-0046   "Preliminary Studies of the Effect of Degrading Infill Walls on the Nonlinear Seismic Response of Steel Frames," by C.Z. Chrysostomou, P. Gergely and J.F. Abel, 12/19/88, (PB89-208383, A05, MF-A01).

NCEER-88-0047   "Reinforced Concrete Frame Component Testing Facility - Design, Construction, Instrumentation and Operation," by S.P. Pessiki, C. Conley, T. Bond, P. Gergely and R.N. White, 12/16/88, (PB89-174478, A04, MF-A01).

NCEER-89-0001   "Effects of Protective Cushion and Soil Compliancy on the Response of Equipment Within a Seismically Excited Building," by J.A. HoLung, 2/16/89, (PB89-207179, A04, MF-A01).

NCEER-89-0002   "Statistical Evaluation of Response Modification Factors for Reinforced Concrete Structures," by H.H-M. Hwang and J-W. Jaw, 2/17/89, (PB89-207187, A05, MF-A01).

NCEER-89-0003   "Hysteretic Columns Under Random Excitation," by G-Q. Cai and Y.K. Lin, 1/9/89, (PB89-196513, A03, MF-A01).

NCEER-89-0004   "Experimental Study of `Elephant Foot Bulge' Instability of Thin-Walled Metal Tanks," by Z-H. Jia and R.L. Ketter, 2/22/89, (PB89-207195, A03, MF-A01).

NCEER-89-0005   "Experiment on Performance of Buried Pipelines Across San Andreas Fault," by J. Isenberg, E. Richardson and T.D. O'Rourke, 3/10/89, (PB89-218440, A04, MF-A01). This report is available only through NTIS (see address given above).

NCEER-89-0006   "A Knowledge-Based Approach to Structural Design of Earthquake-Resistant Buildings," by M. Subramani, P. Gergely, C.H. Conley, J.F. Abel and A.H. Zaghw, 1/15/89, (PB89-218465, A06, MF-A01).

NCEER-89-0007   "Liquefaction Hazards and Their Effects on Buried Pipelines," by T.D. O'Rourke and P.A. Lane, 2/1/89, (PB89-218481, A09, MF-A01).

NCEER-89-0008   "Fundamentals of System Identification in Structural Dynamics," by H. Imai, C-B. Yun, O. Maruyama and M. Shinozuka, 1/26/89, (PB89-207211, A04, MF-A01).

NCEER-89-0009   "Effects of the 1985 Michoacan Earthquake on Water Systems and Other Buried Lifelines in Mexico," by A.G. Ayala and M.J. O'Rourke, 3/8/89, (PB89-207229, A06, MF-A01).

NCEER-89-R010   "NCEER Bibliography of Earthquake Education Materials," by K.E.K. Ross, Second Revision, 9/1/89, (PB90-125352, A05, MF-A01). This report is replaced by NCEER-92-0018.

NCEER-89-0011   "Inelastic Three-Dimensional Response Analysis of Reinforced Concrete Building Structures (IDARC-3D), Part I - Modeling," by S.K. Kunnath and A.M. Reinhorn, 4/17/89, (PB90-114612, A07, MF-A01). This report is available only through NTIS (see address given above).

NCEER-89-0012   "Recommended Modifications to ATC-14," by C.D. Poland and J.O. Malley, 4/12/89, (PB90-108648, A15, MF-A01).

NCEER-89-0013   "Repair and Strengthening of Beam-to-Column Connections Subjected to Earthquake Loading," by M. Corazao and A.J. Durrani, 2/28/89, (PB90-109885, A06, MF-A01).

NCEER-89-0014   "Program EXKAL2 for Identification of Structural Dynamic Systems," by O. Maruyama, C-B. Yun, M. Hoshiya and M. Shinozuka, 5/19/89, (PB90-109877, A09, MF-A01).

NCEER-89-0015   "Response of Frames With Bolted Semi-Rigid Connections, Part I - Experimental Study and Analytical Predictions," by P.J. DiCorso, A.M. Reinhorn, J.R. Dickerson, J.B. Radziminski and W.L. Harper, 6/1/89, to be published.

NCEER-89-0016   "ARMA Monte Carlo Simulation in Probabilistic Structural Analysis," by P.D. Spanos and M.P. Mignolet, 7/10/89, (PB90-109893, A03, MF-A01).

NCEER-89-P017   "Preliminary Proceedings from the Conference on Disaster Preparedness - The Place of Earthquake Education in Our Schools," Edited by K.E.K. Ross, 6/23/89, (PB90-108606, A03, MF-A01).

NCEER-89-0017   "Proceedings from the Conference on Disaster Preparedness - The Place of Earthquake Education in Our Schools," Edited by K.E.K. Ross, 12/31/89, (PB90-207895, A012, MF-A02). This report is available only through NTIS (see address given above).

NCEER-89-0018   "Multidimensional Models of Hysteretic Material Behavior for Vibration Analysis of Shape Memory Energy Absorbing Devices, by E.J. Graesser and F.A. Cozzarelli, 6/7/89, (PB90-164146, A04, MF-A01).

NCEER-89-0019   "Nonlinear Dynamic Analysis of Three-Dimensional Base Isolated Structures (3D-BASIS)," by S. Nagarajaiah, A.M. Reinhorn and M.C. Constantinou, 8/3/89, (PB90-161936, A06, MF-A01). This report has been replaced by NCEER-93-0011.

NCEER-89-0020   "Structural Control Considering Time-Rate of Control Forces and Control Rate Constraints," by F.Y. Cheng and C.P. Pantelides, 8/3/89, (PB90-120445, A04, MF-A01).

NCEER-89-0021   "Subsurface Conditions of Memphis and Shelby County," by K.W. Ng, T-S. Chang and H-H.M. Hwang, 7/26/89, (PB90-120437, A03, MF-A01).

NCEER-89-0022   "Seismic Wave Propagation Effects on Straight Jointed Buried Pipelines," by K. Elhmadi and M.J. O'Rourke, 8/24/89, (PB90-162322, A10, MF-A02).

NCEER-89-0023   "Workshop on Serviceability Analysis of Water Delivery Systems," edited by M. Grigoriu, 3/6/89, (PB90-127424, A03, MF-A01).

NCEER-89-0024   "Shaking Table Study of a 1/5 Scale Steel Frame Composed of Tapered Members," by K.C. Chang, J.S. Hwang and G.C. Lee, 9/18/89, (PB90-160169, A04, MF-A01).

NCEER-89-0025   "DYNA1D: A Computer Program for Nonlinear Seismic Site Response Analysis - Technical Documentation," by Jean H. Prevost, 9/14/89, (PB90-161944, A07, MF-A01). This report is available only through NTIS (see address given above).

NCEER-89-0026   "1:4 Scale Model Studies of Active Tendon Systems and Active Mass Dampers for Aseismic Protection," by A.M. Reinhorn, T.T. Soong, R.C. Lin, Y.P. Yang, Y. Fukao, H. Abe and M. Nakai, 9/15/89, (PB90-173246, A10, MF-A02). This report is available only through NTIS (see address given above).

NCEER-89-0027   "Scattering of Waves by Inclusions in a Nonhomogeneous Elastic Half Space Solved by Boundary Element Methods," by P.K. Hadley, A. Askar and A.S. Cakmak, 6/15/89, (PB90-145699, A07, MF-A01).

NCEER-89-0028   "Statistical Evaluation of Deflection Amplification Factors for Reinforced Concrete Structures," by H.H.M. Hwang, J-W. Jaw and A.L. Ch'ng, 8/31/89, (PB90-164633, A05, MF-A01).

NCEER-89-0029   "Bedrock Accelerations in Memphis Area Due to Large New Madrid Earthquakes," by H.H.M. Hwang, C.H.S. Chen and G. Yu, 11/7/89, (PB90-162330, A04, MF-A01).

NCEER-89-0030   "Seismic Behavior and Response Sensitivity of Secondary Structural Systems," by Y.Q. Chen and T.T. Soong, 10/23/89, (PB90-164658, A08, MF-A01).

NCEER-89-0031   "Random Vibration and Reliability Analysis of Primary-Secondary Structural Systems," by Y. Ibrahim, M. Grigoriu and T.T. Soong, 11/10/89, (PB90-161951, A04, MF-A01).

NCEER-89-0032   "Proceedings from the Second U.S. - Japan Workshop on Liquefaction, Large Ground Deformation and Their Effects on Lifelines, September 26-29, 1989," Edited by T.D. O'Rourke and M. Hamada, 12/1/89, (PB90-209388, A22, MF-A03).

NCEER-89-0033   "Deterministic Model for Seismic Damage Evaluation of Reinforced Concrete Structures," by J.M. Bracci, A.M. Reinhorn, J.B. Mander and S.K. Kunnath, 9/27/89, (PB91-108803, A06, MF-A01).

NCEER-89-0034   "On the Relation Between Local and Global Damage Indices," by E. DiPasquale and A.S. Cakmak, 8/15/89, (PB90-173865, A05, MF-A01).

NCEER-89-0035   "Cyclic Undrained Behavior of Nonplastic and Low Plasticity Silts," by A.J. Walker and H.E. Stewart, 7/26/89, (PB90-183518, A10, MF-A01).

NCEER-89-0036   "Liquefaction Potential of Surficial Deposits in the City of Buffalo, New York," by M. Budhu, R. Giese and L. Baumgrass, 1/17/89, (PB90-208455, A04, MF-A01).

NCEER-89-0037   "A Deterministic Assessment of Effects of Ground Motion Incoherence," by A.S. Veletsos and Y. Tang, 7/15/89, (PB90-164294, A03, MF-A01).

NCEER-89-0038   "Workshop on Ground Motion Parameters for Seismic Hazard Mapping," July 17-18, 1989, edited by R.V. Whitman, 12/1/89, (PB90-173923, A04, MF-A01).

NCEER-89-0039   "Seismic Effects on Elevated Transit Lines of the New York City Transit Authority," by C.J. Costantino, C.A. Miller and E. Heymsfield, 12/26/89, (PB90-207887, A06, MF-A01).

NCEER-89-0040   "Centrifugal Modeling of Dynamic Soil-Structure Interaction," by K. Weissman, Supervised by J.H. Prevost, 5/10/89, (PB90-207879, A07, MF-A01).

NCEER-89-0041   "Linearized Identification of Buildings With Cores for Seismic Vulnerability Assessment," by I-K. Ho and A.E. Aktan, 11/1/89, (PB90-251943, A07, MF-A01).

NCEER-90-0001   "Geotechnical and Lifeline Aspects of the October 17, 1989 Loma Prieta Earthquake in San Francisco," by T.D. O'Rourke, H.E. Stewart, F.T. Blackburn and T.S. Dickerman, 1/90, (PB90-208596, A05, MF-A01).

NCEER-90-0002   "Nonnormal Secondary Response Due to Yielding in a Primary Structure," by D.C.K. Chen and L.D. Lutes, 2/28/90, (PB90-251976, A07, MF-A01).

NCEER-90-0003   "Earthquake Education Materials for Grades K-12," by K.E.K. Ross, 4/16/90, (PB91-251984, A05, MF-A05). This report has been replaced by NCEER-92-0018.

NCEER-90-0004   "Catalog of Strong Motion Stations in Eastern North America," by R.W. Busby, 4/3/90, (PB90-251984, A05, MF-A01).

NCEER-90-0005   "NCEER Strong-Motion Data Base: A User Manual for the GeoBase Release (Version 1.0 for the Sun3)," by P. Friberg and K. Jacob, 3/31/90 (PB90-258062, A04, MF-A01).

NCEER-90-0006   "Seismic Hazard Along a Crude Oil Pipeline in the Event of an 1811-1812 Type New Madrid Earthquake," by H.H.M. Hwang and C-H.S. Chen, 4/16/90, (PB90-258054, A04, MF-A01).

NCEER-90-0007   "Site-Specific Response Spectra for Memphis Sheahan Pumping Station," by H.H.M. Hwang and C.S. Lee, 5/15/90, (PB91-108811, A05, MF-A01).

NCEER-90-0008   "Pilot Study on Seismic Vulnerability of Crude Oil Transmission Systems," by T. Ariman, R. Dobry, M. Grigoriu, F. Kozin, M. O'Rourke, T. O'Rourke and M. Shinozuka, 5/25/90, (PB91-108837, A06, MF-A01).

NCEER-90-0009   "A Program to Generate Site Dependent Time Histories: EQGEN," by G.W. Ellis, M. Srinivasan and A.S. Cakmak, 1/30/90, (PB91-108829, A04, MF-A01).

NCEER-90-0010   "Active Isolation for Seismic Protection of Operating Rooms," by M.E. Talbott, Supervised by M. Shinozuka, 6/8/9, (PB91-110205, A05, MF-A01).

NCEER-90-0011   "Program LINEARID for Identification of Linear Structural Dynamic Systems," by C-B. Yun and M. Shinozuka, 6/25/90, (PB91-110312, A08, MF-A01).

NCEER-90-0012   "Two-Dimensional Two-Phase Elasto-Plastic Seismic Response of Earth Dams," by A.N. Yiagos, Supervised by J.H. Prevost, 6/20/90, (PB91-110197, A13, MF-A02).

NCEER-90-0013   "Secondary Systems in Base-Isolated Structures: Experimental Investigation, Stochastic Response and Stochastic Sensitivity," by G.D. Manolis, G. Juhn, M.C. Constantinou and A.M. Reinhorn, 7/1/90, (PB91-110320, A08, MF-A01).

NCEER-90-0014   "Seismic Behavior of Lightly-Reinforced Concrete Column and Beam-Column Joint Details," by S.P. Pessiki, C.H. Conley, P. Gergely and R.N. White, 8/22/90, (PB91-108795, A11, MF-A02).

NCEER-90-0015   "Two Hybrid Control Systems for Building Structures Under Strong Earthquakes," by J.N. Yang and A. Danielians, 6/29/90, (PB91-125393, A04, MF-A01).

NCEER-90-0016   "Instantaneous Optimal Control with Acceleration and Velocity Feedback," by J.N. Yang and Z. Li, 6/29/90, (PB91-125401, A03, MF-A01).

NCEER-90-0017   "Reconnaissance Report on the Northern Iran Earthquake of June 21, 1990," by M. Mehrain, 10/4/90, (PB91-125377, A03, MF-A01).

NCEER-90-0018   "Evaluation of Liquefaction Potential in Memphis and Shelby County," by T.S. Chang, P.S. Tang, C.S. Lee and H. Hwang, 8/10/90, (PB91-125427, A09, MF-A01).

NCEER-90-0019   "Experimental and Analytical Study of a Combined Sliding Disc Bearing and Helical Steel Spring Isolation System," by M.C. Constantinou, A.S. Mokha and A.M. Reinhorn, 10/4/90, (PB91-125385, A06, MF-A01). This report is available only through NTIS (see address given above).

NCEER-90-0020   "Experimental Study and Analytical Prediction of Earthquake Response of a Sliding Isolation System with a Spherical Surface," by A.S. Mokha, M.C. Constantinou and A.M. Reinhorn, 10/11/90, (PB91-125419, A05, MF-A01).

NCEER-90-0021   "Dynamic Interaction Factors for Floating Pile Groups," by G. Gazetas, K. Fan, A. Kaynia and E. Kausel, 9/10/90, (PB91-170381, A05, MF-A01).

NCEER-90-0022   "Evaluation of Seismic Damage Indices for Reinforced Concrete Structures," by S. Rodriguez-Gomez and A.S. Cakmak, 9/30/90, PB91-171322, A06, MF-A01).

NCEER-90-0023   "Study of Site Response at a Selected Memphis Site," by H. Desai, S. Ahmad, E.S. Gazetas and M.R. Oh, 10/11/90, (PB91-196857, A03, MF-A01).

NCEER-90-0024   "A User's Guide to Strongmo: Version 1.0 of NCEER's Strong-Motion Data Access Tool for PCs and Terminals," by P.A. Friberg and C.A.T. Susch, 11/15/90, (PB91-171272, A03, MF-A01).

NCEER-90-0025   "A Three-Dimensional Analytical Study of Spatial Variability of Seismic Ground Motions," by L-L. Hong and A.H.-S. Ang, 10/30/90, (PB91-170399, A09, MF-A01).

NCEER-90-0026   "MUMOID User's Guide - A Program for the Identification of Modal Parameters," by S. Rodriguez-Gomez and E. DiPasquale, 9/30/90, (PB91-171298, A04, MF-A01).

NCEER-90-0027   "SARCF-II User's Guide - Seismic Analysis of Reinforced Concrete Frames," by S. Rodriguez-Gomez, Y.S. Chung and C. Meyer, 9/30/90, (PB91-171280, A05, MF-A01).

NCEER-90-0028   "Viscous Dampers: Testing, Modeling and Application in Vibration and Seismic Isolation," by N. Makris and M.C. Constantinou, 12/20/90 (PB91-190561, A06, MF-A01).

NCEER-90-0029   "Soil Effects on Earthquake Ground Motions in the Memphis Area," by H. Hwang, C.S. Lee, K.W. Ng and T.S. Chang, 8/2/90, (PB91-190751, A05, MF-A01).

NCEER-91-0001 "Proceedings from the Third Japan-U.S. Workshop on Earthquake Resistant Design of Lifeline Facilities and Countermeasures for Soil Liquefaction, December 17-19, 1990," edited by T.D. O'Rourke and M. Hamada, 2/1/91, (PB91-179259, A99, MF-A04).

NCEER-91-0002 "Physical Space Solutions of Non-Proportionally Damped Systems," by M. Tong, Z. Liang and G.C. Lee, 1/15/91, (PB91-179242, A04, MF-A01).

NCEER-91-0003 "Seismic Response of Single Piles and Pile Groups," by K. Fan and G. Gazetas, 1/10/91, (PB92-174994, A04, MF-A01).

NCEER-91-0004 "Damping of Structures: Part 1 - Theory of Complex Damping," by Z. Liang and G. Lee, 10/10/91, (PB92-197235, A12, MF-A03).

NCEER-91-0005 "3D-BASIS - Nonlinear Dynamic Analysis of Three Dimensional Base Isolated Structures: Part II," by S. Nagarajaiah, A.M. Reinhorn and M.C. Constantinou, 2/28/91, (PB91-190553, A07, MF-A01). This report has been replaced by NCEER-93-0011.

NCEER-91-0006 "A Multidimensional Hysteretic Model for Plasticity Deforming Metals in Energy Absorbing Devices," by E.J. Graesser and F.A. Cozzarelli, 4/9/91, (PB92-108364, A04, MF-A01).

NCEER-91-0007 "A Framework for Customizable Knowledge-Based Expert Systems with an Application to a KBES for Evaluating the Seismic Resistance of Existing Buildings," by E.G. Ibarra-Anaya and S.J. Fenves, 4/9/91, (PB91-210930, A08, MF-A01).

NCEER-91-0008 "Nonlinear Analysis of Steel Frames with Semi-Rigid Connections Using the Capacity Spectrum Method," by G.G. Deierlein, S-H. Hsieh, Y-J. Shen and J.F. Abel, 7/2/91, (PB92-113828, A05, MF-A01).

NCEER-91-0009 "Earthquake Education Materials for Grades K-12," by K.E.K. Ross, 4/30/91, (PB91-212142, A06, MF-A01). This report has been replaced by NCEER-92-0018.

NCEER-91-0010 "Phase Wave Velocities and Displacement Phase Differences in a Harmonically Oscillating Pile," by N. Makris and G. Gazetas, 7/8/91, (PB92-108356, A04, MF-A01).

NCEER-91-0011 "Dynamic Characteristics of a Full-Size Five-Story Steel Structure and a 2/5 Scale Model," by K.C. Chang, G.C. Yao, G.C. Lee, D.S. Hao and Y.C. Yeh," 7/2/91, (PB93-116648, A06, MF-A02).

NCEER-91-0012 "Seismic Response of a 2/5 Scale Steel Structure with Added Viscoelastic Dampers," by K.C. Chang, T.T. Soong, S-T. Oh and M.L. Lai, 5/17/91, (PB92-110816, A05, MF-A01).

NCEER-91-0013 "Earthquake Response of Retaining Walls; Full-Scale Testing and Computational Modeling," by S. Alampalli and A-W.M. Elgamal, 6/20/91, to be published.

NCEER-91-0014 "3D-BASIS-M: Nonlinear Dynamic Analysis of Multiple Building Base Isolated Structures," by P.C. Tsopelas, S. Nagarajaiah, M.C. Constantinou and A.M. Reinhorn, 5/28/91, (PB92-113885, A09, MF-A02).

NCEER-91-0015 "Evaluation of SEAOC Design Requirements for Sliding Isolated Structures," by D. Theodossiou and M.C. Constantinou, 6/10/91, (PB92-114602, A11, MF-A03).

NCEER-91-0016 "Closed-Loop Modal Testing of a 27-Story Reinforced Concrete Flat Plate-Core Building," by H.R. Somaprasad, T. Toksoy, H. Yoshiyuki and A.E. Aktan, 7/15/91, (PB92-129980, A07, MF-A02).

NCEER-91-0017 "Shake Table Test of a 1/6 Scale Two-Story Lightly Reinforced Concrete Building," by A.G. El-Attar, R.N. White and P. Gergely, 2/28/91, (PB92-222447, A06, MF-A02).

NCEER-91-0018 "Shake Table Test of a 1/8 Scale Three-Story Lightly Reinforced Concrete Building," by A.G. El-Attar, R.N. White and P. Gergely, 2/28/91, (PB93-116630, A08, MF-A02).

NCEER-91-0019 "Transfer Functions for Rigid Rectangular Foundations," by A.S. Veletsos, A.M. Prasad and W.H. Wu, 7/31/91, to be published.

NCEER-91-0020 "Hybrid Control of Seismic-Excited Nonlinear and Inelastic Structural Systems," by J.N. Yang, Z. Li and A. Danielians, 8/1/91, (PB92-143171, A06, MF-A02).

NCEER-91-0021 "The NCEER-91 Earthquake Catalog: Improved Intensity-Based Magnitudes and Recurrence Relations for U.S. Earthquakes East of New Madrid," by L. Seeber and J.G. Armbruster, 8/28/91, (PB92-176742, A06, MF-A02).

NCEER-91-0022 "Proceedings from the Implementation of Earthquake Planning and Education in Schools: The Need for Change - The Roles of the Changemakers," by K.E.K. Ross and F. Winslow, 7/23/91, (PB92-129998, A12, MF-A03).

NCEER-91-0023 "A Study of Reliability-Based Criteria for Seismic Design of Reinforced Concrete Frame Buildings," by H.H.M. Hwang and H-M. Hsu, 8/10/91, (PB92-140235, A09, MF-A02).

NCEER-91-0024 "Experimental Verification of a Number of Structural System Identification Algorithms," by R.G. Ghanem, H. Gavin and M. Shinozuka, 9/18/91, (PB92-176577, A18, MF-A04).

NCEER-91-0025 "Probabilistic Evaluation of Liquefaction Potential," by H.H.M. Hwang and C.S. Lee," 11/25/91, (PB92-143429, A05, MF-A01).

NCEER-91-0026 "Instantaneous Optimal Control for Linear, Nonlinear and Hysteretic Structures - Stable Controllers," by J.N. Yang and Z. Li, 11/15/91, (PB92-163807, A04, MF-A01).

NCEER-91-0027 "Experimental and Theoretical Study of a Sliding Isolation System for Bridges," by M.C. Constantinou, A. Kartoum, A.M. Reinhorn and P. Bradford, 11/15/91, (PB92-176973, A10, MF-A03).

NCEER-92-0001 "Case Studies of Liquefaction and Lifeline Performance During Past Earthquakes, Volume 1: Japanese Case Studies," Edited by M. Hamada and T. O'Rourke, 2/17/92, (PB92-197243, A18, MF-A04).

NCEER-92-0002 "Case Studies of Liquefaction and Lifeline Performance During Past Earthquakes, Volume 2: United States Case Studies," Edited by T. O'Rourke and M. Hamada, 2/17/92, (PB92-197250, A20, MF-A04).

NCEER-92-0003 "Issues in Earthquake Education," Edited by K. Ross, 2/3/92, (PB92-222389, A07, MF-A02).

NCEER-92-0004 "Proceedings from the First U.S. - Japan Workshop on Earthquake Protective Systems for Bridges," Edited by I.G. Buckle, 2/4/92, (PB94-142239, A99, MF-A06).

NCEER-92-0005 "Seismic Ground Motion from a Haskell-Type Source in a Multiple-Layered Half-Space," A.P. Theoharis, G. Deodatis and M. Shinozuka, 1/2/92, to be published.

NCEER-92-0006 "Proceedings from the Site Effects Workshop," Edited by R. Whitman, 2/29/92, (PB92-197201, A04, MF-A01).

NCEER-92-0007 "Engineering Evaluation of Permanent Ground Deformations Due to Seismically-Induced Liquefaction," by M.H. Baziar, R. Dobry and A-W.M. Elgamal, 3/24/92, (PB92-222421, A13, MF-A03).

NCEER-92-0008 "A Procedure for the Seismic Evaluation of Buildings in the Central and Eastern United States," by C.D. Poland and J.O. Malley, 4/2/92, (PB92-222439, A20, MF-A04).

NCEER-92-0009 "Experimental and Analytical Study of a Hybrid Isolation System Using Friction Controllable Sliding Bearings," by M.Q. Feng, S. Fujii and M. Shinozuka, 5/15/92, (PB93-150282, A06, MF-A02).

NCEER-92-0010 "Seismic Resistance of Slab-Column Connections in Existing Non-Ductile Flat-Plate Buildings," by A.J. Durrani and Y. Du, 5/18/92, (PB93-116812, A06, MF-A02).

NCEER-92-0011 "The Hysteretic and Dynamic Behavior of Brick Masonry Walls Upgraded by Ferrocement Coatings Under Cyclic Loading and Strong Simulated Ground Motion," by H. Lee and S.P. Prawel, 5/11/92, to be published.

NCEER-92-0012 "Study of Wire Rope Systems for Seismic Protection of Equipment in Buildings," by G.F. Demetriades, M.C. Constantinou and A.M. Reinhorn, 5/20/92, (PB93-116655, A08, MF-A02).

NCEER-92-0013   "Shape Memory Structural Dampers: Material Properties, Design and Seismic Testing," by P.R. Witting and F.A. Cozzarelli, 5/26/92, (PB93-116663, A05, MF-A01).

NCEER-92-0014   "Longitudinal Permanent Ground Deformation Effects on Buried Continuous Pipelines," by M.J. O'Rourke, and C. Nordberg, 6/15/92, (PB93-116671, A08, MF-A02).

NCEER-92-0015   "A Simulation Method for Stationary Gaussian Random Functions Based on the Sampling Theorem," by M. Grigoriu and S. Balopoulou, 6/11/92, (PB93-127496, A05, MF-A01).

NCEER-92-0016   "Gravity-Load-Designed Reinforced Concrete Buildings: Seismic Evaluation of Existing Construction and Detailing Strategies for Improved Seismic Resistance," by G.W. Hoffmann, S.K. Kunnath, A.M. Reinhorn and J.B. Mander, 7/15/92, (PB94-142007, A08, MF-A02).

NCEER-92-0017   "Observations on Water System and Pipeline Performance in the Limón Area of Costa Rica Due to the April 22, 1991 Earthquake," by M. O'Rourke and D. Ballantyne, 6/30/92, (PB93-126811, A06, MF-A02).

NCEER-92-0018   "Fourth Edition of Earthquake Education Materials for Grades K-12," Edited by K.E.K. Ross, 8/10/92, (PB93-114023, A07, MF-A02).

NCEER-92-0019   "Proceedings from the Fourth Japan-U.S. Workshop on Earthquake Resistant Design of Lifeline Facilities and Countermeasures for Soil Liquefaction," Edited by M. Hamada and T.D. O'Rourke, 8/12/92, (PB93-163939, A99, MF-E11).

NCEER-92-0020   "Active Bracing System: A Full Scale Implementation of Active Control," by A.M. Reinhorn, T.T. Soong, R.C. Lin, M.A. Riley, Y.P. Wang, S. Aizawa and M. Higashino, 8/14/92, (PB93-127512, A06, MF-A02).

NCEER-92-0021   "Empirical Analysis of Horizontal Ground Displacement Generated by Liquefaction-Induced Lateral Spreads," by S.F. Bartlett and T.L. Youd, 8/17/92, (PB93-188241, A06, MF-A02).

NCEER-92-0022   "IDARC Version 3.0: Inelastic Damage Analysis of Reinforced Concrete Structures," by S.K. Kunnath, A.M. Reinhorn and R.F. Lobo, 8/31/92, (PB93-227502, A07, MF-A02).

NCEER-92-0023   "A Semi-Empirical Analysis of Strong-Motion Peaks in Terms of Seismic Source, Propagation Path and Local Site Conditions, by M. Kamiyama, M.J. O'Rourke and R. Flores-Berrones, 9/9/92, (PB93-150266, A08, MF-A02).

NCEER-92-0024   "Seismic Behavior of Reinforced Concrete Frame Structures with Nonductile Details, Part I: Summary of Experimental Findings of Full Scale Beam-Column Joint Tests," by A. Beres, R.N. White and P. Gergely, 9/30/92, (PB93-227783, A05, MF-A01).

NCEER-92-0025   "Experimental Results of Repaired and Retrofitted Beam-Column Joint Tests in Lightly Reinforced Concrete Frame Buildings," by A. Beres, S. El-Borgi, R.N. White and P. Gergely, 10/29/92, (PB93-227791, A05, MF-A01).

NCEER-92-0026   "A Generalization of Optimal Control Theory: Linear and Nonlinear Structures," by J.N. Yang, Z. Li and S. Vongchavalitkul, 11/2/92, (PB93-188621, A05, MF-A01).

NCEER-92-0027   "Seismic Resistance of Reinforced Concrete Frame Structures Designed Only for Gravity Loads: Part I - Design and Properties of a One-Third Scale Model Structure," by J.M. Bracci, A.M. Reinhorn and J.B. Mander, 12/1/92, (PB94-104502, A08, MF-A02).

NCEER-92-0028   "Seismic Resistance of Reinforced Concrete Frame Structures Designed Only for Gravity Loads: Part II - Experimental Performance of Subassemblages," by L.E. Aycardi, J.B. Mander and A.M. Reinhorn, 12/1/92, (PB94-104510, A08, MF-A02).

NCEER-92-0029   "Seismic Resistance of Reinforced Concrete Frame Structures Designed Only for Gravity Loads: Part III - Experimental Performance and Analytical Study of a Structural Model," by J.M. Bracci, A.M. Reinhorn and J.B. Mander, 12/1/92, (PB93-227528, A09, MF-A01).

NCEER-92-0030   "Evaluation of Seismic Retrofit of Reinforced Concrete Frame Structures: Part I - Experimental Performance of Retrofitted Subassemblages," by D. Choudhuri, J.B. Mander and A.M. Reinhorn, 12/8/92, (PB93-198307, A07, MF-A02).

NCEER-92-0031   "Evaluation of Seismic Retrofit of Reinforced Concrete Frame Structures: Part II - Experimental Performance and Analytical Study of a Retrofitted Structural Model," by J.M. Bracci, A.M. Reinhorn and J.B. Mander, 12/8/92, (PB93-198315, A09, MF-A03).

NCEER-92-0032   "Experimental and Analytical Investigation of Seismic Response of Structures with Supplemental Fluid Viscous Dampers," by M.C. Constantinou and M.D. Symans, 12/21/92, (PB93-191435, A10, MF-A03). This report is available only through NTIS (see address given above).

NCEER-92-0033   "Reconnaissance Report on the Cairo, Egypt Earthquake of October 12, 1992," by M. Khater, 12/23/92, (PB93-188621, A03, MF-A01).

NCEER-92-0034   "Low-Level Dynamic Characteristics of Four Tall Flat-Plate Buildings in New York City," by H. Gavin, S. Yuan, J. Grossman, E. Pekelis and K. Jacob, 12/28/92, (PB93-188217, A07, MF-A02).

NCEER-93-0001   "An Experimental Study on the Seismic Performance of Brick-Infilled Steel Frames With and Without Retrofit," by J.B. Mander, B. Nair, K. Wojtkowski and J. Ma, 1/29/93, (PB93-227510, A07, MF-A02).

NCEER-93-0002   "Social Accounting for Disaster Preparedness and Recovery Planning," by S. Cole, E. Pantoja and V. Razak, 2/22/93, (PB94-142114, A12, MF-A03).

NCEER-93-0003   "Assessment of 1991 NEHRP Provisions for Nonstructural Components and Recommended Revisions," by T.T. Soong, G. Chen, Z. Wu, R-H. Zhang and M. Grigoriu, 3/1/93, (PB93-188639, A06, MF-A02).

NCEER-93-0004   "Evaluation of Static and Response Spectrum Analysis Procedures of SEAOC/UBC for Seismic Isolated Structures," by C.W. Winters and M.C. Constantinou, 3/23/93, (PB93-198299, A10, MF-A03).

NCEER-93-0005   "Earthquakes in the Northeast - Are We Ignoring the Hazard? A Workshop on Earthquake Science and Safety for Educators," edited by K.E.K. Ross, 4/2/93, (PB94-103066, A09, MF-A02).

NCEER-93-0006   "Inelastic Response of Reinforced Concrete Structures with Viscoelastic Braces," by R.F. Lobo, J.M. Bracci, K.L. Shen, A.M. Reinhorn and T.T. Soong, 4/5/93, (PB93-227486, A05, MF-A02).

NCEER-93-0007   "Seismic Testing of Installation Methods for Computers and Data Processing Equipment," by K. Kosar, T.T. Soong, K.L. Shen, J.A. HoLung and Y.K. Lin, 4/12/93, (PB93-198299, A07, MF-A02).

NCEER-93-0008   "Retrofit of Reinforced Concrete Frames Using Added Dampers," by A. Reinhorn, M. Constantinou and C. Li, to be published.

NCEER-93-0009   "Seismic Behavior and Design Guidelines for Steel Frame Structures with Added Viscoelastic Dampers," by K.C. Chang, M.L. Lai, T.T. Soong, D.S. Hao and Y.C. Yeh, 5/1/93, (PB94-141959, A07, MF-A02).

NCEER-93-0010   "Seismic Performance of Shear-Critical Reinforced Concrete Bridge Piers," by J.B. Mander, S.M. Waheed, M.T.A. Chaudhary and S.S. Chen, 5/12/93, (PB93-227494, A08, MF-A02).

NCEER-93-0011   "3D-BASIS-TABS: Computer Program for Nonlinear Dynamic Analysis of Three Dimensional Base Isolated Structures," by S. Nagarajaiah, C. Li, A.M. Reinhorn and M.C. Constantinou, 8/2/93, (PB94-141819, A09, MF-A02).

NCEER-93-0012   "Effects of Hydrocarbon Spills from an Oil Pipeline Break on Ground Water," by O.J. Helweg and H.H.M. Hwang, 8/3/93, (PB94-141942, A06, MF-A02).

NCEER-93-0013   "Simplified Procedures for Seismic Design of Nonstructural Components and Assessment of Current Code Provisions," by M.P. Singh, L.E. Suarez, E.E. Matheu and G.O. Maldonado, 8/4/93, (PB94-141827, A09, MF-A02).

NCEER-93-0014   "An Energy Approach to Seismic Analysis and Design of Secondary Systems," by G. Chen and T.T. Soong, 8/6/93, (PB94-142767, A11, MF-A03).

NCEER-93-0015   "Proceedings from School Sites: Becoming Prepared for Earthquakes - Commemorating the Third Anniversary of the Loma Prieta Earthquake," Edited by F.E. Winslow and K.E.K. Ross, 8/16/93, (PB94-154275, A16, MF-A02).

NCEER-93-0016   "Reconnaissance Report of Damage to Historic Monuments in Cairo, Egypt Following the October 12, 1992 Dahshur Earthquake," by D. Sykora, D. Look, G. Croci, E. Karaesmen and E. Karaesmen, 8/19/93, (PB94-142221, A08, MF-A02).

NCEER-93-0017   "The Island of Guam Earthquake of August 8, 1993," by S.W. Swan and S.K. Harris, 9/30/93, (PB94-141843, A04, MF-A01).

NCEER-93-0018   "Engineering Aspects of the October 12, 1992 Egyptian Earthquake," by A.W. Elgamal, M. Amer, K. Adalier and A. Abul-Fadl, 10/7/93, (PB94-141983, A05, MF-A01).

NCEER-93-0019   "Development of an Earthquake Motion Simulator and its Application in Dynamic Centrifuge Testing," by I. Krstelj, Supervised by J.H. Prevost, 10/23/93, (PB94-181773, A-10, MF-A03).

NCEER-93-0020   "NCEER-Taisei Corporation Research Program on Sliding Seismic Isolation Systems for Bridges: Experimental and Analytical Study of a Friction Pendulum System (FPS)," by M.C. Constantinou, P. Tsopelas, Y-S. Kim and S. Okamoto, 11/1/93, (PB94-142775, A08, MF-A02).

NCEER-93-0021   "Finite Element Modeling of Elastomeric Seismic Isolation Bearings," by L.J. Billings, Supervised by R. Shepherd, 11/8/93, to be published.

NCEER-93-0022   "Seismic Vulnerability of Equipment in Critical Facilities: Life-Safety and Operational Consequences," by K. Porter, G.S. Johnson, M.M. Zadeh, C. Scawthorn and S. Eder, 11/24/93, (PB94-181765, A16, MF-A03).

NCEER-93-0023   "Hokkaido Nansei-oki, Japan Earthquake of July 12, 1993, by P.I. Yanev and C.R. Scawthorn, 12/23/93, (PB94-181500, A07, MF-A01).

NCEER-94-0001   "An Evaluation of Seismic Serviceability of Water Supply Networks with Application to the San Francisco Auxiliary Water Supply System," by I. Markov, Supervised by M. Grigoriu and T. O'Rourke, 1/21/94, (PB94-204013, A07, MF-A02).

NCEER-94-0002   "NCEER-Taisei Corporation Research Program on Sliding Seismic Isolation Systems for Bridges: Experimental and Analytical Study of Systems Consisting of Sliding Bearings, Rubber Restoring Force Devices and Fluid Dampers," Volumes I and II, by P. Tsopelas, S. Okamoto, M.C. Constantinou, D. Ozaki and S. Fujii, 2/4/94, (PB94-181740, A09, MF-A02 and PB94-181757, A12, MF-A03).

NCEER-94-0003   "A Markov Model for Local and Global Damage Indices in Seismic Analysis," by S. Rahman and M. Grigoriu, 2/18/94, (PB94-206000, A12, MF-A03).

NCEER-94-0004   "Proceedings from the NCEER Workshop on Seismic Response of Masonry Infills," edited by D.P. Abrams, 3/1/94, (PB94-180783, A07, MF-A02).

NCEER-94-0005   "The Northridge, California Earthquake of January 17, 1994: General Reconnaissance Report," edited by J.D. Goltz, 3/11/94, (PB94-193943, A10, MF-A03).

NCEER-94-0006   "Seismic Energy Based Fatigue Damage Analysis of Bridge Columns: Part I - Evaluation of Seismic Capacity," by G.A. Chang and J.B. Mander, 3/14/94, (PB94-219185, A11, MF-A03).

NCEER-94-0007   "Seismic Isolation of Multi-Story Frame Structures Using Spherical Sliding Isolation Systems," by T.M. Al-Hussaini, V.A. Zayas and M.C. Constantinou, 3/17/94, (PB94-193745, A09, MF-A02).

NCEER-94-0008   "The Northridge, California Earthquake of January 17, 1994: Performance of Highway Bridges," edited by I.G. Buckle, 3/24/94, (PB94-193851, A06, MF-A02).

NCEER-94-0009   "Proceedings of the Third U.S.-Japan Workshop on Earthquake Protective Systems for Bridges," edited by I.G. Buckle and I. Friedland, 3/31/94, (PB94-195815, A99, MF-A06).

NCEER-94-0010   "3D-BASIS-ME: Computer Program for Nonlinear Dynamic Analysis of Seismically Isolated Single and Multiple Structures and Liquid Storage Tanks," by P.C. Tsopelas, M.C. Constantinou and A.M. Reinhorn, 4/12/94, (PB94-204922, A09, MF-A02).

NCEER-94-0011   "The Northridge, California Earthquake of January 17, 1994: Performance of Gas Transmission Pipelines," by T.D. O'Rourke and M.C. Palmer, 5/16/94, (PB94-204989, A05, MF-A01).

NCEER-94-0012   "Feasibility Study of Replacement Procedures and Earthquake Performance Related to Gas Transmission Pipelines," by T.D. O'Rourke and M.C. Palmer, 5/25/94, (PB94-206638, A09, MF-A02).

NCEER-94-0013   "Seismic Energy Based Fatigue Damage Analysis of Bridge Columns: Part II - Evaluation of Seismic Demand," by G.A. Chang and J.B. Mander, 6/1/94, (PB95-18106, A08, MF-A02).

NCEER-94-0014   "NCEER-Taisei Corporation Research Program on Sliding Seismic Isolation Systems for Bridges: Experimental and Analytical Study of a System Consisting of Sliding Bearings and Fluid Restoring Force/Damping Devices," by P. Tsopelas and M.C. Constantinou, 6/13/94, (PB94-219144, A10, MF-A03).

NCEER-94-0015   "Generation of Hazard-Consistent Fragility Curves for Seismic Loss Estimation Studies," by H. Hwang and J-R. Huo, 6/14/94, (PB95-181996, A09, MF-A02).

NCEER-94-0016   "Seismic Study of Building Frames with Added Energy-Absorbing Devices," by W.S. Pong, C.S. Tsai and G.C. Lee, 6/20/94, (PB94-219136, A10, A03).

NCEER-94-0017   "Sliding Mode Control for Seismic-Excited Linear and Nonlinear Civil Engineering Structures," by J. Yang, J. Wu, A. Agrawal and Z. Li, 6/21/94, (PB95-138483, A06, MF-A02).

NCEER-94-0018   "3D-BASIS-TABS Version 2.0: Computer Program for Nonlinear Dynamic Analysis of Three Dimensional Base Isolated Structures," by A.M. Reinhorn, S. Nagarajaiah, M.C. Constantinou, P. Tsopelas and R. Li, 6/22/94, (PB95-182176, A08, MF-A02).

NCEER-94-0019   "Proceedings of the International Workshop on Civil Infrastructure Systems: Application of Intelligent Systems and Advanced Materials on Bridge Systems," Edited by G.C. Lee and K.C. Chang, 7/18/94, (PB95-252474, A20, MF-A04).

NCEER-94-0020   "Study of Seismic Isolation Systems for Computer Floors," by V. Lambrou and M.C. Constantinou, 7/19/94, (PB95-138533, A10, MF-A03).

NCEER-94-0021   "Proceedings of the U.S.-Italian Workshop on Guidelines for Seismic Evaluation and Rehabilitation of Unreinforced Masonry Buildings," Edited by D.P. Abrams and G.M. Calvi, 7/20/94, (PB95-138749, A13, MF-A03).

NCEER-94-0022   "NCEER-Taisei Corporation Research Program on Sliding Seismic Isolation Systems for Bridges: Experimental and Analytical Study of a System Consisting of Lubricated PTFE Sliding Bearings and Mild Steel Dampers," by P. Tsopelas and M.C. Constantinou, 7/22/94, (PB95-182184, A08, MF-A02).

NCEER-94-0023   "Development of Reliability-Based Design Criteria for Buildings Under Seismic Load," by Y.K. Wen, H. Hwang and M. Shinozuka, 8/1/94, (PB95-211934, A08, MF-A02).

NCEER-94-0024   "Experimental Verification of Acceleration Feedback Control Strategies for an Active Tendon System," by S.J. Dyke, B.F. Spencer, Jr., P. Quast, M.K. Sain, D.C. Kaspari, Jr. and T.T. Soong, 8/29/94, (PB95-212320, A05, MF-A01).

NCEER-94-0025   "Seismic Retrofitting Manual for Highway Bridges," Edited by I.G. Buckle and I.F. Friedland, published by the Federal Highway Administration (PB95-212676, A15, MF-A03).

NCEER-94-0026   "Proceedings from the Fifth U.S.-Japan Workshop on Earthquake Resistant Design of Lifeline Facilities and Countermeasures Against Soil Liquefaction," Edited by T.D. O'Rourke and M. Hamada, 11/7/94, (PB95-220802, A99, MF-E08).

NCEER-95-0001 "Experimental and Analytical Investigation of Seismic Retrofit of Structures with Supplemental Damping: Part 1 - Fluid Viscous Damping Devices," by A.M. Reinhorn, C. Li and M.C. Constantinou, 1/3/95, (PB95-266599, A09, MF-A02).

NCEER-95-0002 "Experimental and Analytical Study of Low-Cycle Fatigue Behavior of Semi-Rigid Top-And-Seat Angle Connections," by G. Pekcan, J.B. Mander and S.S. Chen, 1/5/95, (PB95-220042, A07, MF-A02).

NCEER-95-0003 "NCEER-ATC Joint Study on Fragility of Buildings," by T. Anagnos, C. Rojahn and A.S. Kiremidjian, 1/20/95, (PB95-220026, A06, MF-A02).

NCEER-95-0004 "Nonlinear Control Algorithms for Peak Response Reduction," by Z. Wu, T.T. Soong, V. Gattulli and R.C. Lin, 2/16/95, (PB95-220349, A05, MF-A01).

NCEER-95-0005 "Pipeline Replacement Feasibility Study: A Methodology for Minimizing Seismic and Corrosion Risks to Underground Natural Gas Pipelines," by R.T. Eguchi, H.A. Seligson and D.G. Honegger, 3/2/95, (PB95-252326, A06, MF-A02).

NCEER-95-0006 "Evaluation of Seismic Performance of an 11-Story Frame Building During the 1994 Northridge Earthquake," by F. Naeim, R. DiSulio, K. Benuska, A. Reinhorn and C. Li, to be published.

NCEER-95-0007 "Prioritization of Bridges for Seismic Retrofitting," by N. Basöz and A.S. Kiremidjian, 4/24/95, (PB95-252300, A08, MF-A02).

NCEER-95-0008 "Method for Developing Motion Damage Relationships for Reinforced Concrete Frames," by A. Singhal and A.S. Kiremidjian, 5/11/95, (PB95-266607, A06, MF-A02).

NCEER-95-0009 "Experimental and Analytical Investigation of Seismic Retrofit of Structures with Supplemental Damping: Part II - Friction Devices," by C. Li and A.M. Reinhorn, 7/6/95, (PB96-128087, A11, MF-A03).

NCEER-95-0010 "Experimental Performance and Analytical Study of a Non-Ductile Reinforced Concrete Frame Structure Retrofitted with Elastomeric Spring Dampers," by G. Pekcan, J.B. Mander and S.S. Chen, 7/14/95, (PB96-137161, A08, MF-A02).

NCEER-95-0011 "Development and Experimental Study of Semi-Active Fluid Damping Devices for Seismic Protection of Structures," by M.D. Symans and M.C. Constantinou, 8/3/95, (PB96-136940, A23, MF-A04).

NCEER-95-0012 "Real-Time Structural Parameter Modification (RSPM): Development of Innervated Structures," by Z. Liang, M. Tong and G.C. Lee, 4/11/95, (PB96-137153, A06, MF-A01).

NCEER-95-0013 "Experimental and Analytical Investigation of Seismic Retrofit of Structures with Supplemental Damping: Part III - Viscous Damping Walls," by A.M. Reinhorn and C. Li, 10/1/95, (PB96-176409, A11, MF-A03).

NCEER-95-0014 "Seismic Fragility Analysis of Equipment and Structures in a Memphis Electric Substation," by J-R. Huo and H.H.M. Hwang, 8/10/95, (PB96-128087, A09, MF-A02).

NCEER-95-0015 "The Hanshin-Awaji Earthquake of January 17, 1995: Performance of Lifelines," Edited by M. Shinozuka, 11/3/95, (PB96-176383, A15, MF-A03).

NCEER-95-0016 "Highway Culvert Performance During Earthquakes," by T.L. Youd and C.J. Beckman, available as NCEER-96-0015.

NCEER-95-0017 "The Hanshin-Awaji Earthquake of January 17, 1995: Performance of Highway Bridges," Edited by I.G. Buckle, 12/1/95, to be published.

NCEER-95-0018 "Modeling of Masonry Infill Panels for Structural Analysis," by A.M. Reinhorn, A. Madan, R.E. Valles, Y. Reichmann and J.B. Mander, 12/8/95, (PB97-110886, MF-A01, A06).

NCEER-95-0019 "Optimal Polynomial Control for Linear and Nonlinear Structures," by A.K. Agrawal and J.N. Yang, 12/11/95, (PB96-168737, A07, MF-A02).

NCEER-95-0020   "Retrofit of Non-Ductile Reinforced Concrete Frames Using Friction Dampers," by R.S. Rao, P. Gergely and R.N. White, 12/22/95, (PB97-133508, A10, MF-A02).

NCEER-95-0021   "Parametric Results for Seismic Response of Pile-Supported Bridge Bents," by G. Mylonakis, A. Nikolaou and G. Gazetas, 12/22/95, (PB97-100242, A12, MF-A03).

NCEER-95-0022   "Kinematic Bending Moments in Seismically Stressed Piles," by A. Nikolaou, G. Mylonakis and G. Gazetas, 12/23/95, (PB97-113914, MF-A03, A13).

NCEER-96-0001   "Dynamic Response of Unreinforced Masonry Buildings with Flexible Diaphragms," by A.C. Costley and D.P. Abrams," 10/10/96, (PB97-133573, MF-A03, A15).

NCEER-96-0002   "State of the Art Review: Foundations and Retaining Structures," by I. Po Lam, to be published.

NCEER-96-0003   "Ductility of Rectangular Reinforced Concrete Bridge Columns with Moderate Confinement," by N. Wehbe, M. Saiidi, D. Sanders and B. Douglas, 11/7/96, (PB97-133557, A06, MF-A02).

NCEER-96-0004   "Proceedings of the Long-Span Bridge Seismic Research Workshop," edited by I.G. Buckle and I.M. Friedland, to be published.

NCEER-96-0005   "Establish Representative Pier Types for Comprehensive Study: Eastern United States," by J. Kulicki and Z. Prucz, 5/28/96, (PB98-119217, A07, MF-A02).

NCEER-96-0006   "Establish Representative Pier Types for Comprehensive Study: Western United States," by R. Imbsen, R.A. Schamber and T.A. Osterkamp, 5/28/96, (PB98-118607, A07, MF-A02).

NCEER-96-0007   "Nonlinear Control Techniques for Dynamical Systems with Uncertain Parameters," by R.G. Ghanem and M.I. Bujakov, 5/27/96, (PB97-100259, A17, MF-A03).

NCEER-96-0008   "Seismic Evaluation of a 30-Year Old Non-Ductile Highway Bridge Pier and Its Retrofit," by J.B. Mander, B. Mahmoodzadegan, S. Bhadra and S.S. Chen, 5/31/96, (PB97-110902, MF-A03, A10).

NCEER-96-0009   "Seismic Performance of a Model Reinforced Concrete Bridge Pier Before and After Retrofit," by J.B. Mander, J.H. Kim and C.A. Ligozio, 5/31/96, (PB97-110910, MF-A02, A10).

NCEER-96-0010   "IDARC2D Version 4.0: A Computer Program for the Inelastic Damage Analysis of Buildings," by R.E. Valles, A.M. Reinhorn, S.K. Kunnath, C. Li and A. Madan, 6/3/96, (PB97-100234, A17, MF-A03).

NCEER-96-0011   "Estimation of the Economic Impact of Multiple Lifeline Disruption: Memphis Light, Gas and Water Division Case Study," by S.E. Chang, H.A. Seligson and R.T. Eguchi, 8/16/96, (PB97-133490, A11, MF-A03).

NCEER-96-0012   "Proceedings from the Sixth Japan-U.S. Workshop on Earthquake Resistant Design of Lifeline Facilities and Countermeasures Against Soil Liquefaction, Edited by M. Hamada and T. O'Rourke, 9/11/96, (PB97-133581, A99, MF-A06).

NCEER-96-0013   "Chemical Hazards, Mitigation and Preparedness in Areas of High Seismic Risk: A Methodology for Estimating the Risk of Post-Earthquake Hazardous Materials Release," by H.A. Seligson, R.T. Eguchi, K.J. Tierney and K. Richmond, 11/7/96, (PB97-133565, MF-A02, A08).

NCEER-96-0014   "Response of Steel Bridge Bearings to Reversed Cyclic Loading," by J.B. Mander, D-K. Kim, S.S. Chen and G.J. Premus, 11/13/96, (PB97-140735, A12, MF-A03).

NCEER-96-0015   "Highway Culvert Performance During Past Earthquakes," by T.L. Youd and C.J. Beckman, 11/25/96, (PB97-133532, A06, MF-A01).

NCEER-97-0001   "Evaluation, Prevention and Mitigation of Pounding Effects in Building Structures," by R.E. Valles and A.M. Reinhorn, 2/20/97, (PB97-159552, A14, MF-A03).

NCEER-97-0002   "Seismic Design Criteria for Bridges and Other Highway Structures," by C. Rojahn, R. Mayes, D.G. Anderson, J. Clark, J.H. Hom, R.V. Nutt and M.J. O'Rourke, 4/30/97, (PB97-194658, A06, MF-A03).

NCEER-97-0003   "Proceedings of the U.S.-Italian Workshop on Seismic Evaluation and Retrofit," Edited by D.P. Abrams and G.M. Calvi, 3/19/97, (PB97-194666, A13, MF-A03).

NCEER-97-0004   "Investigation of Seismic Response of Buildings with Linear and Nonlinear Fluid Viscous Dampers," by A.A. Seleemah and M.C. Constantinou, 5/21/97, (PB98-109002, A15, MF-A03).

NCEER-97-0005   "Proceedings of the Workshop on Earthquake Engineering Frontiers in Transportation Facilities," edited by G.C. Lee and I.M. Friedland, 8/29/97, (PB98-128911, A25, MR-A04).

NCEER-97-0006   "Cumulative Seismic Damage of Reinforced Concrete Bridge Piers," by S.K. Kunnath, A. El-Bahy, A. Taylor and W. Stone, 9/2/97, (PB98-108814, A11, MF-A03).

NCEER-97-0007   "Structural Details to Accommodate Seismic Movements of Highway Bridges and Retaining Walls," by R.A. Imbsen, R.A. Schamber, E. Thorkildsen, A. Kartoum, B.T. Martin, T.N. Rosser and J.M. Kulicki, 9/3/97, (PB98-108996, A09, MF-A02).

NCEER-97-0008   "A Method for Earthquake Motion-Damage Relationships with Application to Reinforced Concrete Frames," by A. Singhal and A.S. Kiremidjian, 9/10/97, (PB98-108988, A13, MF-A03).

NCEER-97-0009   "Seismic Analysis and Design of Bridge Abutments Considering Sliding and Rotation," by K. Fishman and R. Richards, Jr., 9/15/97, (PB98-108897, A06, MF-A02).

NCEER-97-0010   "Proceedings of the FHWA/NCEER Workshop on the National Representation of Seismic Ground Motion for New and Existing Highway Facilities," edited by I.M. Friedland, M.S. Power and R.L. Mayes, 9/22/97, (PB98-128903, A21, MF-A04).

NCEER-97-0011   "Seismic Analysis for Design or Retrofit of Gravity Bridge Abutments," by K.L. Fishman, R. Richards, Jr. and R.C. Divito, 10/2/97, (PB98-128937, A08, MF-A02).

NCEER-97-0012   "Evaluation of Simplified Methods of Analysis for Yielding Structures," by P. Tsopelas, M.C. Constantinou, C.A. Kircher and A.S. Whittaker, 10/31/97, (PB98-128929, A10, MF-A03).

NCEER-97-0013   "Seismic Design of Bridge Columns Based on Control and Repairability of Damage," by C-T. Cheng and J.B. Mander, 12/8/97, (PB98-144249, A11, MF-A03).

NCEER-97-0014   "Seismic Resistance of Bridge Piers Based on Damage Avoidance Design," by J.B. Mander and C-T. Cheng, 12/10/97, (PB98-144223, A09, MF-A02).

NCEER-97-0015   "Seismic Response of Nominally Symmetric Systems with Strength Uncertainty," by S. Balopoulou and M. Grigoriu, 12/23/97, (PB98-153422, A11, MF-A03).

NCEER-97-0016   "Evaluation of Seismic Retrofit Methods for Reinforced Concrete Bridge Columns," by T.J. Wipf, F.W. Klaiber and F.M. Russo, 12/28/97, (PB98-144215, A12, MF-A03).

NCEER-97-0017   "Seismic Fragility of Existing Conventional Reinforced Concrete Highway Bridges," by C.L. Mullen and A.S. Cakmak, 12/30/97, (PB98-153406, A08, MF-A02).

NCEER-97-0018   "Loss Asssessment of Memphis Buildings," edited by D.P. Abrams and M. Shinozuka, 12/31/97, (PB98-144231, A13, MF-A03).

NCEER-97-0019   "Seismic Evaluation of Frames with Infill Walls Using Quasi-static Experiments," by K.M. Mosalam, R.N. White and P. Gergely, 12/31/97, (PB98-153455, A07, MF-A02).

NCEER-97-0020   "Seismic Evaluation of Frames with Infill Walls Using Pseudo-dynamic Experiments," by K.M. Mosalam, R.N. White and P. Gergely, 12/31/97, (PB98-153430, A07, MF-A02).

NCEER-97-0021   "Computational Strategies for Frames with Infill Walls: Discrete and Smeared Crack Analyses and Seismic Fragility," by K.M. Mosalam, R.N. White and P. Gergely, 12/31/97, (PB98-153414, A10, MF-A02).

NCEER-97-0022   "Proceedings of the NCEER Workshop on Evaluation of Liquefaction Resistance of Soils," edited by T.L. Youd and I.M. Idriss, 12/31/97, (PB98-155617, A15, MF-A03).

MCEER-98-0001   "Extraction of Nonlinear Hysteretic Properties of Seismically Isolated Bridges from Quick-Release Field Tests," by Q. Chen, B.M. Douglas, E.M. Maragakis and I.G. Buckle, 5/26/98, (PB99-118838, A06, MF-A01).

MCEER-98-0002   "Methodologies for Evaluating the Importance of Highway Bridges," by A. Thomas, S. Eshenaur and J. Kulicki, 5/29/98, (PB99-118846, A10, MF-A02).

MCEER-98-0003   "Capacity Design of Bridge Piers and the Analysis of Overstrength," by J.B. Mander, A. Dutta and P. Goel, 6/1/98, (PB99-118853, A09, MF-A02).

MCEER-98-0004   "Evaluation of Bridge Damage Data from the Loma Prieta and Northridge, California Earthquakes," by N. Basoz and A. Kiremidjian, 6/2/98, (PB99-118861, A15, MF-A03).

MCEER-98-0005   "Screening Guide for Rapid Assessment of Liquefaction Hazard at Highway Bridge Sites," by T. L. Youd, 6/16/98, (PB99-118879, A06, not available on microfiche).

MCEER-98-0006   "Structural Steel and Steel/Concrete Interface Details for Bridges," by P. Ritchie, N. Kauhl and J. Kulicki, 7/13/98, (PB99-118945, A06, MF-A01).

MCEER-98-0007   "Capacity Design and Fatigue Analysis of Confined Concrete Columns," by A. Dutta and J.B. Mander, 7/14/98, (PB99-118960, A14, MF-A03).

MCEER-98-0008   "Proceedings of the Workshop on Performance Criteria for Telecommunication Services Under Earthquake Conditions," edited by A.J. Schiff, 7/15/98, (PB99-118952, A08, MF-A02).

MCEER-98-0009   "Fatigue Analysis of Unconfined Concrete Columns," by J.B. Mander, A. Dutta and J.H. Kim, 9/12/98, (PB99-123655, A10, MF-A02).

MCEER-98-0010   "Centrifuge Modeling of Cyclic Lateral Response of Pile-Cap Systems and Seat-Type Abutments in Dry Sands," by A.D. Gadre and R. Dobry, 10/2/98, (PB99-123606, A13, MF-A03).

MCEER-98-0011   "IDARC-BRIDGE: A Computational Platform for Seismic Damage Assessment of Bridge Structures," by A.M. Reinhorn, V. Simeonov, G. Mylonakis and Y. Reichman, 10/2/98, (PB99-162919, A15, MF-A03).

MCEER-98-0012   "Experimental Investigation of the Dynamic Response of Two Bridges Before and After Retrofitting with Elastomeric Bearings," by D.A. Wendichansky, S.S. Chen and J.B. Mander, 10/2/98, (PB99-162927, A15, MF-A03).

MCEER-98-0013   "Design Procedures for Hinge Restrainers and Hinge Sear Width for Multiple-Frame Bridges," by R. Des Roches and G.L. Fenves, 11/3/98, (PB99-140477, A13, MF-A03).

MCEER-98-0014   "Response Modification Factors for Seismically Isolated Bridges," by M.C. Constantinou and J.K. Quarshie, 11/3/98, (PB99-140485, A14, MF-A03).

MCEER-98-0015   "Proceedings of the U.S.-Italy Workshop on Seismic Protective Systems for Bridges," edited by I.M. Friedland and M.C. Constantinou, 11/3/98, (PB2000-101711, A22, MF-A04).

MCEER-98-0016   "Appropriate Seismic Reliability for Critical Equipment Systems: Recommendations Based on Regional Analysis of Financial and Life Loss," by K. Porter, C. Scawthorn, C. Taylor and N. Blais, 11/10/98, (PB99-157265, A08, MF-A02).

MCEER-98-0017   "Proceedings of the U.S. Japan Joint Seminar on Civil Infrastructure Systems Research," edited by M. Shinozuka and A. Rose, 11/12/98, (PB99-156713, A16, MF-A03).

MCEER-98-0018   "Modeling of Pile Footings and Drilled Shafts for Seismic Design," by I. PoLam, M. Kapuskar and D. Chaudhuri, 12/21/98, (PB99-157257, A09, MF-A02).

MCEER-99-0001 "Seismic Evaluation of a Masonry Infilled Reinforced Concrete Frame by Pseudodynamic Testing," by S.G. Buonopane and R.N. White, 2/16/99, (PB99-162851, A09, MF-A02).

MCEER-99-0002 "Response History Analysis of Structures with Seismic Isolation and Energy Dissipation Systems: Verification Examples for Program SAP2000," by J. Scheller and M.C. Constantinou, 2/22/99, (PB99-162869, A08, MF-A02).

MCEER-99-0003 "Experimental Study on the Seismic Design and Retrofit of Bridge Columns Including Axial Load Effects," by A. Dutta, T. Kokorina and J.B. Mander, 2/22/99, (PB99-162877, A09, MF-A02).

MCEER-99-0004 "Experimental Study of Bridge Elastomeric and Other Isolation and Energy Dissipation Systems with Emphasis on Uplift Prevention and High Velocity Near-source Seismic Excitation," by A. Kasalanati and M. C. Constantinou, 2/26/99, (PB99-162885, A12, MF-A03).

MCEER-99-0005 "Truss Modeling of Reinforced Concrete Shear-flexure Behavior," by J.H. Kim and J.B. Mander, 3/8/99, (PB99-163693, A12, MF-A03).

MCEER-99-0006 "Experimental Investigation and Computational Modeling of Seismic Response of a 1:4 Scale Model Steel Structure with a Load Balancing Supplemental Damping System," by G. Pekcan, J.B. Mander and S.S. Chen, 4/2/99, (PB99-162893, A11, MF-A03).

MCEER-99-0007 "Effect of Vertical Ground Motions on the Structural Response of Highway Bridges," by M.R. Button, C.J. Cronin and R.L. Mayes, 4/10/99, (PB2000-101411, A10, MF-A03).

MCEER-99-0008 "Seismic Reliability Assessment of Critical Facilities: A Handbook, Supporting Documentation, and Model Code Provisions," by G.S. Johnson, R.E. Sheppard, M.D. Quilici, S.J. Eder and C.R. Scawthorn, 4/12/99, (PB2000-101701, A18, MF-A04).

MCEER-99-0009 "Impact Assessment of Selected MCEER Highway Project Research on the Seismic Design of Highway Structures," by C. Rojahn, R. Mayes, D.G. Anderson, J.H. Clark, D'Appolonia Engineering, S. Gloyd and R.V. Nutt, 4/14/99, (PB99-162901, A10, MF-A02).

MCEER-99-0010 "Site Factors and Site Categories in Seismic Codes," by R. Dobry, R. Ramos and M.S. Power, 7/19/99, (PB2000-101705, A08, MF-A02).

MCEER-99-0011 "Restrainer Design Procedures for Multi-Span Simply-Supported Bridges," by M.J. Randall, M. Saiidi, E. Maragakis and T. Isakovic, 7/20/99, (PB2000-101702, A10, MF-A02).

MCEER-99-0012 "Property Modification Factors for Seismic Isolation Bearings," by M.C. Constantinou, P. Tsopelas, A. Kasalanati and E. Wolff, 7/20/99, (PB2000-103387, A11, MF-A03).

MCEER-99-0013 "Critical Seismic Issues for Existing Steel Bridges," by P. Ritchie, N. Kauhl and J. Kulicki, 7/20/99, (PB2000-101697, A09, MF-A02).

MCEER-99-0014 "Nonstructural Damage Database," by A. Kao, T.T. Soong and A. Vender, 7/24/99, (PB2000-101407, A06, MF-A01).

MCEER-99-0015 "Guide to Remedial Measures for Liquefaction Mitigation at Existing Highway Bridge Sites," by H.G. Cooke and J. K. Mitchell, 7/26/99, (PB2000-101703, A11, MF-A03).

MCEER-99-0016 "Proceedings of the MCEER Workshop on Ground Motion Methodologies for the Eastern United States," edited by N. Abrahamson and A. Becker, 8/11/99, (PB2000-103385, A07, MF-A02).

MCEER-99-0017 "Quindío, Colombia Earthquake of January 25, 1999: Reconnaissance Report," by A.P. Asfura and P.J. Flores, 10/4/99, (PB2000-106893, A06, MF-A01).

MCEER-99-0018 "Hysteretic Models for Cyclic Behavior of Deteriorating Inelastic Structures," by M.V. Sivaselvan and A.M. Reinhorn, 11/5/99, (PB2000-103386, A08, MF-A02).

MCEER-99-0019   "Proceedings of the 7th U.S.- Japan Workshop on Earthquake Resistant Design of Lifeline Facilities and Countermeasures Against Soil Liquefaction," edited by T.D. O'Rourke, J.P. Bardet and M. Hamada, 11/19/99, (PB2000-103354, A99, MF-A06).

MCEER-99-0020   "Development of Measurement Capability for Micro-Vibration Evaluations with Application to Chip Fabrication Facilities," by G.C. Lee, Z. Liang, J.W. Song, J.D. Shen and W.C. Liu, 12/1/99, (PB2000-105993, A08, MF-A02).

MCEER-99-0021   "Design and Retrofit Methodology for Building Structures with Supplemental Energy Dissipating Systems," by G. Pekcan, J.B. Mander and S.S. Chen, 12/31/99, (PB2000-105994, A11, MF-A03).

MCEER-00-0001   "The Marmara, Turkey Earthquake of August 17, 1999: Reconnaissance Report," edited by C. Scawthorn; with major contributions by M. Bruneau, R. Eguchi, T. Holzer, G. Johnson, J. Mander, J. Mitchell, W. Mitchell, A. Papageorgiou, C. Scaethorn, and G. Webb, 3/23/00, (PB2000-106200, A11, MF-A03).

MCEER-00-0002   "Proceedings of the MCEER Workshop for Seismic Hazard Mitigation of Health Care Facilities," edited by G.C. Lee, M. Ettouney, M. Grigoriu, J. Hauer and J. Nigg, 3/29/00, (PB2000-106892, A08, MF-A02).

MCEER-00-0003   "The Chi-Chi, Taiwan Earthquake of September 21, 1999: Reconnaissance Report," edited by G.C. Lee and C.H. Loh, with major contributions by G.C. Lee, M. Bruneau, I.G. Buckle, S.E. Chang, P.J. Flores, T.D. O'Rourke, M. Shinozuka, T.T. Soong, C-H. Loh, K-C. Chang, Z-J. Chen, J-S. Hwang, M-L. Lin, G-Y. Liu, K-C. Tsai, G.C. Yao and C-L. Yen, 4/30/00, (PB2001-100980, A10, MF-A02).

MCEER-00-0004   "Seismic Retrofit of End-Sway Frames of Steel Deck-Truss Bridges with a Supplemental Tendon System: Experimental and Analytical Investigation," by G. Pekcan, J.B. Mander and S.S. Chen, 7/1/00, (PB2001-100982, A10, MF-A02).

MCEER-00-0005   "Sliding Fragility of Unrestrained Equipment in Critical Facilities," by W.H. Chong and T.T. Soong, 7/5/00, (PB2001-100983, A08, MF-A02).

MCEER-00-0006   "Seismic Response of Reinforced Concrete Bridge Pier Walls in the Weak Direction," by N. Abo-Shadi, M. Saiidi and D. Sanders, 7/17/00, (PB2001-100981, A17, MF-A03).

MCEER-00-0007   "Low-Cycle Fatigue Behavior of Longitudinal Reinforcement in Reinforced Concrete Bridge Columns," by J. Brown and S.K. Kunnath, 7/23/00, (PB2001-104392, A08, MF-A02).

MCEER-00-0008   "Soil Structure Interaction of Bridges for Seismic Analysis," I. PoLam and H. Law, 9/25/00, (PB2001-105397, A08, MF-A02).

MCEER-00-0009   "Proceedings of the First MCEER Workshop on Mitigation of Earthquake Disaster by Advanced Technologies (MEDAT-1), edited by M. Shinozuka, D.J. Inman and T.D. O'Rourke, 11/10/00, (PB2001-105399, A14, MF-A03).

MCEER-00-0010   "Development and Evaluation of Simplified Procedures for Analysis and Design of Buildings with Passive Energy Dissipation Systems," by O.M. Ramirez, M.C. Constantinou, C.A. Kircher, A.S. Whittaker, M.W. Johnson, J.D. Gomez and C. Chrysostomou, 11/16/01, (PB2001-105523, A23, MF-A04).

MCEER-00-0011   "Dynamic Soil-Foundation-Structure Interaction Analyses of Large Caissons," by C-Y. Chang, C-M. Mok, Z-L. Wang, R. Settgast, F. Waggoner, M.A. Ketchum, H.M. Gonnermann and C-C. Chin, 12/30/00, (PB2001-104373, A07, MF-A02).

MCEER-00-0012   "Experimental Evaluation of Seismic Performance of Bridge Restrainers," by A.G. Vlassis, E.M. Maragakis and M. Saiid Saiidi, 12/30/00, (PB2001-104354, A09, MF-A02).

MCEER-00-0013   "Effect of Spatial Variation of Ground Motion on Highway Structures," by M. Shinozuka, V. Saxena and G. Deodatis, 12/31/00, (PB2001-108755, A13, MF-A03).

MCEER-00-0014   "A Risk-Based Methodology for Assessing the Seismic Performance of Highway Systems," by S.D. Werner, C.E. Taylor, J.E. Moore, II, J.S. Walton and S. Cho, 12/31/00, (PB2001-108756, A14, MF-A03).

MCEER-01-0001 "Experimental Investigation of P-Delta Effects to Collapse During Earthquakes," by D. Vian and M. Bruneau, 6/25/01, (PB2002-100534, A17, MF-A03).

MCEER-01-0002 "Proceedings of the Second MCEER Workshop on Mitigation of Earthquake Disaster by Advanced Technologies (MEDAT-2)," edited by M. Bruneau and D.J. Inman, 7/23/01, (PB2002-100434, A16, MF-A03).

MCEER-01-0003 "Sensitivity Analysis of Dynamic Systems Subjected to Seismic Loads," by C. Roth and M. Grigoriu, 9/18/01, (PB2003-100884, A12, MF-A03).

MCEER-01-0004 "Overcoming Obstacles to Implementing Earthquake Hazard Mitigation Policies: Stage 1 Report," by D.J. Alesch and W.J. Petak, 12/17/01, (PB2002-107949, A07, MF-A02).

MCEER-01-0005 "Updating Real-Time Earthquake Loss Estimates: Methods, Problems and Insights," by C.E. Taylor, S.E. Chang and R.T. Eguchi, 12/17/01, (PB2002-107948, A05, MF-A01).

MCEER-01-0006 "Experimental Investigation and Retrofit of Steel Pile Foundations and Pile Bents Under Cyclic Lateral Loadings," by A. Shama, J. Mander, B. Blabac and S. Chen, 12/31/01, (PB2002-107950, A13, MF-A03).

MCEER-02-0001 "Assessment of Performance of Bolu Viaduct in the 1999 Duzce Earthquake in Turkey" by P.C. Roussis, M.C. Constantinou, M. Erdik, E. Durukal and M. Dicleli, 5/8/02, (PB2003-100883, A08, MF-A02).

MCEER-02-0002 "Seismic Behavior of Rail Counterweight Systems of Elevators in Buildings," by M.P. Singh, Rildova and L.E. Suarez, 5/27/02. (PB2003-100882, A11, MF-A03).

MCEER-02-0003 "Development of Analysis and Design Procedures for Spread Footings," by G. Mylonakis, G. Gazetas, S. Nikolaou and A. Chauncey, 10/02/02, (PB2004-101636, A13, MF-A03, CD-A13).

MCEER-02-0004 "Bare-Earth Algorithms for Use with SAR and LIDAR Digital Elevation Models," by C.K. Huyck, R.T. Eguchi and B. Houshmand, 10/16/02, (PB2004-101637, A07, CD-A07).

MCEER-02-0005 "Review of Energy Dissipation of Compression Members in Concentrically Braced Frames," by K.Lee and M. Bruneau, 10/18/02, (PB2004-101638, A10, CD-A10).

MCEER-03-0001 "Experimental Investigation of Light-Gauge Steel Plate Shear Walls for the Seismic Retrofit of Buildings" by J. Berman and M. Bruneau, 5/2/03, (PB2004-101622, A10, MF-A03, CD-A10).

MCEER-03-0002 "Statistical Analysis of Fragility Curves," by M. Shinozuka, M.Q. Feng, H. Kim, T. Uzawa and T. Ueda, 6/16/03, (PB2004-101849, A09, CD-A09).

MCEER-03-0003 "Proceedings of the Eighth U.S.-Japan Workshop on Earthquake Resistant Design f Lifeline Facilities and Countermeasures Against Liquefaction," edited by M. Hamada, J.P. Bardet and T.D. O'Rourke, 6/30/03, (PB2004-104386, A99, CD-A99).

MCEER-03-0004 "Proceedings of the PRC-US Workshop on Seismic Analysis and Design of Special Bridges," edited by L.C. Fan and G.C. Lee, 7/15/03, (PB2004-104387, A14, CD-A14).

MCEER-03-0005 "Urban Disaster Recovery: A Framework and Simulation Model," by S.B. Miles and S.E. Chang, 7/25/03, (PB2004-104388, A07, CD-A07).

MCEER-03-0006 "Behavior of Underground Piping Joints Due to Static and Dynamic Loading," by R.D. Meis, M. Maragakis and R. Siddharthan, 11/17/03, (PB2005-102194, A13, MF-A03, CD-A00).

MCEER-03-0007 "Seismic Vulnerability of Timber Bridges and Timber Substructures," by A.A. Shama, J.B. Mander, I.M. Friedland and D.R. Allicock, 12/15/03.

MCEER-04-0001 "Experimental Study of Seismic Isolation Systems with Emphasis on Secondary System Response and Verification of Accuracy of Dynamic Response History Analysis Methods," by E. Wolff and M. Constantinou, 1/16/04 (PB2005-102195, A99, MF-E08, CD-A00).

MCEER-04-0002   "Tension, Compression and Cyclic Testing of Engineered Cementitious Composite Materials," by K. Kesner and S.L. Billington, 3/1/04, (PB2005-102196, A08, CD-A08).

MCEER-04-0003   "Cyclic Testing of Braces Laterally Restrained by Steel Studs to Enhance Performance During Earthquakes," by O.C. Celik, J.W. Berman and M. Bruneau, 3/16/04, (PB2005-102197, A13, MF-A03, CD-A00).

MCEER-04-0004   "Methodologies for Post Earthquake Building Damage Detection Using SAR and Optical Remote Sensing: Application to the August 17, 1999 Marmara, Turkey Earthquake," by C.K. Huyck, B.J. Adams, S. Cho, R.T. Eguchi, B. Mansouri and B. Houshmand, 6/15/04, (PB2005-104888, A10, CD-A00).

MCEER-04-0005   "Nonlinear Structural Analysis Towards Collapse Simulation: A Dynamical Systems Approach," by M.V. Sivaselvan and A.M. Reinhorn, 6/16/04, (PB2005-104889, A11, MF-A03, CD-A00).

MCEER-04-0006   "Proceedings of the Second PRC-US Workshop on Seismic Analysis and Design of Special Bridges," edited by G.C. Lee and L.C. Fan, 6/25/04, (PB2005-104890, A16, CD-A00).

MCEER-04-0007   "Seismic Vulnerability Evaluation of Axially Loaded Steel Built-up Laced Members," by K. Lee and M. Bruneau, 6/30/04, (PB2005-104891, A16, CD-A00).

MCEER-04-0008   "Evaluation of Accuracy of Simplified Methods of Analysis and Design of Buildings with Damping Systems for Near-Fault and for Soft-Soil Seismic Motions," by E.A. Pavlou and M.C. Constantinou, 8/16/04, (PB2005-104892, A08, MF-A02, CD-A00).

MCEER-04-0009   "Assessment of Geotechnical Issues in Acute Care Facilities in California," by M. Lew, T.D. O'Rourke, R. Dobry and M. Koch, 9/15/04, (PB2005-104893, A08, CD-A00).

MCEER-04-0010   "Scissor-Jack-Damper Energy Dissipation System," by A.N. Sigaher-Boyle and M.C. Constantinou, 12/1/04 (PB2005-108221).

MCEER-04-0011   "Seismic Retrofit of Bridge Steel Truss Piers Using a Controlled Rocking Approach," by M. Pollino and M. Bruneau, 12/20/04 (PB2006-105795).

MCEER-05-0001   "Experimental and Analytical Studies of Structures Seismically Isolated with an Uplift-Restraint Isolation System," by P.C. Roussis and M.C. Constantinou, 1/10/05 (PB2005-108222).

MCEER-05-0002   "A Versatile Experimentation Model for Study of Structures Near Collapse Applied to Seismic Evaluation of Irregular Structures," by D. Kusumastuti, A.M. Reinhorn and A. Rutenberg, 3/31/05 (PB2006-101523).

MCEER-05-0003   "Proceedings of the Third PRC-US Workshop on Seismic Analysis and Design of Special Bridges," edited by L.C. Fan and G.C. Lee, 4/20/05, (PB2006-105796).

MCEER-05-0004   "Approaches for the Seismic Retrofit of Braced Steel Bridge Piers and Proof-of-Concept Testing of an Eccentrically Braced Frame with Tubular Link," by J.W. Berman and M. Bruneau, 4/21/05 (PB2006-101524).

MCEER-05-0005   "Simulation of Strong Ground Motions for Seismic Fragility Evaluation of Nonstructural Components in Hospitals," by A. Wanitkorkul and A. Filiatrault, 5/26/05 (PB2006-500027).

MCEER-05-0006   "Seismic Safety in California Hospitals: Assessing an Attempt to Accelerate the Replacement or Seismic Retrofit of Older Hospital Facilities," by D.J. Alesch, L.A. Arendt and W.J. Petak, 6/6/05 (PB2006-105794).

MCEER-05-0007   "Development of Seismic Strengthening and Retrofit Strategies for Critical Facilities Using Engineered Cementitious Composite Materials," by K. Kesner and S.L. Billington, 8/29/05 (PB2006-111701).

MCEER-05-0008   "Experimental and Analytical Studies of Base Isolation Systems for Seismic Protection of Power Transformers," by N. Murota, M.Q. Feng and G-Y. Liu, 9/30/05 (PB2006-111702).

MCEER-05-0009   "3D-BASIS-ME-MB: Computer Program for Nonlinear Dynamic Analysis of Seismically Isolated Structures," by P.C. Tsopelas, P.C. Roussis, M.C. Constantinou, R. Buchanan and A.M. Reinhorn, 10/3/05 (PB2006-111703).

MCEER-05-0010   "Steel Plate Shear Walls for Seismic Design and Retrofit of Building Structures," by D. Vian and M. Bruneau, 12/15/05 (PB2006-111704).

MCEER-05-0011   "The Performance-Based Design Paradigm," by M.J. Astrella and A. Whittaker, 12/15/05 (PB2006-111705).

MCEER-06-0001   "Seismic Fragility of Suspended Ceiling Systems," H. Badillo-Almaraz, A.S. Whittaker, A.M. Reinhorn and G.P. Cimellaro, 2/4/06 (PB2006-111706).

MCEER-06-0002   "Multi-Dimensional Fragility of Structures," by G.P. Cimellaro, A.M. Reinhorn and M. Bruneau, 3/1/06 (PB2007-106974, A09, MF-A02, CD A00).

MCEER-06-0003   "Built-Up Shear Links as Energy Dissipators for Seismic Protection of Bridges," by P. Dusicka, A.M. Itani and I.G. Buckle, 3/15/06 (PB2006-111708).

MCEER-06-0004   "Analytical Investigation of the Structural Fuse Concept," by R.E. Vargas and M. Bruneau, 3/16/06 (PB2006-111709).

MCEER-06-0005   "Experimental Investigation of the Structural Fuse Concept," by R.E. Vargas and M. Bruneau, 3/17/06 (PB2006-111710).

MCEER-06-0006   "Further Development of Tubular Eccentrically Braced Frame Links for the Seismic Retrofit of Braced Steel Truss Bridge Piers," by J.W. Berman and M. Bruneau, 3/27/06 (PB2007-105147).

MCEER-06-0007   "REDARS Validation Report," by S. Cho, C.K. Huyck, S. Ghosh and R.T. Eguchi, 8/8/06 (PB2007-106983).

MCEER-06-0008   "Review of Current NDE Technologies for Post-Earthquake Assessment of Retrofitted Bridge Columns," by J.W. Song, Z. Liang and G.C. Lee, 8/21/06 06 (PB2007-106984).

MCEER-06-0009   "Liquefaction Remediation in Silty Soils Using Dynamic Compaction and Stone Columns," by S. Thevanayagam, G.R. Martin, R. Nashed, T. Shenthan, T. Kanagalingam and N. Ecemis, 8/28/06 06 (PB2007-106985).

MCEER-06-0010   "Conceptual Design and Experimental Investigation of Polymer Matrix Composite Infill Panels for Seismic Retrofitting," by W. Jung, M. Chiewanichakorn and A.J. Aref, 9/21/06 (PB2007-106986).

MCEER-06-0011   "A Study of the Coupled Horizontal-Vertical Behavior of Elastomeric and Lead-Rubber Seismic Isolation Bearings," by G.P. Warn and A.S. Whittaker, 9/22/06 (PB2007-108679).

MCEER-06-0012   "Proceedings of the Fourth PRC-US Workshop on Seismic Analysis and Design of Special Bridges: Advancing Bridge Technologies in Research, Design, Construction and Preservation," Edited by L.C. Fan, G.C. Lee and L. Ziang, 10/12/06.

MCEER-06-0013   "Cyclic Response and Low Cycle Fatigue Characteristics of Plate Steels," by P. Dusicka, A.M. Itani and I.G. Buckle, 11/1/06 06 (PB2007-106987).

MCEER-06-0014   "Proceedings of the Second US-Taiwan Bridge Engineering Workshop," edited by W.P. Yen, J. Shen, J-Y. Chen and M. Wang, 11/15/06.

MCEER-06-0015   "User Manual and Technical Documentation for the REDARS^{TM} Import Wizard," by S. Cho, S. Ghosh, C.K. Huyck and S.D. Werner, 11/30/06.

MCEER-06-0016   "Hazard Mitigation Strategy and Monitoring Technologies for Urban and Infrastructure Public Buildings: Proceedings of the China-US Workshops," edited by X.Y. Zhou, A.L. Zhang, G.C. Lee and M. Tong, 12/12/06.

MCEER-07-0001   "Static and Kinetic Coefficients of Friction for Rigid Blocks," by C. Kafali, S. Fathali, M. Grigoriu and A.S. Whittaker, 3/20/07.

MCEER-07-0002   "Hazard Mitigation Investment Decision Making: Organizational Response to Legislative Mandate," by L.A. Arendt, D.J. Alesch and W.J. Petak, 4/9/07.

MCEER-07-0003   "Seismic Behavior of Bidirectional-Resistant Ductile End Diaphragms with Unbonded Braces in Straight or Skewed Steel Bridges," by O. Celik and M. Bruneau, 4/11/07.

MCEER-07-0004   "Modeling Pile Behavior in Large Pile Groups Under Lateral Loading," by A.M. Dodds and G.R. Martin, 4/16/07.

MCEER-07-0005   "Experimental Investigation of Blast Performance of Seismically Resistant Concrete-Filled Steel Tube Bridge Piers," by S. Fujikura, M. Bruneau and D. Lopez-Garcia, 4/20/07.

MCEER-07-0006   "Seismic Analysis of Conventional and Isolated Liquefied Natural Gas Tanks Using Mechanical Analogs," by I.P. Christovasilis and A.S. Whittaker, 5/1/07.

MCEER-07-0007   "Experimental Seismic Performance Evaluation of Isolation/Restraint Systems for Mechanical Equipment – Part 1: Heavy Equipment Study," by S. Fathali and A. Filiatrault, 6/6/07.

MCEER-07-0008   "Seismic Vulnerability of Timber Bridges and Timber Substructures," A.A. Sharma, J.B. Mander, I.M. Friedland and D.R. Allicock, 6/7/07.